Biosphere-Atmosphere Interaction in a One-Dimensional Climate Model of the Tropics

by

Julie E. Kiang

Submitted to the Department of Civil and Environmental Engineering
in partial fulfillment of the requirements for the degree of

Master of Science in Civil and Environmental Engineering

at the

MASSACHUSETTS INSTITUTE OF TECHNOLOGY

January 1999
[February, 1999]

Author .....
Department of Civil and Environmental Engineering
January 15, 1999

Certified by....
Elfatih A.B. Eltahir
Associate Professor
Thesis Supervisor

Accepted by .....
Andrew J. Whittle
Chairman, Department Committee on Graduate Students

Biosphere-Atmosphere Interaction in a One-Dimensional Climate Model of the Tropics

by

Julie E. Kiang

Submitted to the Department of Civil and Environmental Engineering
on January 15, 1999, in partial fulfillment of the
requirements for the degree of
Master of Science in Civil and Environmental Engineering

Abstract

In this study, we develop a one-dimensional model of the tropics which includes two-way interaction between the biosphere and the atmosphere. The model integrates a radiative-convective equlibrium model of the atmosphere, a land surface model including plant growth and competition and a monsoon circulation model which allows for the exchange of heat and moisture between the one-dimensional column and its surroundings. The model is applied to two domains in West Africa to test the sensitivity of the system's equilibrium to perturbations to initial vegetation.

In the coastal domain, the model simulates a stable forest equilibrium. The equilibrium climate and vegetation show reasonable similarity to observations for the same region. The same equilibrium is reached in both our control simulation and our experimental simulation, in which deforestation is simulated by initializing the model with grassland. Modifications to parameters of the empirical monsoon circulation model show that the climate and vegetation in our model domain are sensitive to the strength of the monsoon circulation and also to climatic conditions in adjacent regions. In particular, changes in the monsoon which allowed hot and dry air to penetrate into the model domain from the north strongly affected the equilibrium climate and vegetation. These sensitivity studies indicated that the existence of multiple equilibria in the biosphere-atmosphere system depends not only on the magnitude of the vegetation-induced climate perturbation, but also on whether or not the perturbation extends across a threshold controlling competition between trees and grasses.

In the inland domain, the model simulates a stable grassland equilibrium in both the control simulation and an afforestation experiment. While vegetation conditions in the inland domain strongly affected the energy balance, primarily through changes in surface albedo, they had little effect on precipitation and moisture availability.

Thesis Supervisor: Elfatih A.B. Eltahir
Title: Associate Professor

Acknowledgments

This research was funded in part by NASA Agreement NAGW-5201. In addition, I was fortunate to be supported by an NSF Graduate Research Fellowship, an NSF Traineeship in the Hydrological Sciences, a Ralph M. Parsons Fellowship and a Global Climate Modelling Initiative Fellowship. I am grateful to all the organizations which provided financial support for this research.

Some components of the model developed in this study were provided courtesy of Nilton Renno, now at the University of Arizona, and Jonathan Foley and his group at the University of Wisconsin, Madison. Their advice and patience while I was familiarizing myself with their models is much appreciated. Dave Pollard at NCAR was also helpful during this process.

My research advisor, Elfatih Eltahir, continually challenged me to incorporate new ideas into my work and to strive to be as comprehensive as possible during all phases of the research. My thanks also to the members of my research group, whose friendship, support, and sharing of knowledge were invaluable to the completion of this thesis. Special thanks to Guiling Wang, for many hours of discussion on modeling techniques and simulation results, to Kirsten Findell, for her unflagging support, and to Jeremy Pal, for help during various stages of this work.

My experience at MIT would have been far less enjoyable without the close friendships which I've developed over the past few years. Thanks to all of you for making the East Coast a fun place to live and work, especially Sue and Erica, for helping me to forge a home in the big city, Karen P., for helping to bridge the past and the present, and Jon, for new adventures. Thanks also to my friends and family back home in California and scattered around the world, whose silent cheering have kept my spirits up throughout this process. I am indebted to all of you.

Contents

List of Figures

List of Tables

Chapter 1

Introduction

Since prehistoric times, humans have been altering the earth's environment to make it more hospitable for daily life, to obtain necessary food and shelter, and more recently, to extract economic gain from its vast resources. Over the past few centuries, and particularly within the previous few decades, rapid population growth and technological advances have encouraged swifter and more dramatic changes to natural conditions. These human-wrought changes to the earth have become the subject of great controversy, and to some, cause for great alarm. In particular, numerous studies have suggested that rapid deforestation in the tropics may be significantly impacting both regional and global climate. In the face of this concern, a thorough understanding of the interplay between land surface conditions and climate is warranted, as it can allow us to better manage the earth's resources for future as well as current generations.

The earth's vegetation contributes significantly to the global carbon cycle, acting as a storage reservoir which allows active exchange of carbon with the atmosphere. Vegetation thus has a significant influence on atmospheric carbon dioxide concentrations worldwide. Carbon dioxide is an important greenhouse gas, and changes in vegetation cover affecting carbon dioxide concentrations can influence climate worldwide. While vegetation's role in the carbon cycle has received widespread media coverage, vegetation also affects local or regional climate by impacting the water and energy exchange between the land surface and the

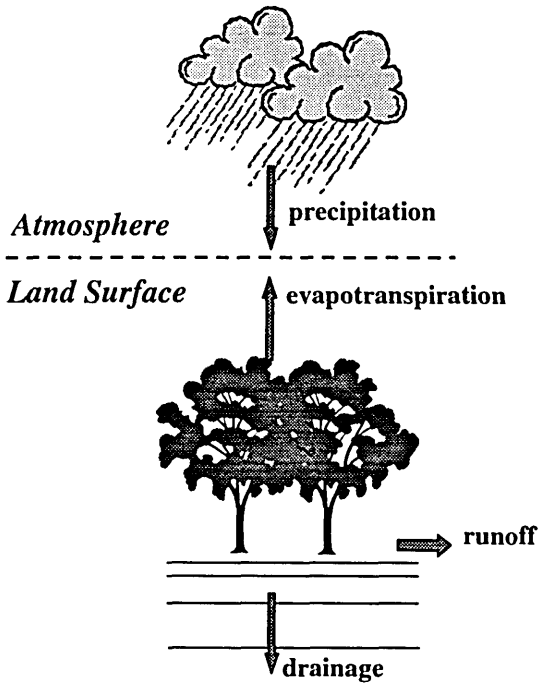

Figure 1-1: Components of the surface water balance.

atmosphere. In fact, these fluxes may have a greater influence on climate than changes in atmospheric carbon dioxide concentrations, especially at a local or regional scale. The effects of vegetation on the fluxes of water and energy between the biosphere and the atmosphere are the focus of this study. Figure 1-1 and Figure 1-2 depict the fluxes comprising the water balance and the energy balance at the biosphere - atmosphere interface. Vegetation affects the strength of these fluxes and the partitioning between them and in this way influences atmospheric and climatic conditions. In turn, local climate affects the types of vegetation which exist in a particular location as different plants have different tolerances for heat, moisture, and light availability, and different strategies for competition when these resources are scarce. This two-way interaction between vegetation and climate determines the equilibrium state of vegetation and climate for a given region.

Speculations on the importance of interactions between the land surface and the atmosphere began centuries ago. It is said that Christopher Columbus noted a decrease in rainfall in the West Indies following deforestation, and attributed

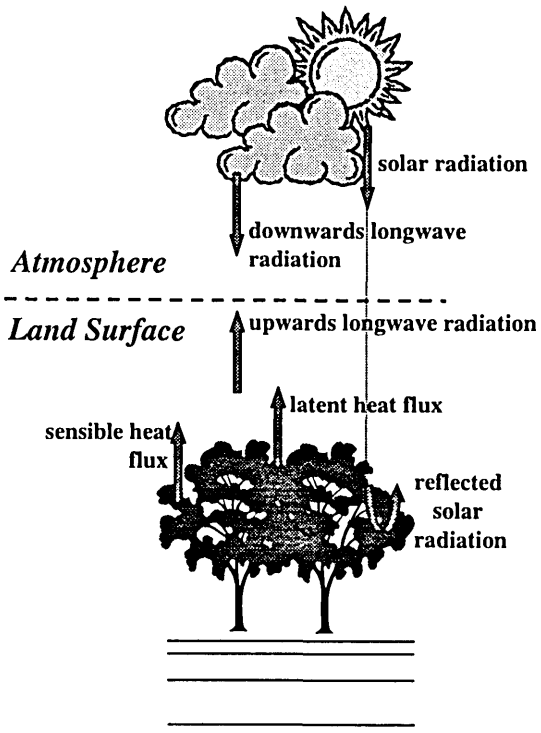

Figure 1-2: Components of the surface energy balance.

the originally high rainfall to the existence of forests on the islands (Meher-Homji 1988). More recently, scientific research has led to improved understanding of the role of vegetation in determining atmospheric conditions. Significant research activity has been undertaken to predict the response of global and regional climate to deforestation. These studies have shown that the control plants exert over moisture and heat fluxes between the land surface and the atmosphere can have significant impacts on atmospheric conditions. Numerous modeling studies of Amazonian deforestation, for example, have consistently shown that large scale deforestation results in a warmer and drier climate in the deforested tropical region (e.g., Lean and Warrilow, 1989; Shukla et al, 1990; Eltahir and Bras, 1994; Sud et al, 1996). However, all of these studies have considered only a one way interaction between vegetation and the climate system. Each of these studies treats vegetation as a static property of the land surface, examining the differences between climate simulated when either grassland or forest dominates the land surface. However, grasslands cannot evolve

into forests, or vice-versa, despite climatic conditions which may favor one dominant vegetation type or the other.

In this study, we address this problem by developing a one-dimensional climate model which allows two way interaction between the biosphere's vegetation and the overlying atmosphere. Plant life responds to changes in climatic conditions, which are in turn influenced by vegetation conditions at the land surface. These changes in climatic conditions can then further influence vegetation at the land surface, and so on in a potential feedback loop. Whether or not inclusion of these two-way feedbacks is important in determining the final equilibrium between vegetation and climate is the subject of this study. If the two-way interaction is indeed important, different initial conditions may result in different equilibrium states. Our model is used to explore the response of the system to perturbations to vegetation at the land surface (e.g., deforestation). Our experiments investigate the possibility of multiple equilibria between vegetation and climate when perturbations to the system are made. Rather than being a predictive tool, our model is intended to elucidate the processes and the constraints which may encourage or inhibit the development of multiple equilibria.

A one-dimensional model was selected for its simplicity and for its ability to isolate local effects from the effects of large scale circulations. The one-dimensional column does, however, have limited interaction with its surroundings. An empirical model, based upon theories of monsoon circulations, is developed to describe the exchange of heat and moisture between the single column and surrounding regions.

The model describes the atmosphere as a one-dimensional column of air whose state is determined by the interplay between radiative forcing, convection, boundary conditions at the land surface, and heat and moisture transport arising from the simulated monsoon circulation. It is suitable for use in tropical areas where the climatic regime is dominated by convection rather than baroclinic frontal systems. Such a condition is characteristic of the tropics, and to some extent, summer in the mid-latitudes. In this study, we confine our work to the tropics, and in particular, West Africa, where the zonal symmetry and clear circulation patterns facilitated development of our empirical model for heat and moisture exchange with

the surroundings.

Following this introduction, Chapter 2 provides background on the modes of interaction between the biosphere and the atmosphere and briefly reviews previous studies on the subject. Chapter 3 outlines some of the important climatological and vegetal characteristics of the tropics, with particular attention to West Africa. Chapter 4 describes our biosphere-atmosphere model, including each of the model's subcomponents. Chapter 5 and Chapter 6 describe the setup of the experimental runs and detail the results of the experiments conducted in two domains, one along the coast of West Africa, and one further inland. Finally, Chapter 7 summarizes the conclusions from this study and suggests areas for further research.

Chapter 2

Biosphere - Atmosphere Interactions

This chapter provides a discussion of theories of biosphere-atmosphere interaction as well as an overview of previous modeling work dealing with biosphere-atmosphere interactions. The effects of atmospheric conditions on vegetation at the land surface are described, along with the role vegetation plays in affecting the atmosphere and climate. This two-way interaction creates the possibility of complicated feedbacks between the biosphere and the atmosphere. The chapter concludes with a discussion of these feedbacks and the potential impacts of land surface changes on monsoon circulations.

2.1 Climatic controls on vegetation

2.1.1 Theory

Global maps of vegetation and climate show a marked correlation between vegetation type and climate. Similar vegetation is found in areas which experience similar climatic regimes. This is not surprising, as plant growth and survival are dependent upon many factors which are related to climate. These factors include (Crawley 1986a, Raven and Johnson 1989, Walter 1985):

- Temperature maxima, minima and averages (daily and annual)
- Temperature ranges (daily and annual)
- Water availability and atmospheric humidity
- Light intensity
- Length of day
- Length of growing season

* Soil type and depth
* Availability of nutrients
* Mechanical factors (e.g., the frequency of fire and wind damage and the amount of grazing by animals)

Climate has a direct effect on the first six of these factors, and indirectly affects the remaining three. Combinations of these factors produce environments in which some plants and not others are able to survive.

While a particular plant may be able to survive in a wide range of climatic conditions, the ability of a plant to thrive in a particular climate is influenced not only by its absolute tolerances to various climatic variables, but also by its ability to compete successfully against other plants vying for the same resources. Laboratory experiments have shown that a plant's "physiological optimum", the conditions under which it is able to maximize growth when there is no competition from other plants, is rarely the same as a plant's "ecological optimum", the conditions under which it is able to maximize growth in the face of competition from other plants (Crawley 1986a). In nature, plants are found where local conditions match their ecological optimum. Typically, a plant is capable of existing in a far greater range of environments than it is actually found to exist in nature, and is limited to the smaller observed range by competition from other plant types.

Some important considerations in assessing the competitiveness of a plant species are its:

- Ability to access resources (light, water, nutrients, soil/space)
- Need for these resources
- Growth and mortality rates
- Differences in seedling needs and established plant needs

The competitiveness of different tropical plant types in various environments are discussed further in Chapter 3.

2.1.2 Previous modeling studies

Existing models which simulate the response of vegetation to climate have ranged from simple models which predict global vegetation patterns, to models including detailed descriptions of individual plants. Two categories of these models are described briefly below.

Equilibrium vegetation models. These types of models predict the equilibrium vegetation for a region given the local climatology. They are typically used at large scales. For example, this type of model is suitable for predicting vegetation cover using the climate produced by a GCM. Because of the large scale at which these models are applied, individual plants and plant species are not modeled. Rather, groupings of plants which share similar climate tolerances, growth and mortality patterns, and physical attributes are lumped together in what are often referred to as plant functional types (Smith et al. 1993). Examples of common plant functional types for the tropics are tropical evergreen trees, tropical raingreen (drought deciduous) trees, C3 grasses and C4 grasses (Foley et al. 1996).

The simplest equilibrium vegetation models are based on correlations between observed global patterns of vegetation and climate. These models often describe vegetation as ecosystems such as tropical forest or tropical savanna, foregoing the use of plant functional types in favor of an even more general description (Prentice et al. 1993).

Other equilibrium vegetation models are more mechanistic. For example, the BIOME model (Prentice et al. 1992) determines equilibrium vegetation by first determining what plant functional types can be expected to be able to survive in a particular climatic regime. This is accomplished by defining physiological limits, or tolerances, of quantities such as maximum and minimum temperature and moisture availability for each plant functional type. After determining which plant functional types could reasonably be expected to survive in a location, competition between the plant functional types is treated indirectly by use of a dominance hierarchy. Certain plant functional types will be excluded from a location by the presence of other plant functional types which are known to compete more successfully for necessary resources (Claussen 1997).

While equilibrium vegetation models have been used to model observed global vegetation patterns, they are designed to predict equilibrium vegetation and are thus unable to model the transient behavior of vegetation (Prentice et al. 1993). However, in considering interactions between vegetation and climate, the transient behavior may be quite important, especially if climatic change outpaces the response time of vegetation. Interactions between vegetation and the climate may preclude transitions from one state to another, thereby influencing the equilibrium state of the system.

Forest stand models/gap models. This class of models provides representation of individual trees and has been used to model the successional behavior of small forest patches. The height, diameter, and other characteristics of individual trees can be predicted. However, these models are suited for scales on the order of 1000 m^2 (Prentice et al. 1993), much smaller than is practical for climate modeling. While useful in forestry, the detailed description of individual trees is not suited for large scales, where the overall canopy structure is a more suitable descriptor of the vegetation.

For integration with climate modeling, there is clearly a need for models which are intermediate in complexity between the two classes of models described above. The Integrated Biosphere Simulator (IBIS) (Foley et al, 1996) is one of a new generation of

models which explicitly represents competition between plants in response to weather conditions experienced during a particular year, but at a scale which is appropriate for use in modeling regional climate. The level of detail in the description of vegetation is similar to that of Surface-Vegetation-Atmosphere Transfer (SVAT) schemes such as the Biosphere-Atmosphere Transfer Scheme (BATS) (Dickinson et al. 1986) and the Simple Biosphere Model (SiB) (Sellers et al. 1986). Like SVAT's, IBIS is designed to provide an atmospheric model with surface energy and moisture fluxes. IBIS is used as the land surface component of our one-dimensional climate model, and is described more fully in Chapter 4.

2.2 Land surface / vegetation controls on climate

2.2.1 Theory

Linkages between the land surface and the atmosphere are evident when one considers both the water and the energy balance at the land surface. Vegetation affects the exchange of both heat and moisture between the land surface and the atmosphere, and can thus play an important role in determining the state of the atmosphere. When these effects are integrated over many weeks, months, or years, it can be seen that vegetation also affects a region's climate.

Figure 1-1 showed the fluxes affecting the water balance at the land surface. Water received at the land surface as precipitation is either returned to the atmosphere through evaporation, removed from the immediate area by surface runoff, or made inaccessible by drainage into deep soil layers and groundwater aquifers. At equilibrium, changes in accessible soil moisture storage (near the surface and within the root zone) are zero. Vegetation affects the partitioning of precipitation into evaporation, runoff, and drainage.

Before precipitation even reaches the ground, a plant's leaves and stems catch, or intercept, some of this water, where it re-evaporates directly to the atmosphere. This evaporation of water is known as interception loss. A plant's leaf area index (LAI)

measures the number of layers of leaves which overlie a unit area of the ground. While leaf shape and orientation also affect interception loss, in general, the greater the LAI, the greater the magnitude of interception loss.

Precipitation which penetrates below the vegetation canopy is known as throughfall. At the ground surface some of this water infiltrates into the soil, and some may become surface runoff. Plant roots can provide preferential channels for infiltration, and leaf litter or other ground debris attributed to vegetation can slow surface flows, allowing more time for infiltration of water into the soil. The water which infiltrates into the soil slowly drains into deeper soil layers and groundwater aquifers. The uptake of water stored in the soils by roots during plant transpiration is a source of moisture to the atmosphere. A plant's root structure determines its ability to extract water from shallow or deep soil layers.

Generally, the existence of vegetation rather than bare soil results in more infiltration, more interception and transpiration, and less surface runoff for the same quantity of precipitation. The specific characteristics of the vegetation affect the degree to which infiltration, runoff and evapotranspiration are affected.

In addition to affecting the water balance, vegetation also affects the energy balance at the land surface. The important fluxes of energy between land and atmosphere were shown in Figure 1-2. Downwards solar (shortwave) radiation and downwards terrestrial (longwave) radiation supply the land surface with energy. Assuming that the downwards ground heat flux is small and that the system is in equilibrium (zero change in heat storage by the land/vegetation), the absorbed energy is returned to the atmosphere by upwelling longwave radiation and by fluxes of latent heat and sensible heat.

Some of the important characteristics of vegetation affecting energy fluxes are its surface roughness, root structure/rooting depth, leaf area, and albedo. Figure 2-1 summarizes the different characteristics of forest and grassland and the effects of these differences on local climate are discussed below using the example of large scale deforestation.

Albedo differences between different types of vegetation and bare ground affect the

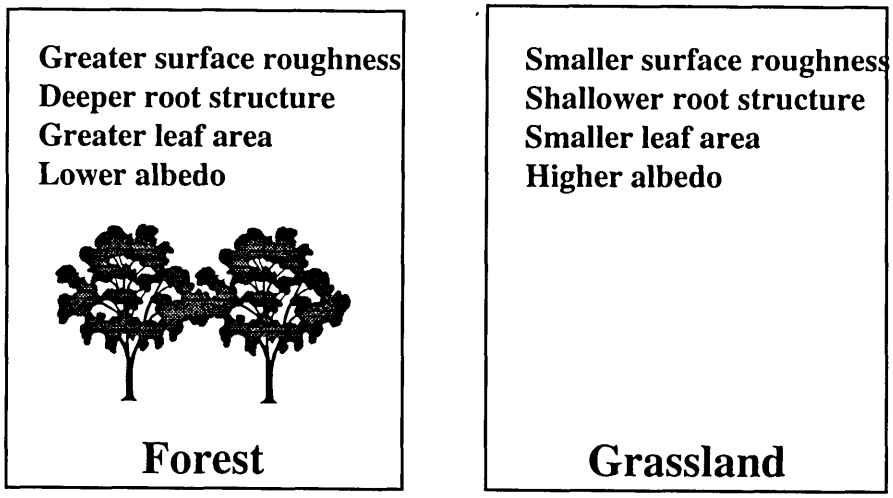

Figure 2-1: Characteristics of vegetation which affect the surface energy balance.

amount of solar radiation which is absorbed at the surface. Forests, which typically have lower albedos than grasslands, absorb more solar radiation. Forest albedos are in the range 12% - 14% while grassland albedos are in the range 16% - 19% (Culf et al. 1995, Bastable et al. 1993). Following deforestation, then, the land surface absorbs significantly less solar radiation.

The cooling effect of the reduction in net solar radiation is counteracted by a decrease in evaporative cooling following deforestation. Vegetation strongly affects the partitioning of energy between latent and sensible heat fluxes. Because of their greater leaf area index, more interception loss takes place from forests than from grasslands. In addition to greater leaf area, trees also have deeper root structures and are able to access deeper soil moisture or groundwater. Thus, transpiration from forest can also exceed that from grassland. Also, because of the greater overall height and variability in height of vegetation in a forest versus grassland, the surface roughness is greater over forests than over grasslands. For all these reasons, total evapotranspiration is usually greater from a forest than from a grassland, and over forest the heat exchange between the land surface and the atmosphere is more strongly dominated by latent heat fluxes than by sensible heat fluxes. Following deforestation, reduced latent heat fluxes result in less evaporative cooling. This results in a warming

of the deforested region as compared to the original forest.

The increased temperatures following deforestation results in increased outgoing longwave radiation. In addition, decreased evapotranspiration implies a smaller atmospheric water vapor content which will tend to diminish the greenhouse effect and result in a smaller downwards longwave radiative flux. These two effects combine to produce a smaller net longwave radiative flux following deforestation. This reduction is combined with the reduction in net solar radiation and results in a reduction in the net allwave radiation. As noted by Eltahir (1996), since the net allwave radiation is the sum of the inputs of energy into the surface, the net allwave radiation must be balanced by fluxes of sensible and latent heat which expel energy into the atmosphere. As already noted, deforestation induces a reduction in latent heat fluxes. Higher temperatures following deforestation imply an increase in the sensible heat flux and the depth of the boundary layer. Thus, a smaller amount of energy is spread over a larger depth of the boundary layer following deforestation and we can expect that over grassland the moist static energy, or boundary layer entropy is smaller than over forest. This reduces the likelihood of local convective precipitation.

The change in evapotranspiration also affects the movement of moisture from the land surface to the atmosphere, which has important implications for atmospheric dynamics. Decreased atmospheric moisture and diminished convective activity suggest that cloudiness will also decrease following deforestation. Decreased cloudiness would increase the downwards shortwave radiative flux at the surface but decrease the downwards longwave radiative flux at the surface. Numerical modeling studies of large scale Amazonian deforestation (e.g., Dickinson and Kennedy (1991) and Lean and Rowntree (1993)) support this view. The actual consequence of deforestation on cloudiness, however, is likely to depend upon the scale of the deforested region. Observational studies have indicated that reduced vegetative cover at smaller scales may actually increase shallow cumulus cloud cover. For example, Cutrim et al. (1995) presented data showing an increase in dry-season afternoon fair-weather cumulus clouds over deforested regions in Amazonia. Rabin and Martin (1996) and Rabin et al. (1990) showed greater shallow cumulus cloud cover over

lightly vegetated versus heavily vegetated landscapes during a drought year in the midwestern United States. It should be noted that the increase in cloud cover in both these studies were observed during dry periods. Again, the scale of the vegetation change is an important consideration, and at the large scales considered in this study, deforestation is expected to result in diminished cloud cover.

In summary then, deforestation results in increased surface albedo and reduced absorbed solar radiation (cooling trend), decreased net longwave radiation (cooling trend), and decreased evapotranspiration (heating trend). The effects of deforestation on cloudiness depend upon the scale of deforestation. The balance of these competing effects have been studied in numerous modeling studies of large scale Amazonian deforestation. These studies generally agree that the net effect of deforestation is a warming of the near surface climate and a decrease in precipitation (e.g., Lean and Warrilow, 1989; Shukla and Sellers, 1990; Dickinson and Kennedy, 1992; Henderson-Sellers et al, 1993; Eltahir and Bras, 1994; and Lean and Rowntree, 1997). The reduction in precipitation can be attributed to a reduction in atmospheric moisture convergence and a reduction in evaporation leading to reduced precipitation recycling. Different studies have shown varying contributions of these two mechanisms to reduced precipitation. This is discussed further in Section 2.2.3.

At long time scales, vegetation has other indirect effects on climate. For example, because vegetation serves as a large carbon storage reservoir, changes in vegetation affect the global carbon balance. If less carbon is stored in vegetation and storage in other reservoirs such as the ocean do not change, decreased vegetation implies that carbon dioxide concentrations in the atmosphere will increase. As carbon dioxide is an important greenhouse gas, changes in atmospheric carbon dioxide concentrations can have important implications for global climate.

Vegetation and climate also both affect nutrient cycling in the soils. Vegetation is dependent on the availability of nutrients in the soil. Nutrient availability is in turn influenced by rates of decay and rates of microbial activity which may change with climatic factors such as temperature and humidity. Hence, interactions between vegetation, climate and nutrient cycling may be important.

Vegetation and climate both also affect soil erosion. Dense vegetation stabilizes the soil matrix, helping to prevent excessive erosion. Characteristics of climate such as the intensity and duration of rainfall events also affect erosion. For example, the high intensity rain events in tropical areas could result in severe erosion if protective vegetation cover is removed. Soil erosion can inhibit the reestablishment of vegetation, and so the interaction between vegetation, climate, and soil erosion may also play an important role in the biosphere-atmosphere system.

While these indirect effects may be quite important in determining the interaction between vegetation and climate, they are beyond the scope of this study.

2.2.2 Observational studies

Observational studies have been conducted at paired forest and grassland sites in the Amazon forest as part of the Amazon Region Micrometeorological Experiment (ARME) and the Anglo-Brazilian Amazonian Climate Observation Study (ABRACOS). A brief overview of some of the results of these studies in the context of forest climate versus grassland climate is given here. These observations showed that net allwave radiation (including both net longwave radiation and net shortwave radiation) was smaller at the cleared sites, in accordance with the theory described above. On average, the net allwave radiation was about 11% less at pasture sites than at forest sites. However, there was no appreciable difference in mean annual temperature and humidity between the forest and pasture sites (Culf et al. 1996). Wright et al. (1992) observed a substantial decrease in evaporation (approximately 45% reduction) during the transition from the wet season to the dry season at a ranchland site in central Amazonia. Based on these observations, they postulated that the dry season evaporation at cleared sites is likely to differ significantly from dry season evaporation over undisturbed forest. Indeed, Shuttleworth (1988)'s observations of evaporation at a nearby forest site exhibited much less seasonality.

While the observed climatological differences over forest and grassland do not match all of the expectations based on theory and modeling studies, this may be due to differences in scale. Only one of the paired forest grassland study sites in ARME

Table 2.1: Results from Modeling Studies of Amazonian Deforestation

Study	ΔT [K]	ΔP [mm/day]	ΔE [mm/day]	ΔRn [W/m2]
Lean and Warrilow (1989)	+2.0	-1.3	-0.6	n/a
Shukla et al. (1990)	+2.5	-1.8	-1.4	-26
Dickinson and Kennedy (1992)	+0.6	-1.4	-0.1	n/a
Henderson-Sellers et al. (1993)	+0.6	-1.6	-0.6	n/a
Eltahir and Bras (1994)	+0.7	-0.4	-0.6	-13
Lean and Rowntree (1997)	+2.3	-0.3	-0.8	n/a

and ABRACOS included both an extensive forest location and an extensive grassland location. At the two other paired locations, one vegetation type was dominant in the area. In such a scenario, development of separate boundary layers over forest and grassland may not have taken place and there may have been significant horizontal mixing of air over the contrasting vegetation types.

2.2.3 Previous modeling studies

As noted in Section 2.2.1, deforestation in the Amazon River basin has been the subject of numerous modeling studies. Using regional climate models or global atmospheric general circulation models (AGCM's), researchers have consistently demonstrated that deforestation of the Amazon is likely to have significant impacts on the regional climate. Most studies agree that large scale deforestation results in less precipitation, less evaporation, and higher surface temperatures (e.g., Lean and Warrilow, 1989; Shukla, Nobre and Sellers, 1990; Dickinson and Kennedy, 1992; Henderson-Sellers et al, 1993; Eltahir and Bras, 1994; and Lean and Rowntree, 1997), as predicted by the theory discussed in the previous section. Table 2.1 summarizes the key results of some of these studies.

However, there is some question as to whether deforestation will increase or decrease moisture convergence, with differing results from different studies, as pointed out by Lean and Rowntree (1997). The change in moisture convergence can be

deduced from the change in the quantity (precipitation - evaporation). Four of the six studies listed in Table 2.1 show a larger decrease in precipitation than in evaporation, implying a decrease in moisture convergence. In contrast, the other two show greater sensitivity of evaporation than precipitation to deforestation. This implies that increased moisture convergence partly compensates for the reduction in evaporation.

It is unclear why these different studies predicted opposing responses in moisture convergence. The conflicting results may be due to differences in the details of the representation of land surface characteristics and topography as discussed by Lean and Rowntree (1997). Eltahir and Bras (1993b) point out that the change in moisture convergence reflects changes in the large scale circulation of the region. The circulation responds to two different processes - changes in precipitation and changes in surface temperature. The complexity of resolving these conflicting responses may contribute to the differing signs in the predicted change in moisture convergence. As the long term mean annual moisture convergence corresponds to the long term mean annual runoff, the change in moisture convergence is an important quantity which bears further study.

A number of studies have also investigated the effects of vegetation on climate in the West Africa region. Xue et al. (1990) used a 2-D zonally averaged model to test the response of climate in West Africa to removal and expansion of the Sahara Desert during the monsoon season. An expansion of the desert to 10N resulted in changes to the July climate which included an average decrease in precipitation of 13% for their entire model domain. The largest changes were seen in the desertification region. In this region, precipitation decreased by 1.5 mm/day, evaporation decreased by 1.7 mm/day, and cloud cover decreased by 7%. In addition, the surface temperature increased by about 1K. When the desert was removed, i.e., vegetation was enhanced in the Sahara region, precipitation increased by an average of 25% over the whole model domain. Over the Sahara region, the change was more dramatic, with an increase in precipitation upwards of 300%. In this experiment, a dipole pattern in the precipitaton change was seen, and south of the Sahara there was actually a decrease

in rainfall. Surface temperature decreased with the enhanced vegetation.

Xue and Shukla (1993) used a general circulation model to study the effects of desertification on the summertime climate of West Africa. Again, rainfall was reduced in the desertification area during the summer monsoon. In addition, a dipole pattern was also seen, in which the reduction in rainfall in the north was accompanied by an increase in rainfall to the south.

Zheng and Eltahir (1998) used a two-dimensional zonally symmetric model to study the role of vegetation in the the dynamics of the West African monsoon. Their model used a very simple scheme for representation of the land surface, using the Budyko dryness index as an indicator of vegetation type. In a perpetual summer experiment simulating deforestation from 5N - 15N, they found that August rainfall in that region was severely impacted by deforestation. The rainfall maximum at 12N was decreased by about one half and the moisture convergence was only about one-third of the value in the control case, indicating a strong effect of vegetation on the monsoon circulation. The location of the imposed vegetation change was seen to strongly affect the magnitude of the climatic change. A desertification experiment showed a smaller response of the summer monsoon to vegetation change in the region north of 15N.

Other modeling studies have tested the sensitivity of climate to land surface changes in extratropical regions. Bonan (1997) used the NCAR Community Climate Model version 2 (CCM2) coupled to NCAR's Land Surface Model (LSM) to study the climatic impact of the replacement of natural vegetation in the United States with agriculture. Agriculture has generally replaced broadleaf deciduous trees, needleleaf evergreen trees and grasses with crop vegetation, although there are exceptions such as in the case of managed forest. Changes from forest to crop generally result in reduced roughness length and reduced leaf and stem area index. While these effects would tend to reduce evapotranspiration, agricultural crops typically have lower stomatal resistances than other plant types. The net result is often to increase evapotranspiration. Shifts to agriculture have had varying effects on surface albedo, by plant type and time of year. Bonan showed that a shift from forest to agriculture

in the eastern United States may have resulted in a cooler springtime climate, due largely to increased latent heat flux and higher surface albedo. These two effects may also have been responsible for a cooler summer over much of the United States in his agricultural U.S. versus natural U.S. simulations. His model also showed changes in precipitation and near-surface atmospheric moisture as a consequence of land use changes.

2.3 Two-way feedbacks

2.3.1 Theory

Because vegetation both influences and is influenced by climate, there is the potential for feedback loops in the vegetation-climate system. A shift in climate may encourage the growth of a particular type of vegetation. If this vegetation type further enhances the climate shift, the system may enter into a positive feedback loop. Conversely, the change in vegetation may trigger a negative feedback, tending to bring the climate (and eventually vegetation) back to its original state.

Charney (1975)'s classic paper on desertification provides an example of a possible feedback between vegetation and climate. Relative to its surroundings, a desert absorbs less solar radiation because of its high albedo. In addition, high surface temperatures result in a large loss of longwave radiative energy. Consequently, a desert is a radiative sink of energy relative to its surroundings. In order to maintain thermal equilibrium, air must descend, resulting in adiabatic warming, over these desert regions. This subsidence further suppresses precipitation, further discouraging the growth of vegetation, in a positive feedback loop. Charney demonstrated this phenomenon in a simple zonal model of the atmosphere.

Over rainforest, the opposite effect encourages precipitation and vegetation growth. Relative to its surroundings, the rainforest is a source of energy, owing to its low albedo and low surface temperature. This creates conditions favoring convection and precipitation, and the availability of water encourages vegetation growth.

These concepts are expanded upon by Eltahir (1996), who considers the effects of vegetation on large scale circulations in the context of a moist atmosphere which is affected not only by radiative changes but also by changes in latent and sensible heat fluxes. Eltahir argues that large scale deforestation results in a reduction in net surface radiation (both shortwave and longwave), necessitating a corresponding decrease in the sum of latent and sensible heat flux in order to maintain the energy balance. This reduces the boundary layer entropy over the deforested region, reducing moist convection. With the reduction in moist convection there is a reduction in the latent heat release in the upper layers of the atmosphere. This results in a cooling of the upper atmosphere relative to its surroundings which causes subsidence over the deforested region. This subsidence weakens the large scale circulation. Because the circulation itself is responsible for creating conditions which favor forest growth, this mechanism again suggests that there may be an important positive feedback between vegetation and climate.

2.3.2 Previous modeling studies

Among the earliest studies of two-way vegetation-climate feedbacks, was research by Gutman et al. (1984). In this work, they defined a dryness index (based upon the ratio of annual net radiation to annual precipitation), which was used to infer the vegetation type at the land surface. Vegetation types were differentiated based on albedo and an index of water availability. Applying these descriptions of vegetation to a zonal model of the land-atmosphere system, they found that changes in the solar constant and atmospheric CO2 levels produced negligible vegetation-climate feedbacks, but cautioned that the simplicity of their model warranted further studies with more realistic models of the globe.

Gutman (1984) expanded this work by testing the sensitivity of the model to perturbations to the initial vegetation cover. He perturbed land surface conditions in different latitude belts to simulate deforestation, desertification and irrigation of the tropical, semi-arid, and desert zones, respectively. In all cases, perturbations to the land surface were reflected in an altered climate, but not to the extent that the

initial perturbations persisted. Gutman found that the impact of the biofeedback was strongest in the area adjacent to the perturbation zone, rather than within the perturbation zone itself.

Claussen (1994) coupled the equilibrium vegetation model, BIOME (discussed in Section 2.1.2), to ECHAM, the global climate model of the Max-Planck Institute for Meteorology. The two models were asynchronously coupled, i.e., monthly mean output from several years of simulation using ECHAM was used as input to BIOME and the resulting equilibrium vegetation distribution predicted by BIOME was used to define surface boundary conditions for a subsequent ECHAM run. This process was repeated until the two models were in equilibrium. Claussen (1997) used an updated version of this model to test the sensitivity of equilibrium vegetation and climate to perturbations to the initial vegetation state. In this study, he focused particularly on the African and Indian monsoon regions by replacing desert vegetation in these regions with rain forest vegetation and vice versa. He found that at equilibrium the forests had reasserted themselves on both continents at locations which had supported forests in the unperturbed simulation. In addition, while there was some enhanced precipitation in arid areas of the Indian subcontinent, the equilibrium vegetation also reverted to its unperturbed state there. However, there was a northward shift in savanna and xerophytic shrub along the desert fringes of the southwest Sahara. In this case, enhanced vegetation seems to have been able to perpetuate itself through feedbacks with the climate system which kept the climate in northern Africa moister than in the unperturbed simulation.

Following a similar asynchronous coupling approach, Texier et al. (1997) coupled the LMD AGCM to BIOME. Incorporation of vegetation feedbacks in simulations of the global climate 6000 B.P. was seen to enhance orbitally induced high-latitude summer warming and to strengthen the West African summer monsoon. The global coverage of tundra and the extent of the Sahara desert were both diminished in their new global equilibrium state.

Foley et al. (1994) also simulated conditions 6000 B.P. with changes in orbital parameters. Using the GENESIS GCM, their simulations produced a 2 K warming in

summer, autumn and winter at high latitudes as compared to simulations of current conditions. This warming is expected to have allowed the northward expansion of boreal forest into what would otherwise be tundra. In Foley et. al.'s simulations, making this vegetation change induced a further warming of approximately 4K in the spring and 1K in other seasons, largely due to the decreased albedo of boreal forest as compared to tundra. This decreased albedo is a consequence of the evergreen forest protruding above the highly reflective snow cover. Bonan et al. (1992) and Bonan et al. (1995) showed similar warming due to an expansion of boreal forest. Levis et al. (1997), using a coupled vegetation and climate model (IBIS-GENESIS), showed that an initially prescribed expansion of boreal forest into tundra regions could be self-sustaining due to the warmer climate induced by forest cover.

Gutman (1984)'s and Gutman et al. (1984)'s studies are limited by the simplicity of both the description of the vegetation and the determination of what vegetation is expected to dominate in a particular latitude belt. Claussen's (1994, 1997), Texier's (1997) and Foley's (1994) work, while incorporating more physical realism, remains limited by the asynchronous coupling and the use of an equilibrium vegetation model in simulating the transient behavior of vegetation. Levis et al. (1997) and Foley et al. (1998) addressed many of the limitations of previous work by coupling IBIS to the GENESIS atmospheric general circulation model. IBIS' structure allowed fully synchronous coupling to the GCM and includes a more complete description of plant competition and interaction with the atmosphere. IBIS is also used as the land surface component of our model, and is described in Section 4.3.

2.4 Monsoon circulations and their sensitivity to land surface conditions

2.4.1 Theory of monsoon circulations

Monsoon regions are marked by a strongly seasonal climate, wet in the summer, and dry in the winter. In the summer months, winds are predominantly from the ocean

to the land, and in the winter months, winds favor the land to ocean direction. The summer winds bring with them moist air from the ocean, initiating heavy rainfall during those months.

This circulation pattern is driven by differential heating of the land and the ocean. During the summer, the land surface absorbs more solar radiation and relative to the ocean, the air over the land region becomes more energetic. One measure of the energy of the near-surface atmosphere is the boundary layer entropy, an increasing function of both temperature and humidity. The boundary layer entropy becomes higher over land than over the sea during the summer, and this induces a circulation moving air from the ocean towards the land (Eltahir and Gong 1996). The rotation of the earth deflects the winds so that rather than straight north-south air movement, we see southwesterlies in the northern hemisphere and northwesterlies in the southern hemisphere. Finally, because the winds also transport moisture, the storage and release of latent heat is also an important component of the monsoon circulation.

During the winter months, the circulation is reversed as the continent loses energy more rapidly than the ocean. Not only is the heat capacity of the ocean larger than that of land, but mixing within the ocean mixed layer allows cooled surface water to sink and to be replaced by warmer water from below. Consequently, the energetics of the land-ocean system is reversed and during the winter months the wind direction also reverses, now blowing from the continent to the ocean.

Figure 2-2 illustrates this seasonal reversal of wind patterns for the West African monsoon, based on NCEP reanalysis data. In the summer months (June, July, August), southerly winds at 1000 mb penetrate as far as 15-20 N. In contrast, these winds to not penetrate far inland from the coast during the winter months (December, January, February) and northeasterlies can dominate as far south as 10N.

Vegetation at the land surface plays an important role in the energy balance at the surface, and can therefore impact the monsoon circulation. As discussed in Section 2.2.1 dense vegetation cover typically has a lower albedo than sparse cover, and thus absorbs more solar radiation. In addition, evapotranspiration from vegetated surfaces is generally greater than that from bare soil, because of the ability

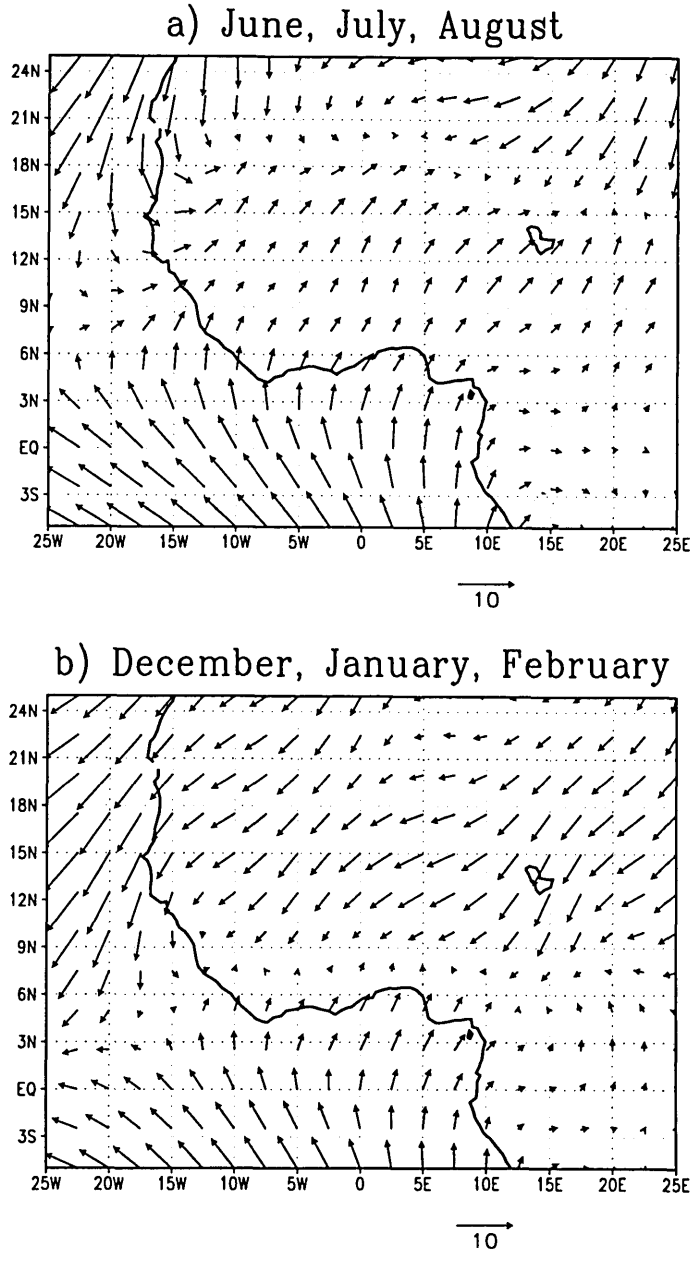

Figure 2-2: (a) Summer (June, July, August) winds over West Africa. (b) Winter (December, January, February) winds over West Africa.

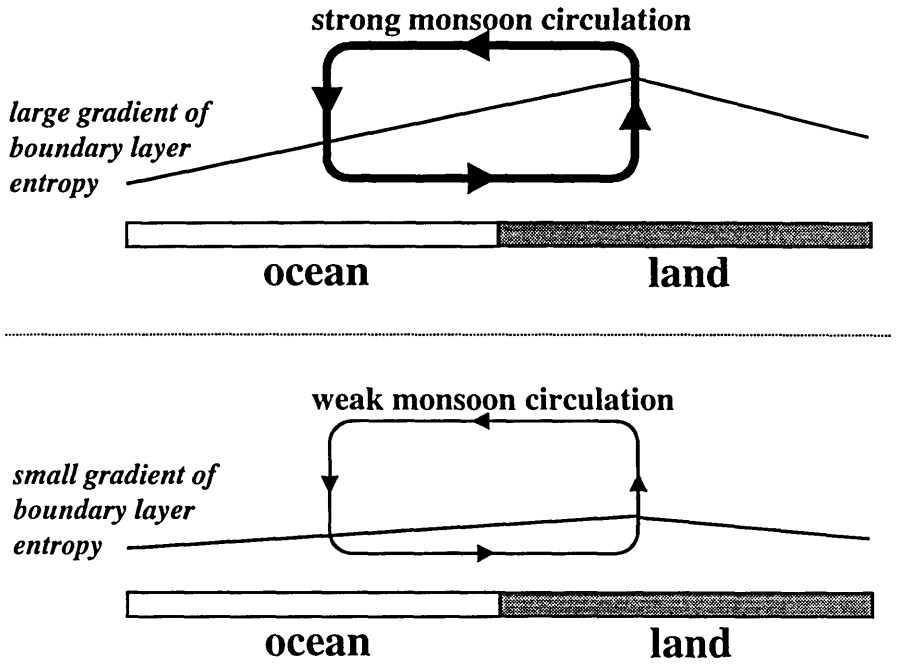

Figure 2-3: A strong gradient in boundary layer entropy is associated with a strong monsoon circulation. Conversely, a weak gradient in boundary layer entropy is associated with a weak monsoon circulation.

of vegetation to access deeper soil water. While there are many other factors to consider, these two mechanisms generally act to increase the available energy at the land surface when there is more vegetation (Eltahir 1996). The energy can be measured in terms of the boundary layer entropy and as discussed by Eltahir (1996), a larger gradient in the boundary layer entropy between land and sea induces a stronger monsoon circulation. This concept is illustrated in Figure 2-3.

Eltahir and Gong (1996), using Geophysical Fluid Dynamics Laboratory (GFDL) data, showed that increased boundary layer entropy is indeed associated with a stronger monsoon circulation in West Africa. Our own data analysis using National Center for Environmental Prediction (NCEP) Reanalysis data confirms this finding. These results are discussed in Chapter 4, in the discussion of the formulation of our empirical monsoon circulation model.

The impact of vegetation on the monsoon is especially important because it constitutes a positive feedback. More vegetation induces a stronger monsoon which

brings with it more precipitation. With additional precipitation, vegetation growth is enhanced, creating a positive feedback on the monsoon circulation. Conversely, inadequate rainfall prevents vegetation growth, which may further diminish the likelihood of a strong monsoon, making the climate increasingly arid. If the feedback between continental vegetation and the strength of the monsoon circulation is significant, changes in vegetation cover may have important impacts on local climate.

2.4.2 Modeling studies of monsoon - vegetation interaction

Fossil pollen, lake sediment and archaeological evidence suggests that in the the early Holocene (approximately 12,000 B.P. to 5,000 B.P.), the Sahara/Sahel boundary in northern Africa was about 5 degrees farther north than it is at present. In addition, the evidence suggest that a moister climate supported more and larger lakes between 15N and 30N ((Kutzbach et al. 1996). Kutzbach et al conducted simulations in which the earth's orbital parameters were altered to reflect those during the early Holocene. These simulations showed an enhancement of the African summer monsoon. However, the intensification of the monsoon was not sufficient to match the climate inferred from paleorecords nor to support the vegetation found in fossil pollen records. Kutzbach et al then showed that by changing vegetation and soil characteristics (replacing desert with grassland and desert soil with more loamy soil), the monsoon was further enhanced and vegetation was able to encroach further into the present day Sahara.

As described in Section 2.3.2, Claussen (1997) also showed enhancement of the African summer monsoon in simulations with enhanced vegetation in northern Africa. Zheng and Eltahir (1997) simulated conditions in West Africa using a zonal model. Vegetation at the land surface was represented very simply using the Budyko dryness index. Their simulations showed a diminished monsoon circulation following a degradation in vegetation near the coast, from 5N to 15N. Their model did not, however, show a significant response to a desertification further inland, from 15N to 20N.

Sud and Smith (1985) studied the response of the Indian monsoon to changes in land surface characteristics. They showed that an increased surface albedo and a

reduction in surface roughness both significantly reduced the intensity of the monsoon circulation. Both of these changes in land surface characteristics are consistent with a decrease in vegetation. Sud and Smith also eliminated evapotranspiration in one simulation, but found that the resulting increase in moisture convergence was able to compensate for the elimination of that moisture source, and precipitation was not significantly changed.

Miller et al. (1997) simulated the climate (and monsoon) of the Australian continent for different vegetation types in the continental interior. They showed a 2 mm/day to 3mm/day increase in summertime precipitation for an Australian interior with broadleaf deciduous trees and loamy soil as compared to simulations with the current vegetation and soils.

Chapter 3

Climatology and Ecology of West Africa

West Africa serves as the area of focus for the numerical experiments in this study and this chapter provides an overview of the climatology and ecology of the region. The coast of West Africa lies at approximately 5N, and our study focuses on the 10 degrees of latitude extending from the coast to 15N. This region is marked by strong zonal symmetry in both climate and vegetation. Most of the region lies between sea level and 2000 feet (Espenshade 1990), and the relatively flat topography does not play a major role in the climate of the region as a whole.

As we saw in the previous chapter, climate and vegetation are inextricably connected, and it is difficult to talk about one without mentioning the other. The following sections are labeled individually as the 'Climate of West Africa' and the 'Vegetation of West Africa,' but each uses information about the other to explain the observed distributions of climate and vegetation.

3.1 Climate of West Africa

The Hadley cell is the dominant atmospheric circulation pattern in the tropics. It is a thermally driven circulation which arises due to differential heating of the surface layers of the atmosphere. Higher energy near the equator induces a circulation with

rising motion near the equator and sinking motion at about 30N. The actual location of the rising and sinking branches of the Hadley cell varies throughout the year and from region to region.

The climate of West Africa is also affected by the monsoon circulation, the position of the ITCZ, and variability in solar insolation. The variability of precipitation in West Africa is governed largely by the monsoon circulation. Like the Hadley circulation, the monsoon circulation is thermally driven, but arises due to differential heating between the land and the ocean rather than differential heating due to distance from the equator. The monsoon brings West Africa strong seasonality. The summer is characterized by southerly winds bringing abundant rainfall. In the winter, the winds reverse, and hot and dry harmattan winds from the north inhibit rainfall in much of West Africa. A more complete discussion of monsoon dynamics is given in Chapter 2.

The strength of the monsoon circulation varies with distance from the coast. Along the coast of West Africa, the monsoon winds are predominantly southerly, blowing from the ocean to the land. Throughout most of the year, they bring coastal West Africa a steady supply of moisture from the tropical Atlantic Ocean. Even in the winter, the winds rarely reverse (see Figure 2-2). However, they do decrease in magnitude and precipitation is diminished in the winter months. On occasion, the harmattan winds from the north do penetrate as far as the coast, bringing with them the hot, dusty air from the desert regions to the north (Rumney 1968). Moving away from the coast, the seasonal reversal of winds is more evident, and the moisture-rich southerly winds penetrate into the interior for a shorter duration. For example, at 15N, southerly monsoon winds are only experienced for about four months, June to August. During the remainder of the year, hot and dry northerly winds suppress rainfall. Figure 3-1 shows the decreasing precipitation and the increasing length of the dry season at three stations in West Africa beginning near the coast and moving northwards. Figure 3-1 also shows the decrease in mean annual precipitation away from the coast.

The penetration of the monsoon winds corresponds to the location of the

intertropical convergence zone (ITCZ), a low pressure region which marks the confluence of northerly and southerly winds. It also marks the location of the rising branch of the Hadley cell. During the summer months, the ITCZ moves northward over West Africa, typically reaching its northernmost position at about 20N. In this convergence area, there is mass lifting of air, which increases the likelihood of precipitation. In addition, the entire region is under the influence of the moist monsoon winds from the Atlantic Ocean. The ITCZ shifts southwards again at the end of the summer, but in the West African region typically stays northward of 6N throughout the year (Ayoade 1983).

Along with the decrease in precipitation is a general decrease in moisture availability. The total evapotranspiration and the specific humidity of the atmosphere both decrease away from the coast, as seen in Figure 3-2 and Figure 3-3.

Because of its proximity to the equator, the coastal area receives relatively steady and high solar insolation year round. As a result of the large and steady input of energy, the region is warm and the seasonal cycle in temperature is muted. Moving farther northwards, or inland, one moves farther from the equator, and there is enhanced seasonality in both the solar insolation and the temperature. Figure 3-4 shows the change in seasonality of temperature moving inland, as recorded at three stations progressively moving farther inland from the coast.

Figure 3-4 also shows that the mean annual surface temperature increases moving northward. This is somewhat counterintuitive, as one might expect colder temperatures farther from the equator. The observations can be understood by also considering the trends in net radiation, precipitation and evapotranspiration. Like temperature, solar insolation at the surface increases northwards, as seen in Figure 3-5. At the top of the atmosphere, however, the downwards solar flux decreases northwards, as expected. (See Figure 3-5.) The atmosphere, then, must be acting to moderate the solar flux at the surface. The increase in incoming solar radiation at the surface can be explained by decreased cloudiness and atmospheric vapor content, consistent with decreased precipitation. A reduction in the atmospheric albedo, due mainly to reduced cloud albedo allows more sunlight to penetrate to the land surface.

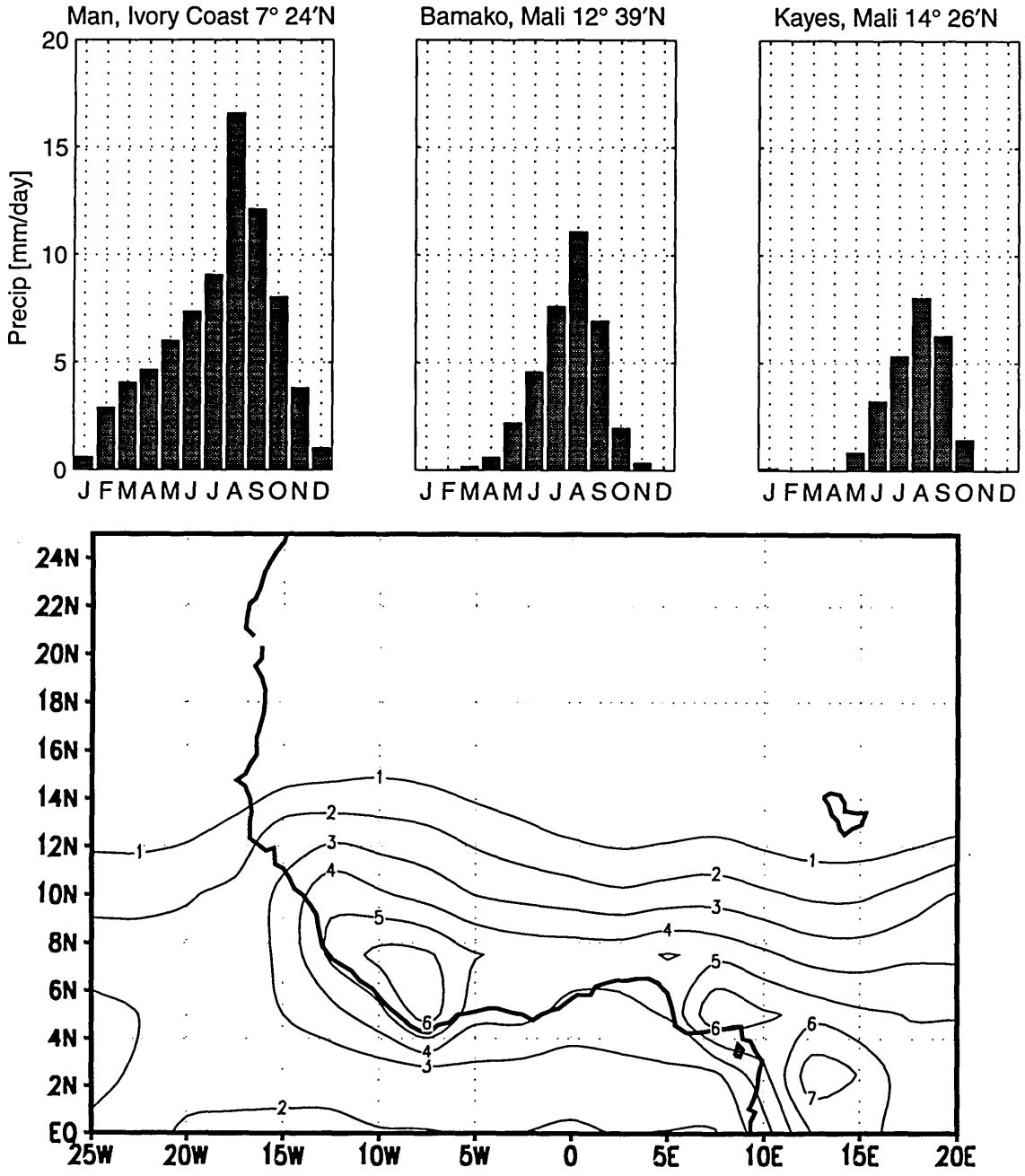

Figure 3-1: The upper panel shows the monthly precipitation [mm/day] at 3 stations in West Africa. (Source: Rumney, 1968) The lower panel shows the mean annual precipitation [mm/day] in West Africa as given by the NCEP reanalysis climatology (1982-1994).

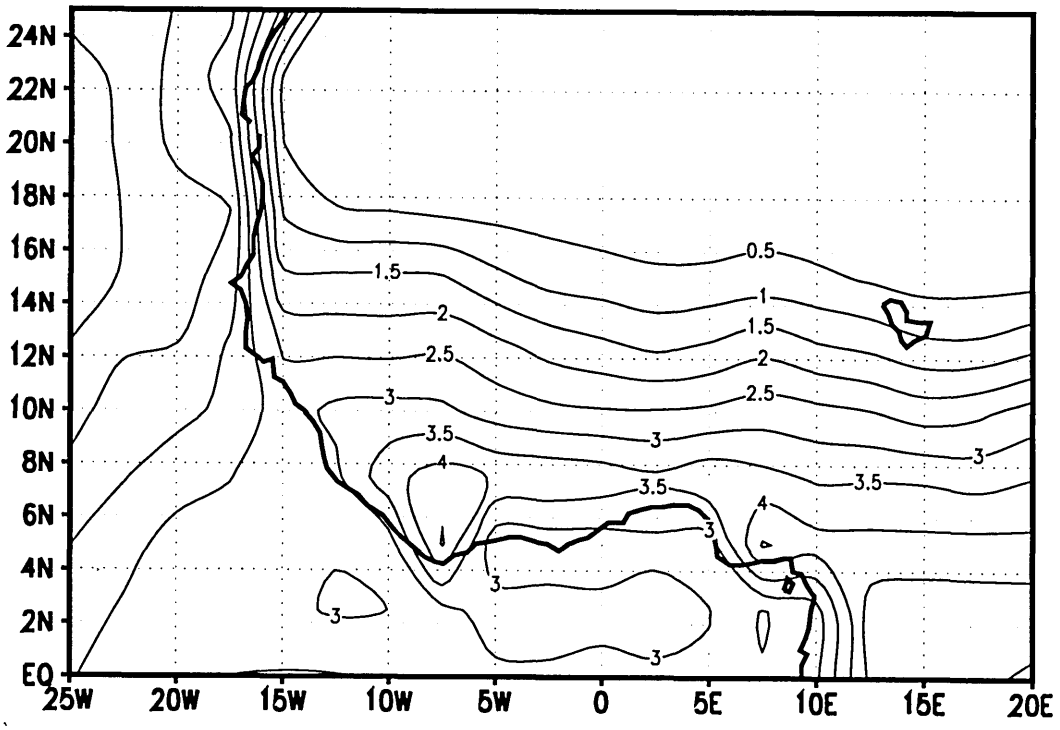

Figure 3-2: Evapotranspiration [mm/day], NCEP reanalysis climatology (1982-1994).

The net solar radiation is also higher inland, as compared to near the coast (see Figure 3-6). Even after factoring in surface albedo differences (forest near the coast has a lower albedo than grassland further inland), the land surface absorbs more solar radiation inland than it does near the coast. Consequently, there is more available solar energy. However, as seen in Figure 3-7, the net longwave radiation is much smaller towards the north, with the result that the net allwave radiation (Figure 3-8) is smaller in northern West Africa than in coastal West Africa. Despite the reduction in radiative energy input, temperatures in northern West Africa are higher than near the coast because of the reduction in evapotranspiration, shown in Figure 3-2. Reduced evapotranspiration implies a decrease in latent cooling of the surface layers of the atmosphere, and increased temperatures near the surface. This highlights the importance of the Bowen ratio, or the partitioning of energy between latent heat and sensible heat.

It is important to note that while the temperature in West Africa increases

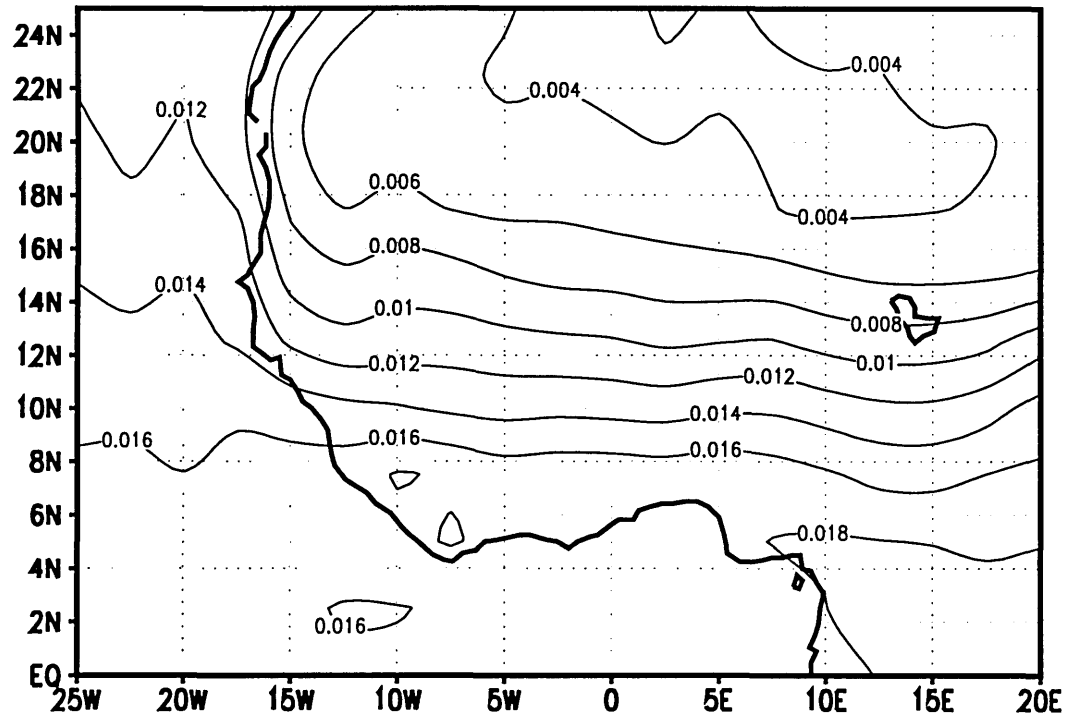

Figure 3-3: Specific humidity [kg/kg], NCEP reanalysis climatology (1982-1994).

northwards, the total moist static energy or boundary layer entropy of the system does not. These quantities are a function not only of temperature, but also of specific humidity. Because of the high latent heat of vaporization of water, water vapor is a large store of energy, which can be released upon condensation. As was seen in Figure 3-3, the specific humidity of the atmosphere is greater near the coast. Figure 3-9 shows that the boundary layer entropy near the coast is higher than the boundary layer entropy further inland, consistent with the observation that the coastal area receives greater total input of radiative energy.

3.2 Vegetation of West Africa

In general, competition between vegetation types in tropical regions depends primarily on the varying abilities of species to capture light and water. The structure of plant communities in the tropics generally depends on competition for only one resource at

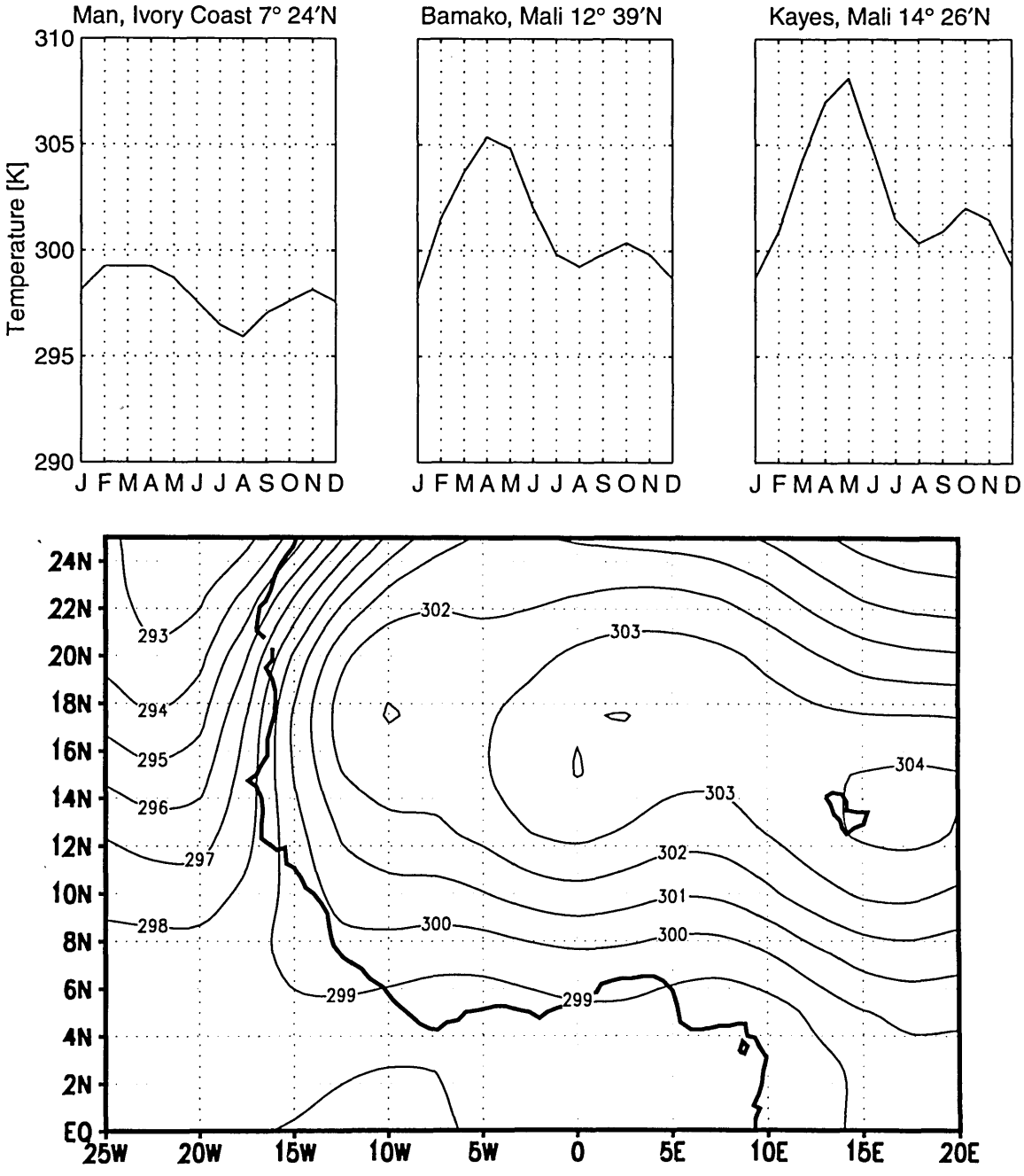

Figure 3-4: The upper panel shows the average monthly temperature [K] at 3 stations in West Africa. (Source: Rumney, 1968) The lower panel shows the mean annual temperature [K] in West Africa as given by the NCEP reanalysis climatology (1982-1994).

(a) Downwards Shortwave Flux at Surface

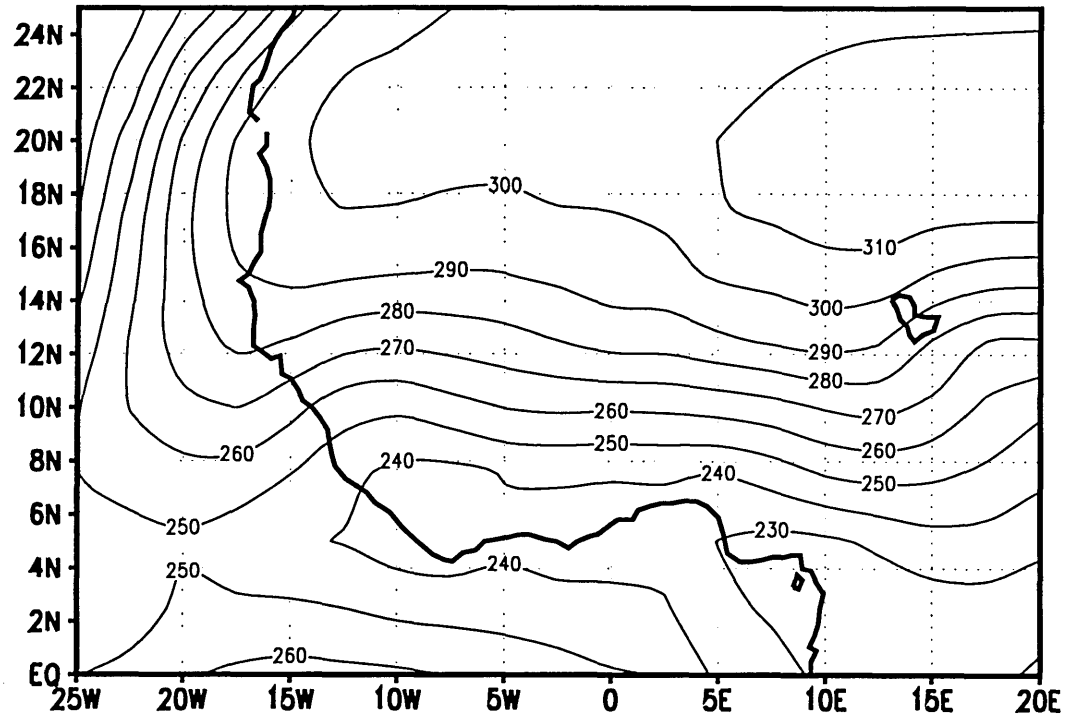

(b) Downwards Shortwave Flux at Top of Atmosphere

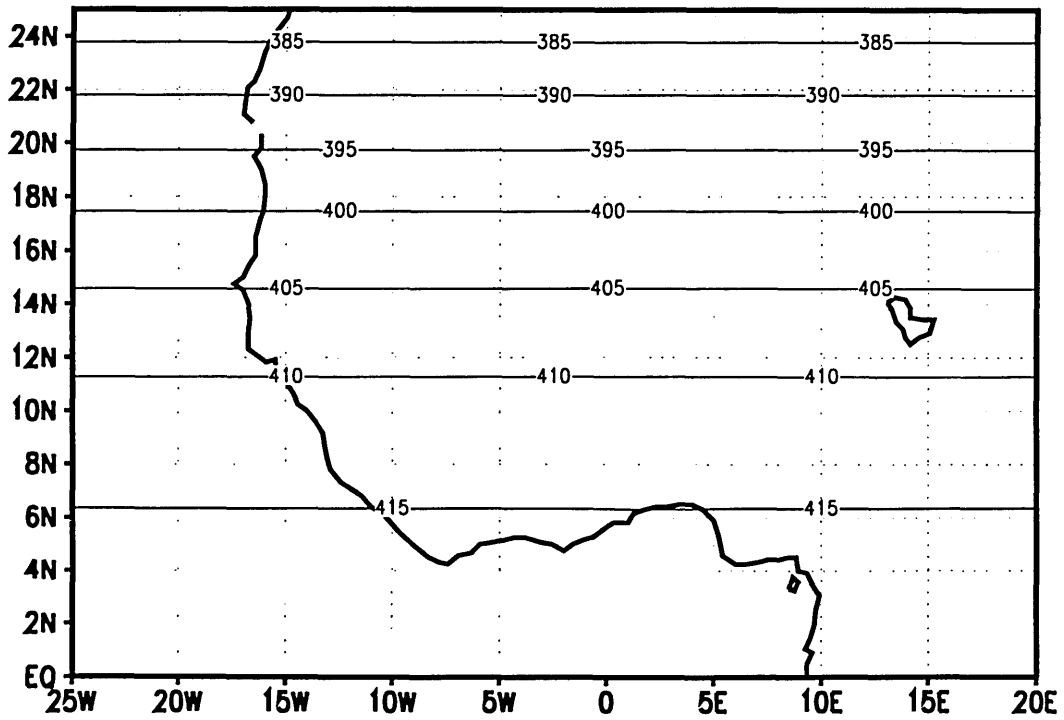

Figure 3-5: Shortwave radiative flux [W/m^2], NCEP reanalysis climatology (1982-1994) at (a) the surface (b) the top of the atmosphere.

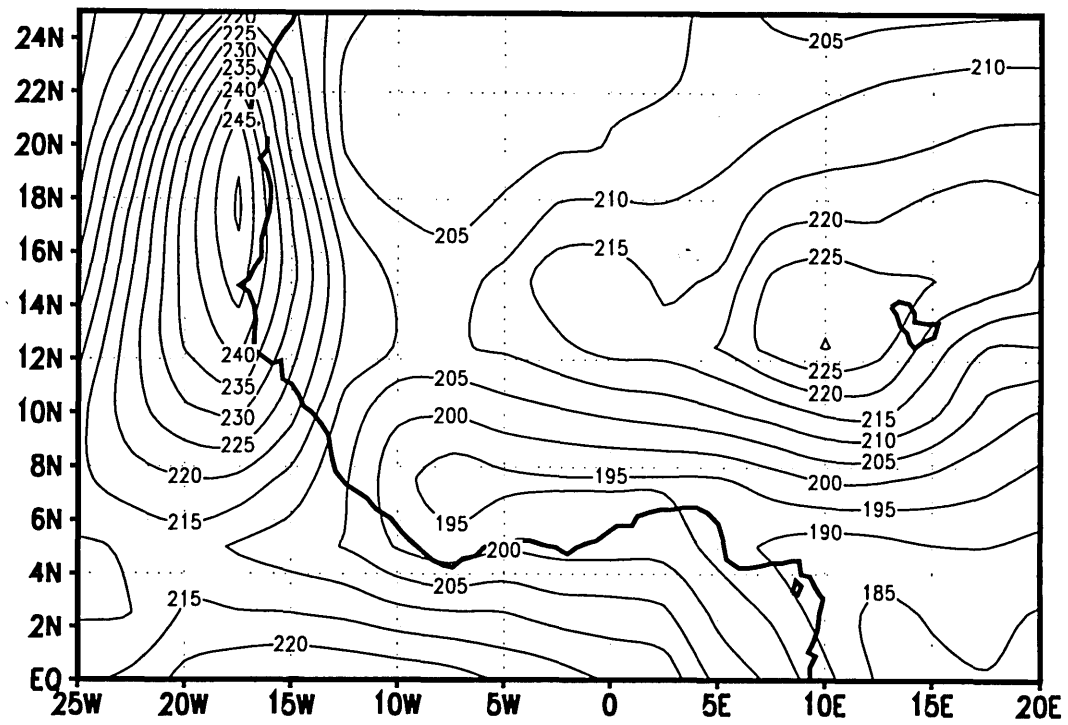

Figure 3-6: Net shortwave radiation [W/m^2], NCEP reanalysis climatology (1982-1994).

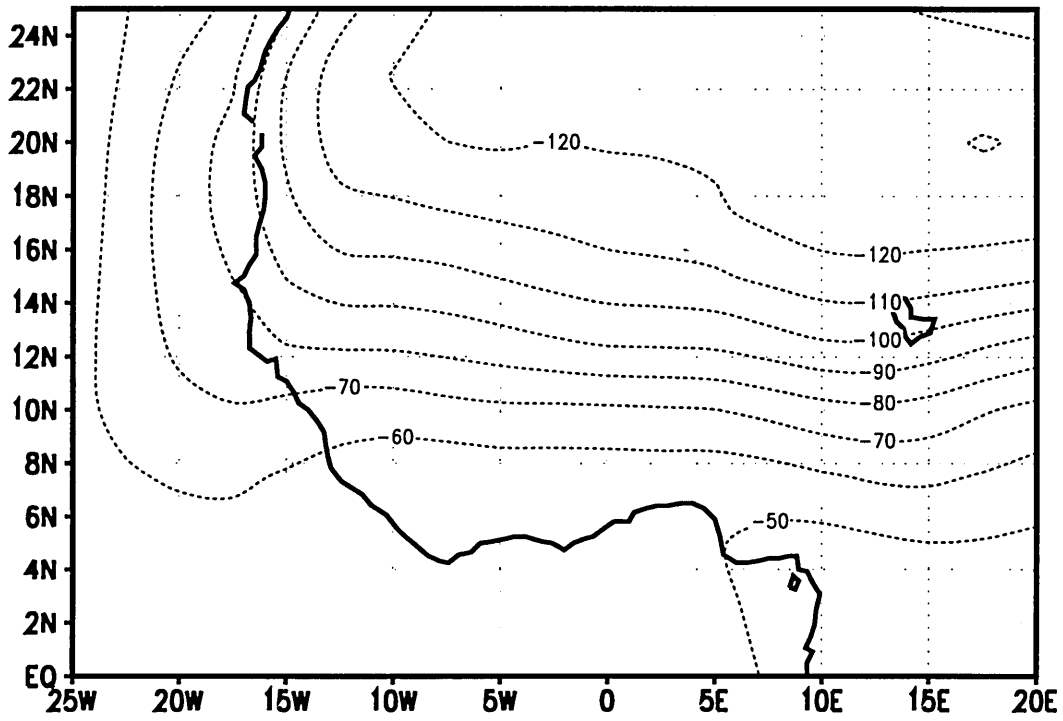

Figure 3-7: Net longwave radiation [W/m^2], NCEP reanalysis climatology (1982-1994).

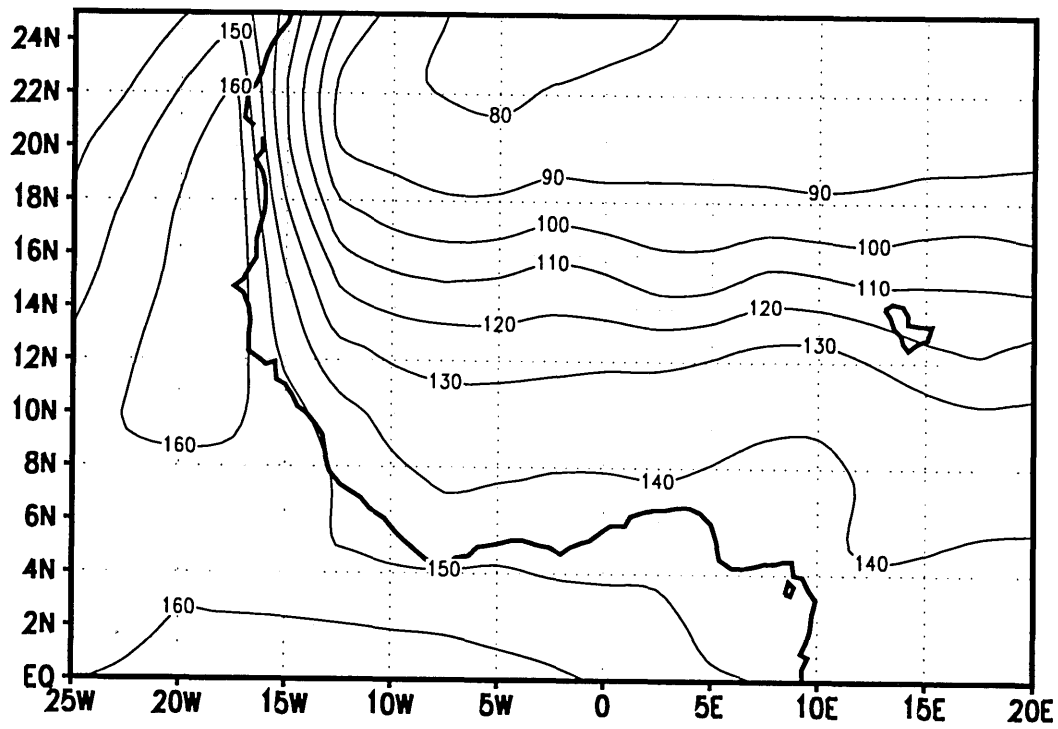

Figure 3-8: Net allwave radiation [W/m^2], NCEP reanalysis climatology (1982-1994).

a time. This competition is summarized well by Pires and Prance (1985):

> *"...under optimal conditions (when there is no lack of water) the biomass tends to be high and the plants tall, and the plants use cover (which produces shade) as a means of eliminating competitors since there is no competition for water. When there is a shortage of water, the plants cannot produce a large biomass, and are unable to cover all of the three-dimensional space which is available. Consequently, the sun penetrates to the ground and light is, therefore, not an object of competition."*

In fact, the vegetation found in the tropics bears out this description of plant competition. Regions in the tropics which have an abundant supply of water are dominated by forests, since trees compete more effectively for light. As the availability of water diminishes, vegetation becomes sparser, transitioning from forest to savanna to grassland and finally to desert, as plants which are better able to obtain and

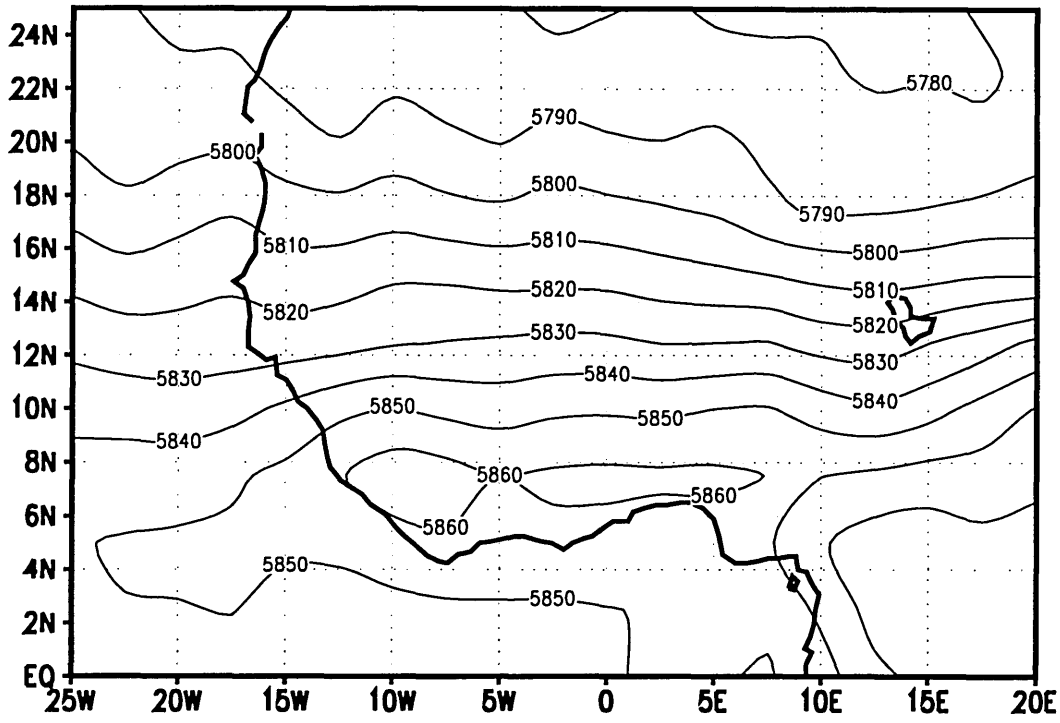

Figure 3-9: Boundary layer entropy [J/kg/K], NCEP reanalysis climatology (1982-1994).

conserve water become dominant. In West Africa, there is a pronounced gradient in both water availability and vegetation type, and the region provides a clear example of the correlation between vegetation type and climatic constraints. Both rainfall and vegetation decrease northwards in a highly zonal pattern. High rainfall rates near the coast are associated with tropical rain forests, and as rainfall drops off moving northwards, the vegetation changes to savanna, grassland and finally desert.

3.2.1 Tropical forest

In humid areas, where water is not limiting, the tropical forests dominate. Forest regions are characterized by high rainfall, warm temperatures and lush vegetation. By forming a closed canopy through which very little light penetrates, they are able to exclude competition from lower canopy species such as grasses. In regions where the mean annual rainfall exceeds about 3-4 mm/day and is relatively constant year-round, the forest is made up primarily of evergreen species (Rumney 1968). Where there is no shortage of water, it is an advantage to continue transpiring and photosynthesizing throughout the year. With less rainfall, the evergreen forest transitions into a more deciduous forest. The deciduous trees are able to conserve water during the dry season by dropping their leaves, and this gives them a competitive advantage over evergreen trees, which continue to transpire and lose water throughout the year.

In West Africa, areas of semi-deciduous forest are generally confined to narrow transition regions between the forest and savanna. The height of the forest canopy may reach 30m - 50m, with emergent trees 10m - 20m higher (Rumney 1968). In these conditions, the forest floor receives very little light, suppressing the growth of a significant understory of shrubs or grasses.

Some typical quantitative measures of vegetation include net primary productivity (NPP), accumulated biomass, and leaf area index (LAI). Net primary productivity is the rate at which plants fix carbon into new tissues, after their needs for maintenance respiration have been considered. Even in a mature ecosystem, the NPP is not zero, as dead tissues must continually be replaced. The biomass is simply the total amount of carbon found in plant material. The LAI is the area of (multiple) layers of leaves which

overlie a unit area of the ground. Due to the placement and orientation of leaves, light can often penetrate below multiple layers of leaves. Tropical forest ecosystems are highly productive and can achieve large biomass. Evergreen forests can achieve slightly higher values of NPP, biomass and LAI than deciduous forests. Table 3.1 shows the range of values which have been reported for these quantities.

3.2.2 Savanna and grassland

As water becomes less plentiful, grasses begin to have a competitive advantage over trees. Because trees cannot develop closed canopies on the limited water supply, they are unable to exclude grasses on the basis of competition for light. Grasses have dense root systems which are more concentrated in the surface layers of the soil, allowing more immediate access to rainfall as it infiltrates into the ground. In addition, most grasses in West Africa are perennial, meaning that while their aboveground tissues wither in the dry season, their below ground tissues remain intact, and they grow year after year from these roots. They are generally able to grow faster and taller, and thus outcompete annuals, which must grow from seed each year (Crawley 1986b). The water conserved by allowing above-ground tissues to die back each year during the dry season gives grasses an advantage over woody plant types in areas with a prolonged dry season.

Thus, as rainfall becomes more seasonal and is received in lesser quantities, grasses can fare better than trees. The forest then transitions into savanna, a region in which trees and grasses coexist. Grasses are typically the dominant plant type, with some scattered deciduous trees. The typical dry season in these savanna/grassland areas may last from 3 to 5 months. In West Africa, transitions from forest to savanna are often abrupt, due to frequent wildfires in the savanna. The frequent fires inhibit the establishment of new trees (Rumney 1968). Those trees which do survive on the savanna have often developed thick, fire resistant bark, or other means of surviving fire. As rainfall diminishes still further, the number of trees also diminishes and the savanna gives way to open grassland with very few trees. The distinction betweeen savanna and grassland is imprecise, as grasses are the dominant vegetation of both.

Adaptation to withstand extreme cold or large variations in temperature are not a factor in plant competition in the tropics. Adaptation to persistent high temperatures, however, has become a competitive advantage for tropical grasses, as compared to grasses which flourish in temperate regions. Most plants utilize the Calvin cycle to fix carbon during photosynthesis and are known as C3 plants. In the Calvin cycle, the enzyme ribulose 1,5 bisphosphate (RuBP) carboxylase catalyzes the formation of ribulose 1,5 biphosphate, a five carbon sugar. This is one of the key steps in photosynthesis. However, RuBP carboxylase also catalyzes the oxidation of the RuBP sugar in a process called photorespiration. Photorespiration essentially undoes the work of photosynthesis. C3 plants routinely lose between one fourth and one half of their photosynthetically fixed carbon to photorespiration. In tropical regions, the problem is even more severe, because the oxidative activity of the RuBP carboxylase enzyme increases with temperature. At high temperatures, the amount of carbon lost due to photorespiration can exceed one half of that produced by photosynthesis. (Raven and Johnson, 1989)

Plants have taken various steps to combat this problem, including development of a different photosynthetic pathway. This altered pathway is used by C4 plants to carry out photosynthesis. C4 plants expend additional energy to concentrate CO_2 in the cells which use RuBP carboxylase. In this manner, the oxidation of the RuBP sugar is inhibited and the loss of carbon due to photorespiration is decreased. Although this manner of carrying out photosynthesis is more energy intensive, the overall process is more efficient because of the reduction in photorespiration. Tropical grasses which carry out C4 photosynthesis are thus more competitive than their C3 counterparts in hot climates. (Raven and Johnson, 1989)

Rumney (1968) reports tropical grasses which grow to heights of between 1m and sometimes as much as 5m in Africa. Elephant grass, for example, can reach heights of several meters (Collinson 1977). Taller grasses are generally found in wetter areas, and shorter and sparser grasses nearer the desert fringes. Table 3.1 give typical values of NPP, biomass and LAI for tropical grasslands and savanna as a single category of ecosystem.

Table 3.1: Typical values of NPP, biomass and LAI for tropical ecosystems.

	NPP [kg-C/m^2/yr]		biomass [kg-C/m^2]		LAI [m^2/m^2]	
	range	typical value	range	typical value	range	typical value
Tropical Evergreen Forest	1-3.5	2	6-80	45	6-16	8
Tropical Deciduous Forest	1-3	1.5	6-60	40	6-10	-
Tropical Grassland-Savanna	≤ 2	1	.2-15	4	1-5	-
Desert	≤ 0.2	-	≤ 4	-	≤ 1	-

Source: Whittaker, 1975, Lieth, 1973 and Larcher, 1995

3.2.3 Desert

As moisture becomes even more scarce, the savanna and grassland give way to desert. The desert is a region with very little available moisture, and plants have adapted to these arid environments through various water conserving techniques. For example, some plants utilize CAM photosynthesis, taking in CO_2 at night and then keeping their stomata closed during the day, when there is higher potential evaporation. An additional concern for plants in desert regions is to avoid overheating, particularly because by reducing water loss during transpiration they also lose the benefit of latent cooling. Thorny leaves and stems are typical defenses against predation by herbivours which have few available food choices.

The arid conditions preclude high rates of NPP, accumulation of biomass or LAI in desert environments. Table 3.1 gives some typical values for desert regions.

Chapter 4

Model Description

The model used in this study consists of several sub-models coupled into a single integrated framework. The principal components of the integrated model are a one-dimensional radiative convective equilibrium model, a land surface model which includes vegetation dynamics, and a model which supplies the one-dimensional atmospheric column with horizontal fluxes of heat and moisture, allowing it to interact with its surroundings. Each of the submodels are described in this chapter. Figure 4-1 depicts our experimental setup very simply. The model domain interacts with a "desert" region to the north and an "ocean" region to the south. Within the model domain, the model finds its own equilibrium vegetation and climate state. The experimental simulations, described in Chapter 5 and Chapter 6, test the response of the vegetation-climate system to different initial vegetation conditions.

We chose to work within a one-dimensional framework in order to utilize a simplified system in which the effects of vegetation could be more easily isolated. Since the only large scale influences are those described by our monsoon circulation model, we are better able to isolate local effects. In addition, a one-dimensional model requires far less computer time than a three dimensional model, and thus allows more comprehensive testing of the response of the system to different forcings and initial conditions.

While our model includes detailed representations of land surface and atmospheric processes, simplifications introduced by its one-dimensional nature must be kept

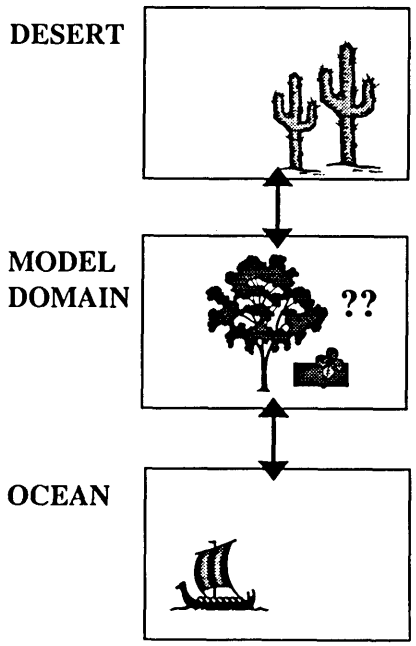

Figure 4-1: An illustration of our model's interaction with its surroundings. How does this interaction and characteristics of the land surface affect the vegetation-climate equilibrium?

in mind when analysing simulation results. Our model is intended to be used in a mechanistic study of land-vegetation-atmosphere interactions which facilitates improved understanding of the important processes in this complex system. It is not intended as a strict representation of reality which can be used in any predictive sense.

4.1 Atmospheric Component: Radiative-Convective Equilibrium Model

The model utilizes a radiative-convective equilibrium model to simulate the atmosphere. It represents a one-dimensional column of the atmosphere by balancing the effects of radiation and convection. Radiation preferentially warms the lower layers of the atmosphere, and in the absence of fluid motion, the atmosphere would reach an unstable equilibrium, with warmer air underlying cooler air. Convection

creates vigorous motion which moves the warmer air upwards until it reaches a more stable position. The radiative-convective equilibrium model balances these effects by calculating the tendencies of temperature and specific humidity due to radiation and convection and then updating the simulated profiles of temperature and humidity at each timestep. Much of the code used to describe the atmospheric model components was borrowed from earlier work by Nilton de Oliveira Renno (1993).

Our model atmosphere assumes 16 vertical levels, each 56.25 mb thick, extending from the surface to about 100 mb. These same levels are used throughout the coupled model, but are further subdivided in the radiation code. Above the model layers which are explicitly simulated by the radiative-convective model, the atmosphere is assumed to be in a state of radiative equilibrium. The water vapor mixing ratio in this statospheric layer is fixed at values taken from the AFGL standard atmosphere. Elsewhere in the atmosphere, the water vapor mixing ratio is a prognostic variable. The composition of the atmosphere with respect to other gases is held fixed throughout each simulation at values taken from the AFGL standard atmosphere.

Convection scheme. Atmospheric convection is modeled using the cumulus convection scheme (Version 4.1) developed by Emanuel (1991) at MIT. The development of this scheme was motivated by the observation that there is a great deal of inhomogeneity within individual convective clouds. In addition, sub-cloud scale updrafts and downdrafts, rather than cloud-scale circulations, have been observed to be responsible for much of the vertical transport which takes place during cumulus convection. The Emanuel scheme emphasizes the importance of sub-cloud scale updrafts and downdrafts and the microphysics of precipitation formation, fallout and re-evaporation in its representation of cumulus convection.

Convection is triggered when a parcel in reversible adiabatic ascent becomes unstable. The model atmosphere is checked for instability beginning at the surface layer and upwards to a specified maximum height. Vertical transports consist of saturated updrafts and downdrafts, a single unsaturated downdraft driven

by evaporation of falling precipitation, and by compensating subsidence. The main closure parameters are the parcel precipitation efficiencies, the fraction of precipitation that falls through unsaturated air, and the rate of re-evaporation of falling precipitation. Before convection is simulated, dry adiabatic adjustment is performed on the model atmosphere. After moist convection, the model checks for supersaturation and initiates large-scale condensation if necessary.

Radiation scheme. The radiation module used was developed at NASA Goddard by Chou (1986) and Chou et al. (1991). It parameterizes longwave radiation by grouping spectral regions with similar radiative properties and by separating the low pressure region of the atmosphere from the high pressure region. It calculates absorption and transmission of longwave radiation for water vapor, carbon dioxide and ozone. While the scheme is also able to compute the radiative effects of nitrous oxide (N_2O) and methane (CH_4), these gases are not present in our simulated atmosphere.

Incoming solar radiation varies according to the month, day, time of day, and location on the globe. Atmospheric absorption and transmission of solar radiation is controlled by water vapor and ozone. The water vapor parameterization is based upon monochromatic calculations which take into account the variation of temperature with height in the atmosphere.

While the radiation scheme is capable of modeling the radiative effects of clouds, cloud processes (formation and dispersal) are among the least understood of atmospheric processes. In order to eliminate this source of uncertainty and inaccuracy, Renno's (1993) radiative-convective equilibrium model did not simulate the growth and dispersal of clouds. Rather, the model used either zero or fixed cloud cover. In this study, we also chose to simplify the actual processes involved. Rather than representing the full radiative effects of clouds, we assumed an atmospheric and cloud albedo of between 15% and 25% and reduced the incoming solar radiation at the top of the atmosphere to reflect this atmospheric albedo. The actual value of the assumed albedo is fixed throughout the year and was chosen so that mean annual solar radiation simulated at the surface approximated that observed at the surface.

While the effects of clouds on solar radiation are loosely represented in such a manner, the effects of clouds on longwave radiation are not considered.

For the radiation calculations, each of the 16 model levels used elsewhere in the coupled model is further subdivided into 4 sublayers.

4.2 Land Surface Component: Integrated Biosphere Simulator (IBIS)

The Integrated Biosphere Simulator, Version 1.1 (IBIS) was developed by Foley et al. (1996). It is a prototype for a new generation of models incorporating all the components of a traditional surface - vegetation - atmosphere transfer (SVAT) model along with representations of biophysics, terrestrial carbon fluxes, and vegetation dynamics (Foley et al, 1996). As discussed in Chapter 2, IBIS is a suitable bridge between models which work well at the scale of GCM's, but cannot simulate the transient behavior of vegetation, and models which include detailed representations of plant growth and competition, but are ill suited for use at large scales. IBIS consists of four sub-models: a land surface module, a vegetation phenology module, a carbon balance module, and a vegetation dynamics module. The main features of each of these modules are described below.

Land Surface Module. IBIS represents the land surface with two vegetation layers and six soil layers. The water, energy, and momentum budget is conserved at each layer and by the land surface as a whole. For the water budget, IBIS includes representations of interception and throughfall, transpiration, soil evaporation, infiltration and drainage. Latent and sensible heat fluxes, along with ground heat fluxes and radiation exchange are calculated for the energy budget. Snow processes are also simulated by IBIS, but are unimportant in the tropical regions modelled in this study. The model is based on the Land Surface Transfer Model (LSX) (Pollard and Thompson 1993) but includes some modifications, particularly with respect to the effects of vegetation on hydrological processes.

Vegetation Dynamics Module. Nine plant functional types (seven trees types and two grass types) are defined based on leaf form (broadleaf or needleleaf), leaf habit (evergreen or deciduous) and photosynthetic pathway (C3 or C4). Each plant functional type responds differently to climatic constraints which affect plant survival, and vegetation dynamics parameters describe their competiveness for light and water. Their success in this competition can be measured by their leaf area index and by their carbon biomass, both updated annually based upon their net primary productivity during that year.

As discussed in Chapter 2, a plant's competitiveness is based on its:

- ability to access resources (light, water, nutrients, soil/space)
- need for these resources
- growth and mortality rates
- differences in seedling needs and established plant needs

IBIS accounts for the first three of these factors affecting competitiveness. A plant's ability to access light and water, but not other resources, is represented in IBIS. In general, trees have first access to incoming solar radiation, shading the ground below them. Depending on the fractional coverage of the upper canopy (trees), the lower canopy (grasses) can receive very little, and even no sunlight for photosynthesis. In addition, the same amount of incoming solar radiation can result in different quantities of absorbed solar energy depending upon leaf shape and orientation. Further considerations of a plant's need for light are treated indirectly by its needs for the products of photosynthesis.

Trees and grasses have different advantages in competing for water. While grasses, with their shallower root structure, have first access to infiltrating water, trees have better access to deeper storages of soil water or groundwater. These differences are represented with different root profiles for different plant types. The differing needs of plants for water are likewise accounted for in the description of different plant functional types. Drought deciduous plants, for example, are able to conserve water

in times of water scarcity by dropping their leaves. Broadleaf plants generally lose water more readily than do needle leaf plants. C4 plants lose less water during transpiration than do C3 plants.

IBIS represents the different growth rates of plants by specifying different patterns of allocation of carbon to leaves, stems, and roots. In addition, different requirements for maintenance respiration can be specified for each plant functional type. Plant mortality is addressed by specifying the rate at which carbon is replaced in each plant functional type.

Vegetation Phenology Module. At a daily timestep, the vegetation phenology module determines the winter-deciduous and drought-deciduous behavior of the various plant functional types which exist in the model domain. Winter-deciduous plants drop their leaves during the coldest months of the year, as determined by weather experienced during the previous year. Drought-deciduous plants drop their leaves during the least productive months of the year, which correspond to the driest months of the year in regions where there is abundant solar energy.

Carbon Balance Module. The carbon sequestered in each of the plant functional types existing in the model domain are calculated based upon simulated gross photosynthesis rates and the carbon utilized for maintenance respiration and growth respiration. The carbon balance is updated annually, with separate reservoirs in leaves, stems and roots.

Foley et al (1996) used observed climatological values of atmospheric boundary conditions and observed soil types to drive IBIS in a 2 x 2 degree global simulation. Starting with minimal vegetation, IBIS simulated the growth of vegetation and the hydrology of the land surface for 50 years. The results of this simulation show fairly good agreement with observations of equilibrium vegetation types and of hydrologic quantities such as mean annual runoff.

Table 4.1 shows the hydrologic quantities calculated by IBIS in an offline simulation for a single point near the coast of West Africa (6N, 8N). IBIS is forced with

the climatological atmospheric boundary conditions described in Foley et al. (1996) for that point. The NCEP reanalysis data for a nearby point (5E, 7.5N) are also shown in Table 4.1. They are shown merely to demonstrate that the IBIS simulation gives reasonable results. While it would have been possible to develop our own set of boundary conditions using NCEP reanalysis data for a more direct comparison, we chose to use the already prepared database for convenience.

As in Foley et al's (1996) study, precipitation in the offline simulation was delivered to the surface stochastically, using the mean monthly precipitation values given in the climatology. The resulting precipitation input consists of rainstorms of variable duration and time of onset which can be separated by one or more days of zero rainfall. One problem we faced in coupling IBIS to our 1-D atmospheric column was that our modeled precipitation is much more uniform than the observed precipitation. There is a diurnal cycle to precipitation, but rainfall occurs very regularly, falling almost every day during the wet season. This has important implications in the partitioning of rainfall to runoff, infiltration, interception loss, transpiration and soil evaporation. In particular, our simulations showed too much interception loss from forest and too much bare soil evaporation over grassland. In order to address this, we made minor modifications to IBIS to address issues of spatial variability in these two processes.

Table 4.1 also shows results for a simulation run in which the precipitation was not delivered to the land surface in a stochastic fashion. Rather, precipitation in each month is constant, at the monthly mean value given in the climatology. As we can see, interception loss over forest and bare soil evaporation over grassland are both increased. This is a dramatic example of the effects of neglecting temporal variability in precipitation. Over a large modeling domain, especially one dominated by local convection, it is likely that there is some precipitation falling somewhere in the domain most of the time. This becomes represented as slow, steady rain over the entire domain. However, over any particular point in the domain, it is not raining all the time. Rather, an individual point may experience brief downpours followed by longer dry spells. In this way, temporal and spatial variability are linked, and we addressed the temporal uniformity of our simulated precipitation by incorporating

Table 4.1: IBIS standalone run with climatological forcing. Location: 6E, 8N

Variable	NCEP Reanalysis 1982-1994 Climatology	Offline IBIS	
		Stochastic Precip	Constant Monthly Precip
Total Evaporation [mm/day]	3.9	3.5	4.4
Interception Loss [mm/day]	-	1.4	3.0
Transpiration [mm/day]	-	2.1	1.5
Soil Evaporation [mm/day]	-	0.0	-0.2
Runoff [mm/day]	0.7	1.1	0.4
Latent Heat [W/m2]	113	101	133
Sensible Heat [W/m2]	30	36	7
Net Solar [W/m2]	194	176	176
Net Longwave [W/m2]	-54	-41	-39
Net Allwave [W/m2]	140	135	137
Final evergreen LAI	-	5.3	0.0
Final raingreen LAI	-	0.0	5.1

some representation of subgrid variability in precipitation into our formulations of interception and bare soil evaporation.

Interception loss. The oversimulation of interception loss affects plant growth because less water infiltrates into the soil and is then available for transpiration. Furthermore, a leaf cannot transpire when it is wet. Thus, the greater the interception storage, the less transpiration is possible.

IBIS' representation of interception storage utilizes a number of parameters, including W_{max}, the maximum depth of water on a leaf, F_{max}, the maximum wetted fraction of a leaf, and T_{drip}, a decay time for the drainage of intercepted water. Spatial variability in precipitation tends to reduce spatially averaged interception loss (Eltahir and Bras 1993a). This reduction can be explained by two processes. First, spatial variability in precipitation concentrates intercepted water on a smaller wetted fraction of the canopy. Second, because the stored water is pooled into a smaller area, it has a greater depth and drains more quickly.

Table 4.2: IBIS standalone run for fixed evergreen forest with and without modifications for subgrid variability in interception storage and bare soil evaporation.

Variable	Standard	Modified Interception	Modified Soil Evaporation	Modified Both
Total Evaporation [mm/day]	4.4	4.0	4.4	3.8
Interception Loss [mm/day]	2.9	1.6	3.1	1.7
Transpiration [mm/day]	1.7	2.4	1.8	2.5
Soil Evaporation [mm/day]	-0.1	0.0	-0.6	-0.4
Runoff [mm/day]	0.4	0.8	0.4	1.0
Latent Heat [W/m2]	128	116	126	111
Sensible Heat [W/m2]	14	23	15	27
Net Solar [W/m2]	176	176	176	176
Net Longwave [W/m2]	-37	-40	-37	-41
Net Allwave [W/m2]	139	136	139	135

Table 4.3: IBIS standalone run for fixed grassland with and without modifications for subgrid variability in interception storage and bare soil evaporation.

Variable	Standard	Modified Interception	Modified Soil Evaporation	Modified Both
Total Evaporation [mm/day]	3.7	3.4	3.3	2.7
Interception Loss [mm/day]	2.1	0.7	2.9	1.0
Transpiration [mm/day]	1.1	1.7	1.4	2.0
Soil Evaporation [mm/day]	0.5	1.0	-0.9	-0.3
Runoff [mm/day]	1.1	1.4	1.5	2.1
Latent Heat [W/m2]	106	99	96	78
Sensible Heat [W/m2]	15	21	21	35
Net Solar [W/m2]	162	162	162	162
Net Longwave [W/m2]	-42	-44	-45	-50
Net Allwave [W/m2]	120	118	117	112

The first of these processes is addressed through modification of F_{max}, the maximum wetted fraction of a leaf. We make the assumption that the rainfall which contributes to interception storage is distributed over a small fraction of the model domain. According to the method proposed by Eltahir and Bras (1993c), we further assume that the larger the rainfall amount, the larger is this fraction, according to:

$$F_{max} = \frac{P}{P_{climate}} \tag{4.1}$$

where P is the simulated precipitation and $P_{climate}$ is the climatological average precipitation intensity for the region. $P_{climate}$ is set at 62.5 mm/day (about 2.6 mm/hour) and the maximum value of F_{max} is set at 1.0. The increased rate of drainage from the canopy with greater depth of storage is treated even more simply, by decreasing the time constant, T_{drip}. The results of these changes are shown in Table 4.2 for our standalone IBIS simulation using constant monthly precipitation. While the modifications are based on physical reasoning, the parameters must be tuned to a particular location. The values of the parameters used for the simulations shown in Table 4.2 are those obtained by tuning the interception storage parameters discussed above so that the results match the ratio of interception loss to transpiration obtained using the stochastic precipitation input. It is tuned to the ratio obtained using stochastic precipitation input rather than observed ratios as this better reflects the influence of temporal variability on the model's behavior. We see that the modifications have the desired effect - a decrease in interception loss over forest. However, interception loss still contributes a larger share of the total evapotranspiration in these simulations (40%) than has been observed (20%-25%) (Shuttleworth 1988). The same set of parameters was used in our coupled model simulations. This produced a ratio of interception loss to transpiration which approximates that seen in Shuttleworth's observations of tropical rain forest evaporation. The sensitivity of the coupled model to changes in the interception scheme are discussed further in Chapter 5.

Bare soil evaporation. Oversimulation of bare soil evaporation is a problem

because it tends to diminish the differences between different vegetation types. Over grassland, both interception loss and transpiration are decreased relative to forest. However, the compensating increase in bare soil evaporation brings the total evapotranspiration close to the forest value.

We modified IBIS' representation of bare soil evaporation to consider spatial variability in precipitation, as reflected in the spatial variability of the near surface soil saturation. Soil evaporation is calculated as:

$$E_s = \sigma_g \cdot (qgfac(s) \cdot qsat(T_g) - q_{air}) \tag{4.2}$$

where E_s is the evaporation from bare soil, σ_g is an aerodynamic transfer coefficient, $qsat(T_g)$ is the saturation specific humidity of air at the ground temperature, and q_{air} is the specific humidity of the air overlying the ground surface. $qgfac$ is a scaling factor for $qsat(T_g)$ to reflect the degree to which the soil is below saturation. $qgfac$ is normally calculated as a deterministic function of the near surface soil saturation. The near surface soil saturation is highly variable due to variability in the precipitation input. Following Entekhabi and Eagleson (1989), we assumed a gamma distribution for the near surface soil saturation. Integrating, we get the expected value of the parameter, $qgfac$:

$$E(qgfac) = \int qgfac(s) f_s ds \tag{4.3}$$

where f_s is the distribution of the near surface soil saturation. The original $qgfac$ function and the modified function are shown in Figure 4-2. At high soil saturation, $E(qgfac)$, and consequently, soil evaporation are decreased, reflecting the fact that even at high average soil moisture, there remain patches of dry soil. At low soil saturation, $E(qgfac)$, and consequently, soil evaporation increase. This reflects the fact that even at low average soil moiture, there will be some areas of very wet soil. The results of this modification in the formulation of bare soil evaporation are shown in Table 4.2. Negative values of soil evaporation indicate dew formation.

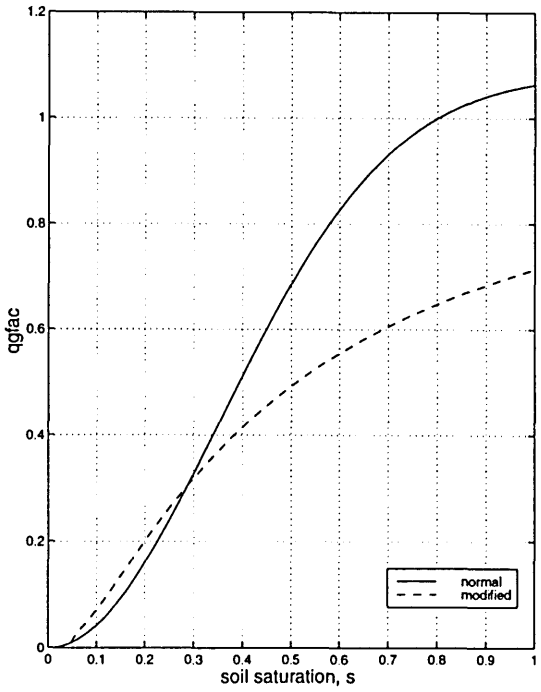

Figure 4-2: The function, $qgfac$, as a function of near surface soil saturation before and after our modification. The modified curve is the expected value of $qgfac$ as a function of the expected value of the near surface soil saturation.

4.3 Monsoon Circulation Model

Traditionally, one-dimensional models have been used most frequently to model either the entire earth as a single column or to model an atmospheric column over an ocean region. In either case, the modeled system can be considered a closed system with respect to water. When a one-dimensional model is used over an ocean region, the ocean surface at the lower boundary provides the atmosphere with an infinite source and sink of moisture. When modeling the entire globe, an ocean surface is also typically used for the lower boundary. At the upper boundary, there is no appreciable leakage of water vapor from the uppermost layers of the atmosphere into space.

When a one-dimensional model is used over land, however, water is continually lost from the system due to horizontal movement of surface and groundwater runoff and due to percolation of soil water into inaccessible groundwater storage. When modeling over very short time periods, the gradual loss of water may be acceptable. However, if the one-dimensional model is used to simulate climate over decades, this loss of water is clearly unacceptable. The column quickly dries out, leaving a wholly unrealistic representation of the natural system. Thus, an added complexity in using one-dimensional models over land is the need to resupply the one-dimensional column with moisture. Furthermore, horizontal fluxes of heat and moisture throughout the atmosphere can significantly affect convection and other atmopsheric processes, and so the vertical and temporal distribution of these fluxes is an important consideration.

Previous one-dimensional models run over land have returned moisture to the system in a variety of ways. The simplest method is to simply prescribe a constant amount of moisture convergence into the atmospheric column (Koster and Eagleson 1990). Others have used a varying convergence amount. For example, da Rocha et al. (1996) used a sinusoidal form for a time-varying assignment of moisture convergence. However, the amount of moisture convergence has a strong effect on the modeled atmosphere, and atmospheric conditions simulated by the model are constrained by using a prescribed convergence. In using a one-dimensional model to simulate climate change, the simulated atmosphere should not be constrained to a limited range of

equilibrium conditions by a prescribed convergence amount. Thus, it is necessary to relate the amount of convergence into the column to conditions within the modeled domain, so that the simulated climate can move independently to any equilibrium. Brubaker et al. (1991) did so by relating the amount of convergence to the difference in humidity between a simulated atmospheric column over land and an adjacent atmospheric column over ocean.

Our convergence model takes a similar approach, but instead of focusing only on humidity, uses Emanuel et al. (1994)'s proposal that the amount of convergence into a region is related to the gradient in boundary layer entropy between the region and its surroundings. The concept that a large gradient in boundary layer entropy induces a strong monsoon circulation in the tropics was discussed in Section 2.4 and illustrated in Figure 2-3. A strong monsoon results in a large flux of air into a region. Conversely, a weak gradient in boundary layer entropy results in a weak monsoon circulation and smaller fluxes of air.

Eltahir and Gong (1996), along with our own data analysis, show that a larger gradient in boundary layer entropy is indeed associated with a stronger monsoon circulation. Although the monsoon circulation is not strictly north-south, our data analysis simplifies the system by considering only the meridional fluxes. We calculated the meridional fluxes of air into two domains in West Africa, shown in Figure 4-3. Both domains extend from 10W to 7.5E. The coastal domain extends from 5N to 10N and the inland domain extends from 10N to 15N. Each domain has an associated ocean region, also shown in Figure 4-3.

The coastal domain, 5N - 10N, exhibits some seasonality in precipitation, but at no time during the year does it become completely dry. Under normal conditions, southerly winds blow across the southern boundary throughout the year. During the summer monsoon, and most of the year, these southerlies extend through 10N. (See Figure 2-2.) In the winter months, however, northerlies bring drier air from the north into the domain. The ocean region for the coastal domain extends from 1.25S - 3.75NN.

The inland domain, 10N to 15N, is a region which is strongly affected by the annual

monsoon. During the winter, northerly winds can blow across the entire domain while in the summer, strong monsoonal winds from the south bring with them moisture-rich air. The "ocean" region extends from 0N to 7.5N. It is larger than the ocean region for the coastal domain and includes both ocean and land. The ocean region was delineated to include the equatorial Atlantic Ocean, as the monsoon circulation is driven by differential heating between land and ocean. The region from 5N - 7.5N, while overlying land, shows less seasonality than areas to the north, and was included along with the ocean region to provide better continuity between the two selected regions.

Figure 4-4 shows the mass flux of air into the coastal domain from the south (across the 5N boundary) and from the north (across the 10N boundary). These fluxes are calculated using the meridional winds, integrated from 1000 mb to 900 mb. They are plotted against the difference in entropy between the coastal domain and the ocean region to the south of the domain. Figure 4-5 show the same plots for the inland domain. These figures were produced using thirteen years of monthly data from the NCEP renalysis project.

The boundary layer entropy for the ocean regions was estimated as the average of the lowest two NCEP levels - 1000mb and 925mb. For the land regions, it was calculated as the average of the lowest three NCEP levels, 1000mb, 925mb, and 850mb. When using the model over the coastal domain, the boundary layer entropy was calculated over the lowest 2 model levels for a total mixed layer depth of 113mb. For the inland domain, the lowest 3 model levels were assumed part of the mixed layer, for a total depth of 169 mb.

The model calculates entropy at every time step, and these values are averaged over the last 20 days for use in calculating the stength of the monsoon circulation. Hence, there is a time lag between changes in the model simulated atmosphere and the response of the monsoon circulation. This was built into the model to account for the time scale of motion from the ocean to the model domain and because the data used to develop the relationship are monthly data. A gaussian filter was used in the averaging, with the peak contribution at 10 days. The gaussian distribution

was chosen to reflect the idea that the atmospheric state long ago is unlikely to be as important as the more recent state of the atmosphere. However, at too short of a time scale, the state of the atmosphere is unlikely to have yet begun to influence the monsoon circulation. The model is sensitive to the length of time chosen for the gaussian average, and this sensitivity should be further examined in future work.

The entropy-flux relationship also shows a hysteresis - the path it takes in the first half of the year tends to be different than the path it takes in the latter half of the year. This is true to varying degrees for the different domains, but creates a seasonal bias in our estimation of the strength of the monsoon. For example, in the coastal domain, the flux from the ocean tends to be underestimated by the monsoon circulation model in the first half of the year while it is overestimated in the last months of the year.

As seen in Figure 4.3, the strength of the monsoon circulation in West Africa, as measured by the magnitude of the meridional fluxes of air, is better correlated with differences in boundary layer entropy between land and ocean than with differences in either temperature or specific humidity alone. In the coastal domain, there is no correlation between temperature gradients and the strength of the monsoon circulation. While there is significant correlation between the gradient in specific humidity and the strength of the monsoon circulation, the difference in boundary layer entropy between land and ocean is a better indicator of the monsoon strength.

Using the NCEP reanalysis data, an empirical relation was found between the gradient of boundary layer entropy between the land surface and the ocean and the fluxes of air into the land region. Using this relationship, along with monthly climatological means of boundary layer entropy over the ocean and the model calculated boundary layer entropy over the model domain, we estimated the flux of air across the model boundaries.

Using these estimated fluxes, the moisture and heat advection into the region are calculated using a simple box model. The moisture tendency is calculated for each

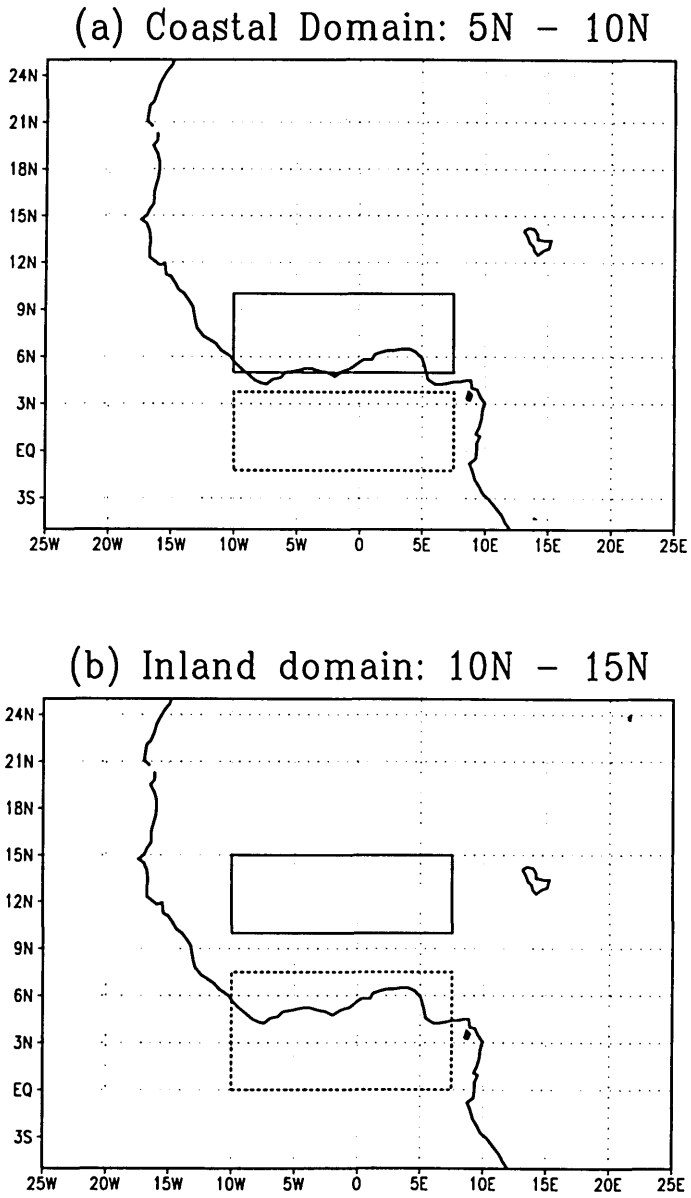

Figure 4-3: The solid box shows the model domain, the dotted box shows the associated ocean region used in developing the empirical monsoon circulation model. (a) Coastal domain (b) Inland domain

(a) Flux from South

(b) Flux from North

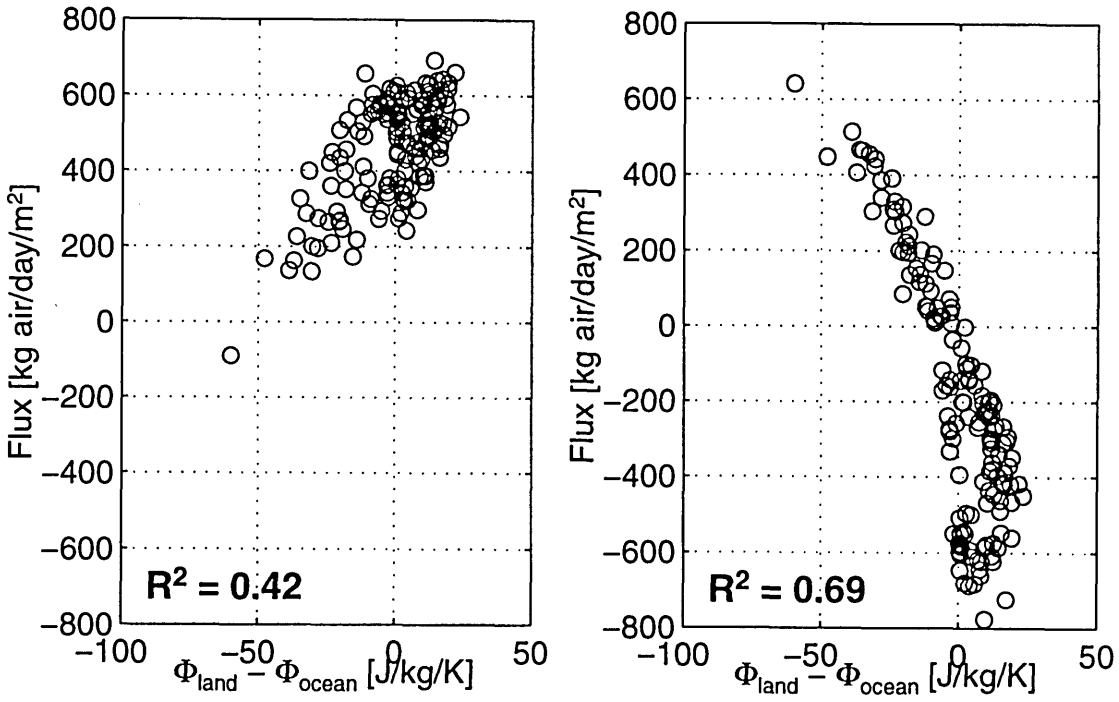

Figure 4-4: Coastal domain: Mass fluxes of air into the domain vs. entropy difference between land and ocean. (a) Flux from south (across 5N). (b) Flux from north (across 10N).

(a) Flux from South

(b) Flux from North

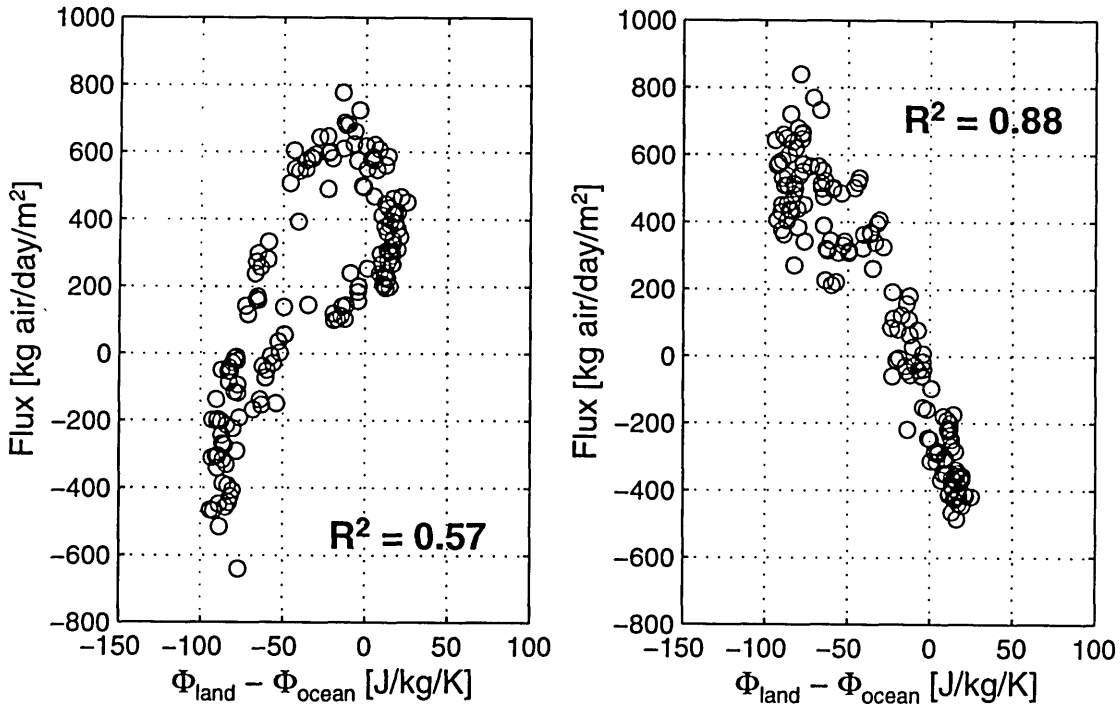

Figure 4-5: Inland domain: Mass fluxes of air into the domain vs. entropy difference between land and ocean. (a) Flux from south (across 10N). (b) Flux from north (across 15N).

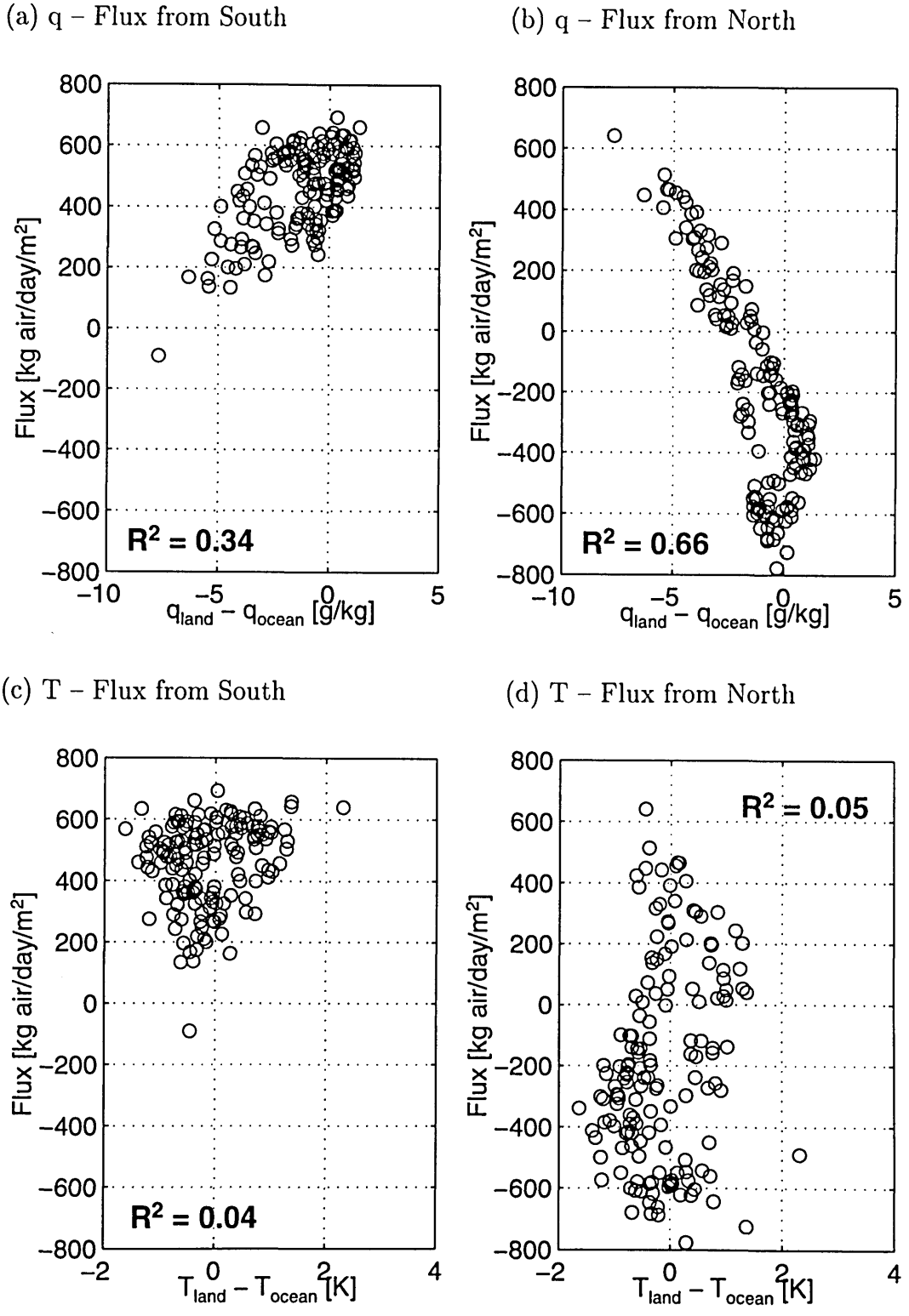

Figure 4-6: Coastal domain: correlation between mass flux of air and differences in specific humidity and temperature. (a) Specific Humidity – Flux from south (across 5N). (b) Specific Humidity – Flux from north (across 10N). (c) Temperature – Flux from south (across 5N). (d) Temperature – Flux from north (across 10N).

level of the modeled atmosphere according to:

$$q_{adv} = \frac{q_{boundary} \cdot M_{flux} + q_{model} \cdot M_{level}}{M_{flux} + M_{level}} \tag{4.4}$$

$$q_{tendency} = q_{adv} - q_{model} \tag{4.5}$$

where q_{adv} is the new specific humidity of the model domain after horizontal advection of moisture has taken place, $q_{boundary}$ is the specific humidity of the advected air, and q_{model} is the current specific humidity of the model domain. M_{flux} is the mass flux of air across the domain boundary, and M_{level} is the mass of air in one level of the model atmosphere. Separate calculations are made for each model level. The temperature tendencies at each model level are calculated similarly:

$$T_{adv} = \frac{T_{ocean} \cdot M_{flux} + T_{model} \cdot M_{level}}{M_{flux} + M_{level}} \tag{4.6}$$

$$T_{tendency} = T_{adv} - T_{model} \tag{4.7}$$

A vertical velocity is deduced from the air mass convergence by assuming that the air is incompressible and applying the principal of continuity. Integrating from the surface upwards, if horizontal fluxes of air bring additional mass into the 1-D model column, then the air is displaced upwards. If the horizontal fluxes take air away from the model column, then subsidence replaces the diverging air with air from above. Accompanying the vertical movement of air is vertical advection of the properties of the air in each level.

4.4 Coupled Model

Our coupled model of the biosphere and atmosphere links each of the individual model components described above into one integrated system. The control simulations and results are described in the following chapters.

Chapter 5

Coastal Domain: Experimental Simulations

The experimental runs investigate the sensitivity of the vegetation-climate equilibrium to perturbations to the initial vegetation condition. In the first set of simulations, the effects of vegetation on only the local land surface-atmosphere exchange are considered. In the second set of simulations, the effects of vegetation are broadened to also include its impacts on the horizontal fluxes of the monsoon circulation. The model's sensitivity to the parameters of our empirical monsoon circulation model is also explored.

The model is run for the two domains described previously in the description of the monsoon circulation model. The experiments for the coastal domain are described in this chapter, while those for the inland domain are discussed in Chapter 6. The coastal domain extends from 10W to 7.5E, and 5N to 10N. It is approximately 1900 km by 550 km and encompasses the coastal forests of West Africa and some savanna at the domain's northern edge. The monsoon circulation model for this region was developed using the ocean region located 10W - 7.5E; 1.25S - 3.75N for calculation of the entropy difference between land and sea. The locations of the coastal domain and the ocean region used for development of the empirical monsoon circulation model were shown in Figure 4-3. Monthly climatological profiles of temperature and specific humdity at the southern and northern domain boundaries are used for the

determination of advected heat and moisture. The incoming solar flux at the top of the atmosphere is calculated for 7.5 N, the center of the domain, and used for the entire region.

As discussed in Chapter 4, the model is run with zero cloud cover. However, the effects of cloud cover on solar radiation are loosely represented by reducing the solar constant by 25% to represent the albedo of the atmosphere. The effects of cloud cover on longwave radiation are not included, although longwave radiation does respond to changes in atmospheric humidity. The atmospheric boundary layer is represented as a mixed layer of constant thickness (113 mb). The sensitivity of the model results to this choice of mixed layer thickness is discussed along with the control simulations.

The soils used in the coastal domain are a medium textured silty loam consisting of 20% sand, 60% silt and 20% clay. According to the soil data of Zobler (1986), this region of West Africa consists of both silty loam and loamy sand (which has a higher sand fraction). The densest forest regions of West Africa correspond to the areas shown to have silty loam. Simulations with a high sand content tend to allow excessive condensation, resulting in large negative evaporation from the soil (Wang, 1998). We thus chose to use the medium textured silty loam throughout the domain. However, further investigation of the model's sensitivity to soil type is warranted in future work.

In each of the following experiments, the linked model is run at a 15 minute timestep. All processes are updated at each timestep except for the following: plant phenology (leaf habit), which is updated daily, and vegetation dynamics (when active), which are updated annually based upon growing conditions experienced during the preceding year. The model atmosphere is divided into 16 equal pressure layers, each 56.25 mb in thickness. As discussed in Section 4.1, the radiation code further subdivides these vertical layers for its calculations. In some simulations, noted in the text, radiative heating and cooling rates are updated only hourly to save computational time. This change does not have an appreciable effect on the model results, as the radiation time scale is much longer than one hour. Unless otherwise stated, the results shown for each simulation are for the equilibrium state of the

vegetation-climate system.

5.1 Control Simulations

We make two "control" runs for the coastal domain to demonstrate the ability of the linked model to predict a reasonable equilibrium climate and vegetation. The first "control" shows the ability of the model to approximate the regional climate and vegetation when using climatological values for the horizontal fluxes of air into the domain. The second control run utilizes our empirical monsoon circulation model to calculate these horizontal fluxes of air. Our experimental runs utilize these two different modes of interaction with the surroundings. One set of experiments looks at the effects of vegetation on climate when it does not affect the regional circulation (i.e., climatological fluxes are used) and another extends the influence of vegetation to include the monsoon circulation (i.e., the monsoon circulation model is used).

5.1.1 Control simulation: Fixed circulation

In the fixed circulation control simulation, the air mass fluxes are fixed for each month of the year, and are taken as the fluxes of air across the southern and northern domain boundaries calculated from the NCEP reanalysis climatology. The air entering the domain advects with it moisture and heat in the same manner as used in the monsoon circulation model. The monthly average temperature and humidity profiles for the advected air are calculated along the domain boundaries from the NCEP reanalysis climatology. Vegetation is initialized as a tropical drought deciduous forest and the fully coupled biosphere-atmosphere model finds its own vegetation-climate equilibrium.

Although West Africa exhibits strong zonal symmetry, there are steep north-south gradients in both land surface and atmospheric variables. Consequently it is difficult to directly compare observational data to results from our large domain, which is assumed to be homogeneous. Our one-dimensional model is an abstraction of reality, including many simplifications of the real system. Nevertheless, the average observed

and simulated climates should bear resemblance to one another.

At equilibrium, the vegetation for the fixed circulation control simulation is deciduous forest. The region from 5N to 10N actually consists of a mixture of evergreen forest, deciduous forest and tall grass savanna. It is not unreasonable, then, for our model to simulate deciduous forest for the entire homogeneous region. The upper panel of Figure 5-1 shows that the LAI is stable at about 6 throughout the run. This value is in the range seen for tropical deciduous forests listed in Table 3.1. In the lower panel of Figure 5-1 we see that the biomass has not yet stabilized by the end of the simulation. An oversight in the model code initialized the biomass at zero at the start of the simulation. This problem is further discussed in Appendix A.

The climate of the fixed circulation control simulation approximates that observed over the model domain. Table 5.1 shows the annual average values of some climatic variables for the control run compared to observed data for the same region. NCEP reanalysis data is given for the observations, rather than station data, because average values over the same spatial domain can easily be taken from the gridded NCEP dataset. However, because some NCEP variables are heavily influenced by the GCM model output, the NCEP "observations" should not be regarded as absolute truth.

The annual average climate compares reasonably well with the NCEP climatology, although the simulated climate is somewhat warmer and drier than NCEP. The partitioning of energy between latent and sensible heat fluxes is in good agreement with the observations. However, it should be noted that the sum of NCEP's latent and sensible heat terms does not equal the NCEP net allwave radiation at the surface. The net solar radiation in our model closely approximates the NCEP value, as the atmospheric albedo was tuned to give a similar incoming and net solar radiation as NCEP. Our model simulates a smaller net longwave radiation, resulting from both a higher simulated surface temperature and a smaller downwards longwave radiative flux. The smaller downwards longwave radiative flux is consistent with the drier atmosphere and lack of representation of cloud cover.

In terms of partitioning of water, precipitation and evaporation are in balance, and there is no runoff. This is a problem with our model in general. Very little runoff

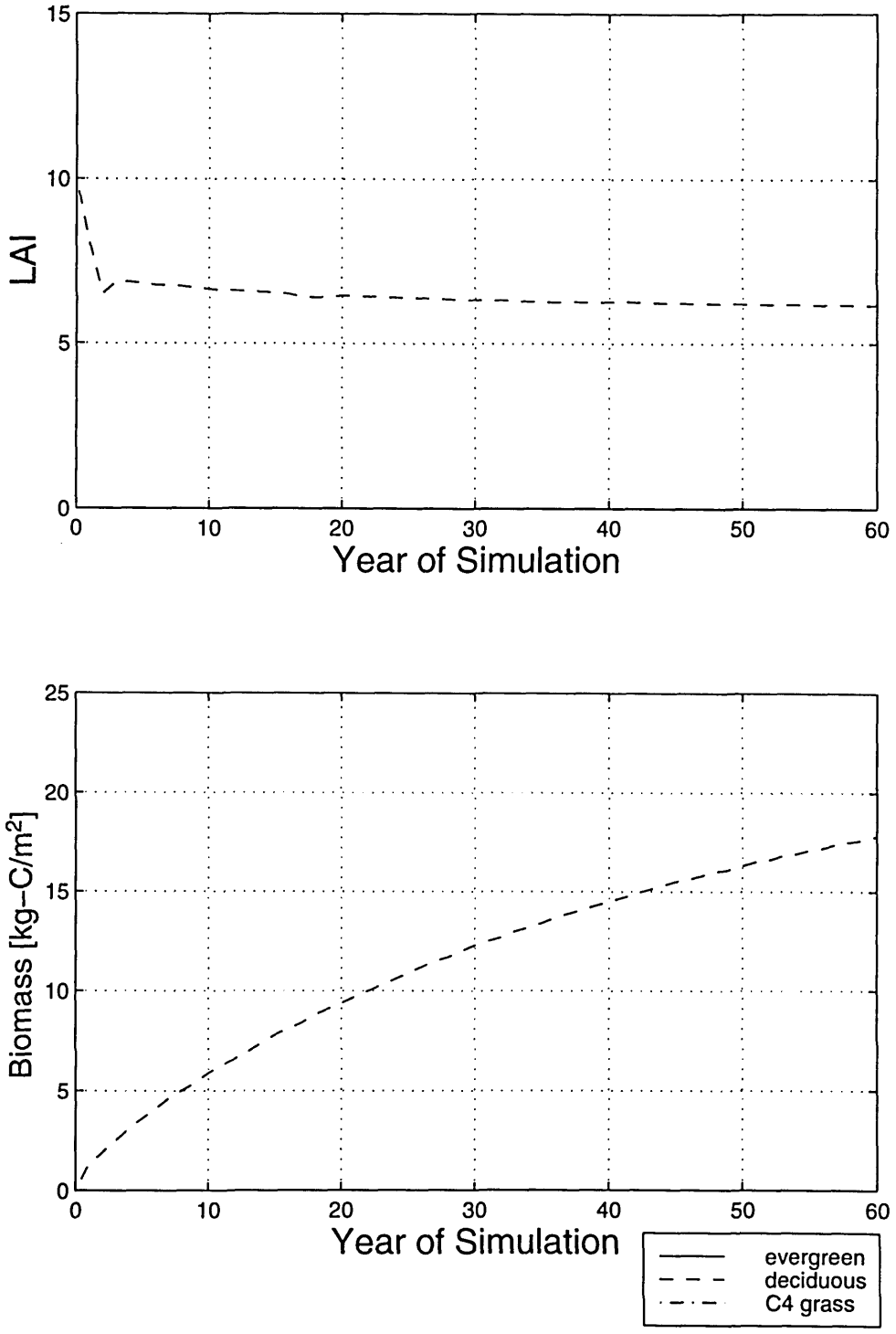

Figure 5-1: Coastal domain, fixed circulation control simulation. The upper panel shows the LAI, which is stable throughout the run. The lower panel shows the biomass, which has not yet stabilized.

Table 5.1: Coastal Domain Control Runs - Simulated Mean Annual Climate with Comparison to NCEP Climatology

Variable	NCEP Reanalysis 1982-1994 Climatology	Model Results	
		Climatological Flux	Flux Relation
T [K]	299.7	301.9	300.6
q [g/kg]	16.4	12.6	13.5
Precipitation [mm/day]	4.4	3.4	4.5
Evapotranspiration [mm/day]	3.4	3.4	4.3
Interception loss [mm/day]	-	1.1	1.2
Transpiration [mm/day]	-	2.3	3.2
Soil Evaporation [mm/day]	-	0.0	-0.1
Runoff [mm/day]	1.1	0.0	0.2
Latent Heat [W/m2]	99	98	125
Sensible Heat [W/m2]	32	30	12
Net Solar [W/m2]	198	202	201
Net Longwave [W/m2]	-57	-76	-68
Net Allwave [W/m2]	141	126	133
Entropy Difference [J/kg/K]	-1.1	-1.4	2.0

is generated in any of our simulations, and it is limited to subsurface runoff. No simulations produced an appreciable amount of surface runoff, even in grassland areas. A possible explanation for this is a lack of sufficient spatial and temporal variability. In our simulations, precipitation occurs every day during the wet season. Storms occur more frequently and with lesser intensity in our simulations, as compared to observations. This precipitation pattern tends to make surface runoff less likely, as precipitation reaching the surface is less likely to exceed the infiltration capacity of the soil or to result in saturation of the uppermost layers of soil. It may also tend to inhibit subsurface runoff as smaller infiltration amounts stay closer to the surface where plants have access to the stored soil moisture.

The seasonal variability of many variables are not simulated well by our model because we do not simulate variable cloud cover. There is no increase in cloudiness during the summer months to attenuate the increase in solar insolation during those same months. In West Africa, the increase in cloudiness during the summer can reduce the number of sunshine hours experienced on an average summer day to less than half the number of hours experienced on an average winter day (Hayward and Oguntoyinbo 1987). This has a strong effect on the downwards solar flux. In fact, both the NCEP reanalysis (see Figure 5-3) and the International Satellite Cloud Climatology Project (ISCCP) data show that the downwards solar flux is actually greater during winter than during the summer in our model domain. In contrast, our model simulations have greater solar radiation in the summertime. This seasonal skew in solar radiation impacts all of the energy fluxes in our model, and also components of the water balance. Despite this, the seasonal variation in our model simulation matches the seasonal variation in the NCEP climatology fairly well, except in the solar radiation field. The seasonality of the NCEP climatology is shown in Figures 5-2 to Figure 5-4. The seasonal variability of our model simulation is shown in Figure 5-5 to Figure 5-7. Figure 5-8 shows soundings of the simulated atmosphere for January 1 (winter) and July 1 (summer).

Our precipitation field shows a comparable amount of seasonal variability as the NCEP data, but is shifted downwards, reflecting the overall lower precipitation

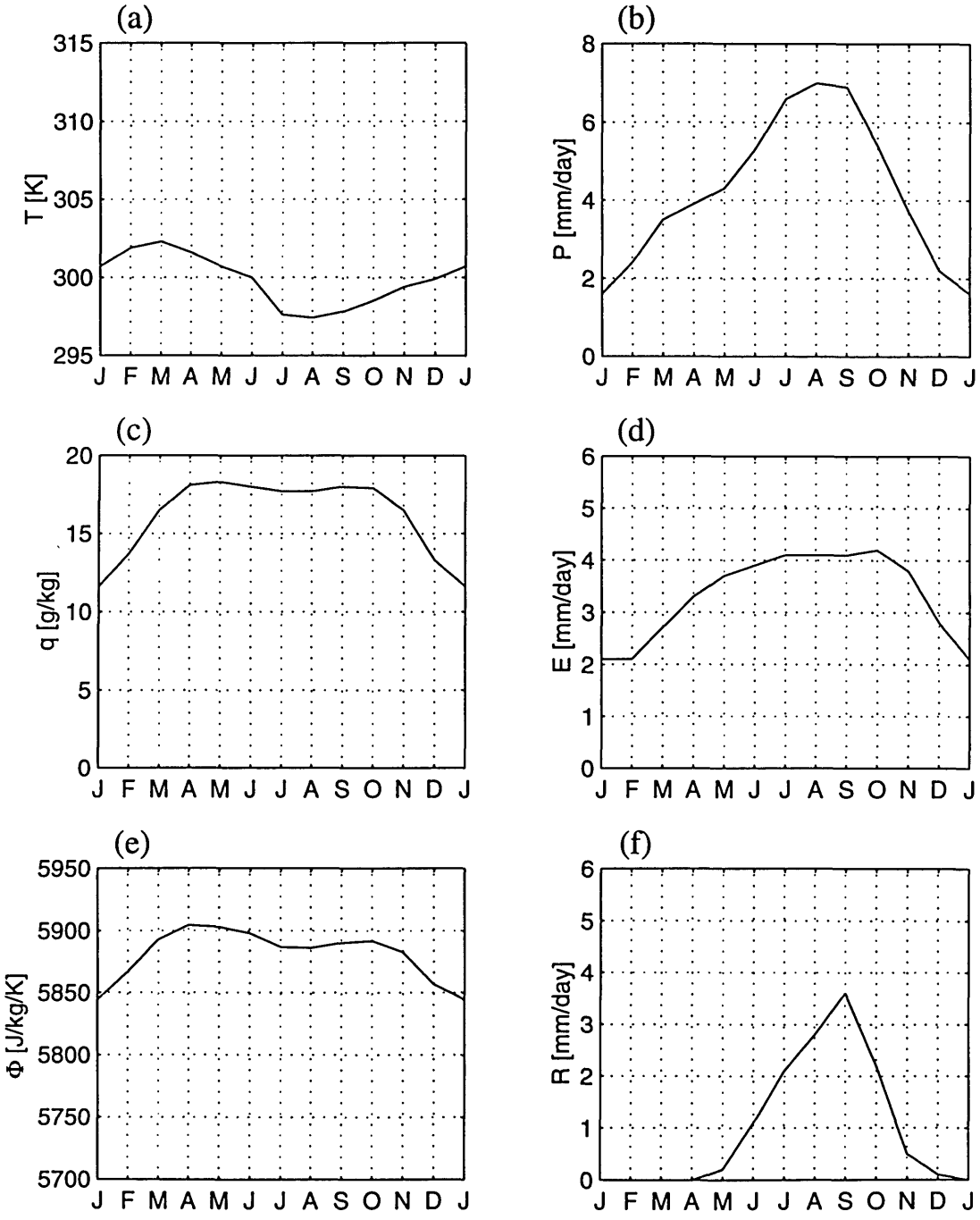

Figure 5-2: Coastal domain: NCEP reanalysis climatology (1982-1994), seasonal cycle of climate. (a) Temperature (b) Precipitation (c) Specific humidity (d) Total evapotranspiration (e) Boundary layer entropy (f) Runoff

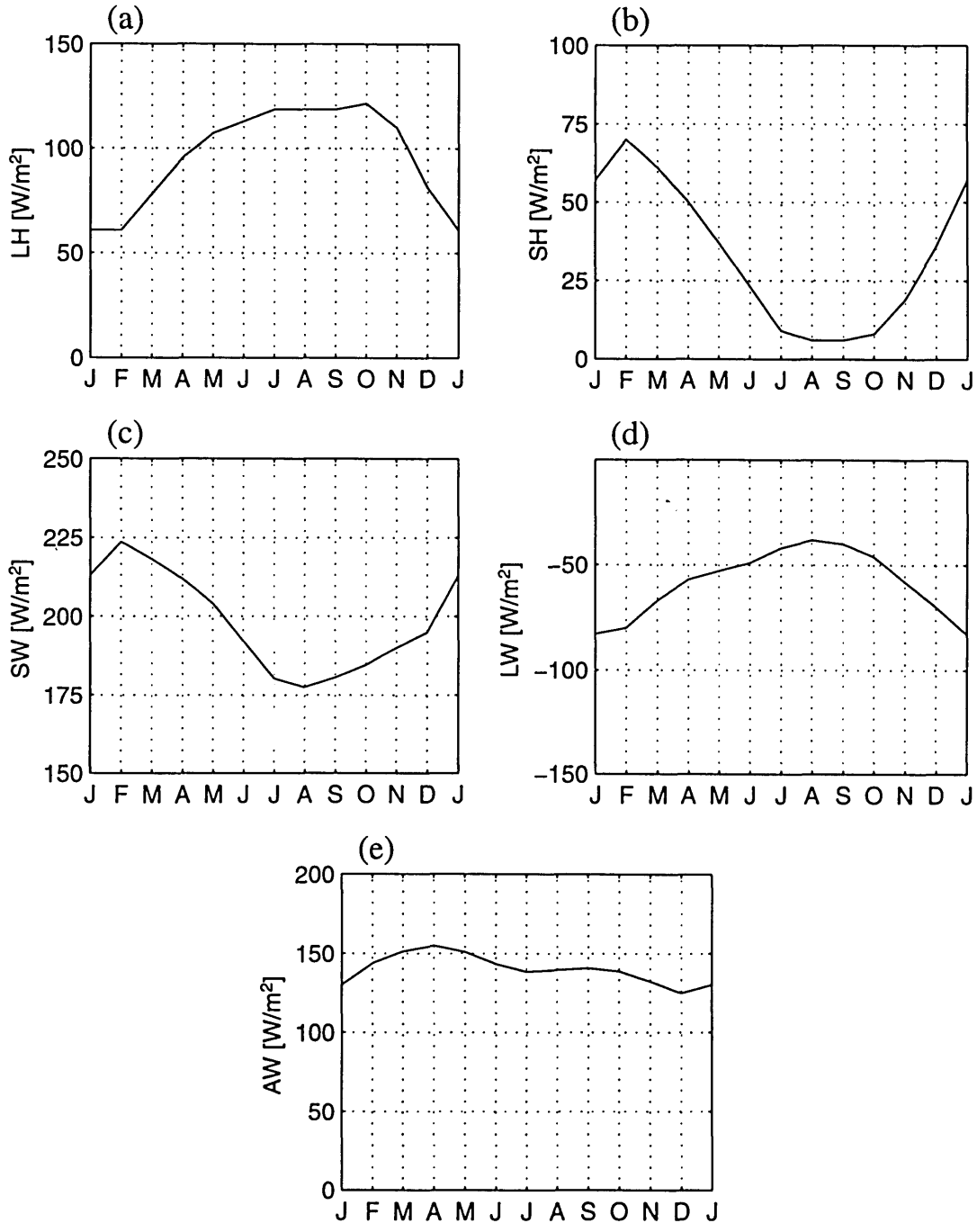

Figure 5-3: Coastal domain: NCEP reanalysis climatology (1982-1994), land-atmosphere energy exchange. (a) Latent heat flux (b) Sensible heat flux (c) Net shortwave radiative flux (d) Net longwave radiative flux (e) Net allwave radiative flux

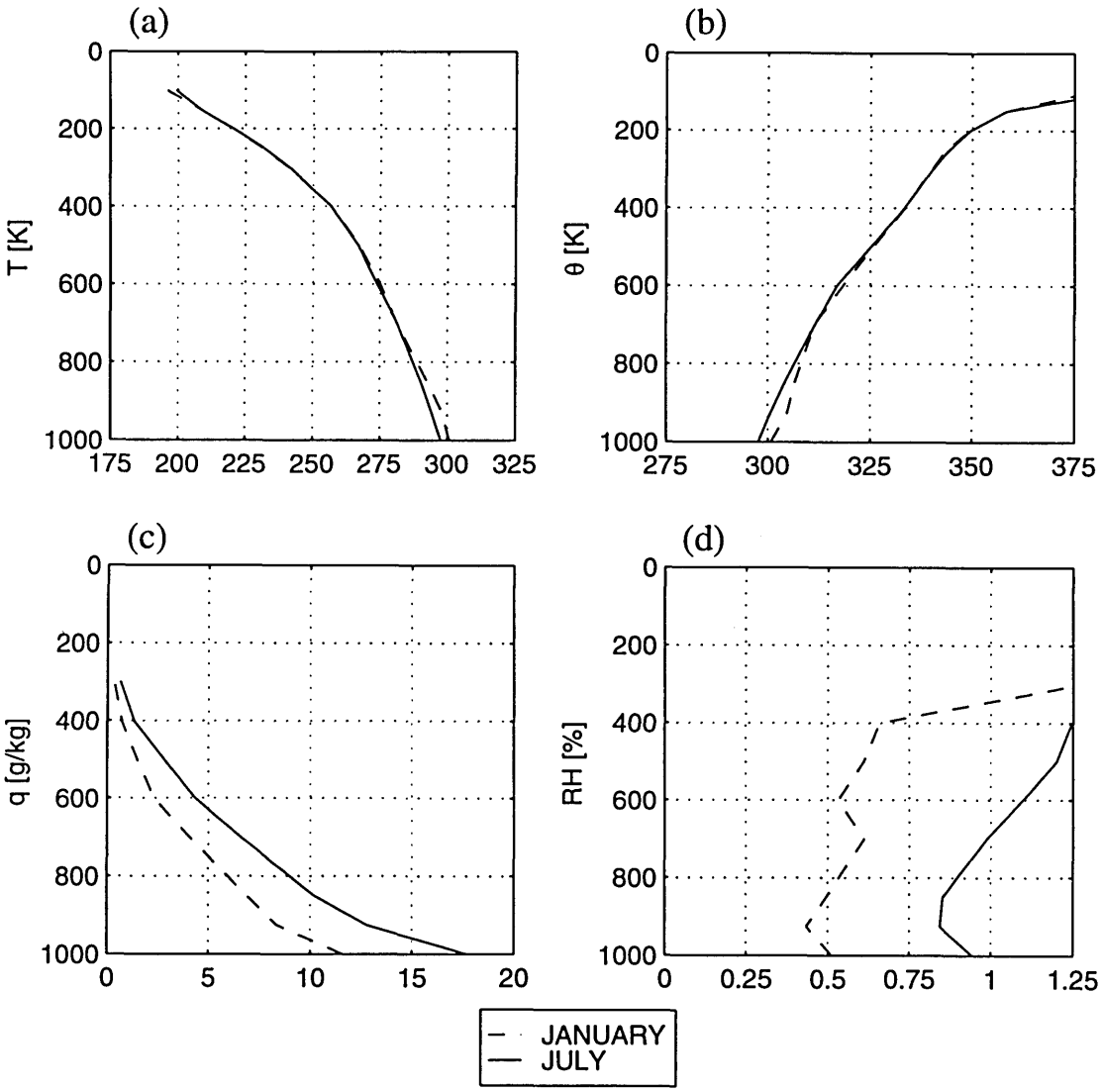

Figure 5-4: Coastal domain: NCEP reanalysis climatology (1982-1994), atmospheric soundings. (a) Absolute temperature (b) Potential temperature (c) Specific humidity (d) Relative humidity

in our simulation. In addition, precipitation rises to its summer maximum much more quickly in our simulation, and remains there for a longer duration. The precipitation in our simulation ranges from a minimum of about 0.5 mm/day in the winter to a maximum of 5.0 mm/day in the summer. Precipitation in the NCEP climatology ranges from 1.6 mm/day to 7.0 mm/day. The total evaporation in our simulation also shows a summer maximum and winter minimum, consistent with the NCEP climatology. The seasonal distribution of specific humidity, temperature, and boundary layer entropy also match the NCEP climatology fairly well. The seasonal variation in energy fluxes show reasonable agreement with the NCEP climatology, with the exception of the solar energy field.

In Figure 5-7, we see that there is strong advection of heat from surrounding regions during the winter months. Both the fluxes of air from the north and from the south contribute to the total heat advection. In the summer, heat advection does little to alter the temperature profile of the model domain.

The moisture advection is positive through most of the year, but negative during the winter months. The sharp peaks seen in the moisture advection are due to abrupt shifts in the profile of advected air at the beginning of each month. The transition from month to month can be smoothed in future work. In the winter, the transport of drier air from surrounding regions decreases the moisture content of the atmosphere. Near-surface air fluxes at the northern boundary are positive (directed into the domain) in DJF, and bring with them dry air from the region north of the model domain. In the remainder of the year, the surface flux at the northern boundary is negative, indicating a southerly wind. In the summer, then, winds bringing moist air from the south of the model domain penetrate the entire length of the domain, keeping the hot and dry air to the north out. Figure 5-7e shows the difference in entropy between the model domain and the ocean region to its south. As expected, the difference becomes larger during the summer months and smaller during the winter months. The total precipitable water in the model atmosphere is shown in Figure 5-7f, and is slightly smaller than NCEP estimates. This is consistent with the drier conditions discussed earlier.

The soundings shown in Figure 5-8 show characteristics which match observations. (See NCEP soundings in Figure 5-4). The absolute temperature is highest at the surface and decreases upwards. The potential temperature, which accounts for pressure differences, shows that the atmosphere is stable, with potentially warmer air overlying the colder surface layers. However, the uppermost layers of the atmosphere are cold compared to observations. The specific humidity profiles show a characteristic concave shape, with specific humidity decreasing rapidly upwards from the surface. This is especially evident in the summer (July 1) profile. The relative humidity in the summer is high near the surface, then bows out to a minimum near 400mb. It then increases rapidly again to reach saturation in the uppermost layers of the atmosphere. This shape is typical of soundings in convecting atmospheres but is less evident in the NCEP sounding. This pattern is absent from the winter profile, due to the absense of vigorous convective motion.

5.1.2 Control simulation: Interactive circulation

The second "control" run, which utilizes our empirical monsoon circulation model, is set up exactly like the fixed circulation control run, but includes variable interaction with the surroundings. Based on the conditions within the model domain, the fluxes of air from the north and from the south are calculated using the empirical formulae described in Section 4.3. These fluxes of air advect with them heat and moisture, according to the properties of the air along the model domain's border, as calculated from the NCEP climatology.

The mean annual values of key variables are shown in Table 5.1 and compared to both the NCEP climatology and the simulated climate of the fixed circulation control simulation for the same region. The seasonal variability in the model simulation is shown in Figure 5-10 to Figure 5-12. The interactive circulation control simulation produced a somewhat moister and cooler climate than the climatological control simulation. In terms of temperature and humidity, it is actually in closer agreement with the NCEP climatology for the region. In addition, there is more precipitation and evaporation in the interactive circulation control simulation. Precipitation exceeds

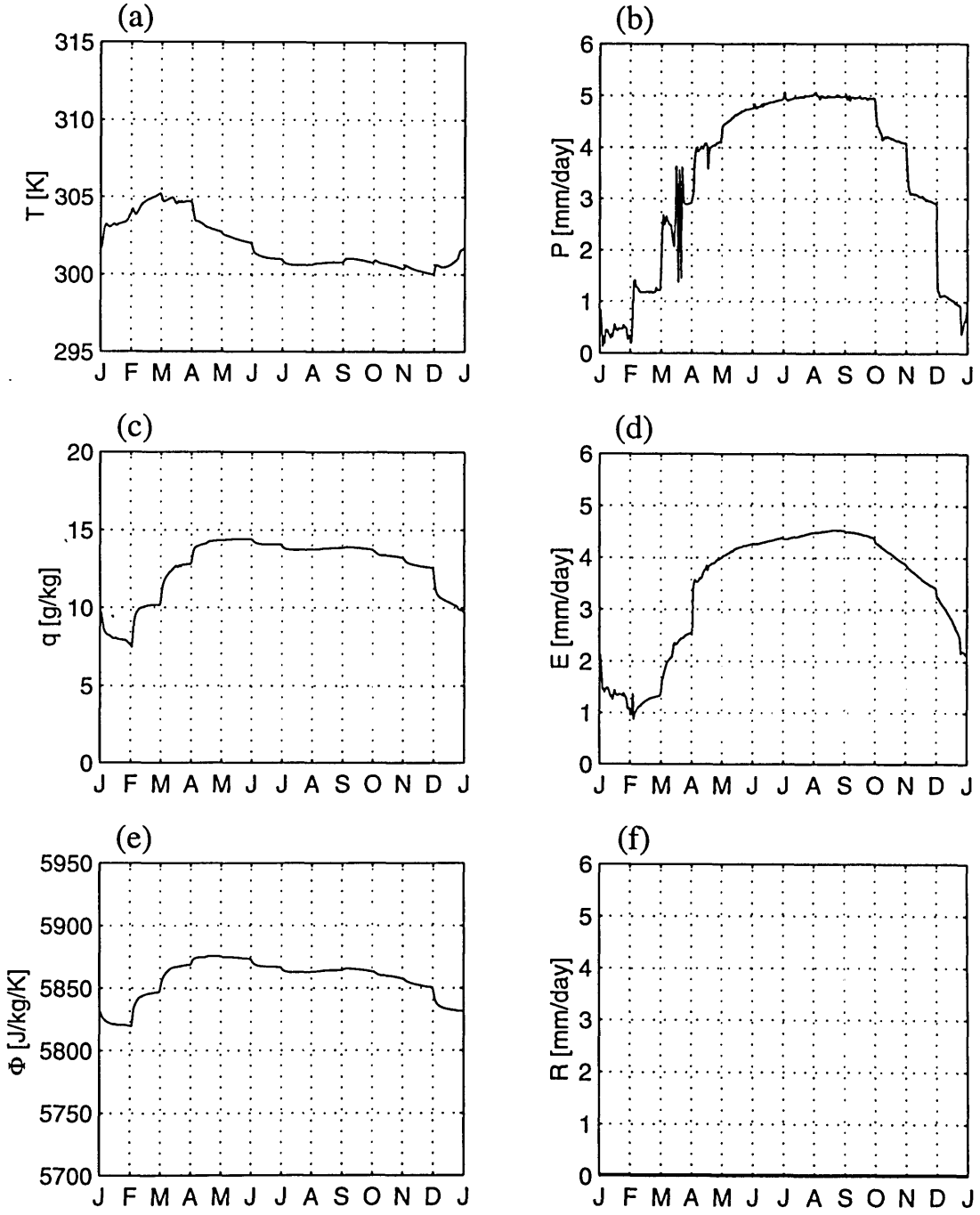

Figure 5-5: Coastal domain: fixed circulation control simulation, seasonal cycle of simulated climate. (a) Temperature (b) Precipitation (c) Specific humidity (d) Total evapotranspiration (e) Boundary layer entropy (f) Runoff

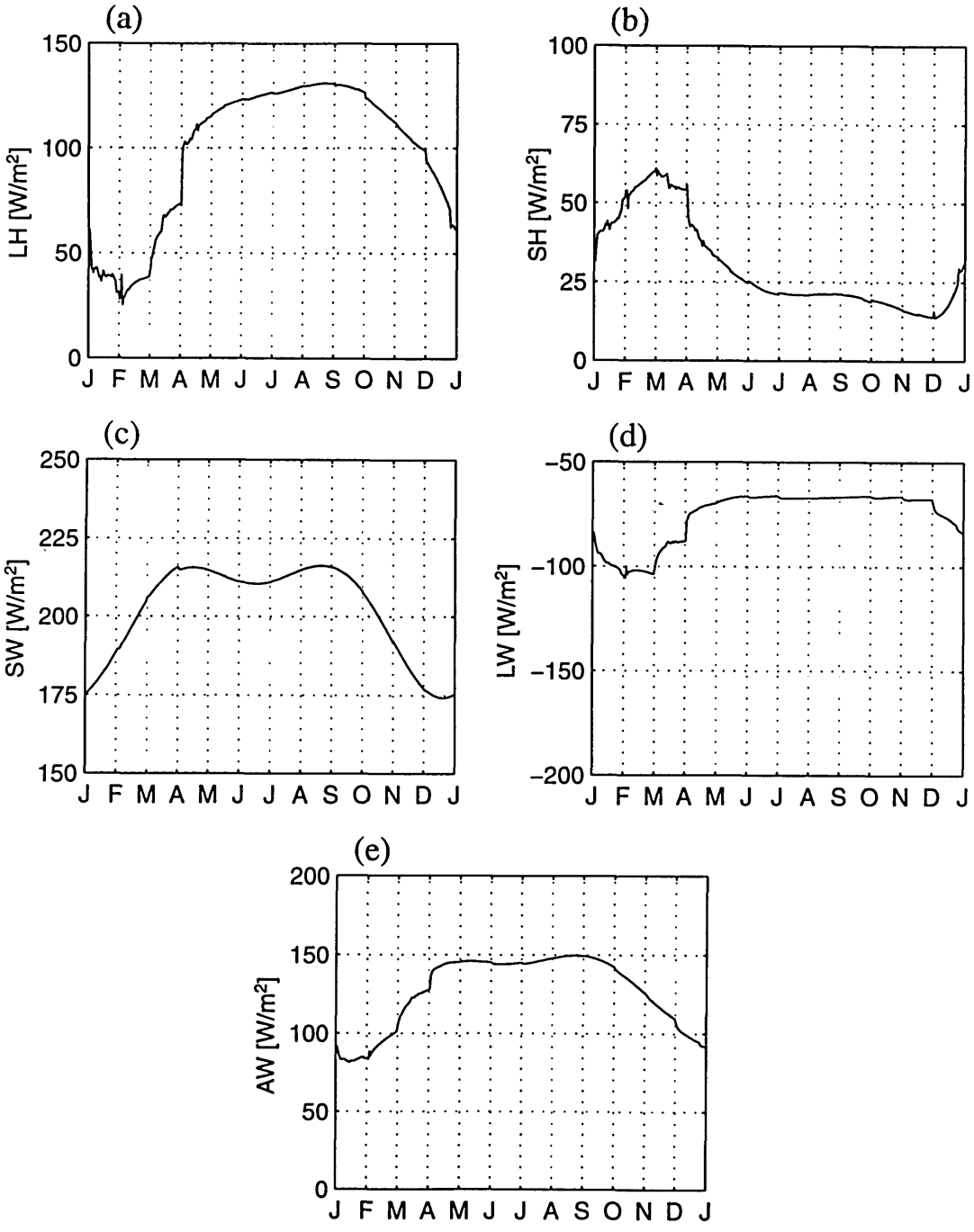

Figure 5-6: Coastal domain: fixed circulation control simulation, land-atmosphere energy exchange. (a) Latent heat flux (b) Sensible heat flux (c) Net shortwave radiative flux (d) Net longwave radiative flux (e) Net allwave radiative flux

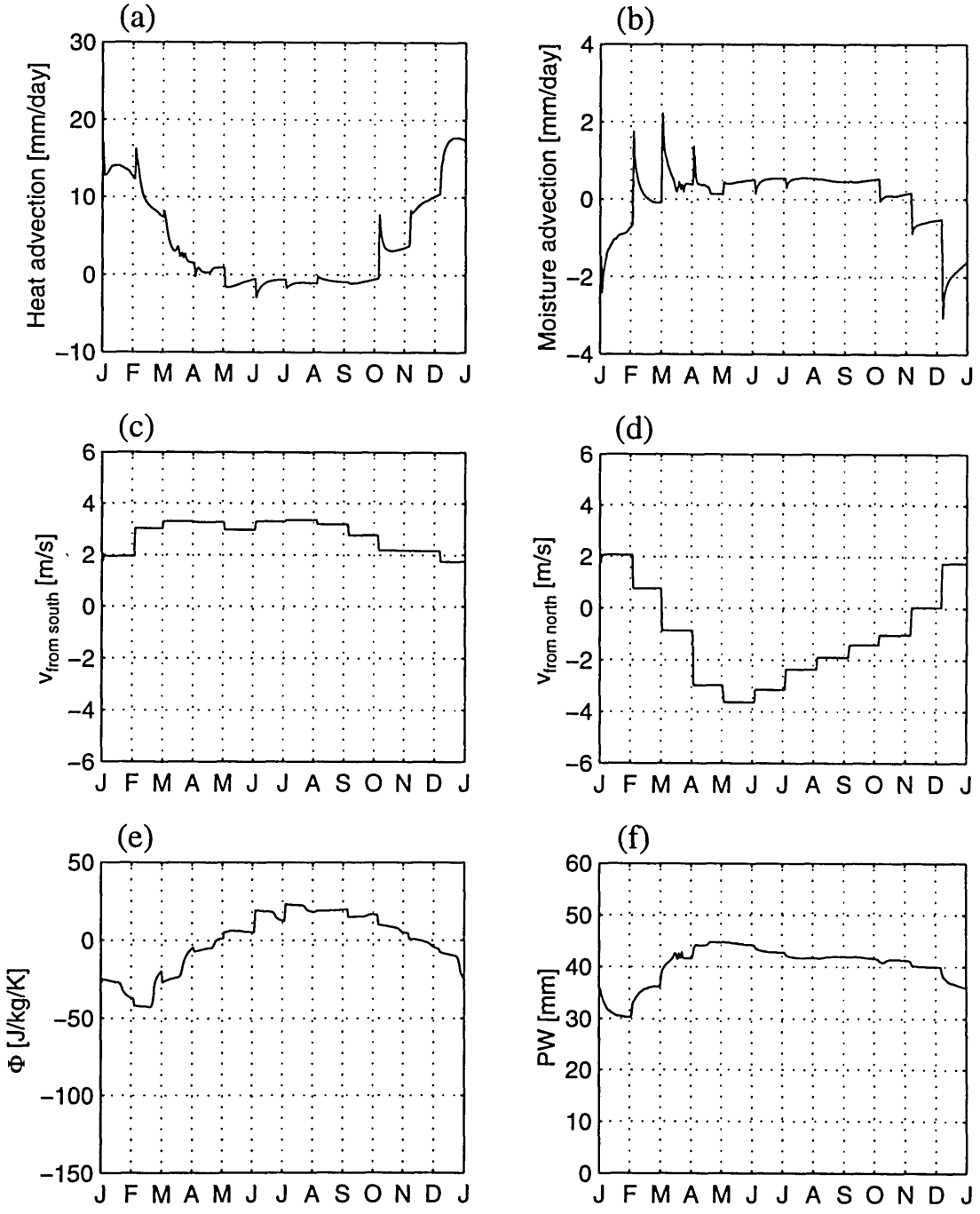

Figure 5-7: Coastal domain: fixed circulation control simulation, monsoon circulation. (a) Heat advection (b) Moisture advection (c) Lowest level wind across southern boundary (d) Lowest level wind across northern boundary (e) Entropy difference between model domain and ocean region (f) Precipitable water

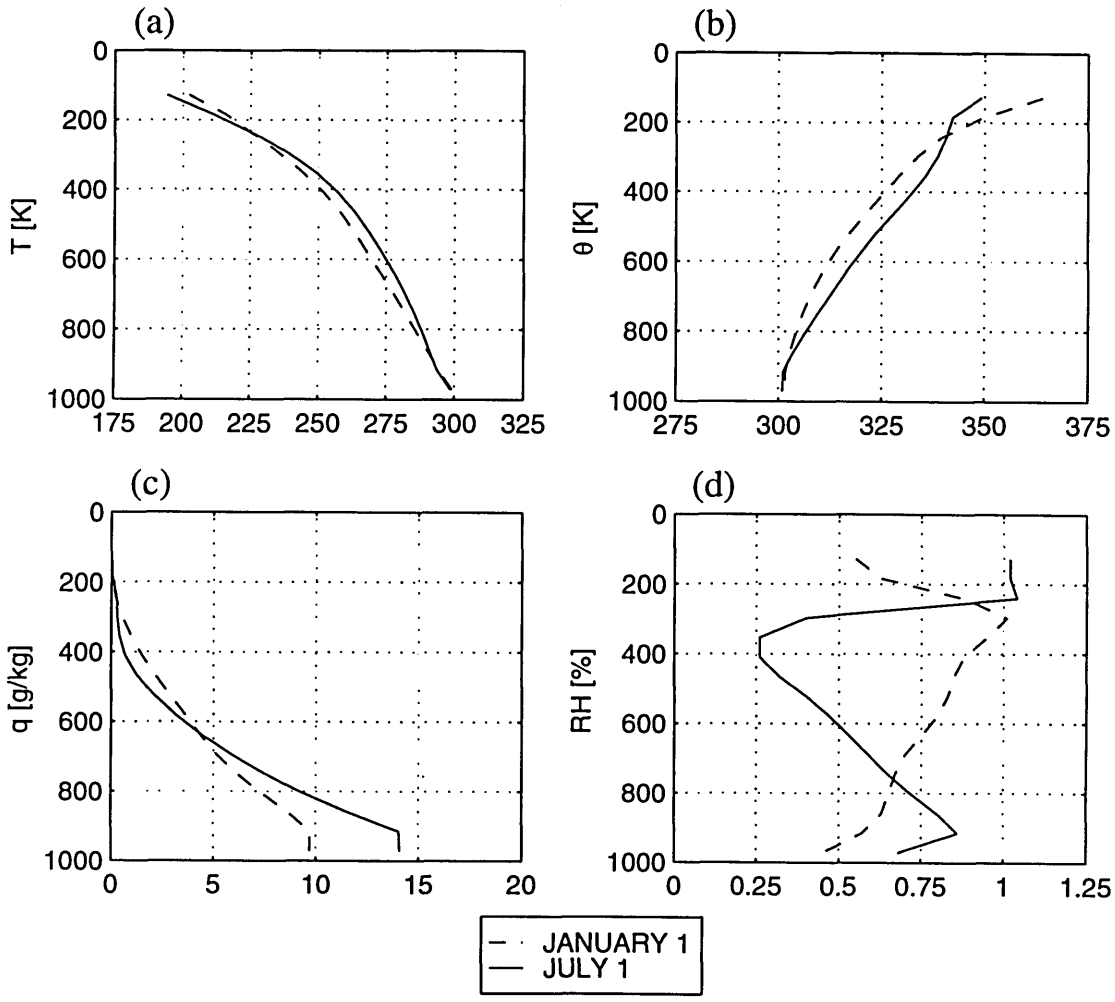

Figure 5-8: Coastal domain: fixed circulation control simulation, atmospheric soundings. (a) Absolute temperature (b) Potential temperature (c) Specific humidity (d) Relative humidity

evaporation, yielding 0.2 mm/day of runoff. Net solar radiation was essentially unchanged, but an increase in net longwave radiation brought the net allwave radiation in closer agreement with observations as well. The change in net longwave radiation is largely due to the 1K drop in surface temperature.

The fluxes of air simulated by the monsoon circulation model do not match the climatological fluxes exactly. However, the simulated fluxes (shown in Figure 5-12) do capture the general seasonal trends observed in the NCEP climatology (shown in Figure 5-7) . The surface flux across the southern domain boundary remains positive throughout the year. The mean annual surface wind speed of 2.7 m/s across the southern boundary is in good agreement with the climatological wind speed. Furthermore, the magnitude of the seasonal variability in surface wind speed matches the climatology quite well.

The fluxes from the north are not simulated as well. There is less seasonality in the simulated fluxes than observed in the climatology, reflected in the smaller amplitude of variability in the surface wind speed. The wind direction is almost always southerly (i.e., directed out of the domain) in the interactive circulation control simulation. During the winter months, the wind speeds drop, and reverse briefly. However, these northerly winds are quite weak as compared to the climatology. Because of the diminished northerlies, there is less advection of hot dry air from the north into the model domain, and the simulated climate remains cooler and moister. The weakening of the monsoon and the resulting penetration of hot, dry winds from the north into the model domain which was seen in the fixed circulation control simulation appears to be the primary cause of the drop in winter atmospheric moisture and precipitation in that simulation. This effect is diminished in the interactive circulation control simulation and hence there is considerably less seasonal variability in this second "control" simulation. This suggests that the strength of the monsoon is important as much for its ability to prevent dry air from penetrating southwards into the model domain from the north as for its ability to bring in additional moisture from the south.

The mean annual entropy difference between the model domain and the ocean

region is larger in this simulation, as compared to both the control simulation and the NCEP climatology. This is due to the increased specific humidity, which has a stronger effect on entropy than the decrease in temperature. The higher boundary layer entropy is consistent with the stronger monsoon. A positive feedback in which the strong monsoon helps to sustain the conditions which created it are likely to have some role in this simulation. The degree to which these feedbacks, rather than imprecision in the empircal monsoon circulation model, cause deviations of the simulated fluxes from the climatological values is difficult to assess.

We also see a slight shift in timing of the peak surface winds, which may be attributed to two effects. First, the entropy over the model domain is averaged over twenty days using a gaussian filter with its peak at 10 days prior to the current timestep. Hence, there is some sluggishness in the response of the system. However, because the empircial relationship was derived from monthly data, we continued to use the 20-day gaussian filter. Second, there is a "hysteresis" in the data used to derive the relationship. In the fluxes from the ocean region to the south, the model tends to underestimate the fluxes of air from February through June. From September to December, it tends to overestimate the fluxes. In a similar but opposite effect, the fluxes across the northern domain boundary tend to be overestimated during April through June, and underestimated from August through November.

The changes in the fluxes of air across the southern and northern domain boundaries result in less seasonal variability than was observed in the fixed circulation control simulation. The diminished penetration of hot dry air from the north seems to be the primary reason for the diminished seasonality. Although the mean annual climate in this simulation compares as well as or better than the mean annual climate in the fixed circulation control simulation to the NCEP climatology, the seasonality of the climate in this simulation does not compare as well. In particular, the distributions of precipitation, temperature, specific humidity, net longwave radiation and sensible heat flux are flattened out in this simulation. Thus, it may be that the ability of the fixed circulation control simulation to approximate the seasonal variability seen in the NCEP data despite the erroneous distribution in solar flux is

due to the strong effects of horizontal advection in shaping the climate.

The soundings in Figure 5-13 also reflect the change in the atmospheric circulation. As before, relative humidity on July 1 shows a bowed out shape, characteristic of rising air. On January 1, this same shape is seen, indicating that rising motion is taking place year round.

Corresponding to the decrease in seasonality, and the increase in rainfall, the equilibrium vegetation for the interactive circulation control simulation is a tropical evergreen forest. Deciduous forests are no longer the most competitive because they drop their leaves during the least productive months of the year, which correspond to those with the driest soils. However, because there is plenty of water and not very much seasonality, there is still adequate water during those months and the plants would do better not to drop their leaves and to instead continue to photosynthesize during those months. Hence, the evergreen forests become dominant in the interactive circulation control simulation. The region sustains a tropical evergreen forest with an LAI of about 10, and a biomass which is approaching 35 kg-C/m^2/yr (see Figure 5-9). The NPP is stable at about 1.8 kg-C/m^2/yr. These values are all in the range of observed values of tropical evergreen forests given in Table 3.1. Again, the biomass has not yet stabilized but any additional growth is unlikely to affect the equilibrium climate or vegetation significantly, as discussed in Appendix A.

5.1.3 Sensitivity to mixed layer depth

The surface mixed layer of the atmosphere is represented in our model by assuming that the air and water vapor are well-mixed. The temperature and specific humidity of the atmospheric layers included in the mixed layer are adjusted to satisfy this assumption at the end of each timestep. There is no representation of the growth and decline of the depth of the mixed layer over the course of the day and the assumed depth does not vary with season.

The sensitivity of the model to the depth of the mixed layer was tested in a series of three simulations. In the 56 mb mixed layer simulation, only the first model layer is considered part of the mixed layer. The 113 mb mixed layer simulation uses the

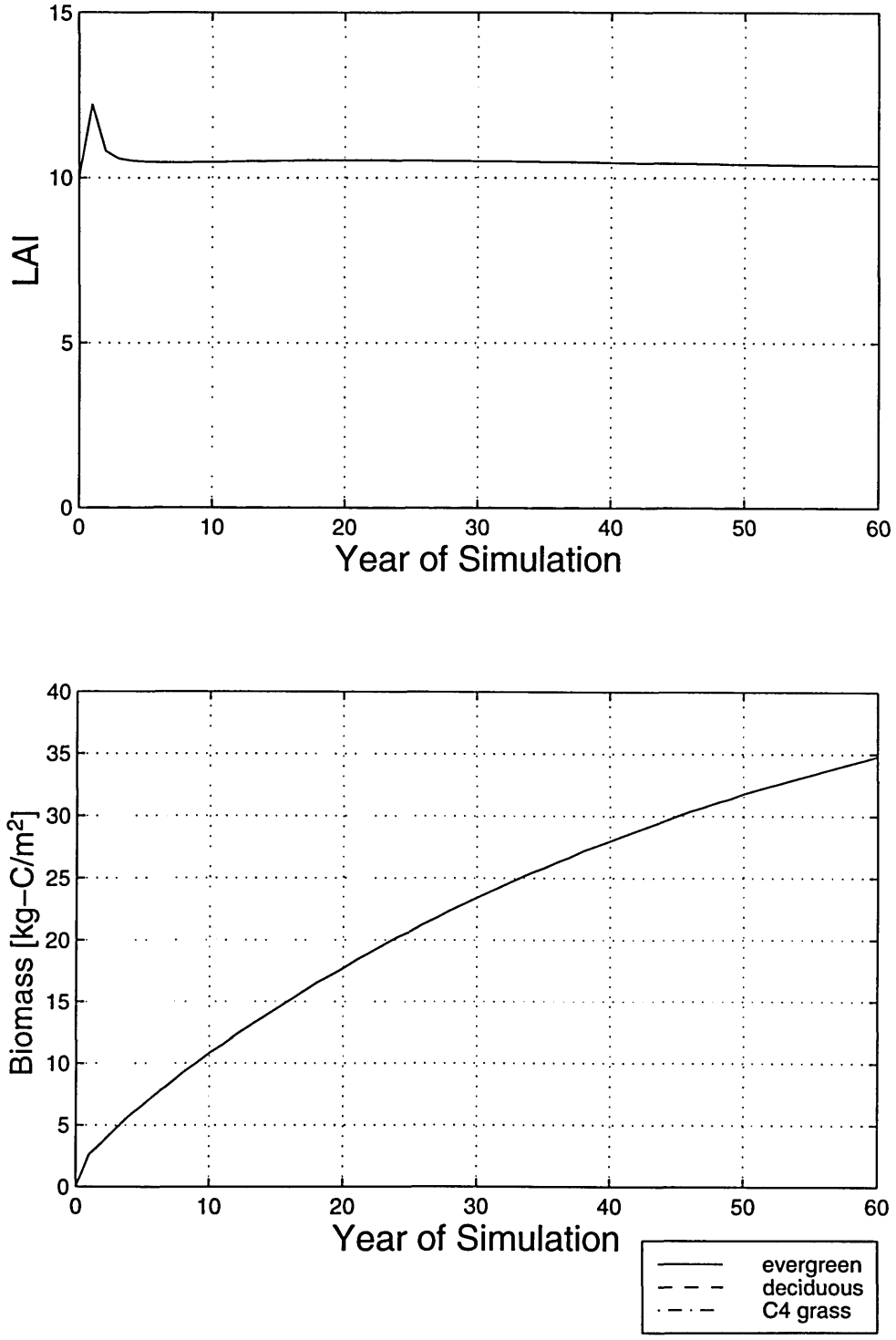

Figure 5-9: Coastal domain, fixed circulation control simulation. The upper panel shows the LAI, which is stable throughout the run. The lower panel shows the biomass, which has not yet stabilized.

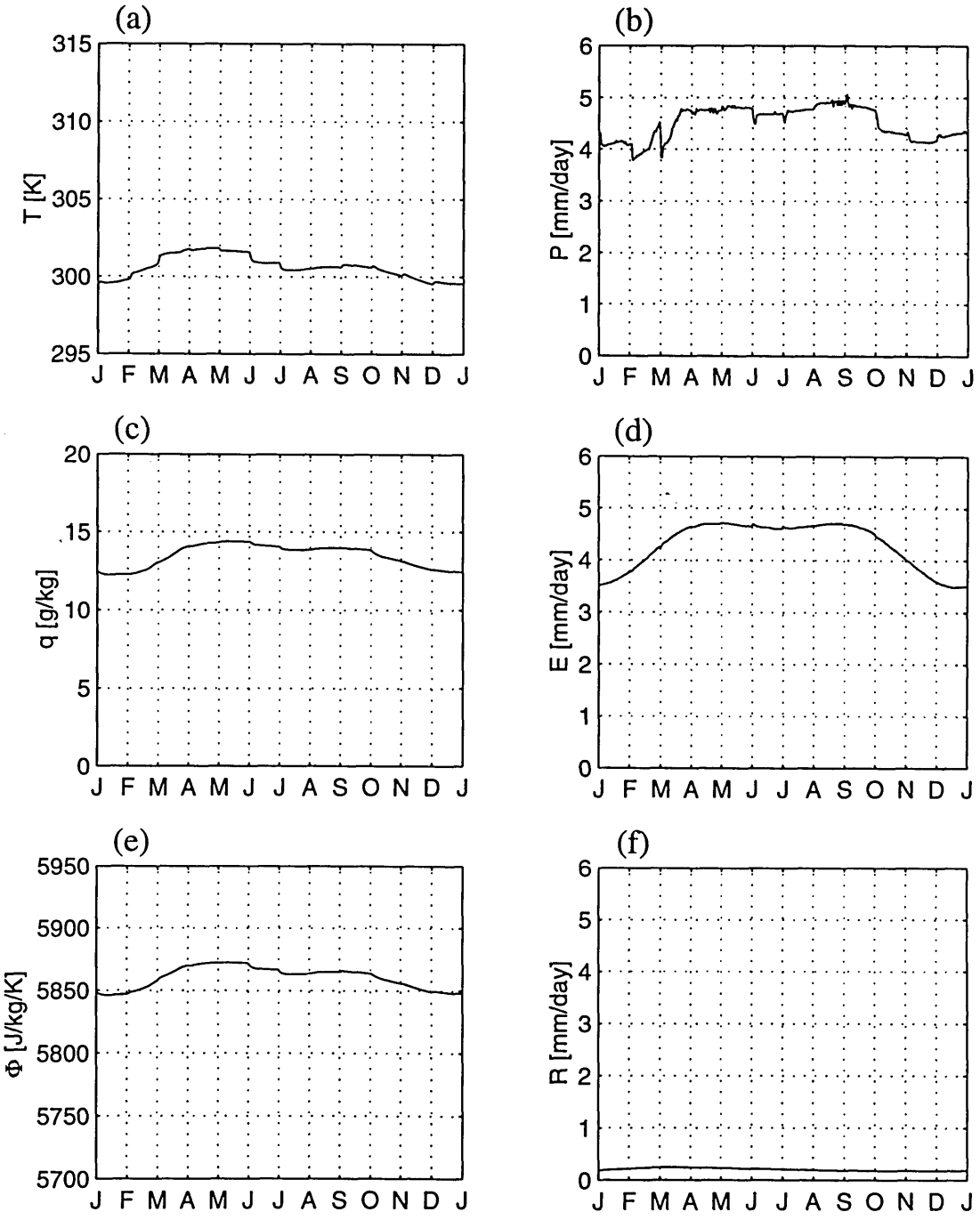

Figure 5-10: Coastal domain: interactive circulation control simulation, seasonal cycle of simulated climate. (a) Temperature (b) Precipitation (c) Specific humidity (d) Total evapotranspiration (e) Boundary layer entropy (f) Runoff

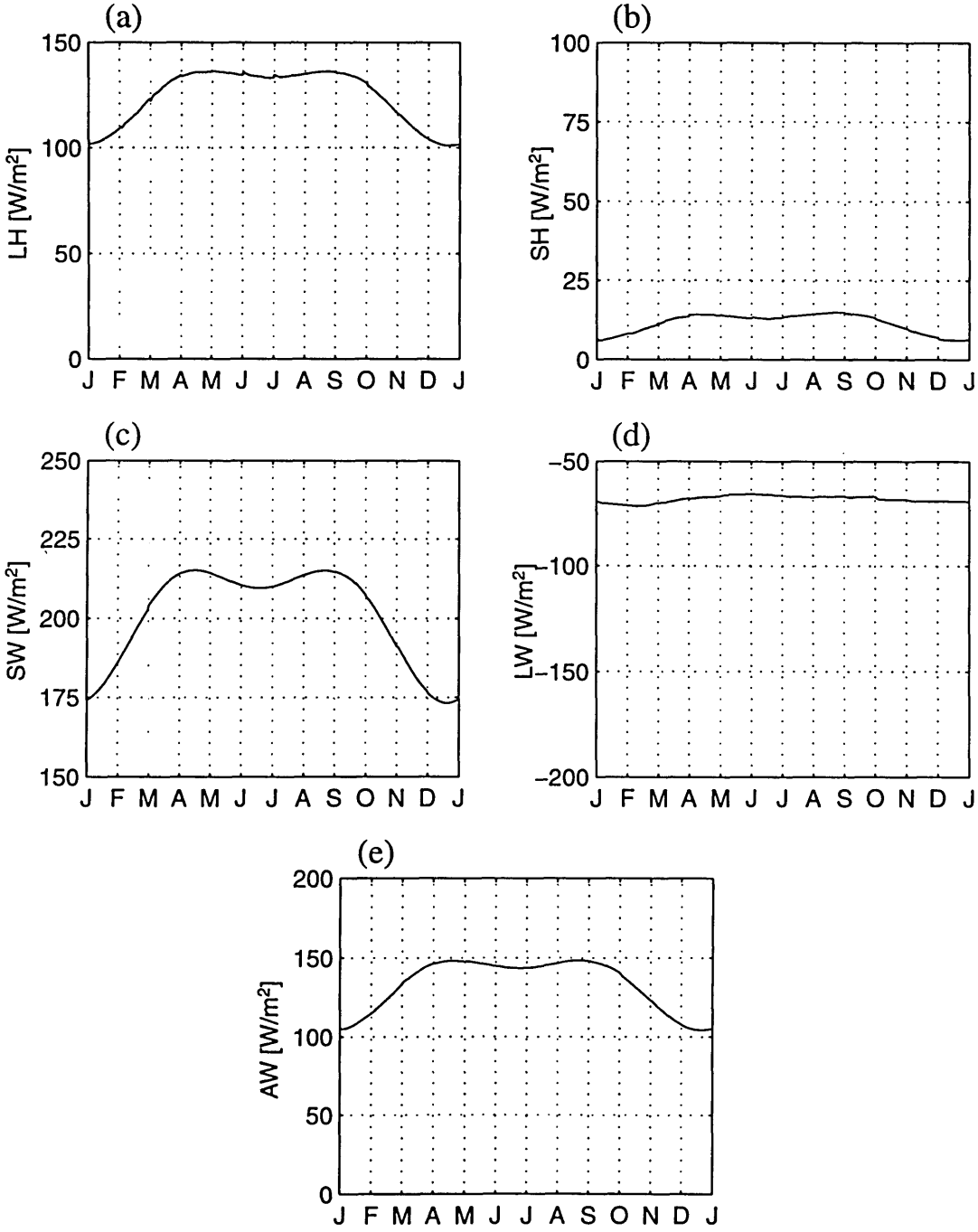

Figure 5-11: Coastal domain: interactive circulation control simulation, land-atmosphere energy exchange. (a) Latent heat flux (b) Sensible heat flux (c) Net shortwave radiative flux (d) Net longwave radiative flux (e) Net allwave radiative flux

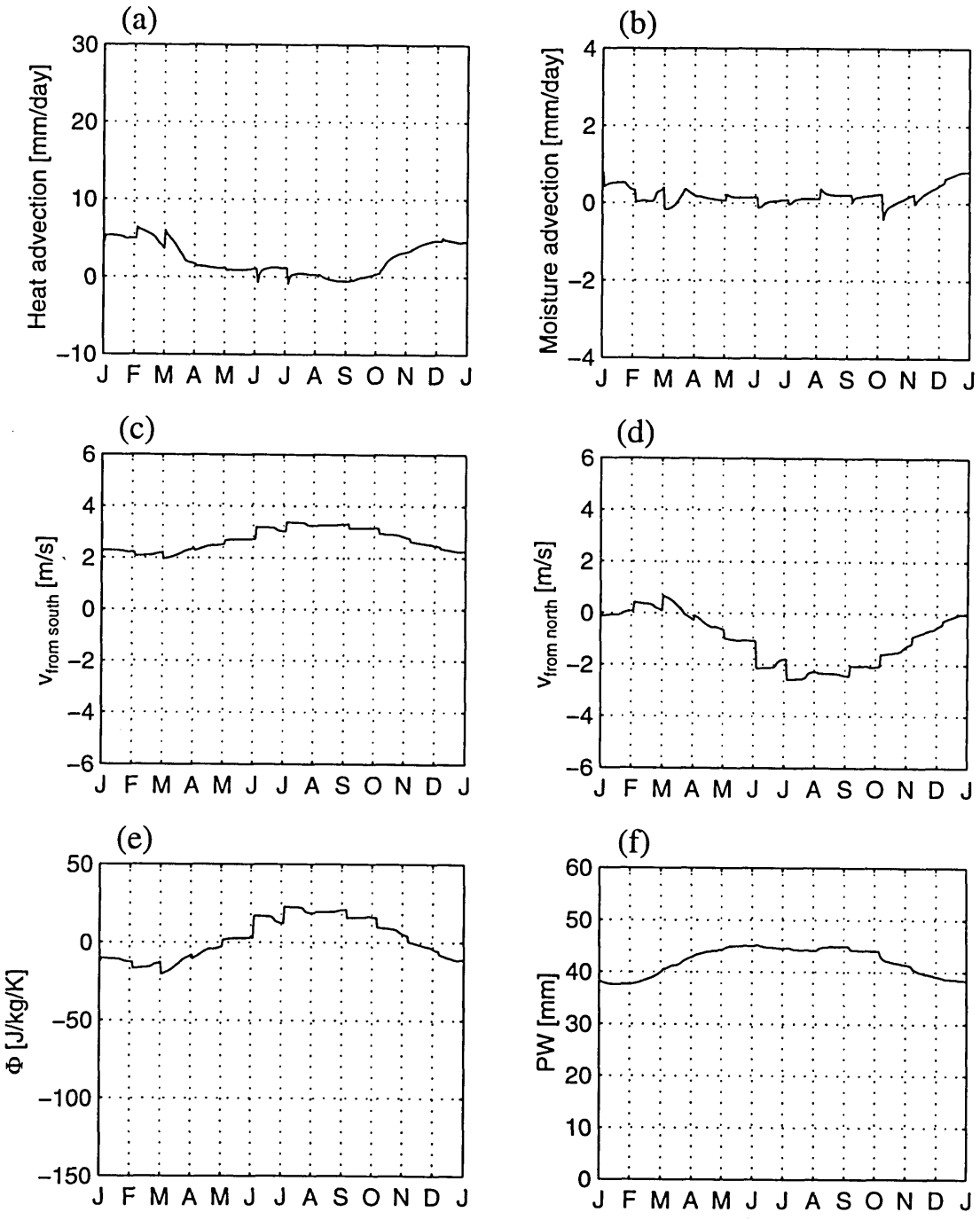

Figure 5-12: Coastal domain: interactive circulation control simulation, monsoon circulation. (a) Heat advection (b) Moisture advection (c) Lowest level wind across southern boundary (d) Lowest level wind across northern boundary (e) Entropy difference between model domain and ocean region (f) Precipitable water

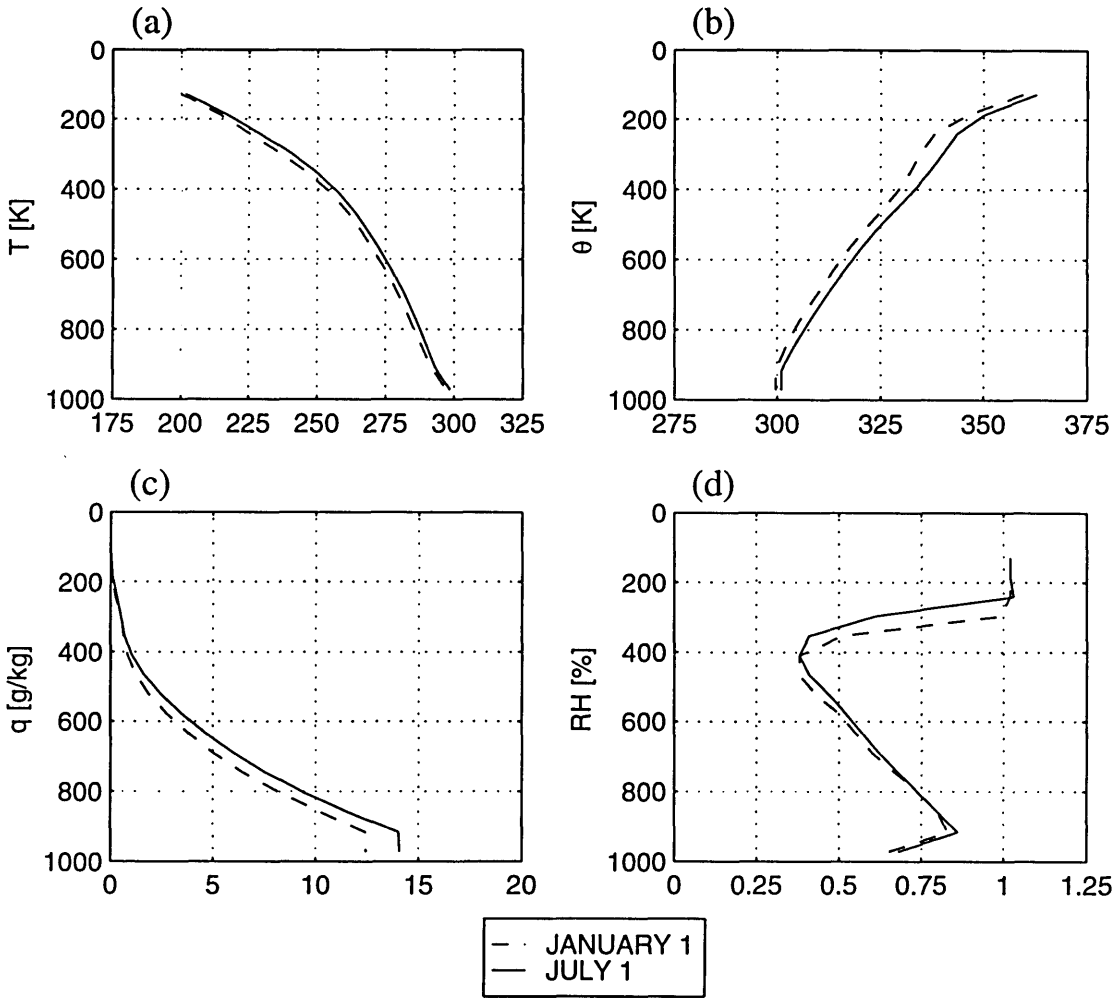

Figure 5-13: Coastal domain: interactive circulation control simulation, atmospheric soundings. (a) Absolute temperature (b) Potential temperature (c) Specific humidity (d) Relative humidity

Table 5.2: Coastal Domain: Sensitivity to Mixed Layer Depth

Variable	56mb Mixed Layer	113mb Mixed Layer	169mb Mixed Layer
T [K]	300.2	300.8	302.0
q [g/kg]	14.1	13.4	12.7
Precip [mm/day]	4.7	4.5	5.0
Evap [mm/day]	4.1	4.3	4.7
Runoff [mm/day]	0.6	0.3	0.3
Latent Heat [W/m2]	118	123	134
Sensible Heat [W/m2]	18	16	8
Net Solar [W/m2]	202	201	201
Net Longwave [W/m2]	-69	-65	-62
Net Allwave [W/m2]	133	136	139

lower two layers, and the 169 mb mixed layer simulation uses the lowest three layers.

As seen in Table 5.2 increasing the depth of the mixed layer warms and dries the surface. As air of higher potential temperature higher in the atmosphere is mixed into the surface mixed layer, it becomes warmer. In addition, air from above the boundary layer has lower moisture content, and mixing it into the surface layer has a drying effect. There is essentially no impact of the mixed layer depth on the surface radiation balance, and small, but apparently non-linear effects on the remaining surface energy fluxes and on precipitation.

A mixed layer depth of 113 mb was selected for our control and experimental simulations as the best approximation for the mixed layer depth over forest.

5.1.4 Sensitivity to modifications in land surface model

As described in Chapter 4, we modified IBIS to incorporate representation of spatial variability in two processes - interception storage and bare soil evaporation. The effects of these modifications depend upon the temporal characteristics of the precipitation at the land surface. Table 5.3 and Table 5.4 show the sensitivity of the mean annual climate in our coupled model to these modifications. They are consistent

Table 5.3: Fixed evergreen forest with and without modifications for subgrid variability in interception storage and bare soil evaporation.

Variable	Standard	Modified Interception	Modified Soil Evaporation	Modified Both
T [K]	299.9	300.6	299.9	300.5
q [g/kg]	13.9	13.5	13.9	13.5
Precipitation [mm/day]	5.3	4.7	5.3	4.7
Total Evaporation [mm/day]	5.3	4.4	5.2	4.5
Interception Loss [mm/day]	4.1	1.1	4.1	1.2
Transpiration [mm/day]	1.2	3.1	1.3	3.4
Soil Evaporation [mm/day]	0.0	0.3	-0.1	-0.1
Runoff [mm/day]	0.0	0.3	0.0	0.2
Latent Heat [W/m2]	152	128	152	129
Sensible Heat [W/m2]	-3	13	-3	12
Net Solar [W/m2]	201	201	201	201
Net Longwave [W/m2]	-56	-63	-56	-63
Net Allwave [W/m2]	145	138	145	138

with the sensitivities for the standalone IBIS simulations discussed in Section 4.2 and help to moderate rates of interception loss and bare soil evaporation.

In Table 5.3 we see that over forest, using the original IBIS representation of interception storage, interception loss accounts for about three quarters of the total evapotranspiration. By including representation of spatial variability in interception storage, interception loss is reduced to about one quarter of the total evapotranspiration. Bare soil evaporation contributes only a small fraction to the total evapotranspiration, and this is unaltered by the modifications to the soil evaporation. Negative values indicate dew formation.

In Table 5.4 we see that changes in the interception scheme also affected the partitioning of evaporation over grassland. Interception loss was reduced by almost 2 mm/day, and both transpiration and soil evaporation increase as a result. The high rate of soil evaporation is reduced when spatial variability in soil evaporation is taken into account.

Table 5.4: Fixed grassland with and without modifications for subgrid variability in interception storage and bare soil evaporation.

Variable	Unmodified	Modified Interception	Modified Soil Evaporation	Modified Both
T [K]	300.3	300.6	300.5	301.0
q [g/kg]	12.9	12.7	12.7	12.4
Precipitation [mm/day]	4.0	3.9	3.8	3.5
Total Evaporation [mm/day]	4.0	3.8	3.8	3.4
Interception Loss [mm/day]	2.5	0.4	2.7	0.4
Transpiration [mm/day]	0.8	1.9	1.1	2.2
Soil Evaporation [mm/day]	0.7	1.5	-0.1	0.7
Runoff [mm/day]	0.0	0.1	0.0	0.2
Latent Heat [W/m2]	117	110	109	97
Sensible Heat [W/m2]	5	12	7	17
Net Solar [W/m2]	189	189	189	189
Net Longwave [W/m2]	-69	-69	-74	-77
Net Allwave [W/m2]	120	120	115	112

5.2 Deforestation Experiments: Fixed Circulation Case

In these experiments we test the sensitivity of the equilibrium climate and vegetation to perturbations to the initial vegetation state. We first simulate conditions with fixed vegetation, to test the sensitivity of the climate to changes at the land surface. Then, vegetation and climate are allowed to interact and through that interaction find their own equilibrium state.

In this experiment, the effects of vegetation changes are limited to those induced by changes in the surface-atmosphere fluxes, and the resulting differences in partitioning of water and energy at the land surface. This experiment tests the degree to which these effects by themselves can affect the local equilibrium between vegetation and climate. Any effects on the large-scale circulation are eliminated by fixing the horizontal fluxes of air at their climatological values. However, while the magnitude

of the fluxes of air are held constant, the horizontal moisture and heat advection depend not only on the magnitude of the fluxes, but also on the difference between the properties in the climatological profile of advected air and the model domain. Thus, the moisture and heat convergence can change with changes in the model atmosphere.

5.2.1 Static vegetation simulations

Table 5.5 shows the equilibrium climate for the climatological control simulation (forest vegetation) described earlier and a sensitivity run in which we hold the vegetation fixed as grassland. Figure 5-14 to Figure 5-17 show the seasonal cycle of the simulated climate when vegetation is held fixed as grassland. We see that while the change in vegetation cover does affect the local climate, the effects are small. Precipitation decreases by only 0.3 mm/day, and evaporation by only 0.4 mm/day. Temperature decreases by 0.4 K and the specific humidity is reduced by 0.2 g/kg. An increase in surface albedo decreases the absorbed solar radiation at the surface by 13 W/m2.

Table 5.6 shows the results of other numerical simulations of tropical deforestation as compared to the results of our simulation. Each of the other studies deals with deforestation of the Amazon basin, which as well as being located in a different region of the world, experiences less seasonality and more rainfall than West Africa. The following comparisons to these studies, then, must be made with some caution. Unlike most experimental work on Amazonian deforestation, our temperature is reduced by deforestation. The observed increase in surface temperature in clearings is due primarily to reduced evaporation and latent cooling, which counteracts the cooling effects of reduced net radiation at the surface. Our model shows only a moderate decrease in evaporation of 0.4 mm/day. Thus, there is only a small change in latent cooling to offset the 16 W/m^2 reduction in net allwave radiation at the surface. Consequently, temperature goes down, rather than up in our model simulations.

Zheng and Eltahir (1998) use a zonally symmetric model of West Africa with a simple land surface scheme to simulate deforestation from 5N-15N in West Africa.

Table 5.5: Coastal Domain: Modelled Forest vs. Grassland

Variable	Climatological Fluxes		Flux Relation	
	Forest	Grass	Forest	Grass
T [K]	301.9	301.5	300.6	301.0
q [g/kg]	12.6	12.4	13.5	12.4
Precipitation [mm/day]	3.4	3.1	4.5	3.5
Total Evaporation [mm/day]	3.4	3.0	4.3	3.4
Interception Loss [mm/day]	1.1	0.5	1.2	0.4
Transpiration [mm/day]	2.3	2.0	3.2	2.2
Soil Evaporation [mm/day]	0.0	0.6	-0.1	0.7
Runoff [mm/day]	0.0	0.1	0.2	0.2
Latent Heat [W/m2]	98	88	125	97
Sensible Heat [W/m2]	30	24	12	17
Net Solar [W/m2]	202	189	201	189
Net Longwave [W/m2]	-76	-79	-68	-77
Net Allwave [W/m2]	126	110	133	112

Their simulation showed a more substantial decrease in summertime precipitation (on the order of one half of their control simulation) than is seen in our simulation. Local effects alone, then, do not seem to produce a magnitude of climatic change similar to previous work on the topic.

5.2.2 Dynamic vegetation simulations

In the experimental run, the initial vegetation is set to grassland and the model finds its own vegetation-climate equilibrium. In this simulation, the initial grassland vegetation quickly gives way to forest. As seen in Figure 5-18 and Figure 5-19, the grass has died by the end of year 10 and forest is well established. After 10 years, the LAI and NPP have stabilized at the same values seen in the equilibrium state of the control simulation, which was initialized with deciduous forest vegetation. In both simulations, biomass is still accumulating at the end of 60 years. The large spike in grass LAI at the beginning of the simulation is due to the error in biomass initialization. The initial biomass is small, allowing high NPP during the first few

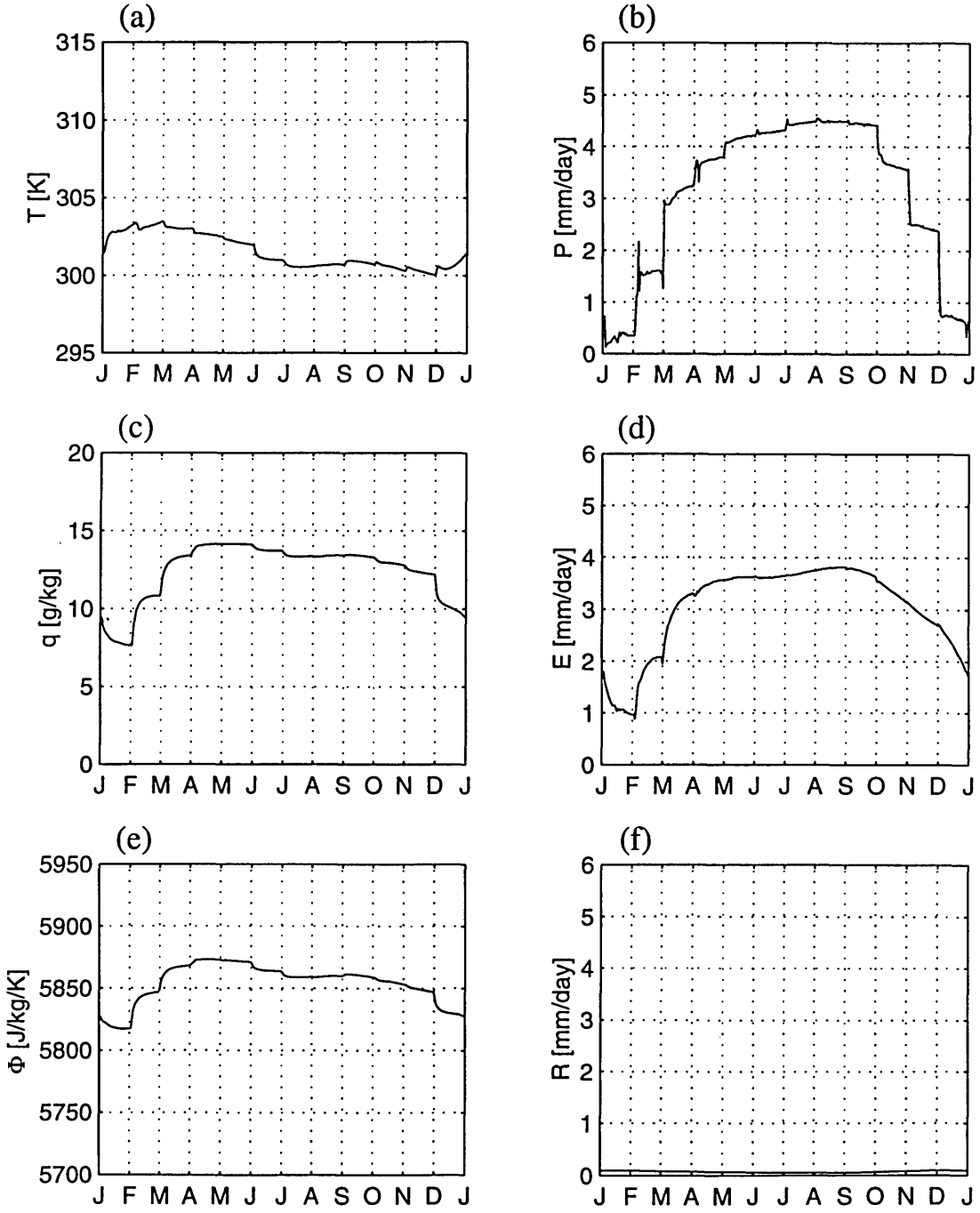

Figure 5-14: Coastal domain: fixed circulation fixed grass simulation, seasonal cycle of simulated climate. (a) Temperature (b) Precipitation (c) Specific humidity (d) Total evapotranspiration (e) Boundary layer entropy (f) Runoff

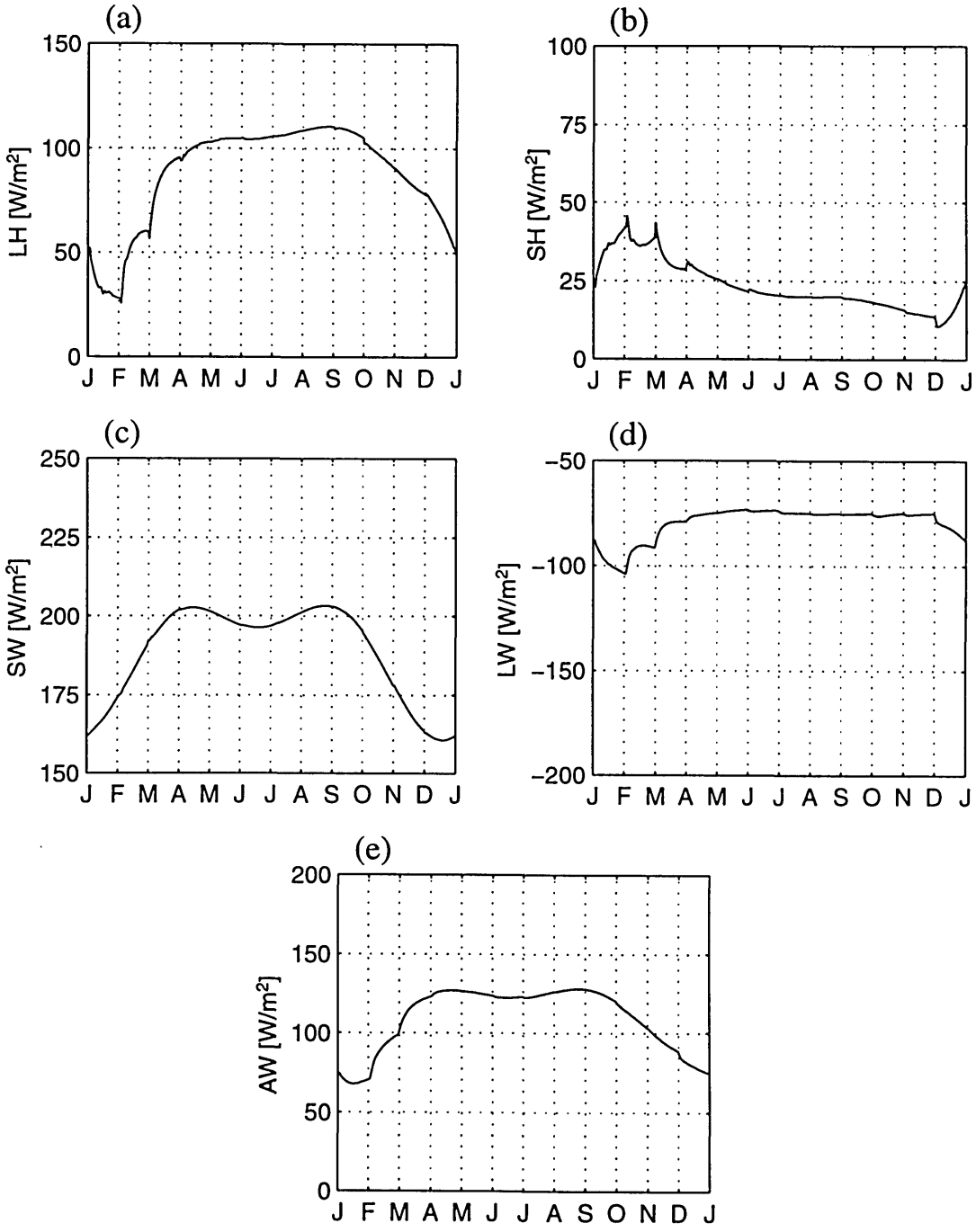

Figure 5-15: Coastal domain: fixed circulation fixed grass simulation, land-atmosphere energy exchange. (a) Latent heat flux (b) Sensible heat flux (c) Net shortwave radiative flux (d) Net longwave radiative flux (e) Net allwave radiative flux

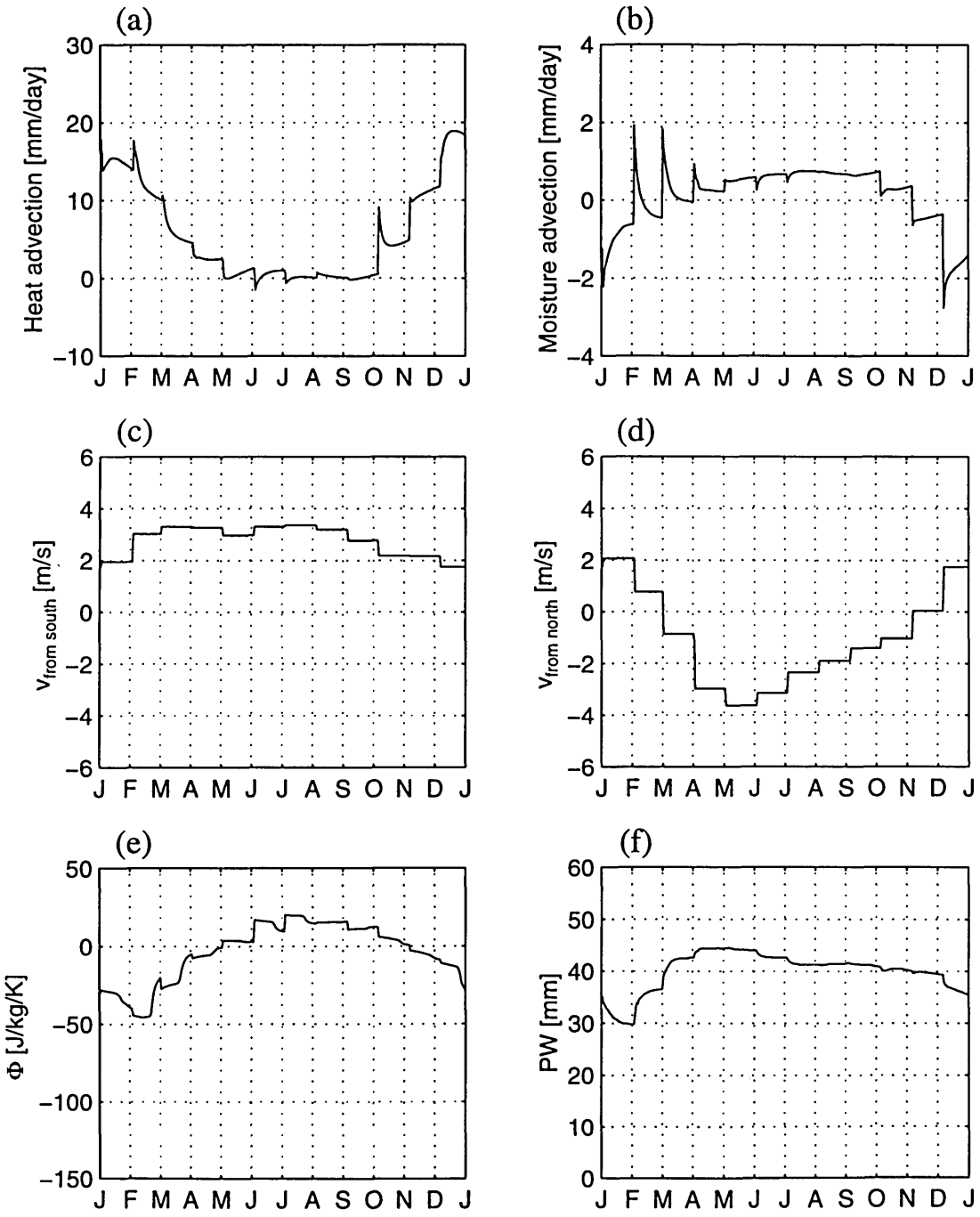

Figure 5-16: Coastal domain: fixed circulation fixed grass simulation, monsoon circulation. (a) Heat advection (b) Moisture advection (c) Lowest level wind across southern boundary (d) Lowest level wind across northern boundary (e) Entropy difference between model domain and ocean region (f) Precipitable water

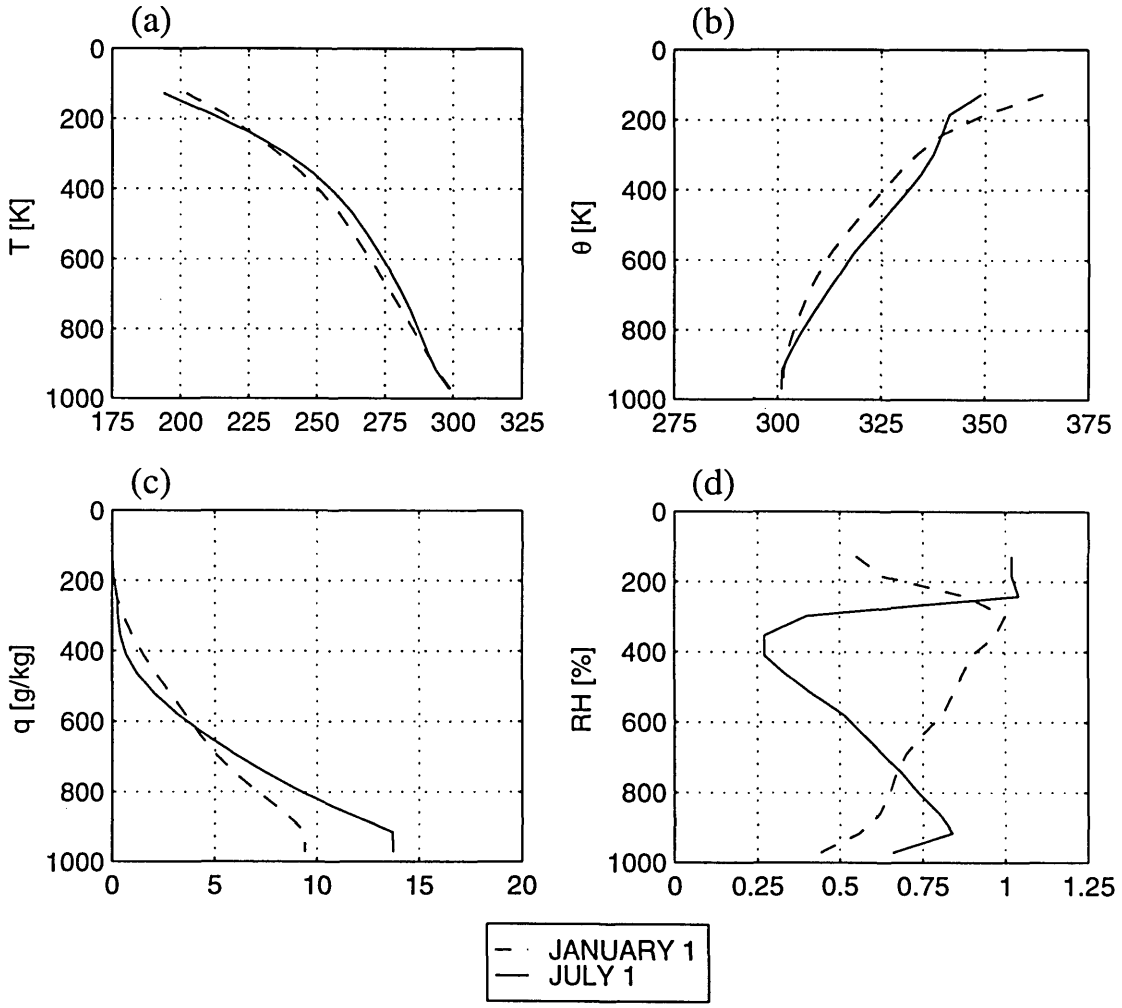

Figure 5-17: Coastal domain: fixed circulation fixed grass simulation, atmospheric soundings. (a) Absolute temperature (b) Potential temperature (c) Specific humidity (d) Relative humidity

Table 5.6: Coastal Domain: Modelled Forest vs. Grassland, Compared to Previous Modeling Studies of Amazonian Deforestation. While strict comparisons should not be made due to the different locations of these studies, we can note that in almost all cases the sign of the changes in the listed variables are the same in our experiments and in the Amazonian deforestation experiments.

Study	ΔT [K]	ΔP [mm/day]	ΔE [mm/day]	ΔRn [W/m2]
Lean and Warrilow (1989)	+2.0	-1.3	-0.6	n/a
Shukla, Nobre and Sellers (1990)	+2.5	-1.8	-1.4	-26
Dickinson and Kennedy (1992)	+0.6	-1.4	-0.1	n/a
Henderson-Sellers et. al. (1993)	+0.6	-1.6	-0.6	n/a
Eltahir and Bras (1994)	+0.7	-0.4	-0.6	-13
Lean and Rowntree (1997)	+2.3	-0.3	-0.8	n/a
This Experiment (fixed circulation)	-0.4	-0.3	-0.4	-16
This Experiment (variable circulation)	+0.4	-1.0	-0.9	-21

years of the simulation. However, as this makes grass more, and not less productive, it is not expected to alter the results of this experiment. The biomass initialization problem is discussed further in Appendix A.

A stable equilibrium is not unexpected for this experiment as only small changes in the simulated climate result from the change in vegetation cover (deforestation). Not unexpectedly, these small changes do not result in a different equilibrium climate and vegetation. In particular, there is only a small decrease in precipitation. Water is the limiting resource in the tropics, and the decrease in precipitation is not enough to restrict the growth and survival of trees. As a result, both vegetation and climate recover after an initial perturbation to the vegetation cover and return to the equilibrium state of the control climate.

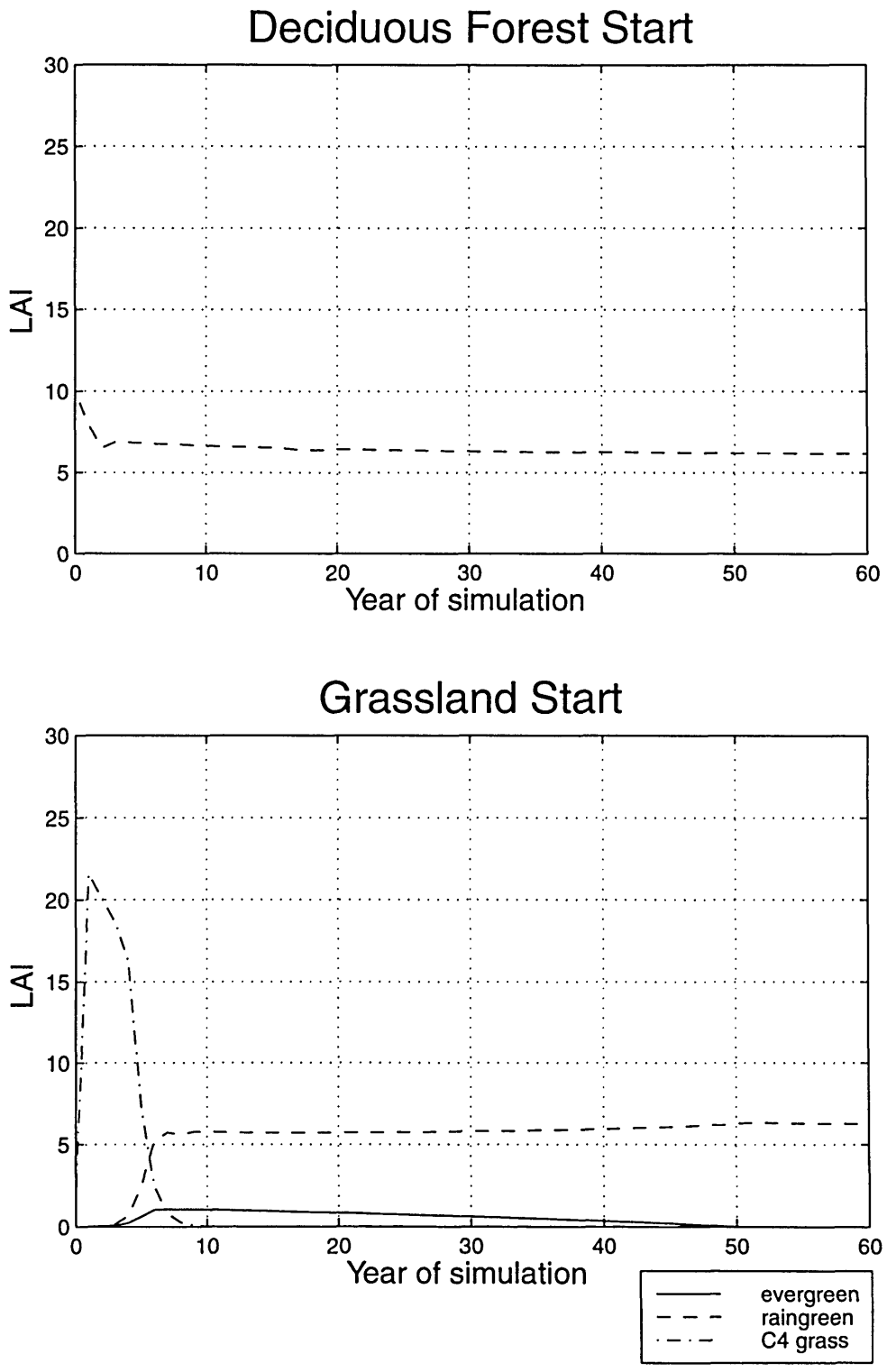

Figure 5-18: Coastal domain, fixed circulation simulations. Vegetation is initialized as either deciduous forest or grassland. The equilibrium vegetation LAI is the same in either case.

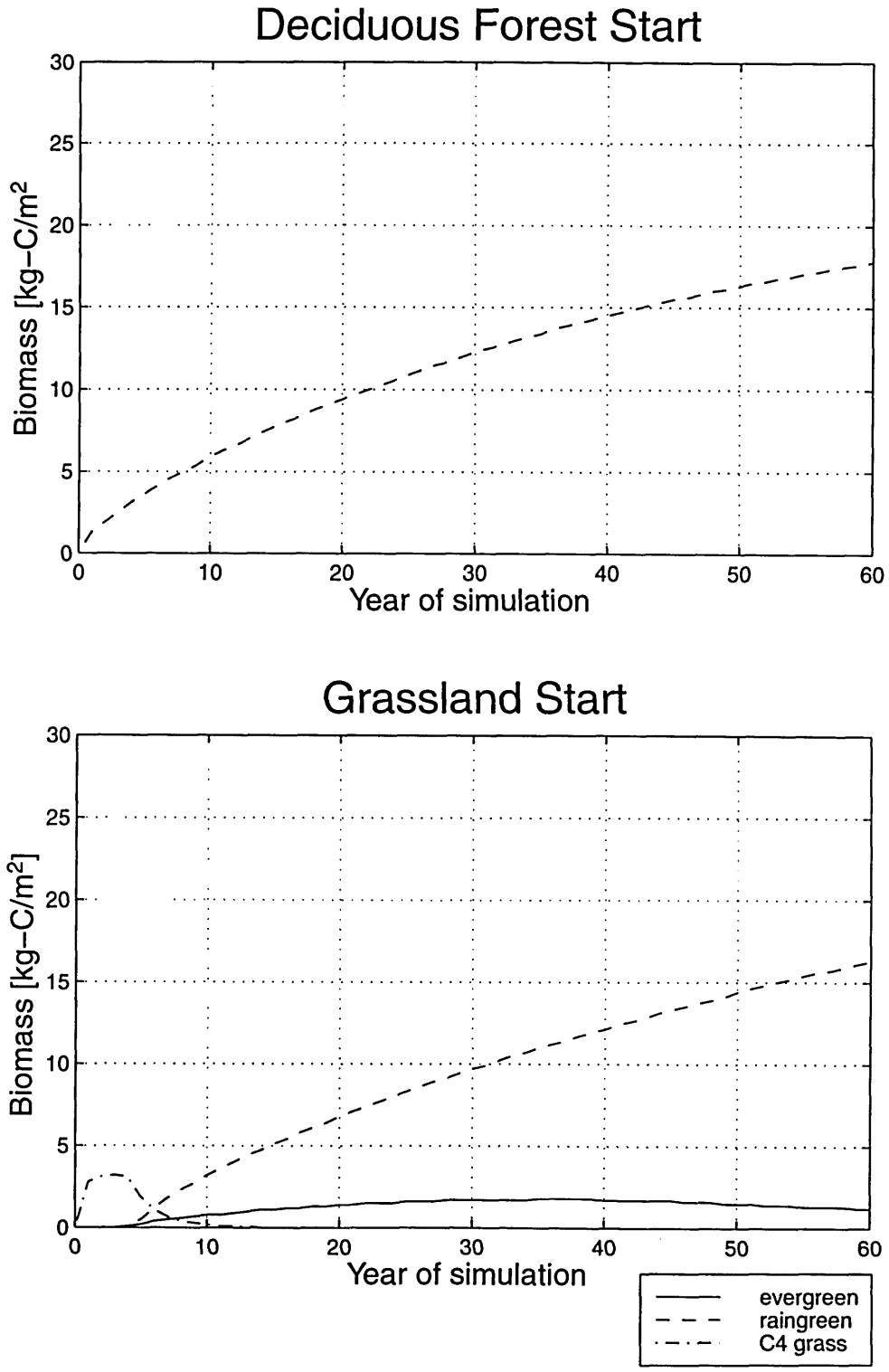

Figure 5-19: Coastal domain, fixed circulation simulations. The equilibrium biomass approaches the same value whether the simulation is initialized as deciduous forest or grassland.

5.3 Deforestation experiments: Interactive Circulation Case

In these experiments, we test the sensitivity of the equilibrium vegetation and climate to changes in initial vegetation when the monsoon circulation is allowed to vary with changing conditions in the model domain. In these simulations, vegetation affects not only the local water and energy balance, but also the strength of the monsoon circulation.

5.3.1 Static vegetation simulations

Table 5.5 shows the sensitivity of the climate to a change in the vegetation. The equilibrium climate of the variable flux control simulation (evergreen forest) are compared to the climate of a simulation in which vegetation is held fixed as grassland. We see more pronounced differences between these two simulations than were seen in the experiment using climatological fluxes of air. Precipitation decreases by 1.0 mm/day, and evaporation by 0.9 mm/day. Temperature increases by 0.4 K and specific humidity decreases by 1.1 g/kg. The net solar radiation is reduced by 12 W/m^2 and the net longwave radiation by 9 W/m^2 for a total reduction in allwave radiation of 21 W/m^2. These changes are more similar to the changes seen in studies of Amazonian deforestation shown in Table 5.6 than were the changes seen in the fixed circulation simulations. The reduction in precipitation is still smaller than that simulated by Zheng and Eltahir (1998).

Figure 5-20 to Figure 5-23 show the seasonality of the fixed grassland climate. There is enhanced drying in the winter, which is related to changes in the monsoon circulation. Because of reduced entropy in the model domain, the monsoons do not penetrate as far inland in the winter, and there are greater fluxes of hot and dry air from the north into the model domain. This tends to perpetuate the already warmer and drier climate.

The enhanced sensitivity to land cover as compared to the fixed circulation

experiments suggests that interaction with the surrounding regions is quite important in determining the climate of a region.

5.3.2 Dynamic vegetation simulations

The model was initialized with grassland and allowed to find its own equilibrium vegetation and climate in this experimental simulation. As with the fixed circulation experiment, while the changes in vegetation cover affect the climate, the changes are not sufficient to prevent the forest of the control simulation from re-establishing itself. The development of LAI and biomass over the length of the simulation are shown in Figure 5-24 and Figure 5-25. While the biomass has not yet stabilized, the equilibrium vegetation is clearly forest. The equilibrium climate and vegetation are the same in both the simulation initialized with grassland vegetation and the simulation initialized with forest vegetation.

5.4 Sensitivity of Results to Slope of Empirical Flux Relationships

In these simulations, we test the sensitivity of our results to the slope of the empirical function used to model the monsoon circulation. The sensitivities to both an increase and a decrease in the slope of the relationship are tested. When there is no difference in entropy between land and sea, we use the same value for the mass flux of air, but this mass flux either increases or decreases more rapidly as the entropy difference departs from zero. The radiative heating and cooling rates were updated only hourly in these simulations, to save computational time.

Table 5.7 shows the mean annual climate for simulations in which the slope of the flux relationship at one boundary (northern or southern) was modified. They will be referred to as simulation SouthX2, for the doubled slope at the southern boundary, simulation South÷2 for the halved slope at the southern boundary, simulation NorthX2, for the doubled slope at the northern boundary, and simulation North÷2,

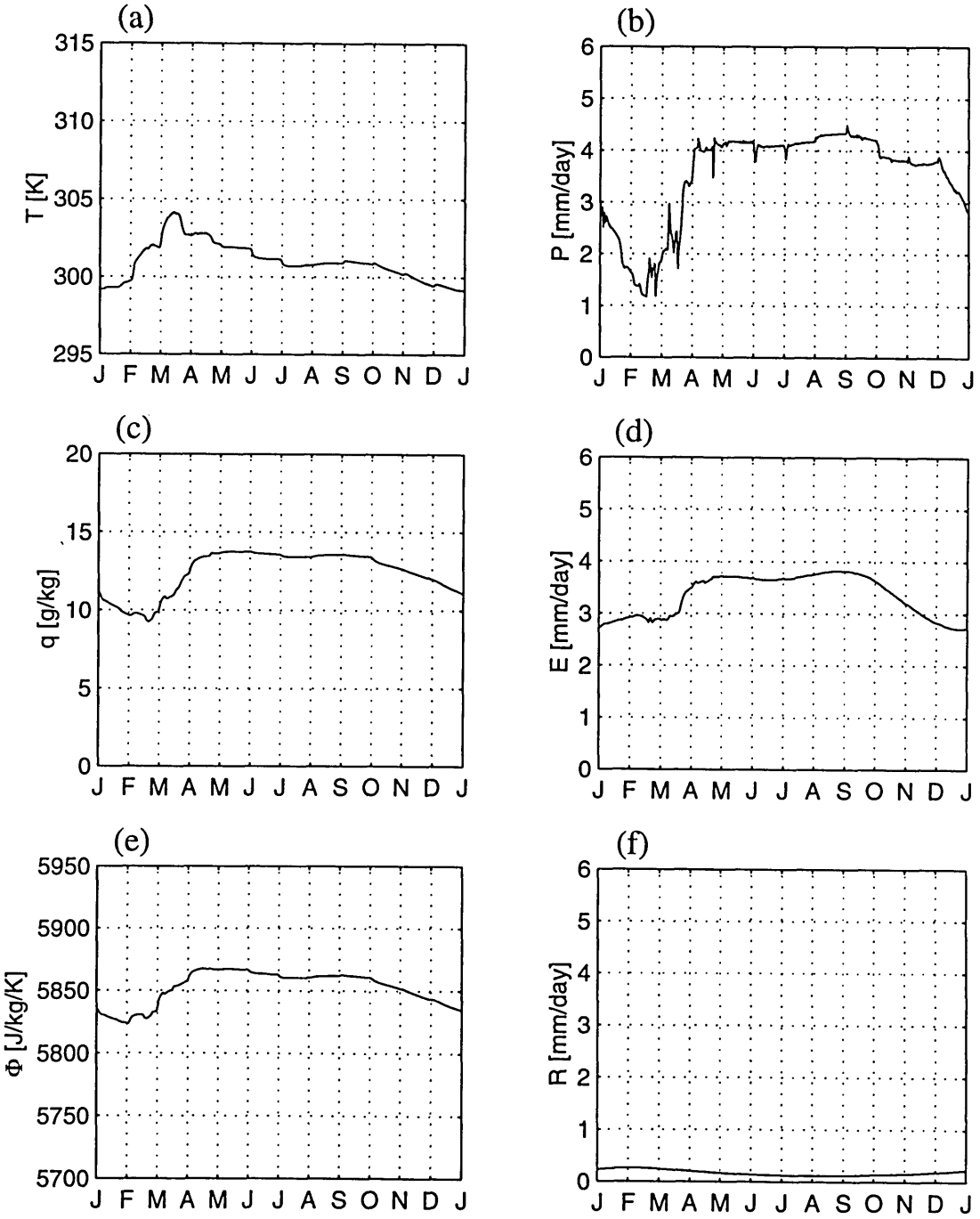

Figure 5-20: Coastal domain: interactive circulation fixed grass simulation, seasonal cycle of simulated climate. (a) Temperature (b) Precipitation (c) Specific humidity (d) Total evapotranspiration (e) Boundary layer entropy (f) Runoff

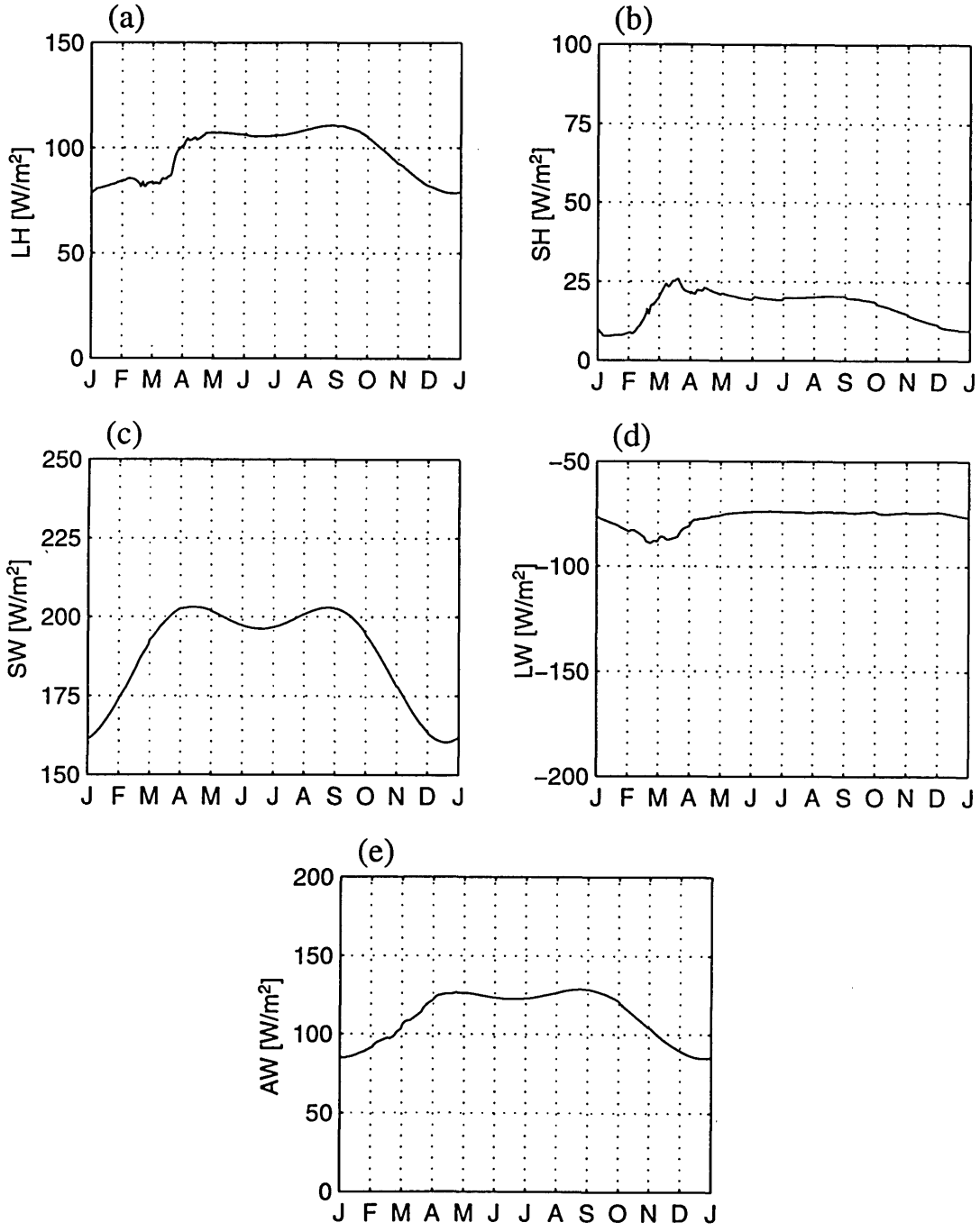

Figure 5-21: Coastal domain: interactive circulation fixed grass simulation, land-atmosphere energy exchange. (a) Latent heat flux (b) Sensible heat flux (c) Net shortwave radiative flux (d) Net longwave radiative flux (e) Net allwave radiative flux

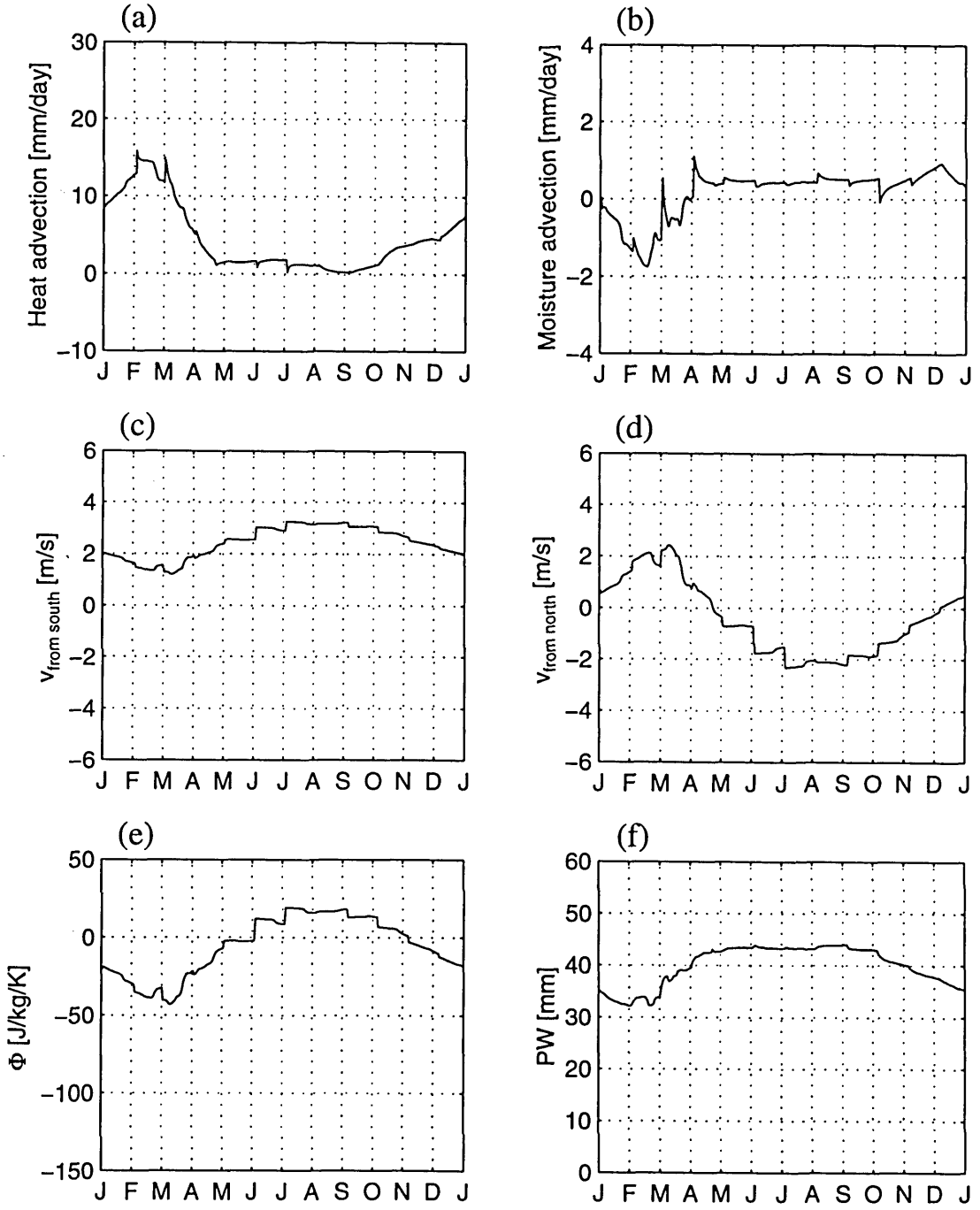

Figure 5-22: Coastal domain: interactive circulation fixed grass simulation, monsoon circulation. (a) Heat advection (b) Moisture advection (c) Lowest level wind across southern boundary (d) Lowest level wind across northern boundary (e) Entropy difference between model domain and ocean region (f) Precipitable water

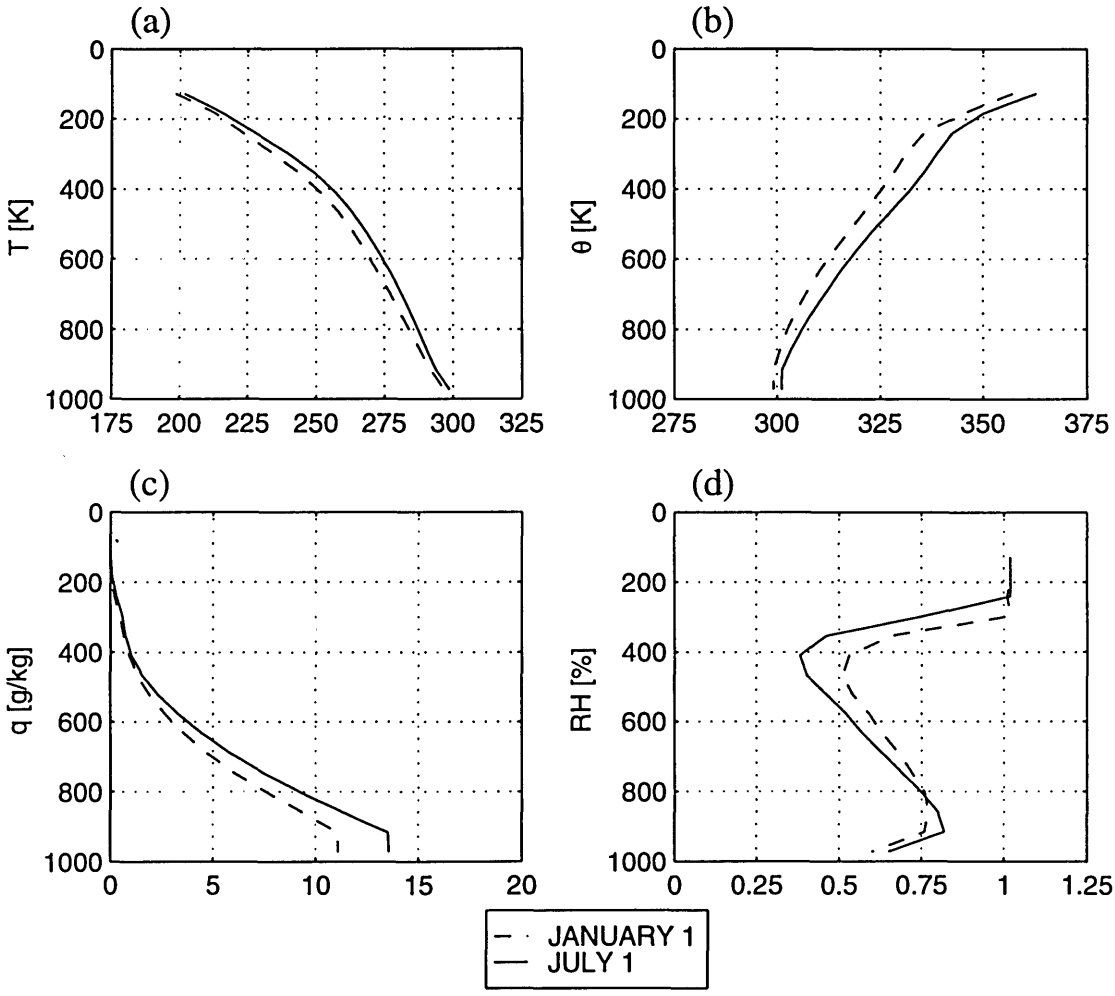

Figure 5-23: Coastal domain: interactive circulation fixed grass simulation, atmospheric soundings. (a) Absolute temperature (b) Potential temperature (c) Specific humidity (d) Relative humidity

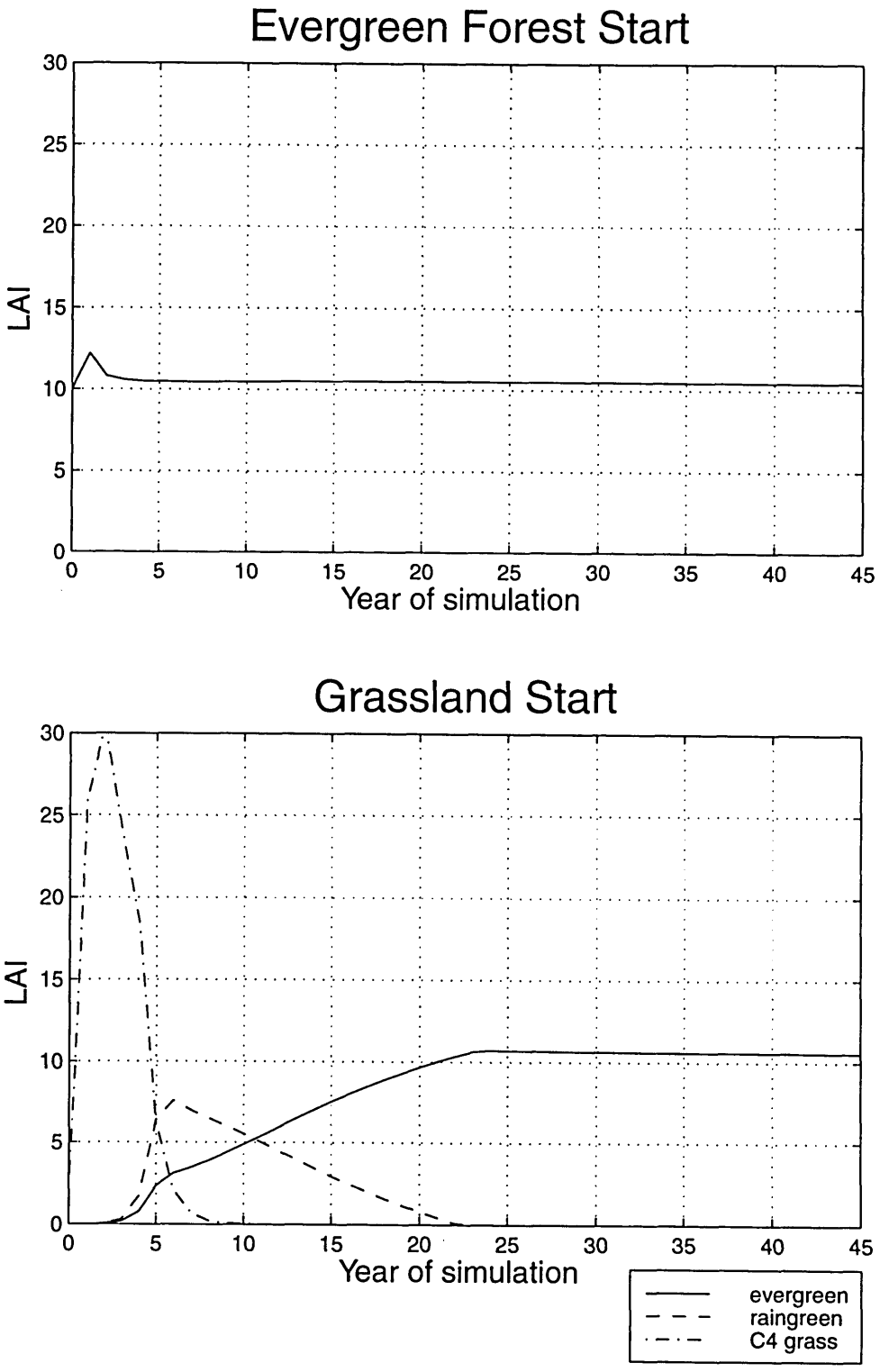

Figure 5-24: Coastal domain: Whether the initial vegetation is forest or grassland, the model simulates the same equilibrium vegetation and climate (evergreen forest), here represented by the leaf area index (LAI).

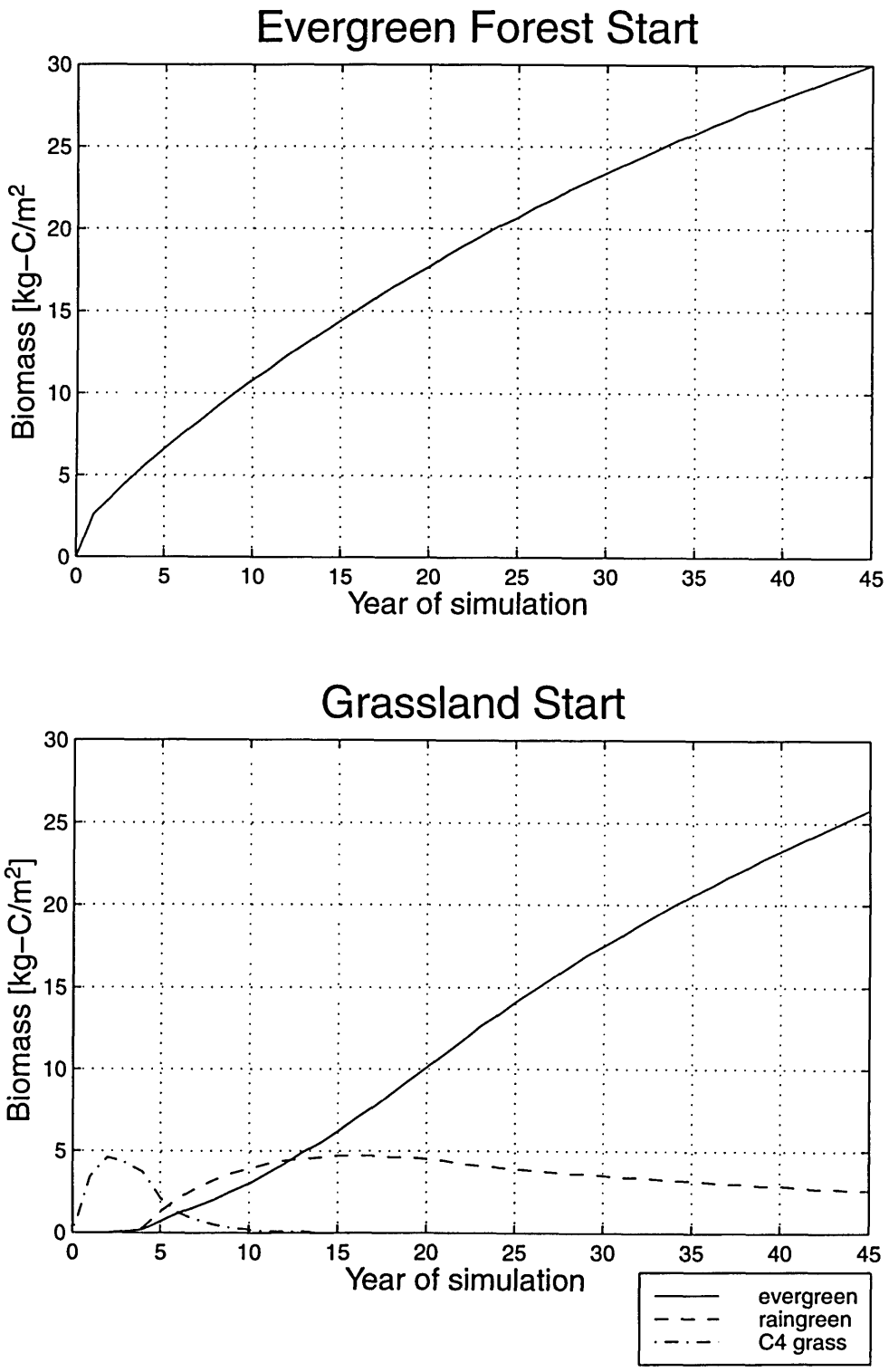

Figure 5-25: Coastal domain: The equilibrium biomass approaches the same value whether the simulation is initialized as forest or grassland.

for the halved slope at the northen boundary. As seen in the table, the changes from the control simulation are modest, except in simulation NorthX2, which showed a 25% drop in precipitation and 1.7K increase in temperature as compared to the interactive circulation control simulation.

Doubling the slope of the relationship for fluxes from the south increases the seasonality of the simulated climate, as can be seen in Figure 5-26 to Figure 5-28. The main differences seem to arise during the winter months, when less moisture is advected from the south, reducing the entropy of the model domain and allowing hot and dry air from the north to penetrate into the domain. By halving the slope of the flux relationship, the seasonality is flattened out (not shown). Due to similar reasoning, doubling the slope of the empirical relationship for fluxes from the north enhances the seasonality of the simulated climate (see Figure 5-29 to Figure 5-31). As seen in Figure 5-31, there is more penetration of hot and dry air from the north during the winter, sharply drying the atmosphere in those months. Conversely, by decreasing the slope, the seasonality is reduced due to diminished penetration of the dry winds (not shown).

Each of these simulations resulted in equilibrium forest vegetation. Except in simulation NorthX2, the large mean annual precipitation and flat seasonal distribution of rainfall was such that evergreen trees were the dominant plant type. In experiment NorthX2, the precipitation was reduced and seasonality enhanced to such a degree that deciduous forest became dominant.

5.4.1 Static vegetation simulations

The sensitivity of the climate simulated with a modified flux relationship to changes in vegetation was tested by holding grass fixed throughout a simulation until the climate reached equilibrium. Table 5.8 and Table 5.9 compare the mean annual climate for the simulated equilibrium forest and fixed grassland for SouthX2, South÷2, NorthX2, and North÷2.

The sensitivity of simulations SouthX2 and South÷2 to land cover is similar to that which was seen for the control simulation and associated sensitivity run.

Table 5.7: Coastal Domain: Sensitivity of forested domain to the slope of the empirical flux relationships.

Variable	Control	Flux relation for southern boundary		Flux relation for northern boundary	
		2XSlope (ever)	0.5XSlope (ever)	2XSlope (decid)	0.5XSlope (ever)
T [K]	300.6	300.8	300.7	302.3	300.6
q [g/kg]	13.5	12.8	13.6	12.1	13.5
Precipitation [mm/day]	4.5	4.1	4.6	3.4	4.5
Total Evaporation [mm/day]	4.3	4.1	4.3	3.4	4.3
Interception Loss [mm/day]	1.2	1.3	1.2	1.1	1.2
Transpiration [mm/day]	3.2	2.9	3.2	2.2	3.2
Soil Evaporation [mm/day]	-0.1	-0.1	-0.1	0.0	-0.1
Runoff [mm/day]	0.2	0.0	0.2	0.0	0.2
Latent Heat [W/m2]	125	118	125	98	124
Sensible Heat [W/m2]	12	16	12	28	12
Net Solar [W/m2]	201	202	202	202	202
Net Longwave [W/m2]	-68	-70	-68	-78	-68
Net Allwave [W/m2]	126	132	134	134	134
Entropy Difference [J/kg/K]	-1.4	-2.9	3.0	-4.8	2.2

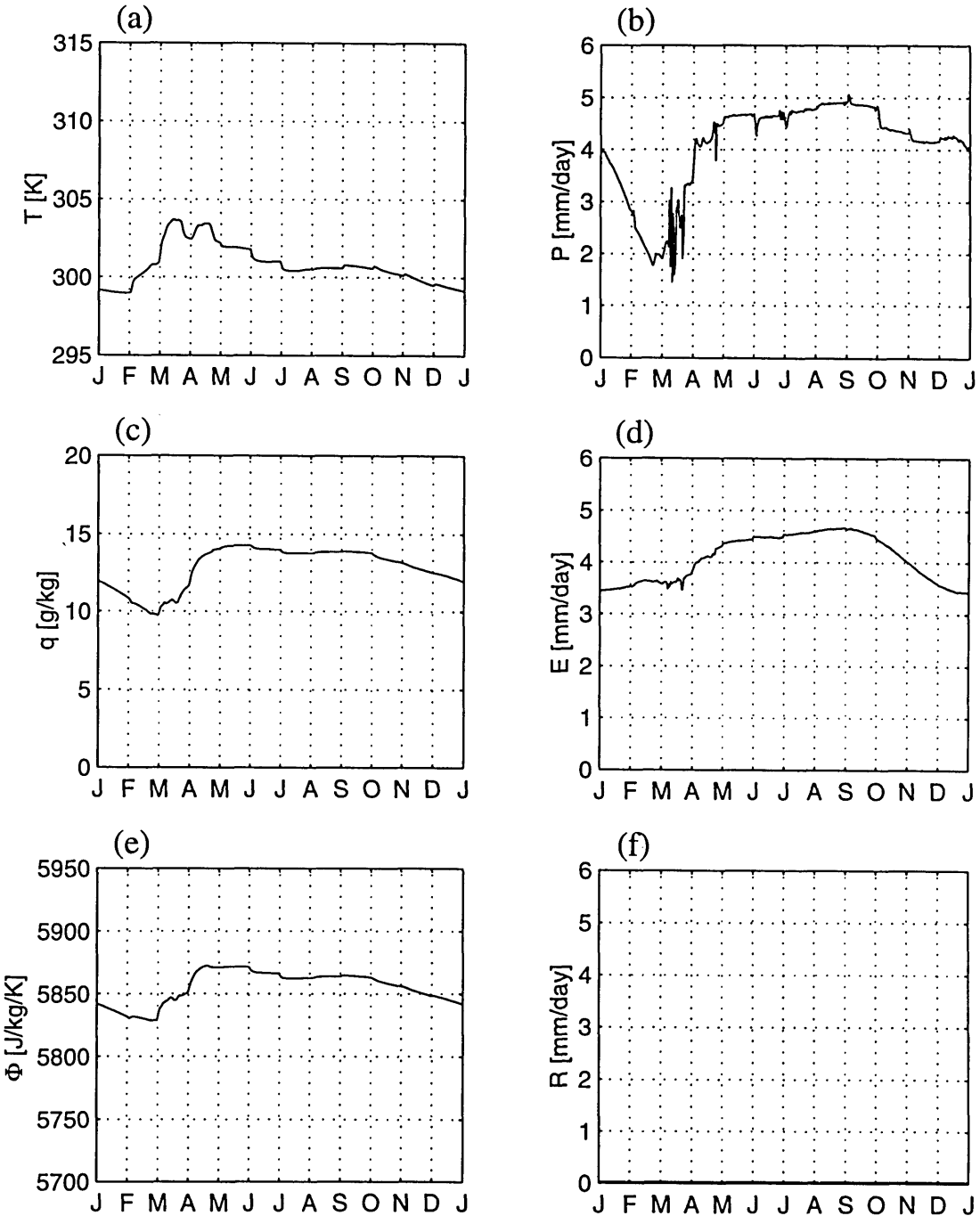

Figure 5-26: Coastal domain: SouthX2, seasonal cycle of simulated climate. (a) Temperature (b) Precipitation (c) Specific humidity (d) Total evapotranspiration (e) Boundary layer entropy (f) Runoff

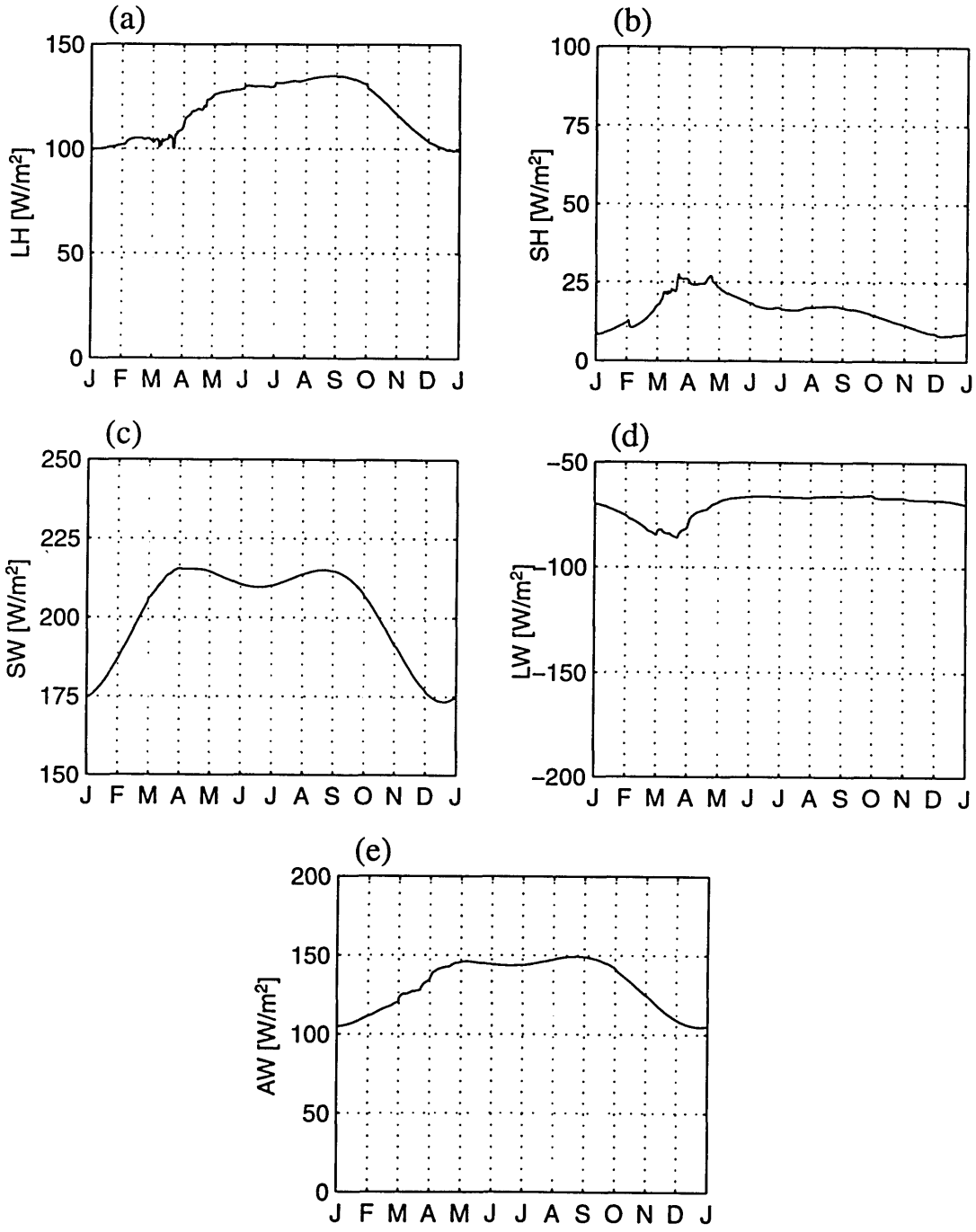

Figure 5-27: Coastal domain: SouthX2: Land-atmosphere energy exchange (a) Latent heat flux (b) Sensible heat flux (c) Net shortwave radiative flux (d) Net longwave radiative flux (e) Net allwave radiative flux

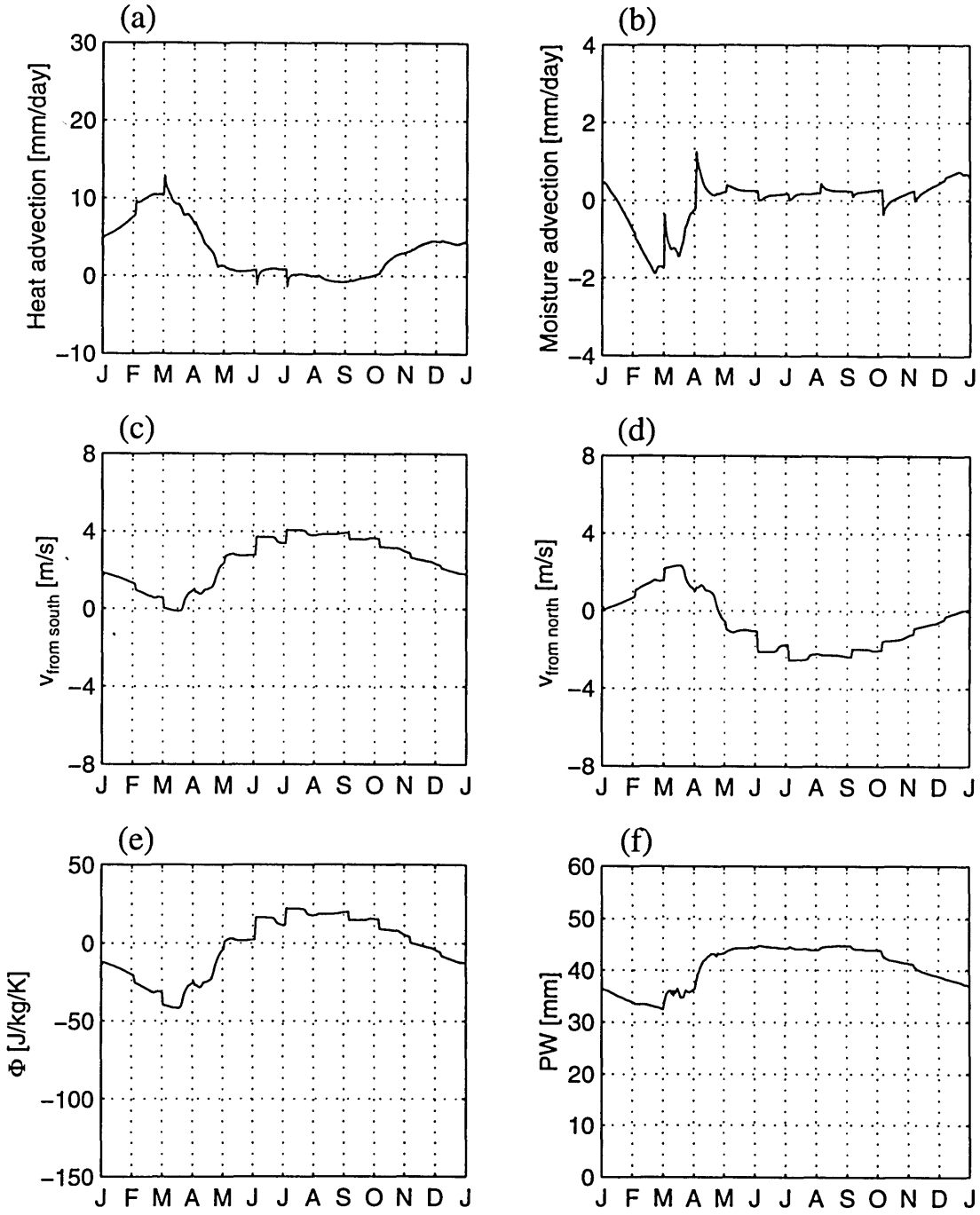

Figure 5-28: Coastal domain: SouthX2, Monsoon circulation. (a) Heat advection (b) Moisture advection (c) Lowest level wind across southern boundary (d) Lowest level wind across northern boundary (e) Entropy difference between model domain and ocean region (f) Precipitable water

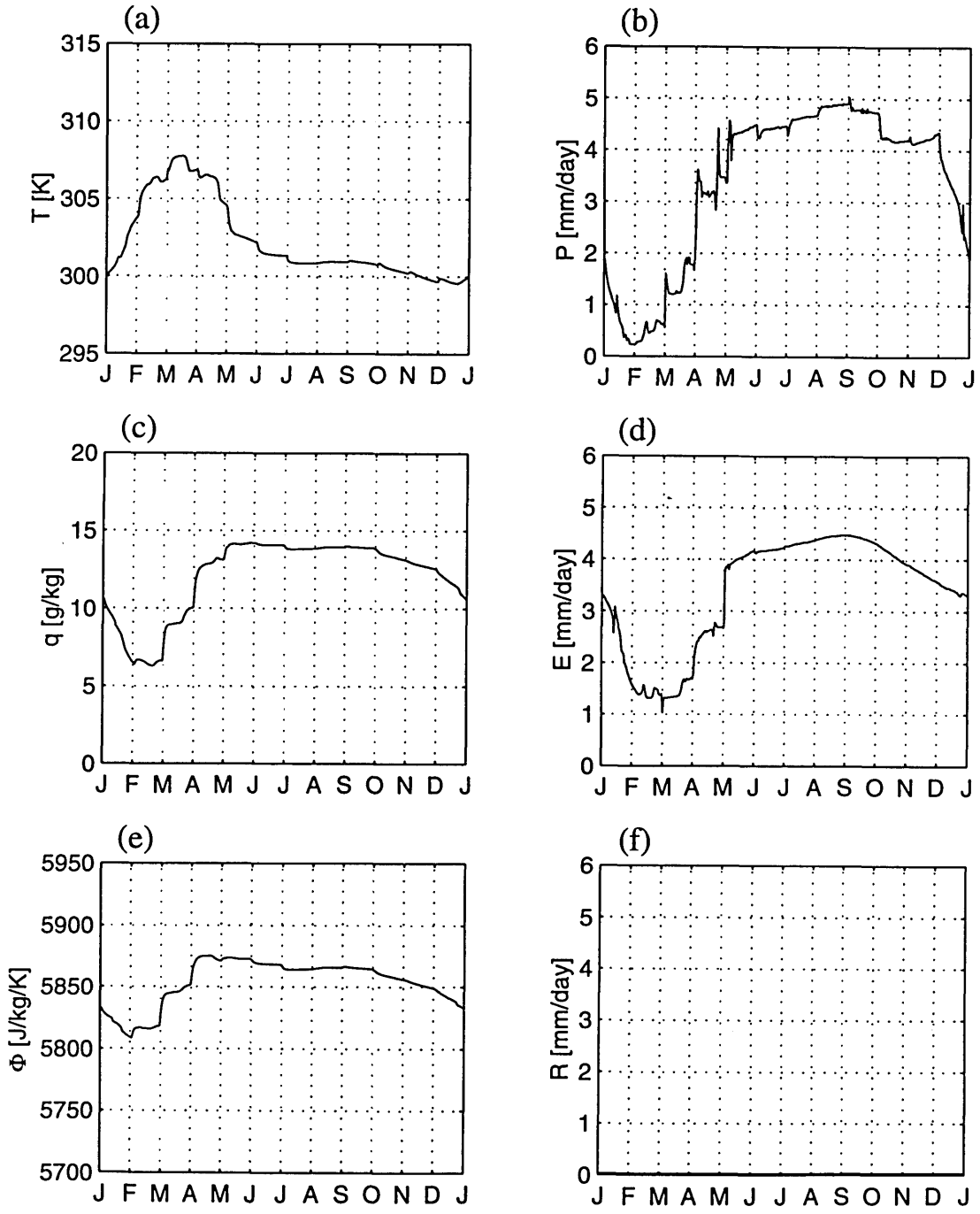

Figure 5-29: Coastal domain: NorthX2, seasonal cycle of simulated climate. (a) Temperature (b) Precipitation (c) Specific humidity (d) Total evapotranspiration (e) Boundary layer entropy (f) Runoff

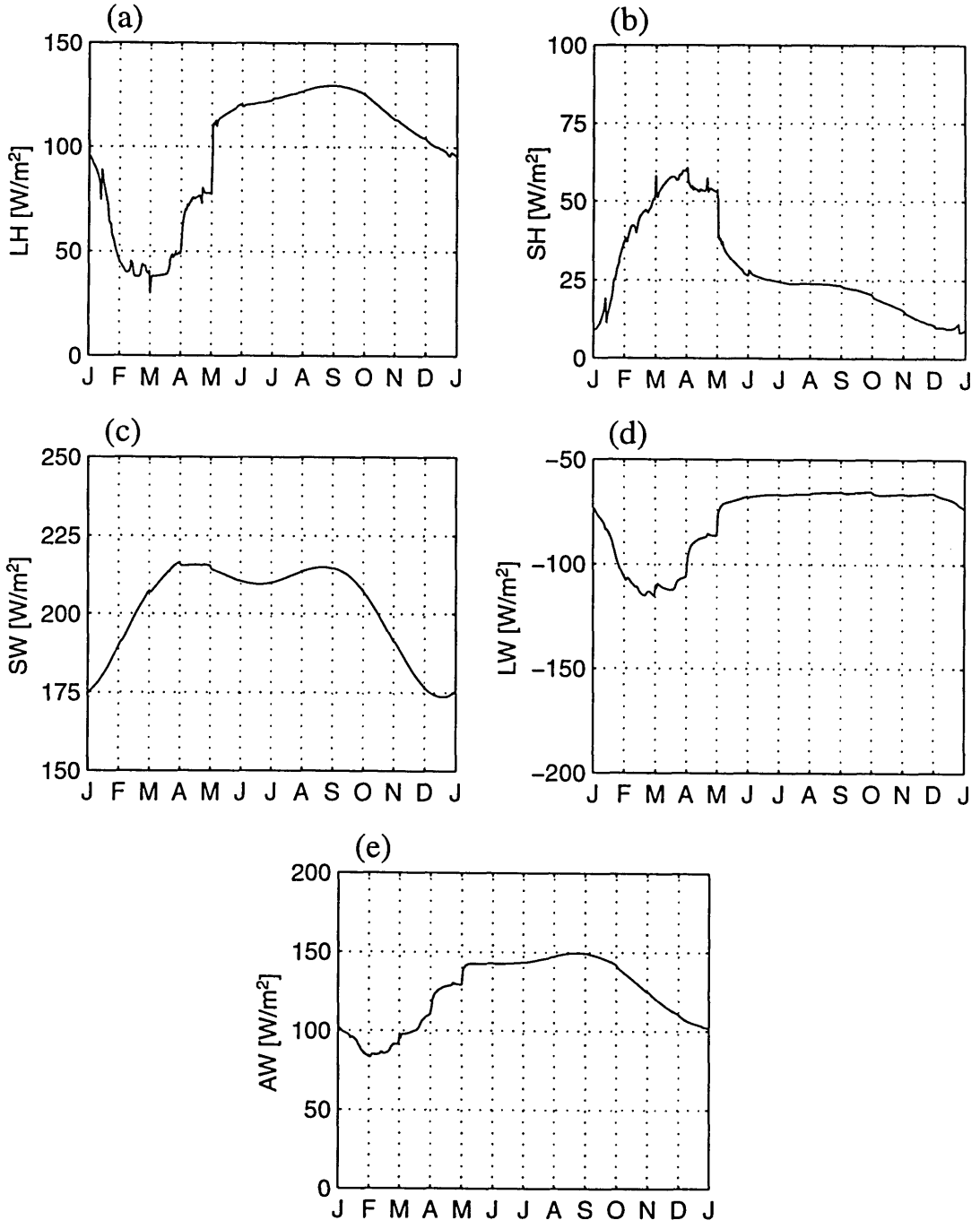

Figure 5-30: Coastal Domain: NorthX2, Land-atmosphere energy exchange. (a) Latent heat flux (b) Sensible heat flux (c) Net shortwave radiative flux (d) Net longwave radiative flux (e) Net allwave radiative flux

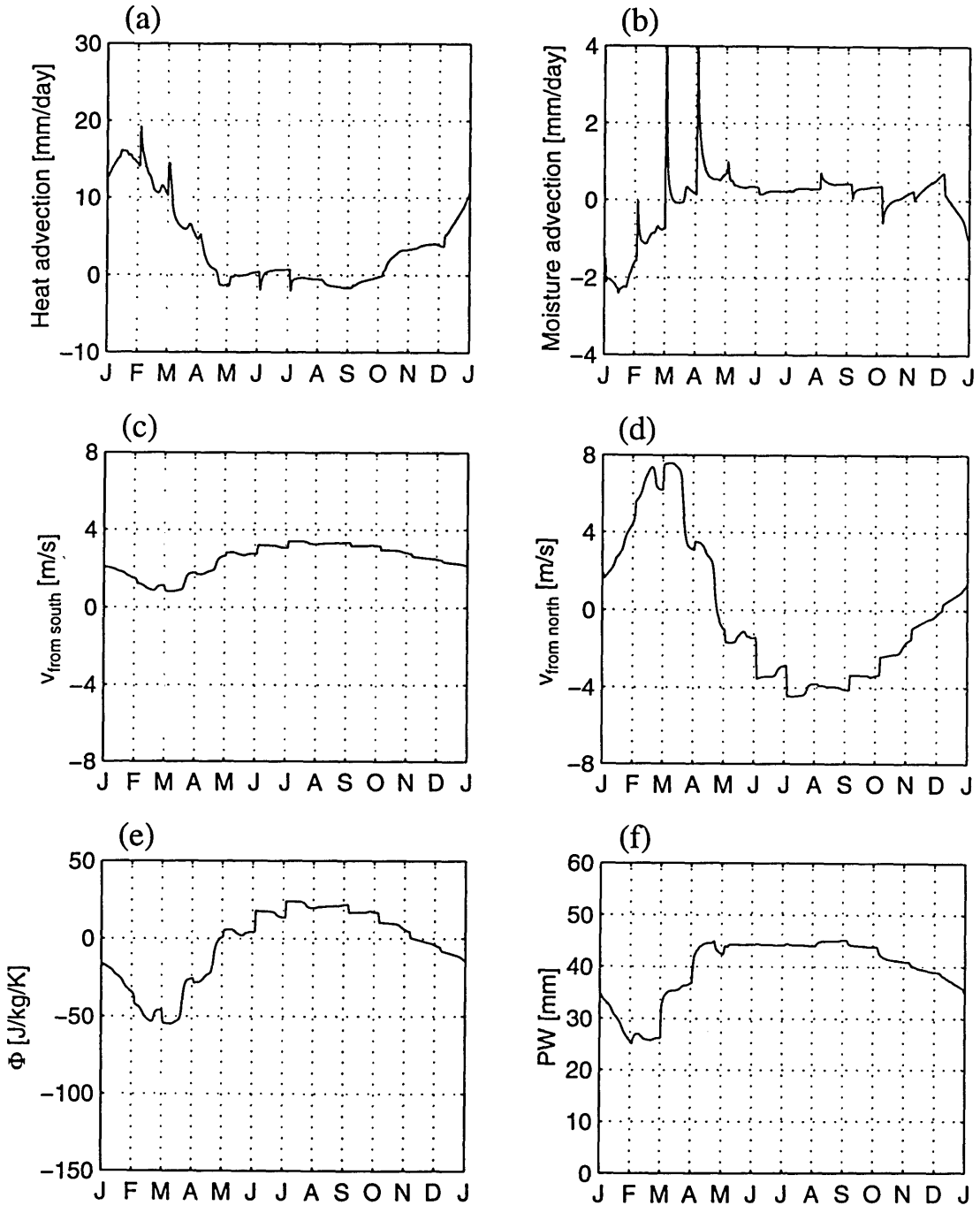

Figure 5-31: Coastal domain: NorthX2, Monsoon circulation. (a) Heat advection (b) Moisture advection (c) Lowest level wind across southern boundary (d) Lowest level wind across northern boundary (e) Entropy difference between model domain and ocean region (f) Precipitable water

Table 5.8: Coastal Domain: Modelled Forest vs. Grassland, with modified monsoon circulation (Experiments SouthX2 and South÷2

Variable	Ocean Flux 2.0 X Slope		Ocean Flux 0.5 X Slope	
	Forest	Grass	Forest	Grass
T [K]	300.8	301.4	300.7	300.9
q [g/kg]	12.8	11.6	13.6	12.7
Precipitation [mm/day]	4.1	3.2	4.6	3.7
Total Evaporation [mm/day]	4.1	3.1	4.3	3.4
Interception Loss [mm/day]	1.3	0.5	1.2	0.4
Transpiration [mm/day]	2.9	2.0	3.2	2.3
Soil Evaporation [mm/day]	-0.1	0.6	-0.1	0.7
Runoff [mm/day]	0.0	0.1	0.2	0.3
Latent Heat [W/m2]	118	88	125	100
Sensible Heat [W/m2]	16	21	12	16
Net Solar [W/m2]	202	190	202	189
Net Longwave [W/m2]	-70	-82	-68	-75
Net Allwave [W/m2]	132	108	134	114
Entropy Difference [J/kg/K]	-2.9	-11.6	3.0	-3.8

Figure 5-32 to Figure 5-34 show the seasonal variation in the simulated climate for SouthX2, with fixed grassland vegetation. The winter drying is enhanced, giving a longer and more severe dry season. Enhanced seasonality in temperature, specific humidity, latent heat and sensible heat are also seen.

Simulation North÷2 shows less sensitivity to vegetation type than the other simulations. Temperature remains unchanged, and precipitation is decreased by only 0.5 mm/day. Simulation NorthX2 has a drier equilibrium climate for forest than the other simulations, but also shows only moderate sensitivity to the land cover. As in other grassland sensitivity tests, there is enhanced seasonality, which can be seen in Figure 5-35 to Figure 5-37.

Table 5.9: Coastal Domain: Modelled Forest vs. Grassland, with modified monsoon circulation (Experiments NorthX2 and North÷2

Variable	Desert Flux 2.0 X Slope		Desert Flux 0.5 X Slope	
	Forest	Grass	Forest	Grass
T [K]	302.3	302.3	300.6	300.6
q [g/kg]	12.1	11.6	13.5	12.9
Precipitation [mm/day]	3.4	2.9	4.5	4.0
Total Evaporation [mm/day]	3.4	2.9	4.3	3.5
Interception Loss [mm/day]	1.1	0.5	1.2	0.4
Transpiration [mm/day]	2.2	1.8	3.2	2.3
Soil Evaporation [mm/day]	0.0	0.6	-0.1	0.7
Runoff [mm/day]	0.0	0.0	0.2	0.6
Latent Heat [W/m2]	98	84	124	101
Sensible Heat [W/m2]	28	24	12	16
Net Solar [W/m2]	202	190	202	189
Net Longwave [W/m2]	-78	-84	-68	-75
Net Allwave [W/m2]	124	106	134	124
Entropy Difference [J/kg/K]	-4.8	-8.7	2.2	-2.9

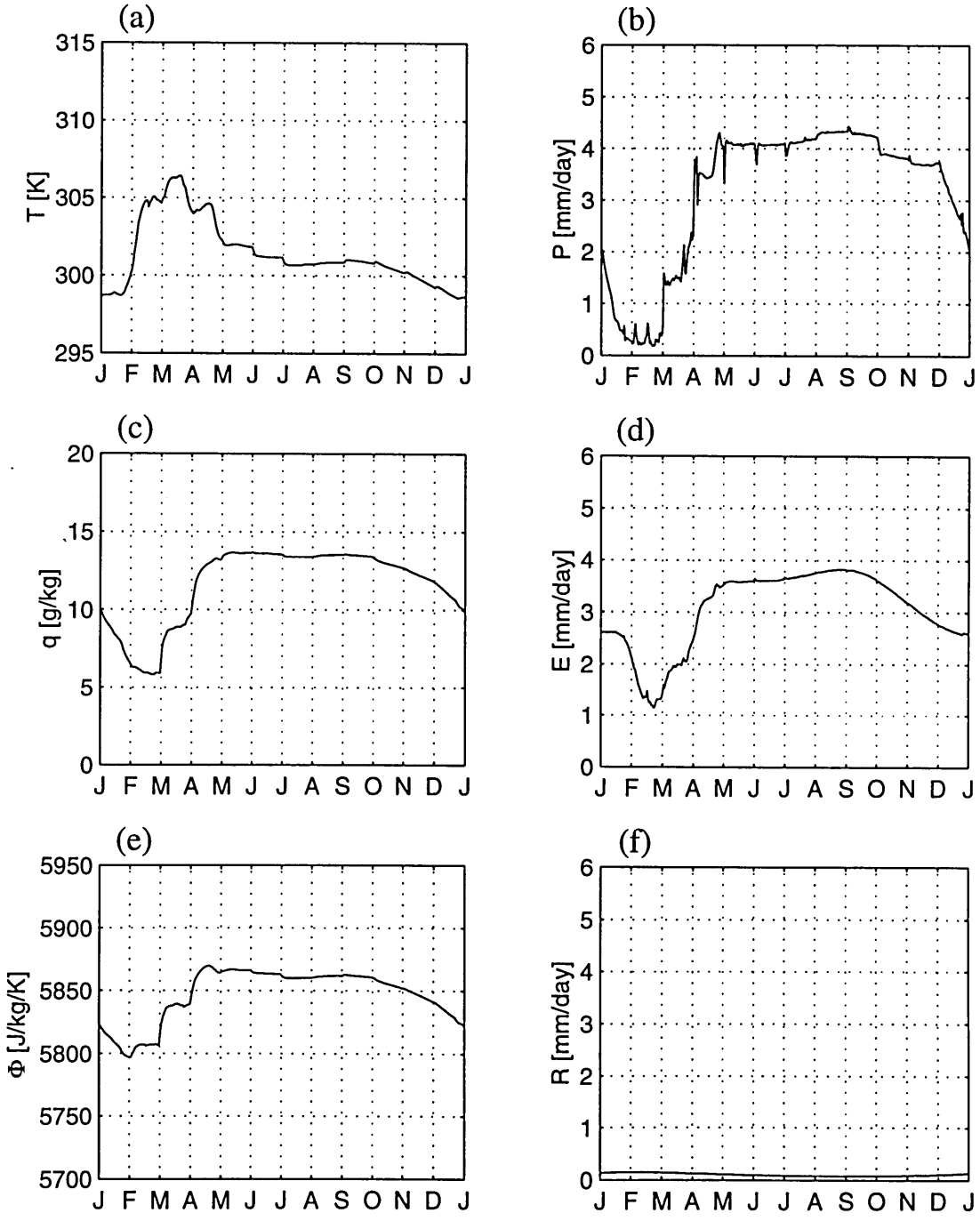

Figure 5-32: Coastal domain: SouthX2 with fixed grass, seasonal cycle of simulated climate. (a) Temperature (b) Precipitation (c) Specific humidity (d) Total evapotranspiration (e) Boundary layer entropy (f) Runoff

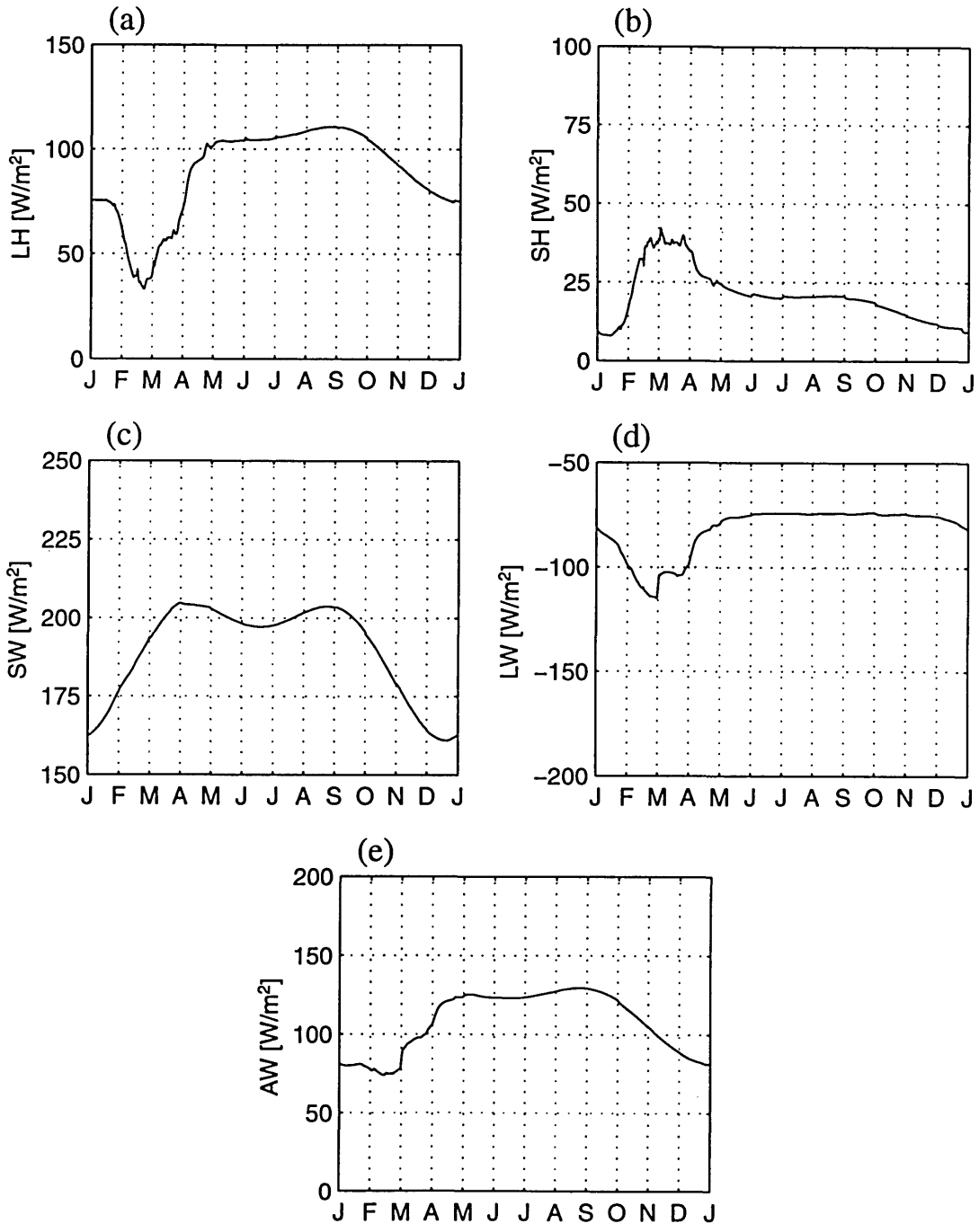

Figure 5-33: Coastal domain: SouthX2 with fixed grass, land-atmosphere energy exchange. (a) Latent heat flux (b) Sensible heat flux (c) Net shortwave radiative flux (d) Net longwave radiative flux (e) Net allwave radiative flux

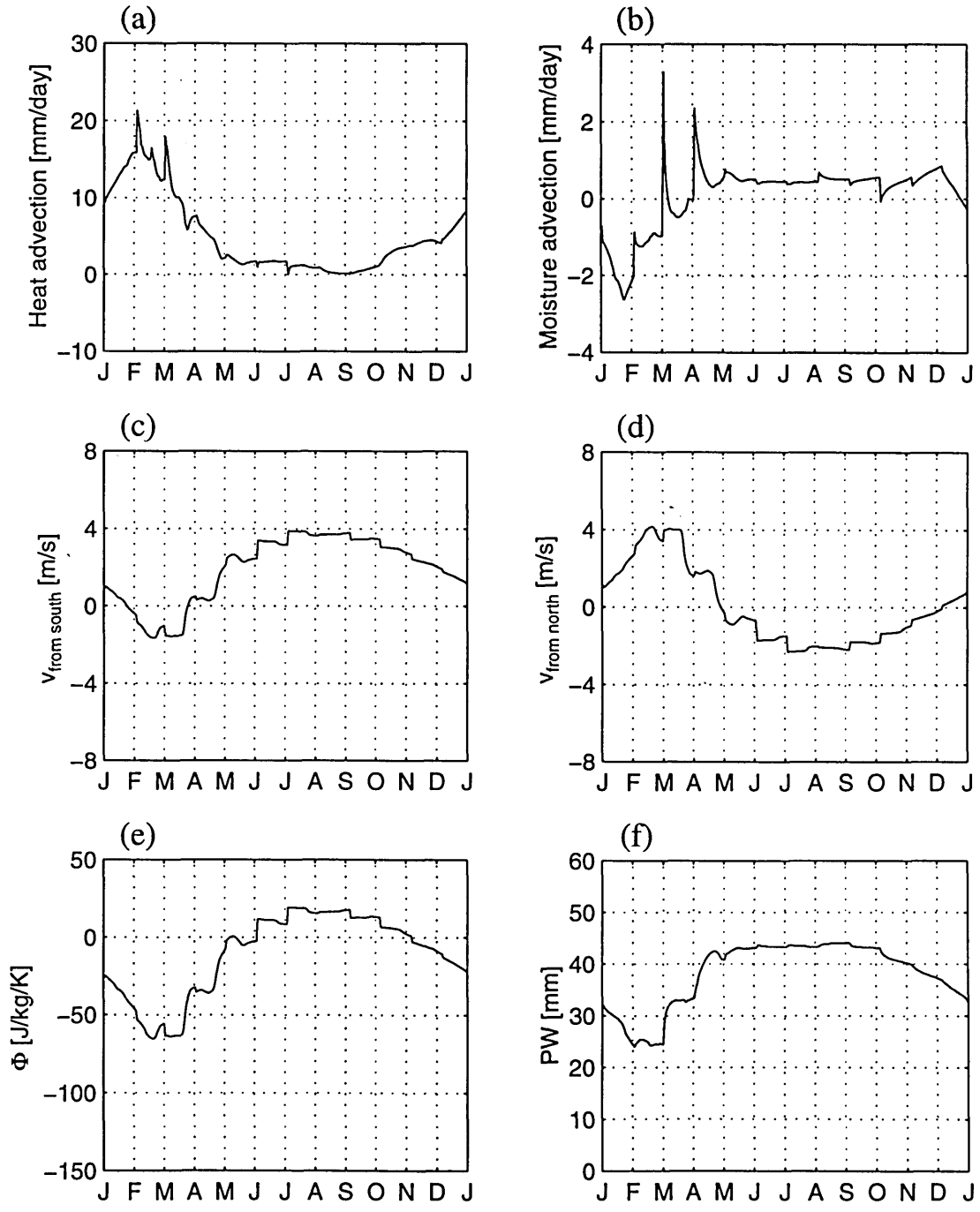

Figure 5-34: Coastal domain: SouthX2 with fixed grass, monsoon circulation. (a) Heat advection (b) Moisture advection (c) Lowest level wind across southern boundary (d) Lowest level wind across northern boundary (e) Entropy difference between model domain and ocean region (f) Precipitable water

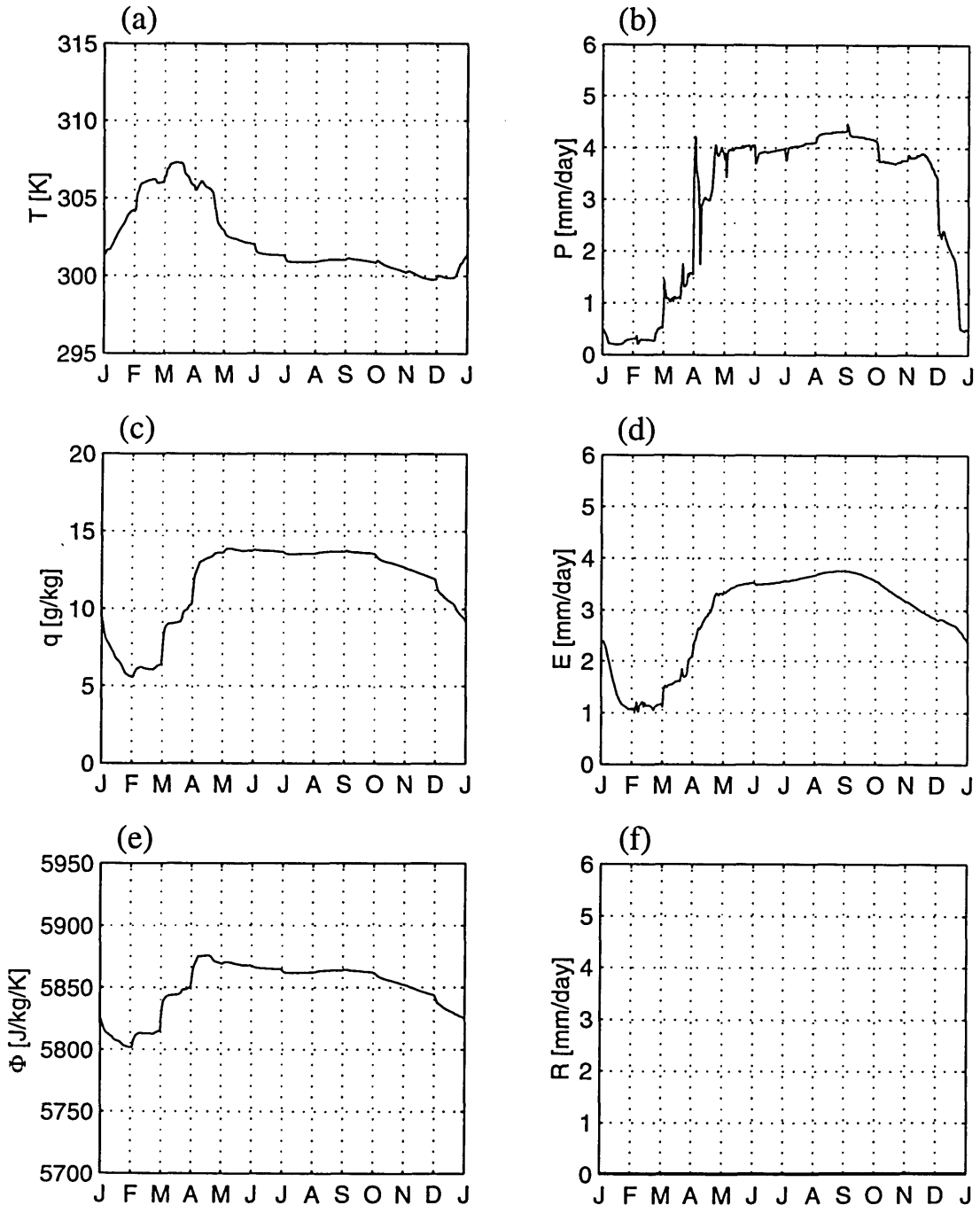

Figure 5-35: Coastal domain: NorthX2 with fixed grass, seasonal cycle of simulated climate. (a) Temperature (b) Precipitation (c) Specific humidity (d) Total evapotranspiration (e) Boundary layer entropy (f) Runoff

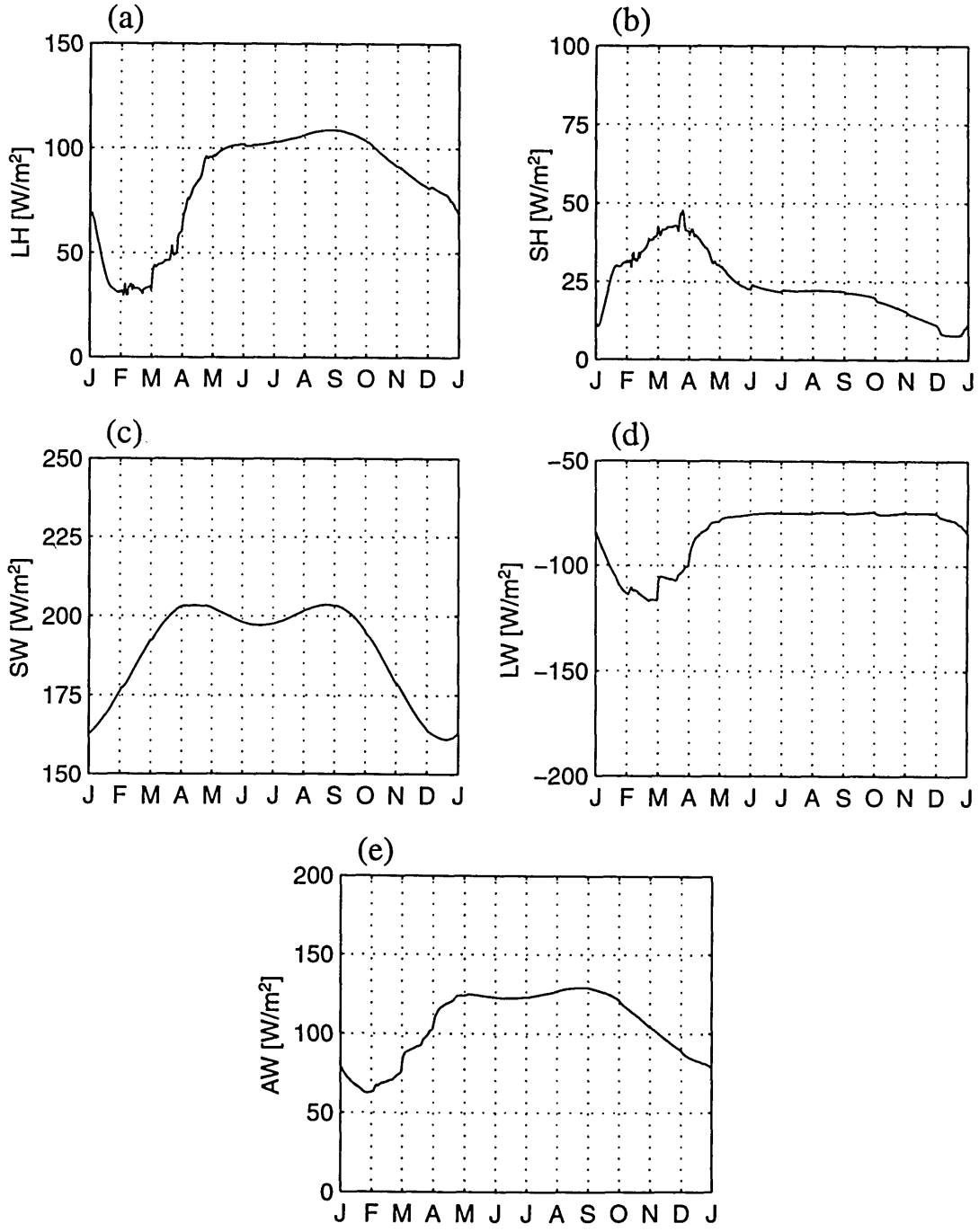

Figure 5-36: Coastal domain: NorthX2 with fixed grass, land-atmosphere energy exchange. (a) Latent heat flux (b) Sensible heat flux (c) Net shortwave radiative flux (d) Net longwave radiative flux (e) Net allwave radiative flux

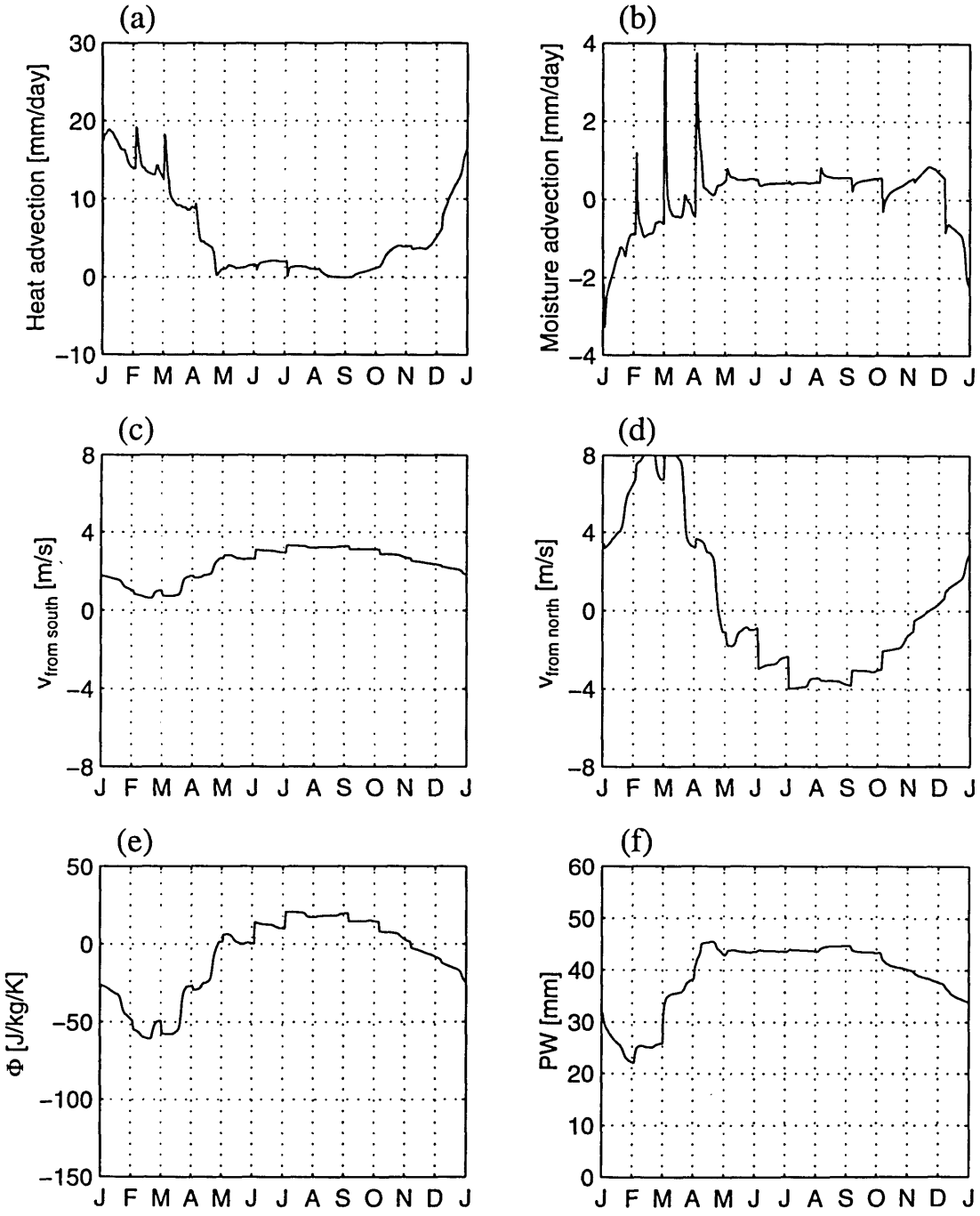

Figure 5-37: Coastal domain: NorthX2 with fixed grass, monsoon circulation. (a) Heat advection (b) Moisture advection (c) Lowest level wind across southern boundary (d) Lowest level wind across northern boundary (e) Entropy difference between model domain and ocean region (f) Precipitable water

Table 5.10: Coastal Domain: Summary of equilibrium vegetation.

	Evergreen Start	*Deciduous Start*	*Grassland Start*
South Slope ÷ 2	ever	-	ever
South Slope x 2	ever	-	ever
North Slope ÷ 2	ever	-	ever
North Slope x 2	decid	decid	decid

5.4.2 Dynamic vegetation simulations

Table 5.10 summarizes the results of our dynamic vegetation simulations for the modified slope simulations. In no case did the equilibrium vegetation and climate change with a different initial vegetation condition. This suggests that forest vegetation is very stable in our model domain, and that this result is not sensitive to the parameters in our monsoon circulation model. Although climate becomes drier and more seasonal after deforestation, the changes are not of significant magnitude to change the dominant vegetation type.

5.5 Sensitivity of Results to Properties of the Advected Air

The model displays high sensitivity to the monsoon circulation model, especially to the specification of fluxes at the northern boundary. As such, we explored this sensitivity further with simulations in which we changed the properties of the advected air at the northern boundary. Instead of using the properties observed at 10N, the actual boundary, we used the atmospheric humidity and temperature profiles at 15N to calculate horizontal moisture and heat advection. This simulates a dramatic change

(desertification) in climatic conditions to the north of the model domain. In these simulations, the radiative heating and cooling rates of the atmosphere are updated hourly. The equilibrium climate of this simulation when initialized as deciduous forest is shown in Table 5.11. The simulation will be referred to as simulation Advect15.

This change in the profile of advected air results in a substantially drier climate in the winter. During these months, the weakened circulation allows penetration of southerlies into the 5N-10N region, bringing in dry and hot air from the north. Precipitation drops to an annual average of 2.5 mm/day, just 55% of the precipitation of the control simulation. Evapotranspiration also decreases to 2.5 mm/day, and there is no runoff. The decrease in evapotranspiration results in a decrease in latent cooling of the near surface air, and temperature increases by 2.7K as compared to the control run. With a smaller latent heat flux, there is a compensating increase in the sensible heat flux of 28 W/m^2 and the Bowen ratio increases from 0.1 to 0.5. The outgoing longwave radiation increases due to the higher surface temperatures, and the smaller atmospheric water content reduces the downwards longwave radiative flux. The combination of these two effects decreases the net longwave radiation at the surface by 24 W/m^2. This is the main contribution to the 16% reduction in net allwave radiation - from 133 W/m^2 to 112 W/m^2.

In addition to the change in mean annual climate, there is also a significant enhancement of seasonality with the altered profile of advected air. Figure 5-38 to Figure 5-41 show the seasonality of atmospheric and surface variables. In particular, we may note that precipitation is less than 1 mm/day from about February to the beginning of June. In contrast, there was little seasonality in precipitation in the control simulation - it varied from about 4 mm/day in the winter to just under 5 mm/day in the summer. Correspondingly, simulation Advect15 also shows strong seasonality in evaporation, specific humidity, and total precipitable water. During the dry season, during which total evapotranspiration is small, the decrease in latent cooling triggers a rapid rise in temperature to 310K from a minimum of just under 300K. The entropy range for this simulation is more than 60 J/kg/K, as compared to a much more limited range of about 25 J/kg/K in the control simulation. With this

variability in entropy also comes increased variability in the strength of the monsoon circulation. The surface wind across the southern boundary ranges from a minimum near 0 m/s in April to a maximum of about 3.5 m/s in September. In the control simulation, the range of variation is about half that, from about 2 m/s to 3.5 m/s. The surface wind across the northern boundary also shows greater seasonality, and is positive (directed into the domain) for 7 months of the year. In general, the monsoon circulation is seen to be much weaker in the winter than in the control simulation. The weaker circulation allows more desert air into the model domain, further reducing the energy of air in the model domain and thus further weakening the monsoon. This feedback becomes more important in this simulation because the advected air (profile at 15N) is less energetic than the advected air in the control simulation (profile at 10N).

The equilibrium vegetation for this simulation with diminished moisture and enhanced seasonality is deciduous forest. However, the forest has a small LAI of only about 4. The stable NPP and the accumulated biomass at the end of 45 years are less than one half that of the interactive circulation control simulation.

5.5.1 Static Vegetation Simulations

The sensitivity of this simulation to the vegetation at the land surface is tested by holding the vegetation fixed as grass and allowing the climate to reach equilibrium. The differences between the equilibrium climates with grass and forest are shown in Table 5.11. The seasonality of the climate with fixed grassland vegetation (Figure 5-42 to Figure 5-45) can be compared to the climate with equilibrium forest (Figure 5-38 to Figure 5-41). The climate is drier and cooler over grassland. Precipitation and total evaporation both decrease by 0.4 mm/day. The temperature effects of reduced evaporation are more than compensated for by a reduction in net radiation, which arises due to a reduction in both net solar and net longwave radiation. This results in a 0.6K reduction in temperature. The net solar radiation decreases by 17 W/m^2 due to increased surface albedo. The net longwave radiation decreases by 16 W/m^2 due to less incoming longwave radiation.

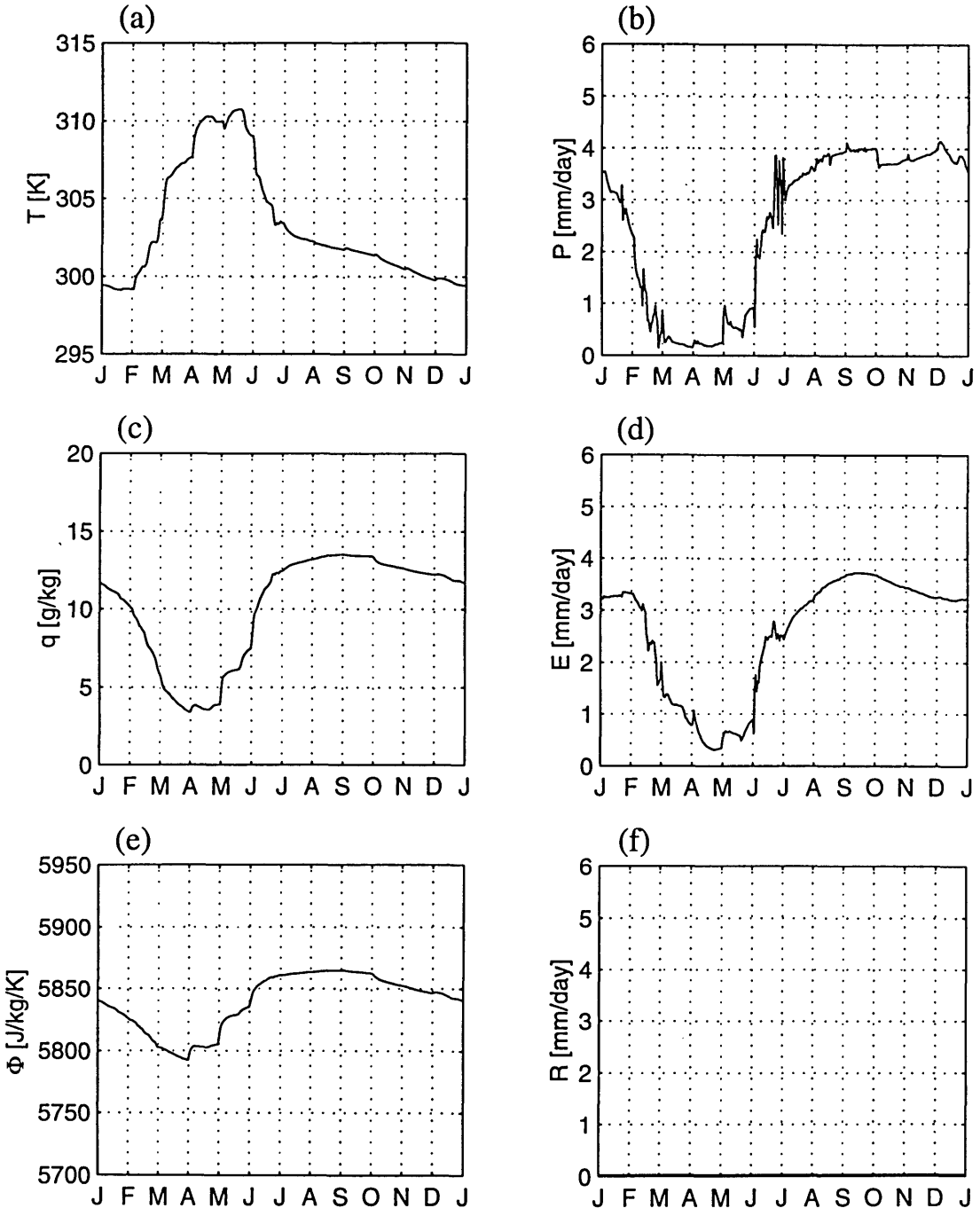

Figure 5-38: Coastal domain: Advect15, seasonal cycle of simulated climate. (a) Temperature (b) Precipitation (c) Specific humidity (d) Total evapotranspiration (e) Boundary layer entropy (f) Runoff

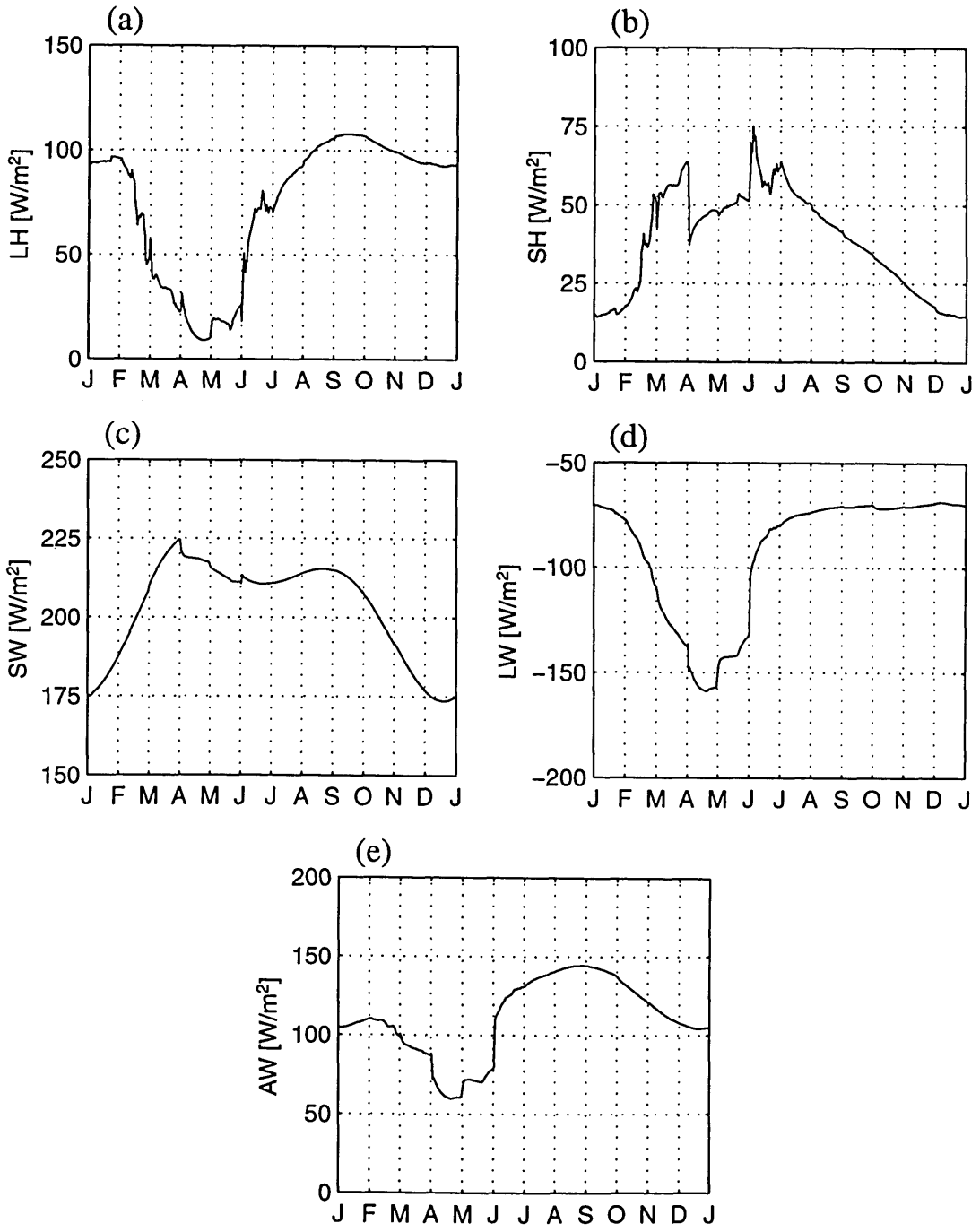

Figure 5-39: Coastal domain: Advect15, land-atmosphere energy exchange. (a) Latent heat flux (b) Sensible heat flux (c) Net shortwave radiative flux (d) Net longwave radiative flux (e) Net allwave radiative flux

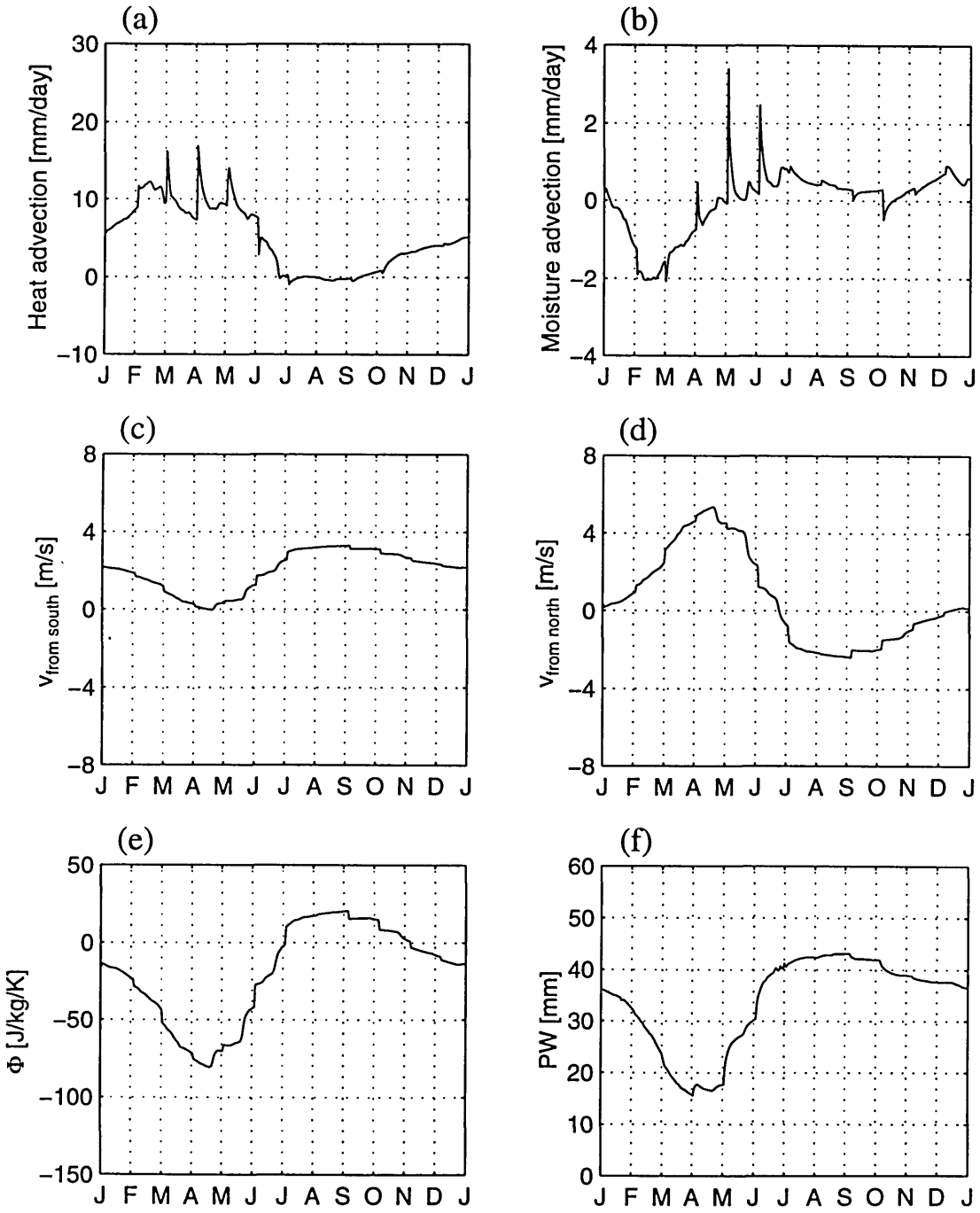

Figure 5-40: Coastal domain: Advect15, monsoon circulation. (a) Heat advection (b) Moisture advection (c) Lowest level wind across southern boundary (d) Lowest level wind across northern boundary (e) Entropy difference between model domain and ocean region (f) Precipitable water

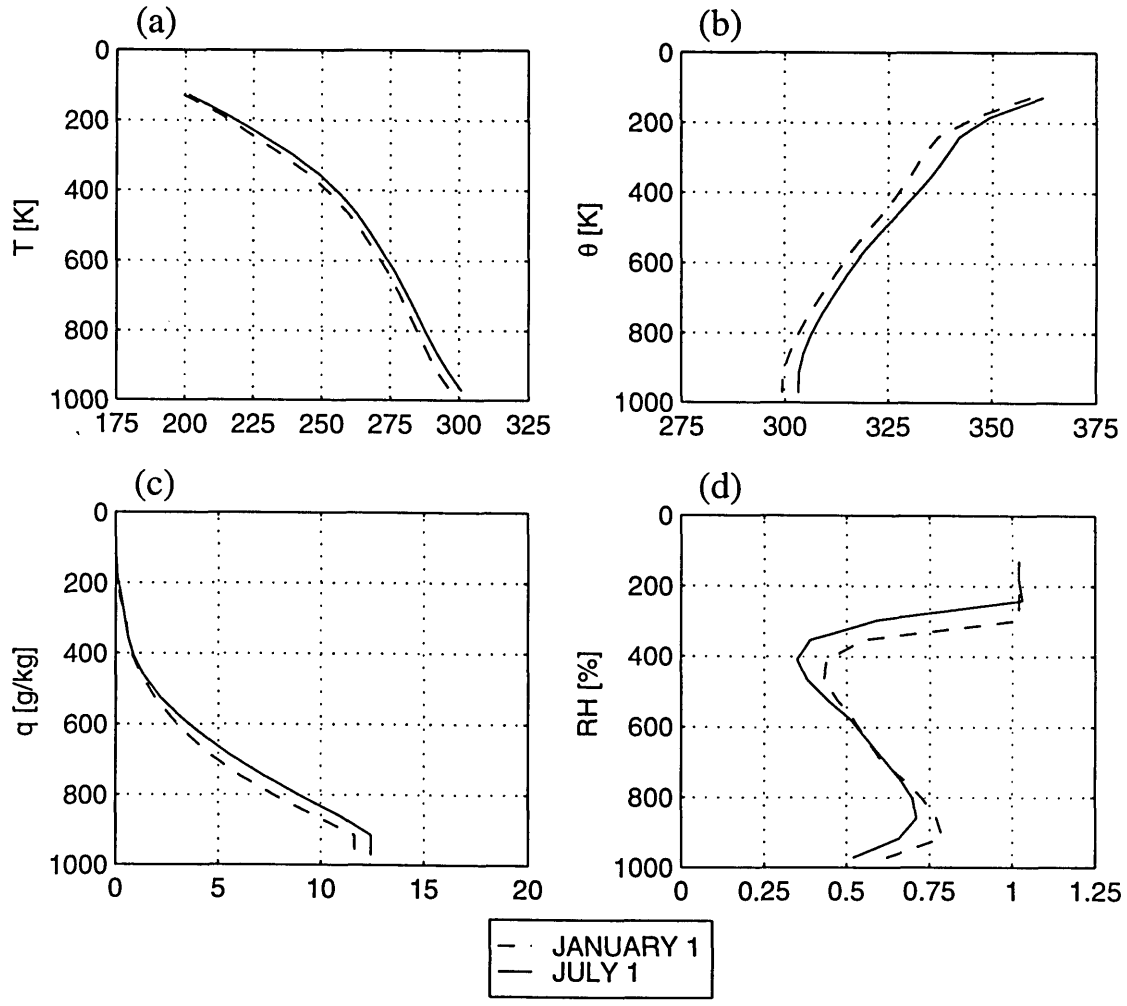

Figure 5-41: Coastal domain: Advect15, atmospheric soundings. (a) Absolute temperature (b) Potential temperature (c) Specific humidity (d) Relative humidity

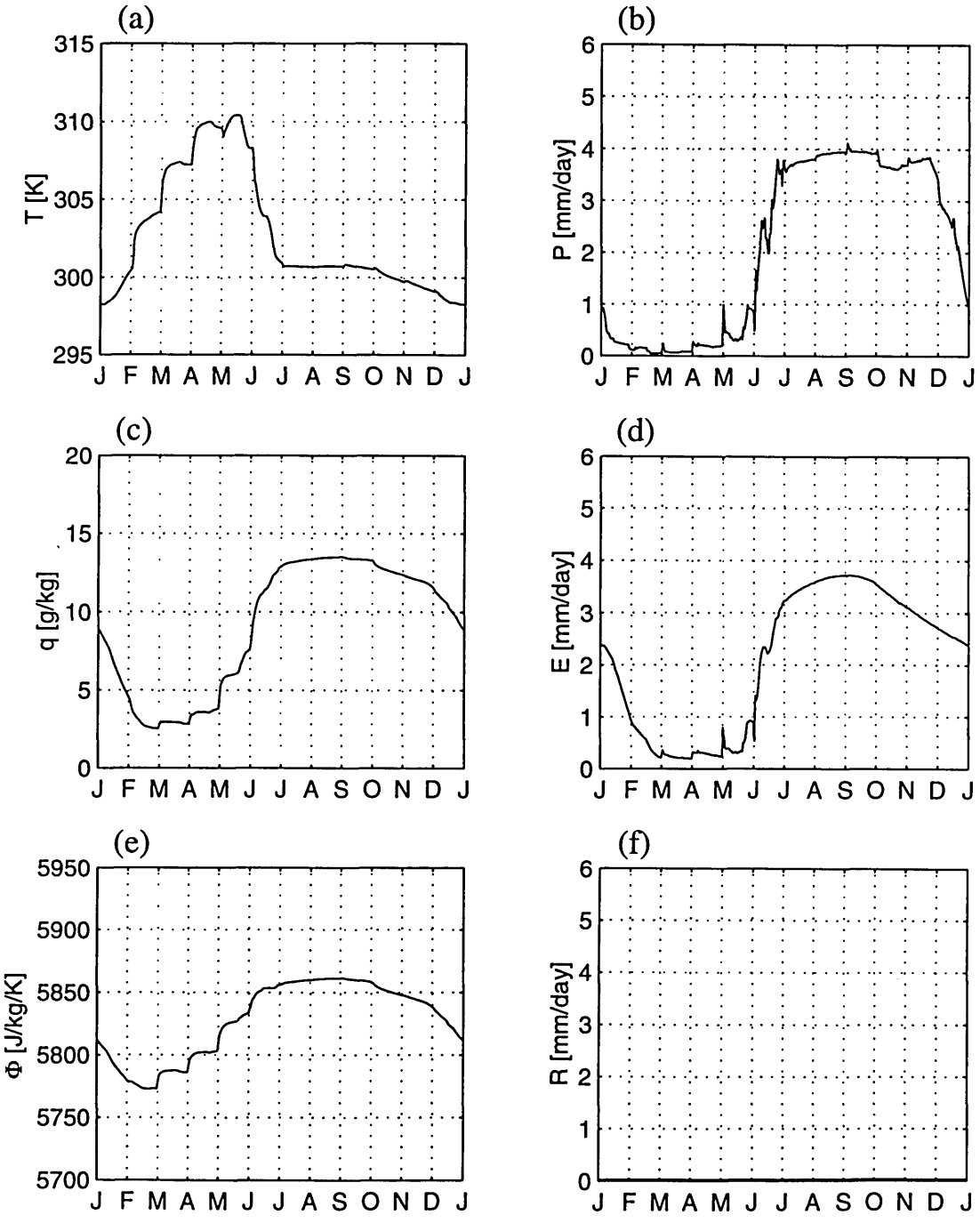

Figure 5-42: Coastal domain: Advect15 with grass initialization, seasonal cycle of simulated climate. (a) Temperature (b) Precipitation (c) Specific humidity (d) Total evapotranspiration (e) Boundary layer entropy (f) Runoff

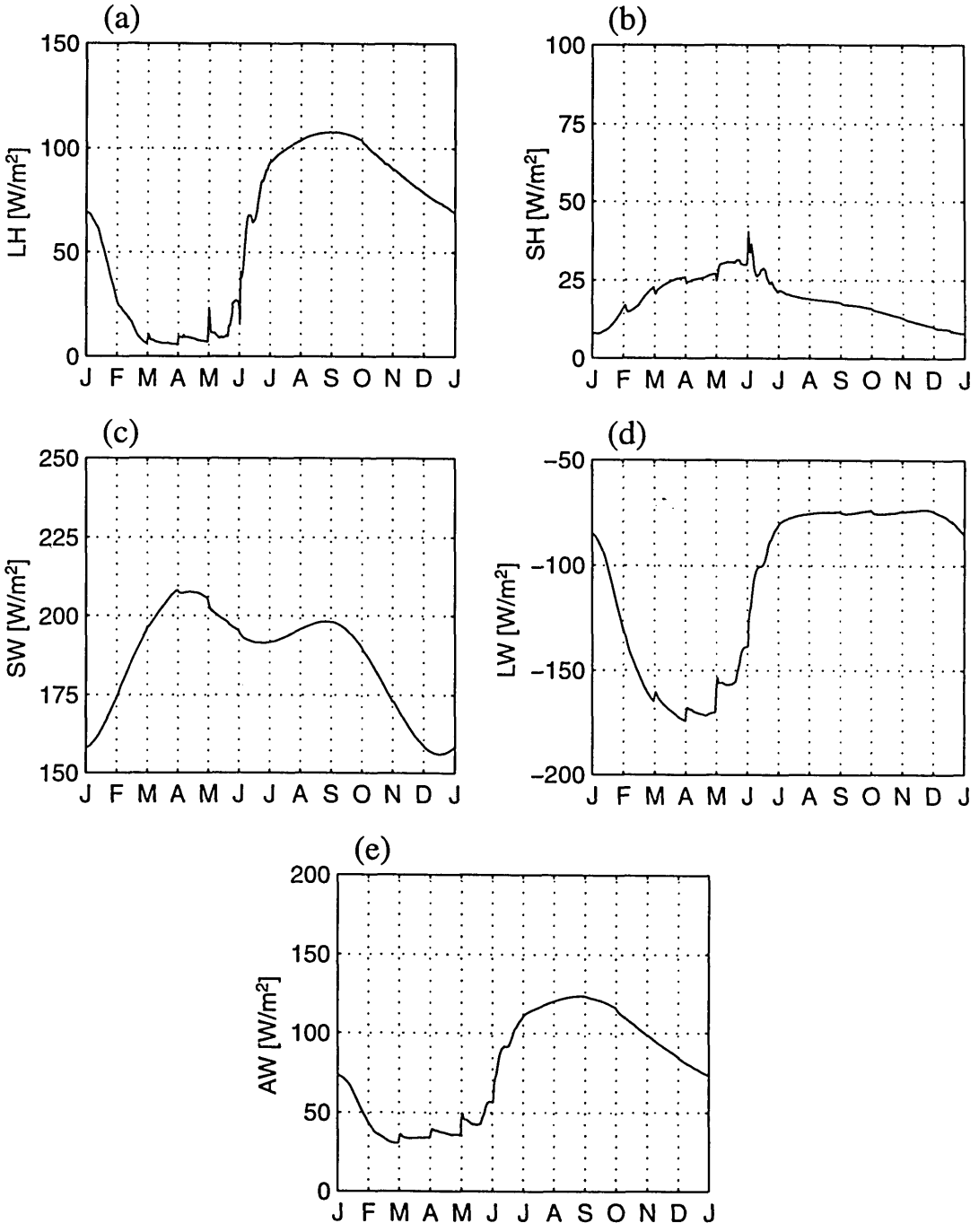

Figure 5-43: Coastal domain: Advect15 with grass initialization, land-atmosphere energy exchange. (a) Latent heat flux (b) Sensible heat flux (c) Net shortwave radiative flux (d) Net longwave radiative flux (e) Net allwave radiative flux

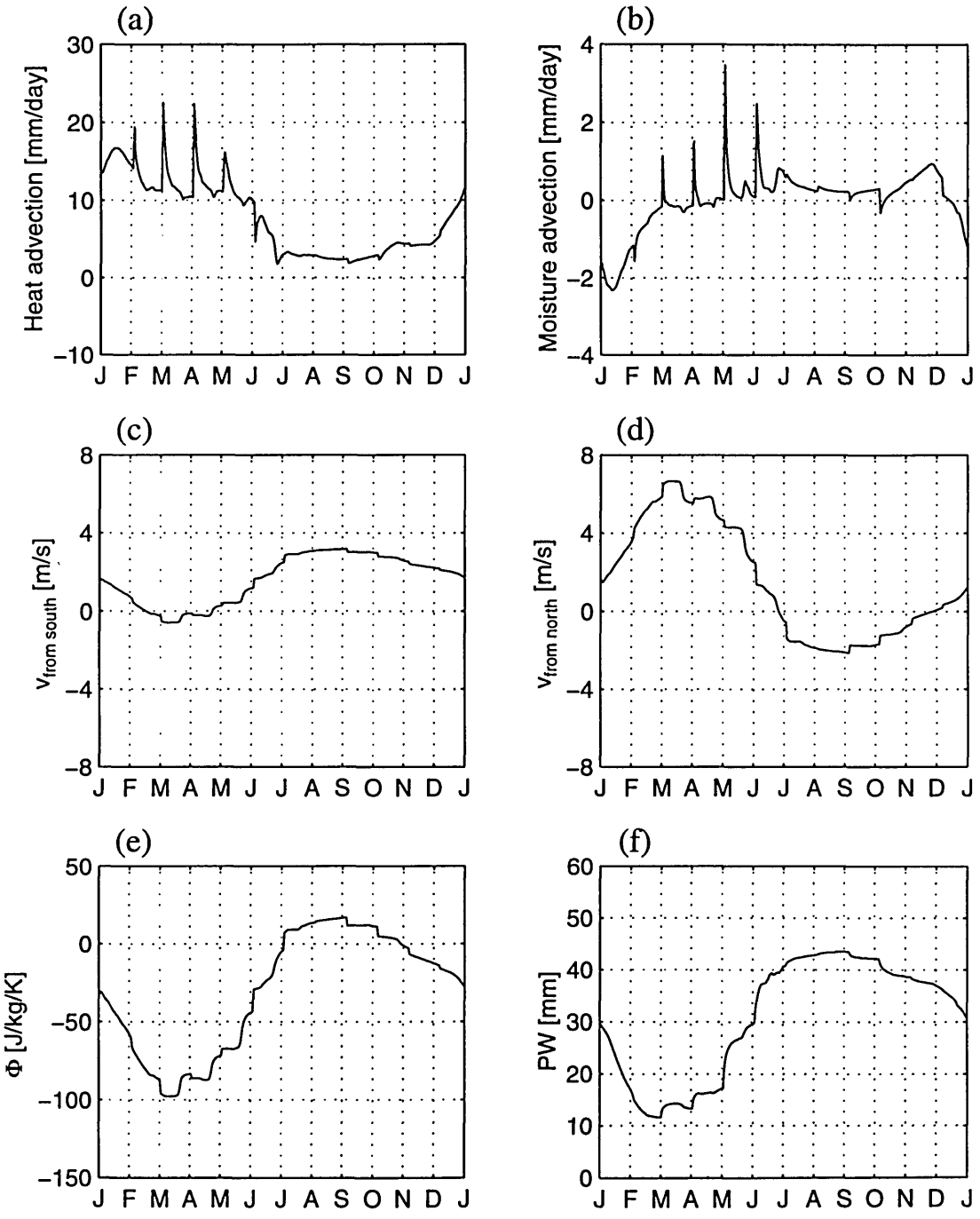

Figure 5-44: Coastal domain: Advect15 with grass initialization, monsoon circulation. (a) Heat advection (b) Moisture advection (c) Lowest level wind across southern boundary (d) Lowest level wind across northern boundary (e) Entropy difference between model domain and ocean region (f) Precipitable water

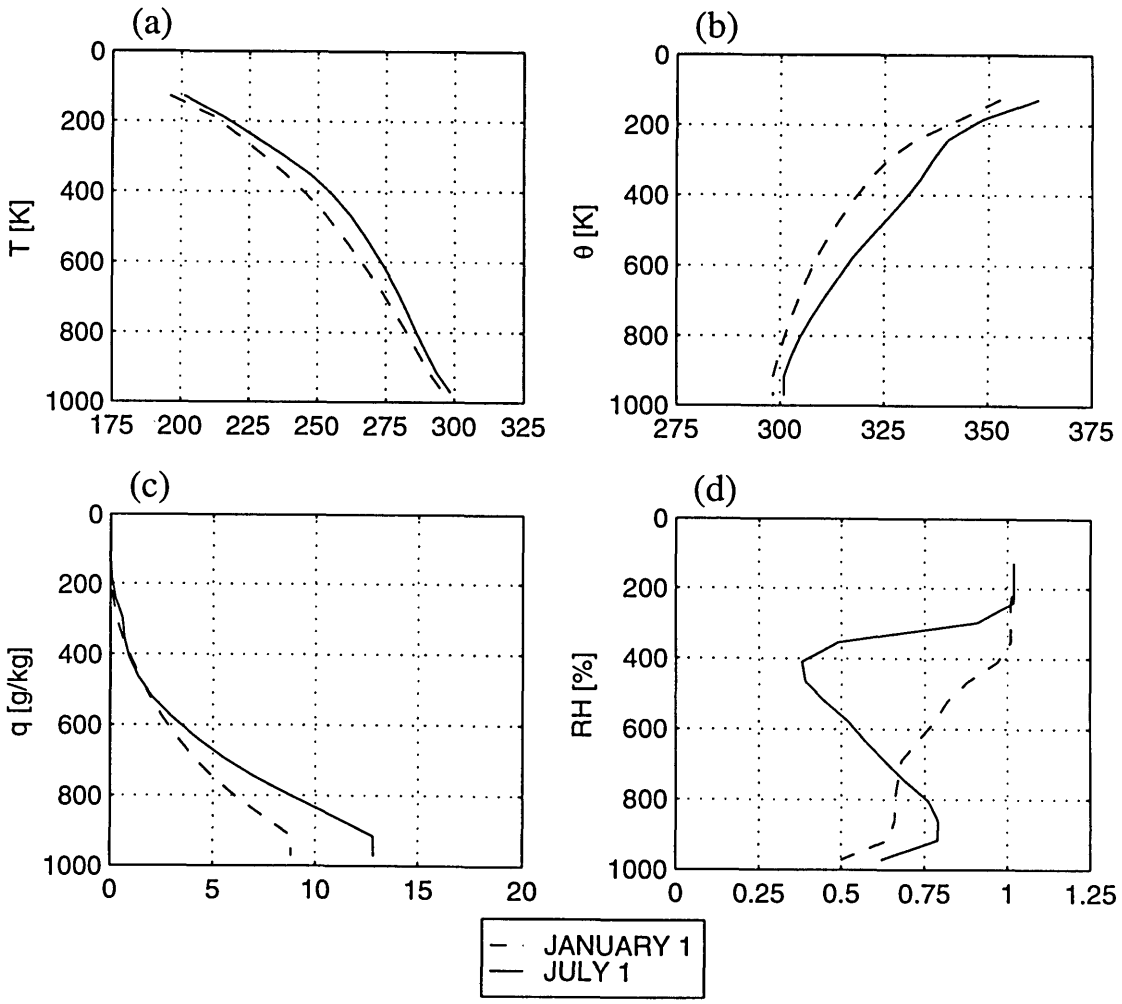

Figure 5-45: Coastal domain: Advect15 with grass initialization, atmospheric soundings. (a) Absolute temperature (b) Potential temperature (c) Specific humidity (d) Relative humidity

Table 5.11: Coastal Domain: Modelled Forest vs. Grassland, with modified profile of advected air (Experiment Advect15)

Variable	Control	Desert Advection Profile at 15N	
		Forest	Grass
T [K]	300.6	303.3	302.7
q [g/kg]	13.5	10.1	9.1
Precipitation [mm/day]	4.5	2.5	2.1
Total Evaporation [mm/day]	4.3	2.5	2.1
Interception Loss [mm/day]	1.2	0.9	0.5
Transpiration [mm/day]	3.2	1.6	1.8
Soil Evaporation [mm/day]	-0.1	0.1	-0.2
Runoff [mm/day]	0.2	0.0	0.0
Latent Heat [W/m2]	125	74	61
Sensible Heat [W/m2]	12	40	19
Net Solar [W/m2]	201	204	187
Net Longwave [W/m2]	-68	-92	-108
Net Allwave [W/m2]	133	112	79

5.5.2 Dynamic vegetation simulations

When vegetation is initialized as grass, and the model is allowed to find its own equilibrium state for vegetation and climate, it settles into a different equilibrium than when the simulation is initialized with deciduous forest. The competition between forest and grass is regulated largely by the availability of moisture, and the change in precipitation in this experiment happens to straddle the threshold defining the dominance of forest and the dominance of grassland.

The evolution of LAI and biomass in the two simulations (forest start and grass start) are shown in Figure 5-46 and Figure 5-47. The equilibrium grassland has a high LAI of about 11, which is higher than any observations reported in Table 3.1. In part, this may be a limitation in IBIS' representation of grassland. However, the biomass and the NPP of the stable grassland are reasonable, at 2.2 kg-C/m^2 and 1.0 kg-C/m^2/yr, respectively.

While the LAI and NPP of the equilibrium grassland is greater than that of the

equilibrium deciduous forest, the biomass of the forest is significantly higher than that of the grassland. This is reasonable since forest can dominate simply by shading the ground, even if its rates of growth and photosynthesis are actually slower.

The fact that a change in the properties of the advected air has such a dramatic effect both on the equilibrium climate and vegetation has important implications. Namely, land use changes can affect not only the local region, but also neighboring regions. If desertification of land in an adjacent region brings hotter and drier air into a domain, this simulation shows that it can have potentially serious effects. The importance of conditions in neighboring regions on biofeedbacks was also seen by Gutman (1984). In his simulations, biofeedback was strongest in the regions adjacent to his perturbation zone, and not within it. These results imply a large role of horizontal advection in the moderation of climate, and point to the need for two-dimensional or three-dimensional modeling to explore this idea further.

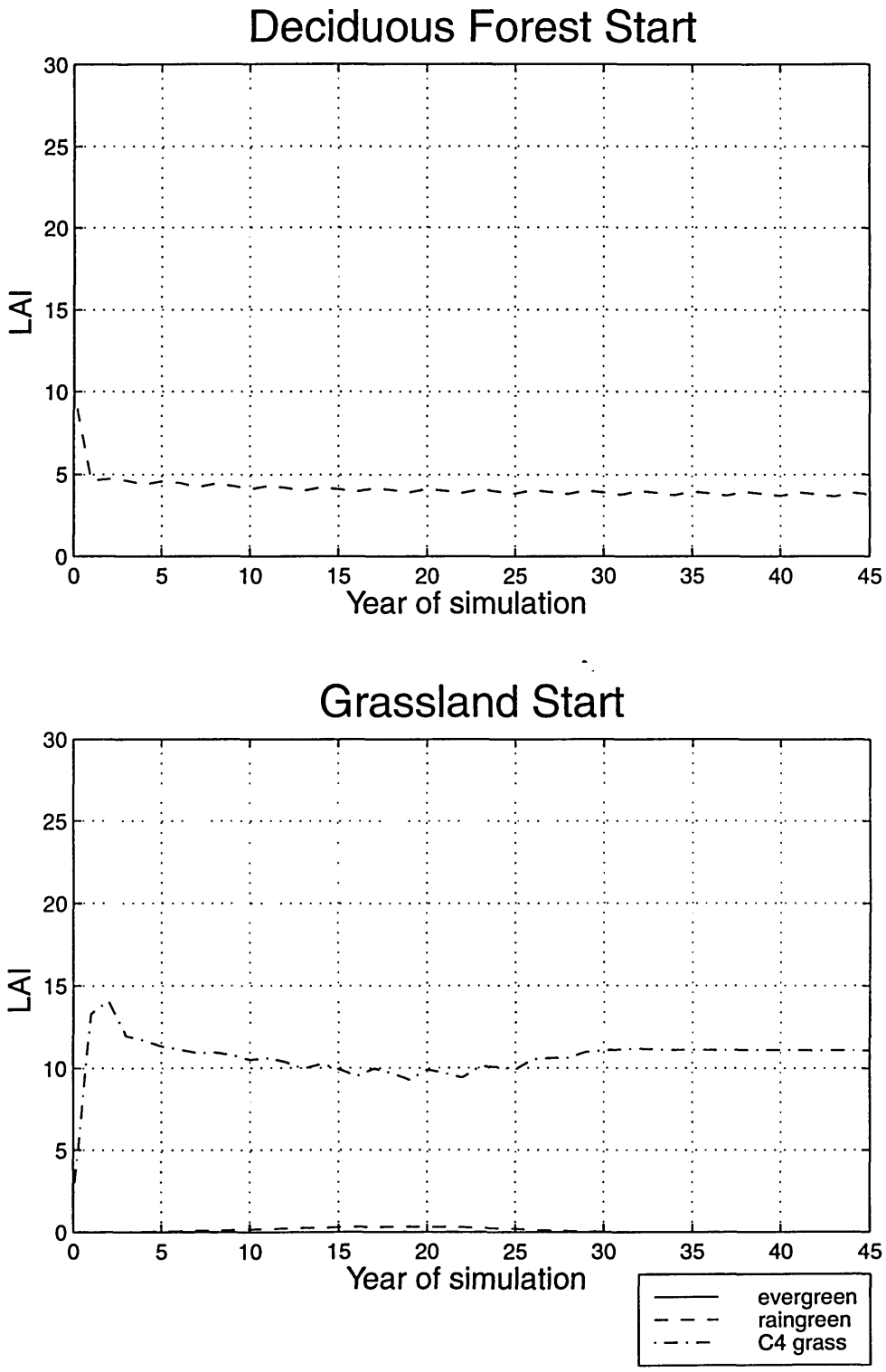

Figure 5-46: Coastal domain: Advect15, the equilibrium vegetation, here described by LAI, is different when the simulation is initialized with forest versus grassland.

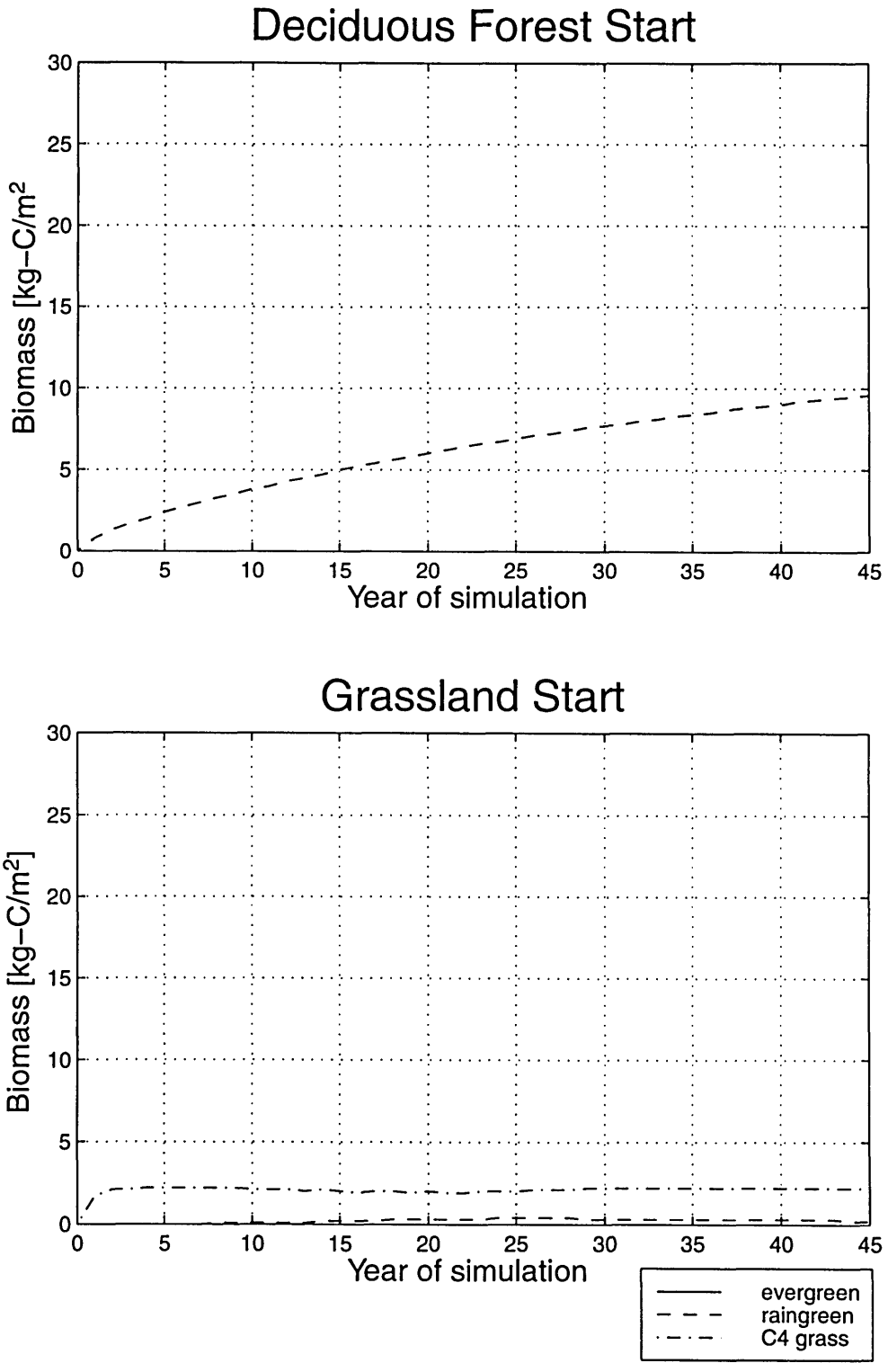

Figure 5-47: Coastal domain: Advect15, the equilibrium vegetation, here described by biomass, is different when the simulation is initialized with forest versus grassland.

Chapter 6

Inland Domain: Experimental Simulations

The inland domain extends from 10W to 7.5 E, and 10N to 15N. As discussed in Chapter 4, the seasonal effects of the monsoon are strong in this region. Observed vegetation in this model domain consists primarily of savanna/grassland, with more abundant vegetation near the southern boundary and sparser vegetation near the northern boundary. The location of the model domain and its associated ocean region (for the empirical monsoon circulation model) were shown in Figure 4-3. The "ocean" region is defined as 10W to 7.5E, and 0N-7.5N, and encompasses both a strip of the Atlantic Ocean and the tropical rain forests along the coast of West Africa. Again, advected properties are taken from monthly climatologies along the domain boundaries, and calculations for solar radiation are made for the center of the domain, 12.5N. In this region, the effects of the monsoon are strong, and correlations between the entropy difference between the model domain and an ocean region defined to the south, are high.

The effects of cloud cover on solar radiation are loosely represented by decreasing the solar constant by 15% to represent the effects of the cloud albedo. Due to high sensible heat fluxes and increased turbulent mixing and entrainment at the top of the boundary layer over grassland, the expected equilibrium vegetation of this domain, the height of the mixed layer is set at 180mb for the inland domain.

As in the coastal domain, there are regions of loamy sand and regions of silty loam in the inland domain. Although the loamy sand is more dominant in this region, we again use a soil type of silty loam in the inland domain. This is because our offline IBIS simulations and the experience of other IBIS users shows unusually high condensation resulting in large negative values of soil evaporation when a high sand fraction is used (Wang 1998). Using the silty loam reduces the differences between the inland domain and the coastal domain simply to those due to the different solar forcing and monsoon circulation in each domain.

The timestep of these simulations is 15 minutes for convection and land surface processes. Radiative cooling/heating rates are updated hourly, vegetation phenology is updated daily, and vegetation dynamics is updated annually. The experiments performed for the inland domain are similar, but more limited in scope, than those for the coastal domain. Unless otherwise noted, the results shown are for the equilibrium state of the system.

6.1 Control Simulations

As in the coastal domain, we have two "control" simulations in the inland domain, one in which the horizontal fluxes of air across the northern and southern domain boundaries are set equal to their monthly climatological values, and one in which they are calculated by our monsoon circulation model. Each control simulation is described below.

It should be noted that IBIS (version 1.0) does not simulate mixed tree and grass vegetation well. When vegetation dynamics are active, either trees or grass almost always become the exclusive vegetation type. This was also seen in the coastal domain simulations. While this is a limitation of the model, it should not affect our ability to test differences created by contrasts in land surface vegetation. By contrasting grass and forest, we capture the essence of the effects of the land surface on the climate system.

6.1.1 Control Simulation: Fixed Circulation

In the fixed circulation control simulation, the fluxes of air across the domain boundaries are set equal to the fluxes calculated from the NCEP reanalysis climatology. These climatological fluxes advect with them the properties (temperature and specific humidity) of the air along the domain boundaries. The vegetation is initialized as grassland and the model is run until it finds its own equilibrium between vegetation and climate.

At equilibrium, the vegetation is grassland with an LAI of 1.1 and biomass of 0.2 kg-C/m^2 (see Figure 6-1). The NPP of this system is about 0.10 kg-C/m^2/yr. While the LAI is in the range listed for tropical savanna/grassland in Table 3.1, the biomass and NPP are much smaller. In simulation Advect 15, we saw the opposite problem - while biomass and NPP were in the observed range, the LAI was quite high. It is possible that limitations in IBIS' representation of grassland contributed to these discrepancies between our simulated values of LAI, biomass and NPP and the observed ranges of values for these quantities.

The climate of this simulation agrees reasonably well with the NCEP climatology for the region, but is hotter and drier. However, we should note that water is not conserved in the NCEP climate. In both the NCEP climatology (Figure 6-2 to Figure 6-4) and in our simulation (Figure 6-5 to Figure 6-8), there is considerable seasonality in the variables shown. As in the coastal domain, the lack of variable cloud cover in our model gives the incoming short wave radiation at the land surface the opposite seasonality from that seen in observations. Solar radiation peaks during the summer (wet) season in our simulation, while observations show that enhanced cloud cover during these months actually decreases the incoming solar radiation. This problem with our simulation is reflected in the net solar radiation at the land surface, shown in Figure 6-6.

Aside from the net shortwave radiation and the net allwave radiation, the seasonal variability in our model does not differ significantly from the climatology. In our simulation, the dry season lasts from approximately November through March,

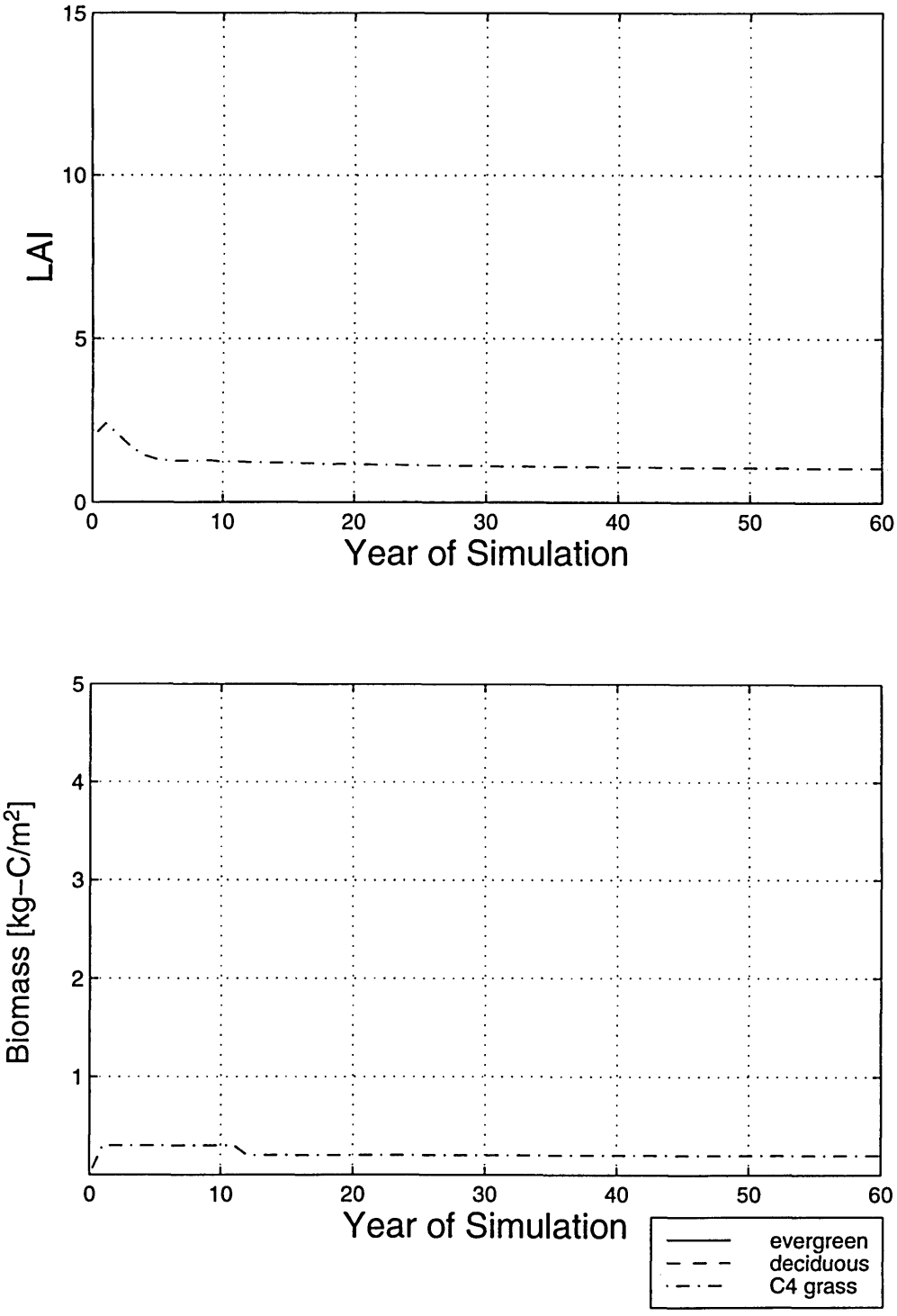

Figure 6-1: Inland domain: Fixed circulation simulations. At equilibrium, grassland is dominant in terms of both LAI and biomass for the control simulation, initialized with grassland.

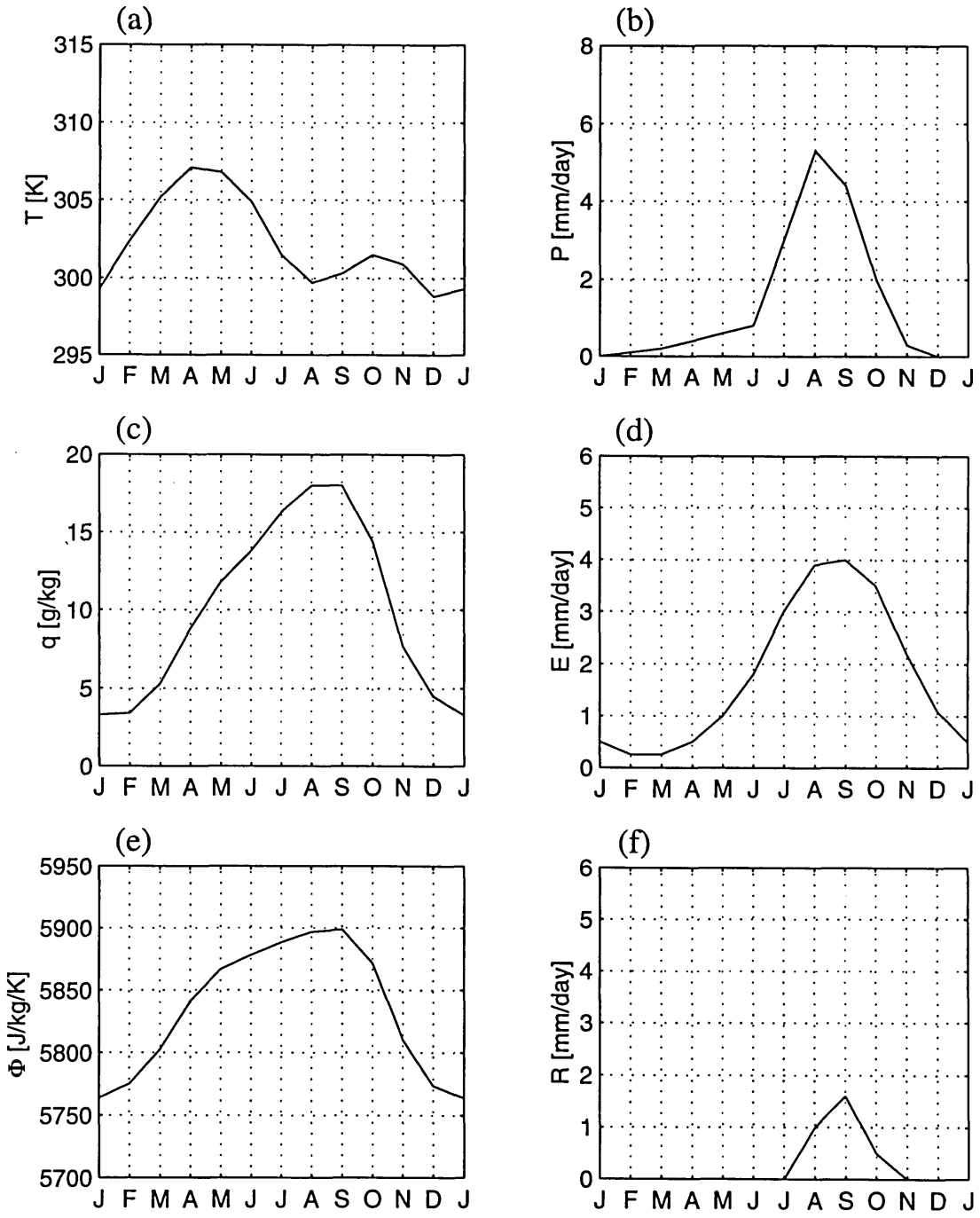

Figure 6-2: Inland domain: NCEP reanalysis climatology (1982-1994), seasonal cycle of climate. (a) Temperature (b) Precipitation (c) Specific humidity (d) Total evapotranspiration (e) Boundary layer entropy (f) Runoff

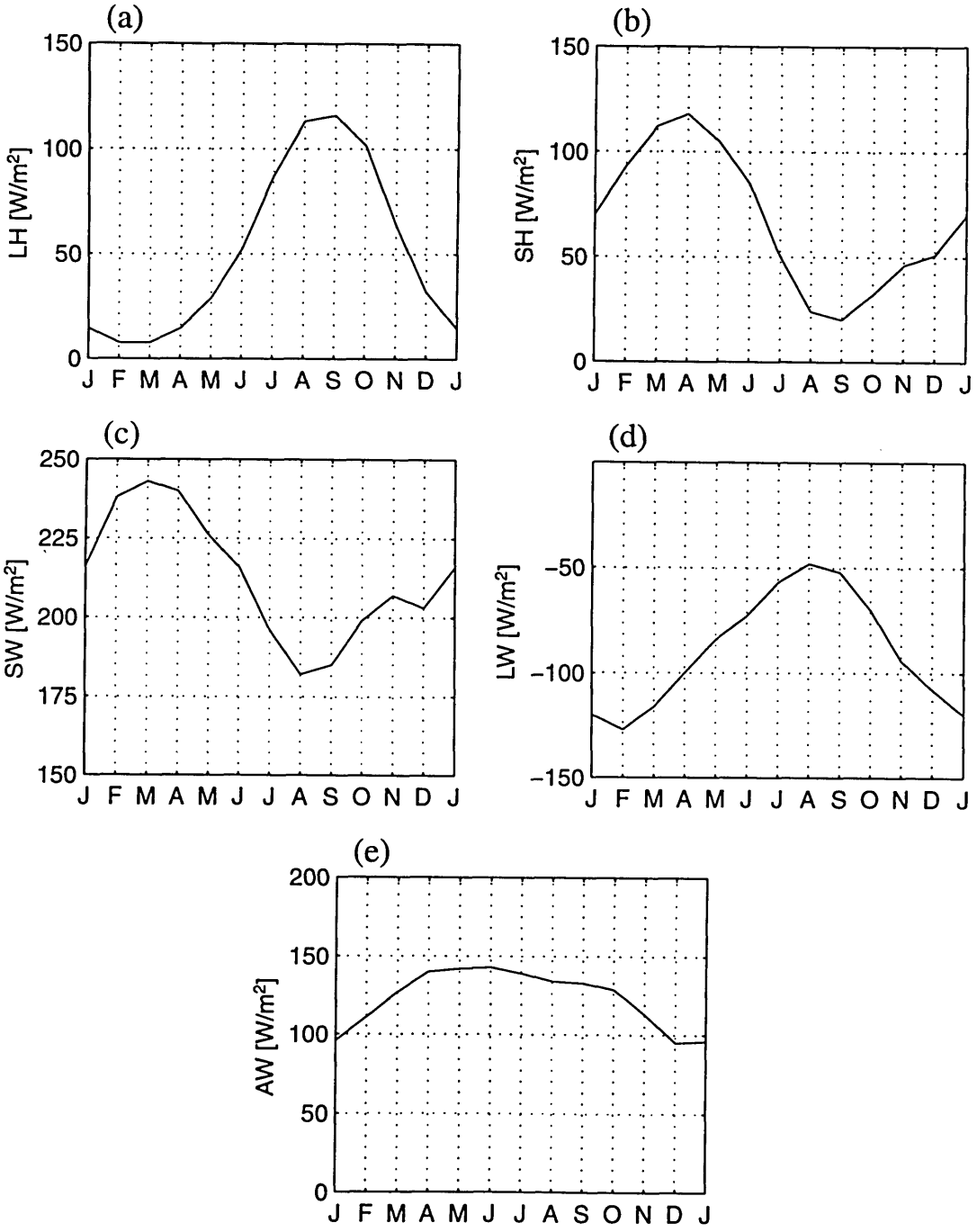

Figure 6-3: Inland domain: NCEP reanalysis climatology (1982-1994), land-atmosphere energy exchange. (a) Latent heat flux (b) Sensible heat flux (c) Net shortwave radiative flux (d) Net longwave radiative flux (e) Net allwave radiative flux

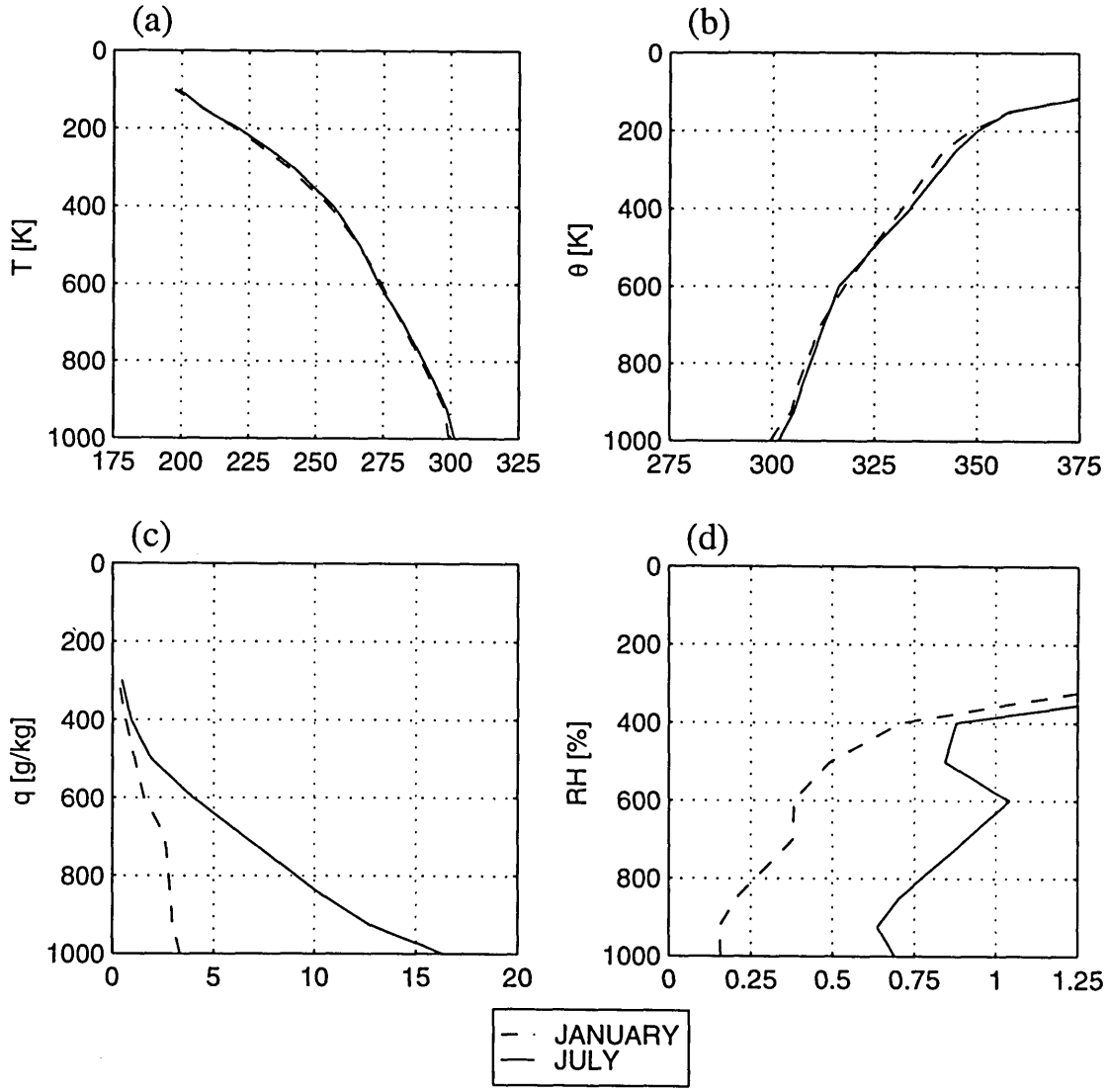

Figure 6-4: Inland domain: NCEP reanalysis climatology (1982-1994), atmospheric soundings. (a) Absolute temperature (b) Potential temperature (c) Specific humidity (d) Relative humidity

although April is also quite dry. During the wet season, precipitation peaks at about 4 mm/day. The NCEP climatology shows a dry season which lasts slightly longer, about November through May, and a wet season with a somewhat higher, but shorter duration peak in precipitation. The transition between the seasons is also more gradual in the NCEP climatology. The evaporation in our simulation shows a very similar seasonal pattern to the climatology, as does the precipitation. It is near zero during the dry season, but increases rapidly during the wet season to a peak of about 4 mm/day. Precipitation and evaporation balance at the annual time scale, and there is no runoff. The specific humidity in our model also shows a notable dry season from about November to March.

The temperature in both our simulation and the NCEP climatology peaks in about April-May and then decreases. The NCEP climatology shows a second, smaller peak in October-November which is not present in our model. Our mean annual temperature is higher than the NCEP climatology, and this is reflected in a higher temperature peak (near 311K) than is seen in the NCEP data (about 307K). The simulated entropy of the model domain compares fairly well with the climatology, ranging from a minimum of about 5760 J/kg/K to a maximum of about 5880 J/kg/K. The entropy calculated from the NCEP data has the same minimum but peaks at a value of about 5900 J/kg/K. The simulated entropy is approximately the same as the NCEP climatology despite biases in temperature and specific humidity because the higher temperature is offset by the decrease in specific humidity.

As before, the large spikes in the moisture and heat advection shown in Figure 6-7 are due to abrupt changes in both the fluxes of air and in the profiles of the advected air each month.

The soundings in Figure 6-8 show the mixed layer which extends through the three lowest layers of the model atmosphere, from the surface to about 830mb. The soundings also show that potential temperature increases with altitude, a stable situation. The moisture content of the atmosphere is seen to vary widely from January 1 to July 1; this is reflected in both the specific humidity and relative humidity plots.

Table 6.1: Inland Domain Control Run - Simulated Mean Annual Climate with Comparison to NCEP Climatology

Variable	NCEP Reanalysis 1982-1994 Climatology	Model Results	
		Climatological Fluxes	Flux Relation
T [K]	302.4	305.8	305.4
q [g/kg]	10.4	8.6	8.1
Precipitation [mm/day]	1.4	1.8	1.9
Total Evaporation [mm/day]	1.9	1.8	1.9
Interception Loss [mm/day]	-	0.4	0.7
Transpiration [mm/day]	-	0.6	0.9
Soil Evaporation [mm/day]	-	0.8	0.3
Runoff [mm/day]	0.3	0.0	0.0
Latent Heat [W/m2]	54	51	54
Sensible Heat [W/m2]	67	41	46
Net Solar [W/m2]	213	218	215
Net Longwave [W/m2]	-87	-127	-117
Net Allwave [W/m2]	126	91	98
Entropy Difference [J/kg/K]	-33	-30	-36

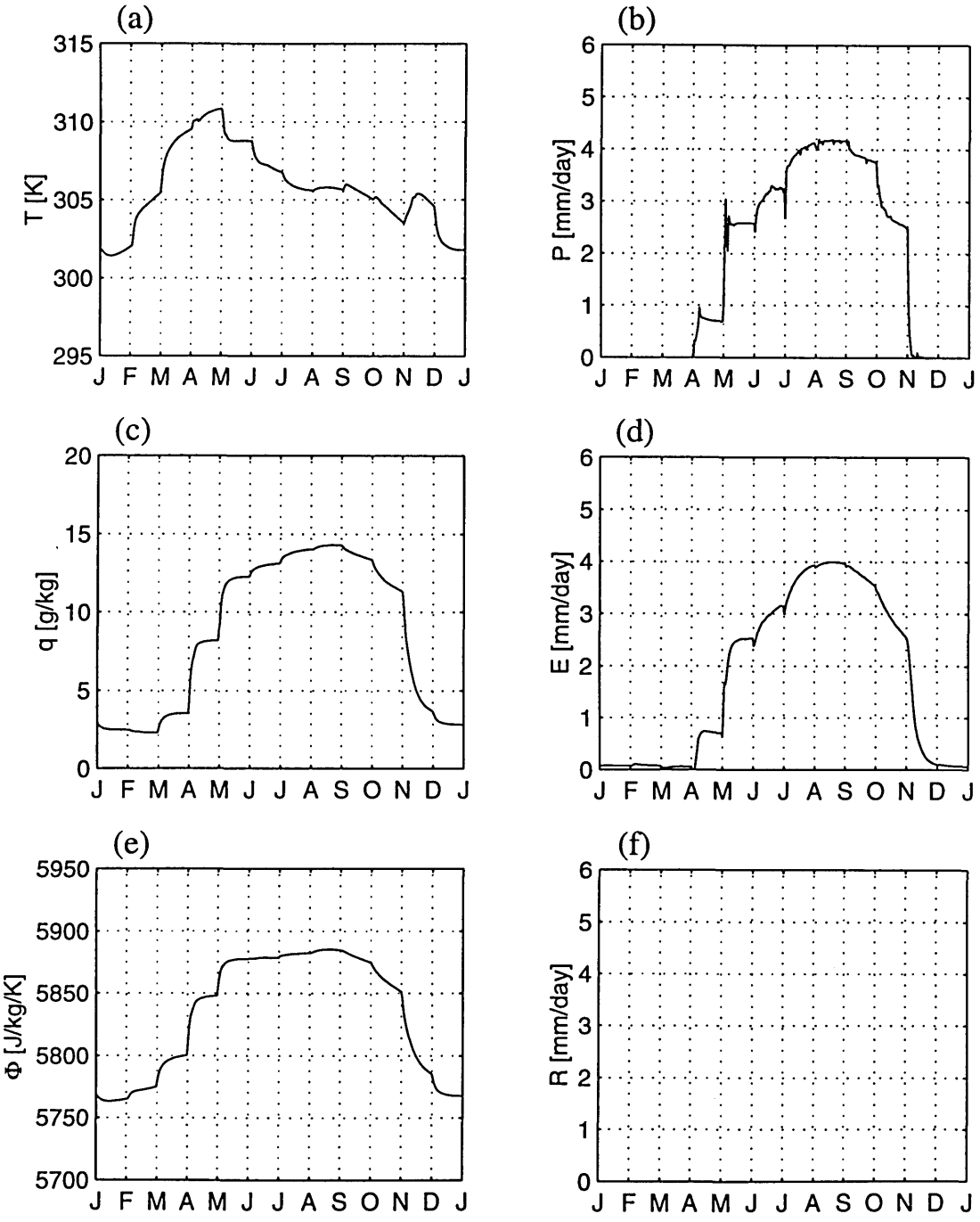

Figure 6-5: Inland domain: fixed circulation control simulation, mean annual climate. (a) Temperature (b) Precipitation (c) Specific humidity (d) Total evapotranspiration (e) Boundary layer entropy (f) Runoff

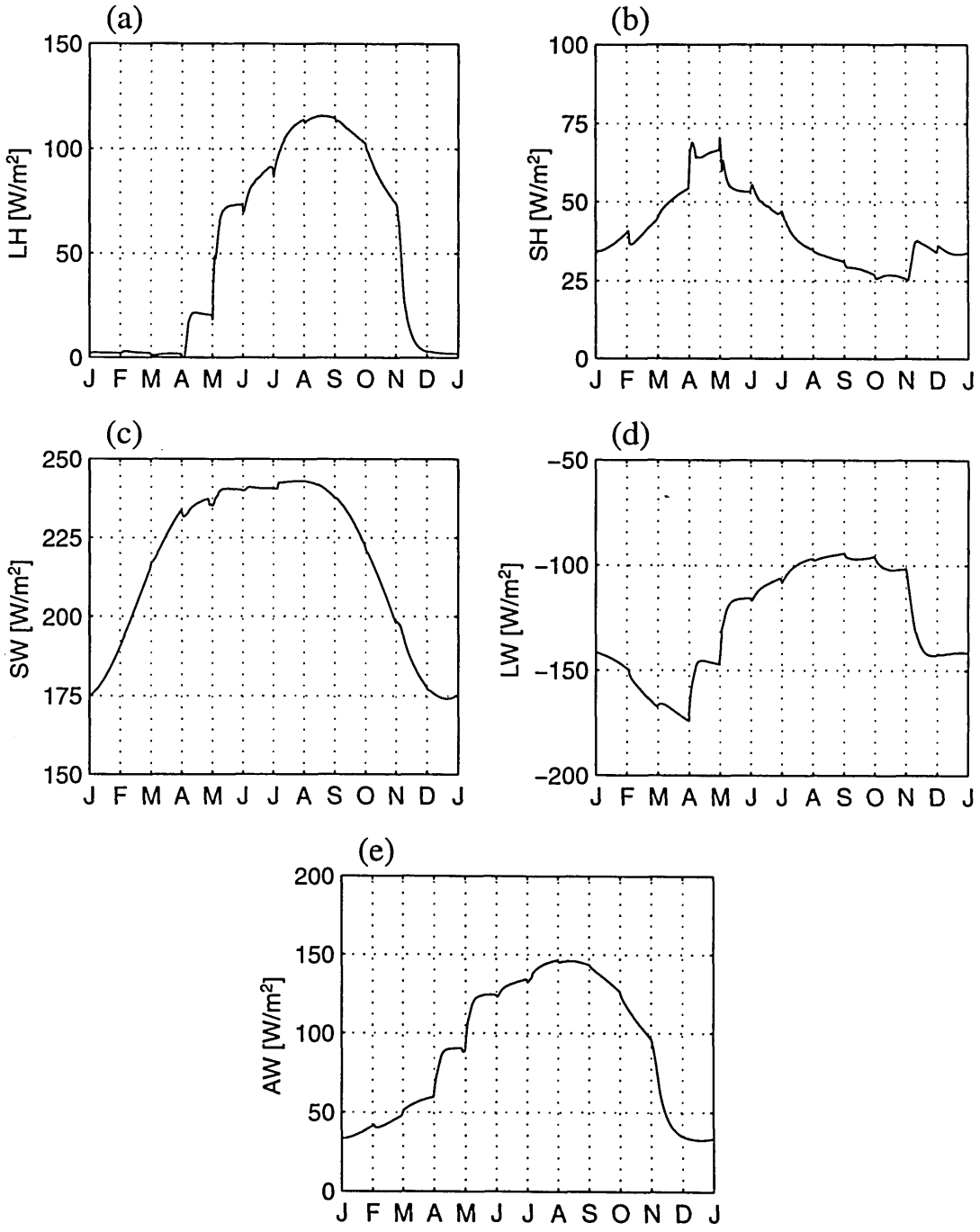

Figure 6-6: Inland domain: fixed circulation control simulation, land-atmosphere energy exchange. (a) Latent heat flux (b) Sensible heat flux (c) Net shortwave radiative flux (d) Net longwave radiative flux (e) Net allwave radiative flux

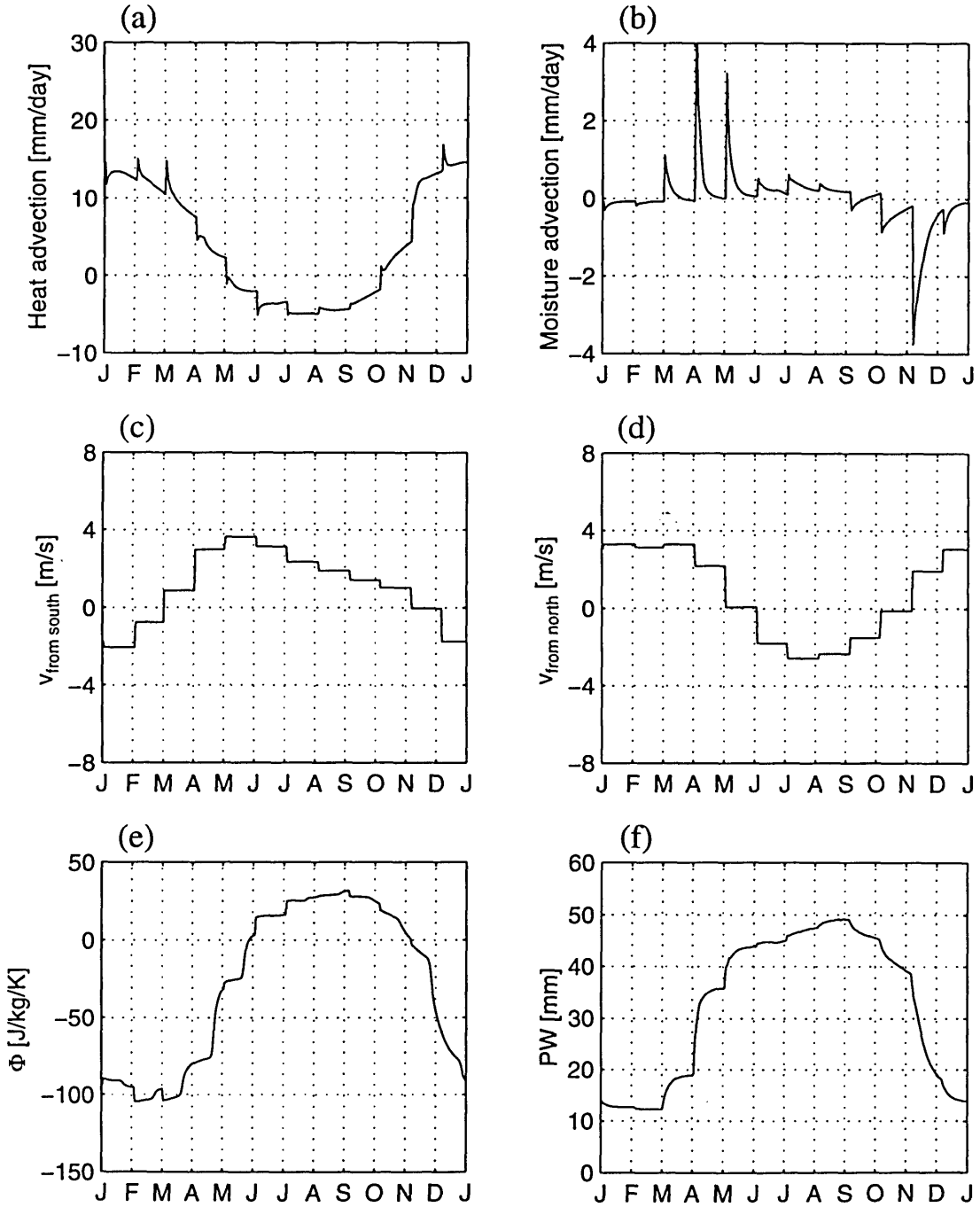

Figure 6-7: Inland domain: fixed circulation control simulation, monsoon circulation. (a) Heat advection (b) Moisture advection (c) Lowest level wind across southern boundary (d) Lowest level wind across northern boundary (e) Entropy difference between model domain and ocean region (f) Precipitable water

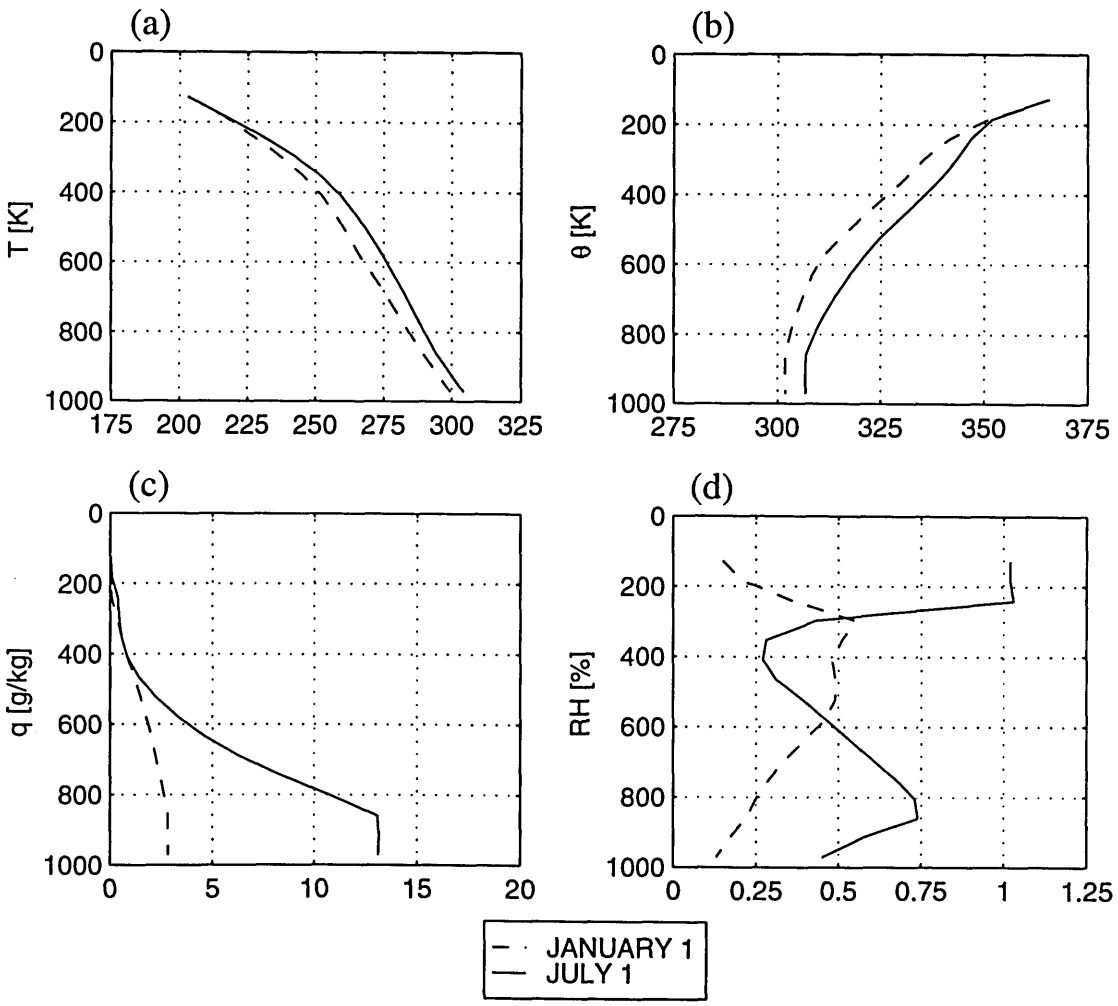

Figure 6-8: Inland domain: fixed circulation control simulation, atmospheric soundings. (a) Absolute temperature (b) Potential temperature (c) Specific humidity (d) Relative humidity

6.1.2 Control Simulation: Interactive Circulation

In the interactive circulation control simulation, we use our empirical monsoon circulation model to calculate the horizontal fluxes of air into the domain. The moisture and heat advection are calculated using the climatological profiles of humidity and temperature along the domain boundaries. This setup gives a more complete representation of our model domain, in which local conditions affect not only the local fluxes but also the monsoon circulation.

The mean annual climate of this simulation is very similar to that of the climatological control simulation (see Table 6.1). The main differences between the two simulations are seen in the seasonality of the climate (see Figure 6-10 to Figure 6-13). The dry season in the interactive circulation control simulation commences one to two months later than in the fixed circulation simulation. This may be due to differences in the timing of the monsoon circulation, which can be examined by looking at the surface winds simulated by the model, and seen in the climatology. In Figure 6-12 we see that the surface winds at the northern boundary agree quite well with those in the climatology (Figure 6-7). However, the dry winds from the north persist for one to two months longer than in the climatology. The influx of moist surface winds across the southern boundary is also delayed, in this case by about 3 months. These two features both contribute to a delay in the onset of precipitation in the interactive circulation control simulation. However, because the wet season actually extends into January, the length of the dry season is actually slightly reduced in this simulation as compared to the fixed circulation control simulation.

The equilibrium vegetation in this run is grassland. It has an LAI of 2.1 and a biomass of 0.4 kg/m^2. Figure 6-9 shows the evolution of LAI and biomass over the length of the run for the control simulation. The NPP is stable at about 0.2 kg/m^2/yr. The increase in vegetative cover in this simulation as compared to the fixed circulation control simulation is the result of the slightly higher mean annual precipitation and slightly longer wet season.

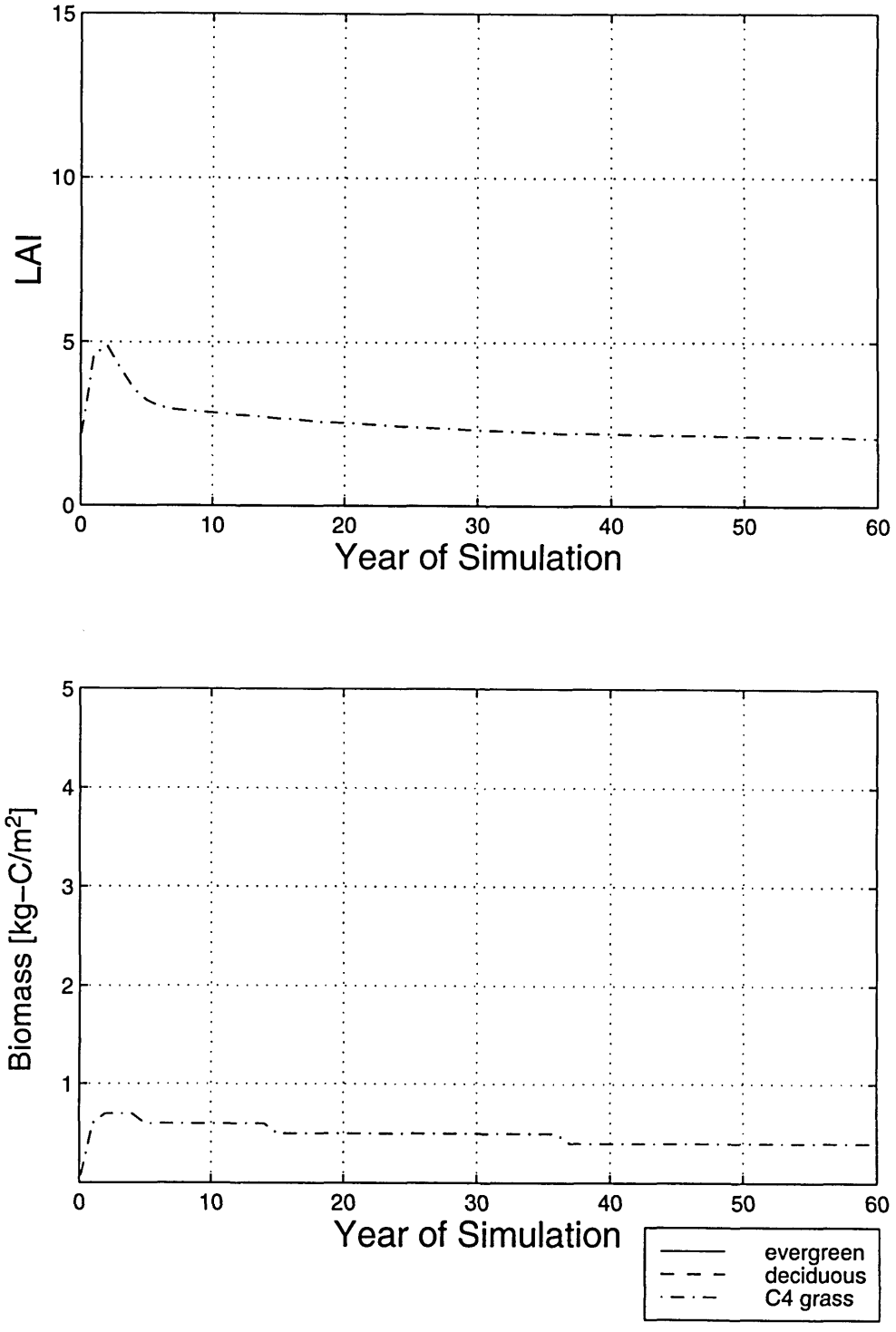

Figure 6-9: Inland domain: Interactive circulation simulations. At equilibrium, grassland is dominant in terms of both LAI and biomass for the control simulation, initialized with grassland.

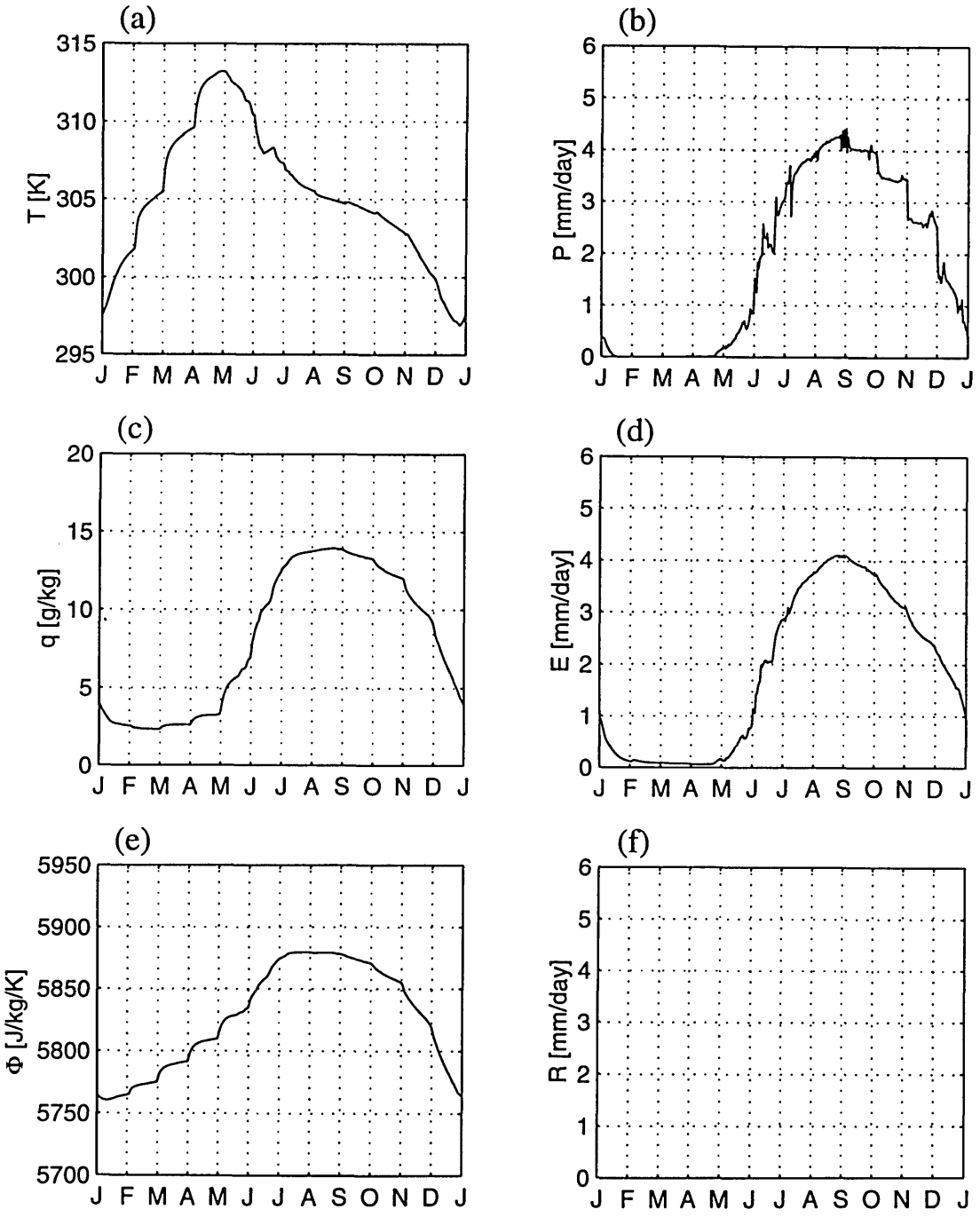

Figure 6-10: Inland domain: interactive circulation control simulation, mean annual climate. (a) Temperature (b) Precipitation (c) Specific humidity (d) Total evapotranspiration (e) Boundary layer entropy (f) Runoff

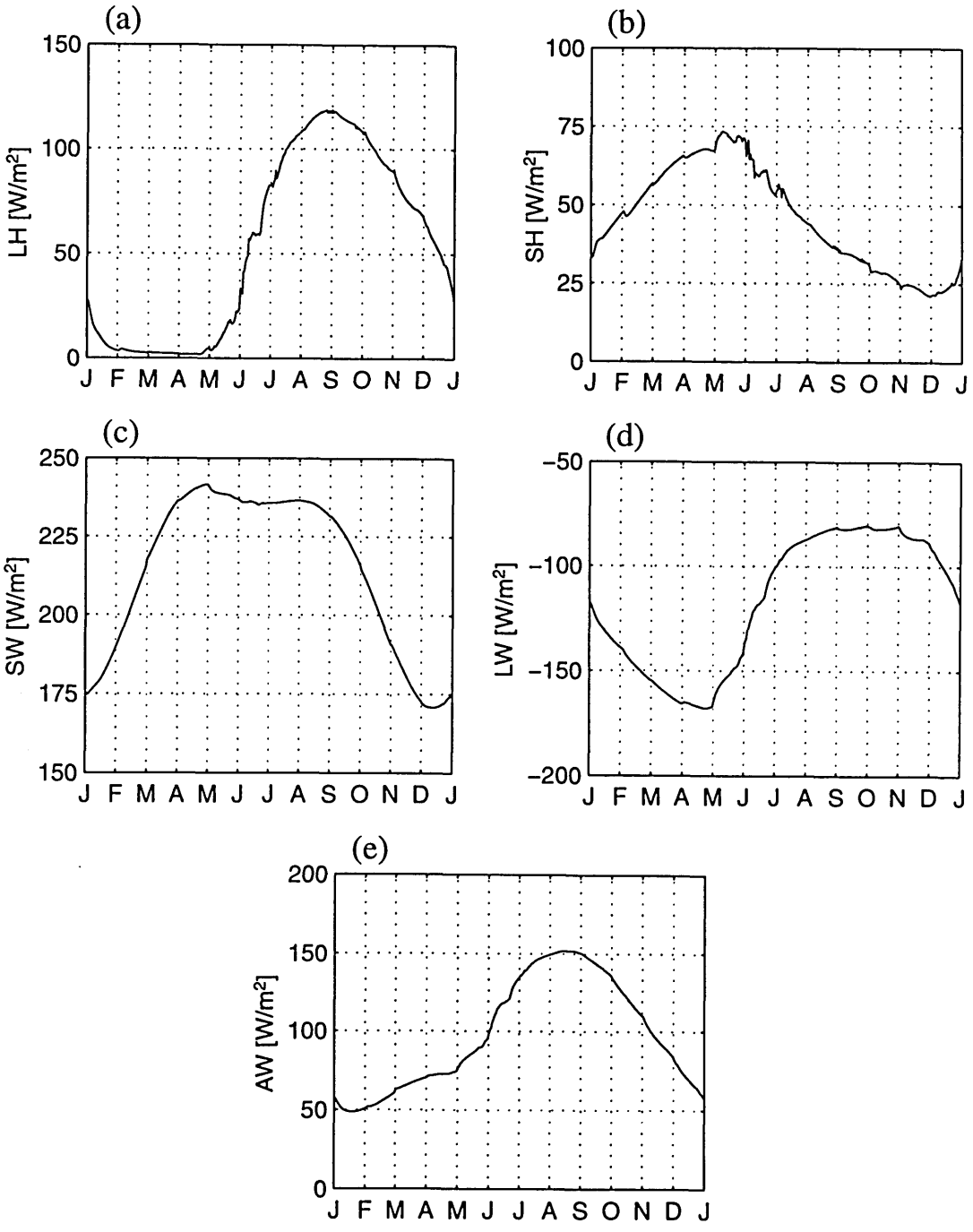

Figure 6-11: Inland domain: interactive circulation control simulation, land-atmosphere energy exchange. (a) Latent heat flux (b) Sensible heat flux (c) Net shortwave radiative flux (d) Net longwave radiative flux (e) Net allwave radiative flux

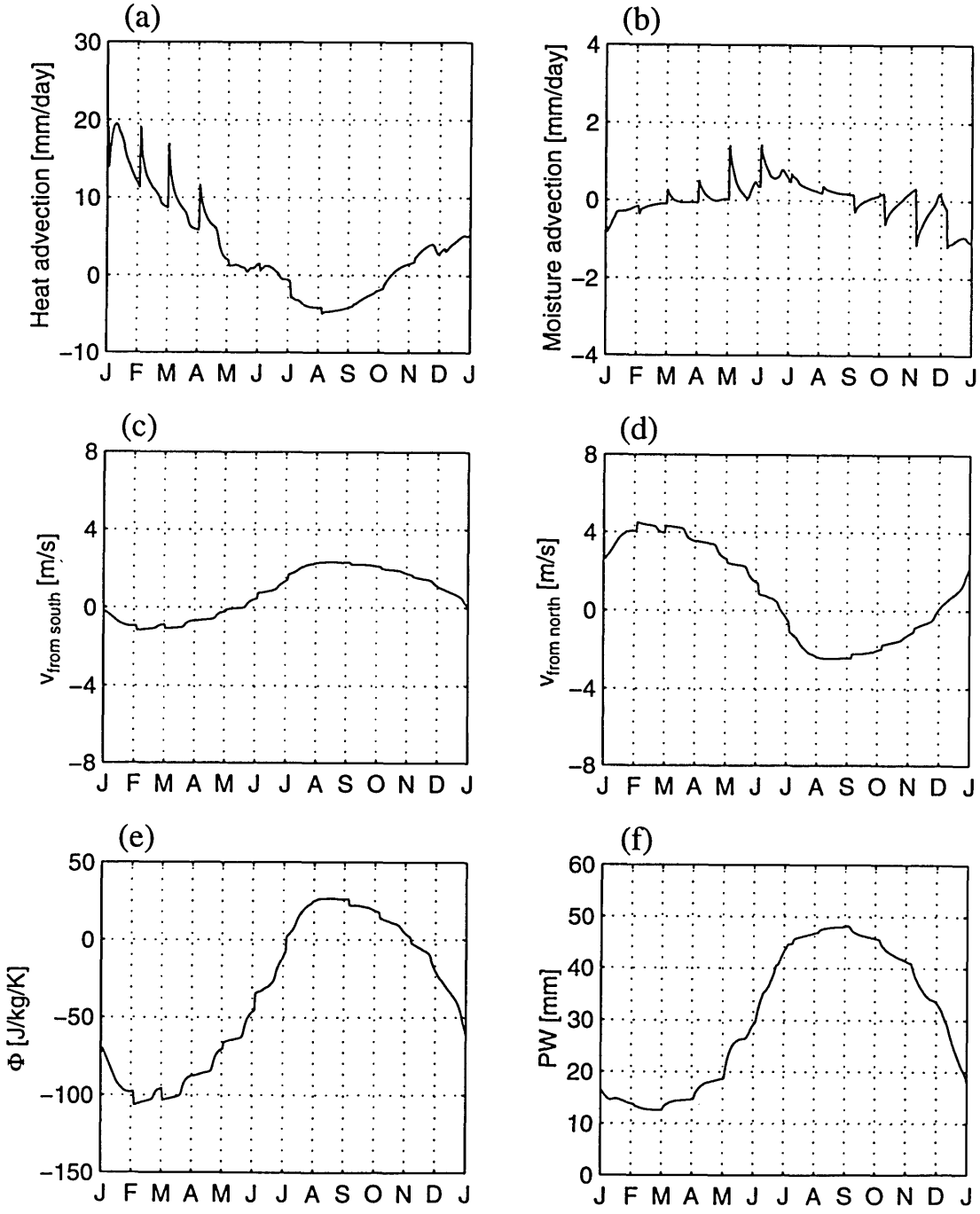

Figure 6-12: Inland domain: interactive circulation control simulation, monsoon circulation. (a) Heat advection (b) Moisture advection (c) Lowest level wind across southern boundary (d) Lowest level wind across northern boundary (e) Entropy difference between model domain and ocean region (f) Precipitable water

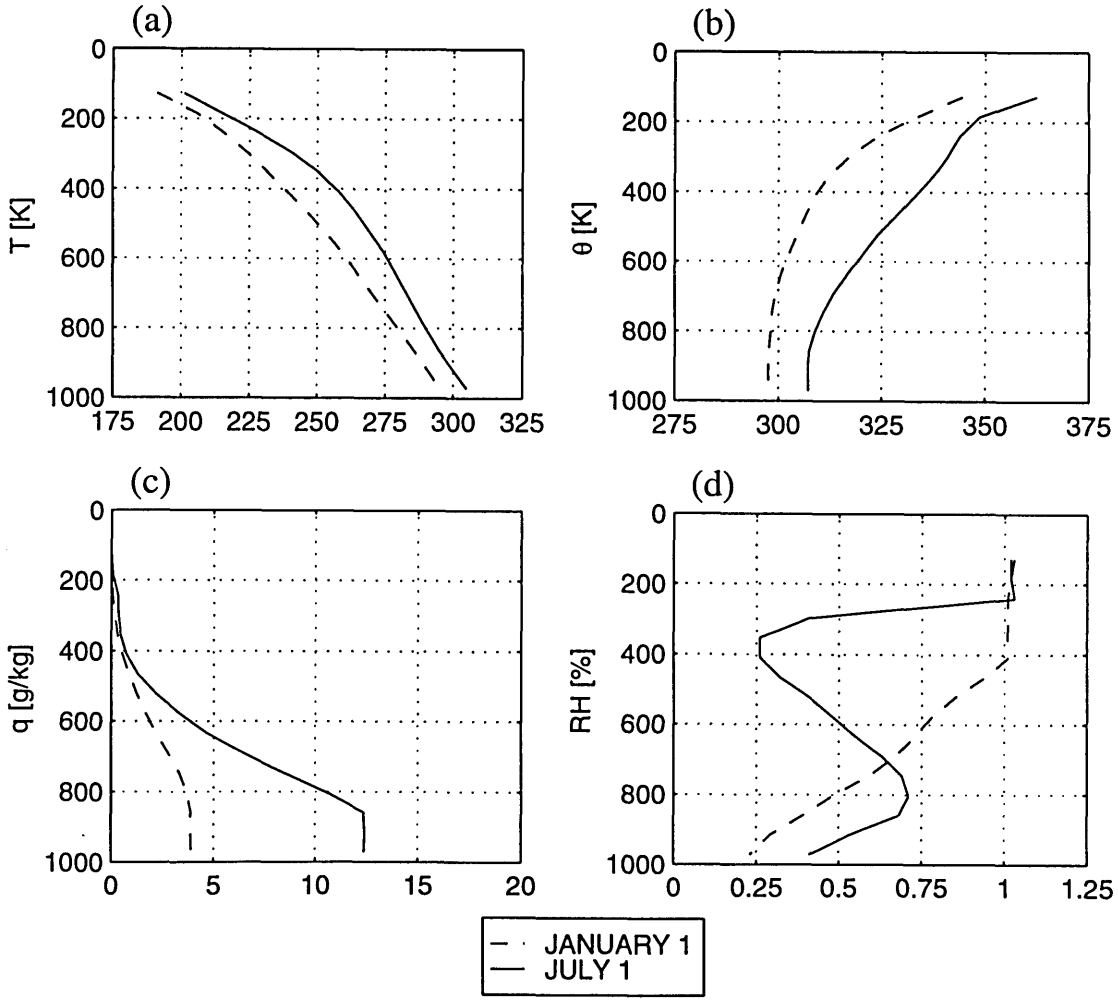

Figure 6-13: Inland domain: interactive circulation control simulation, atmospheric soundings. (a) Absolute temperature (b) Potential temperature (c) Specific humidity (d) Relative humidity

6.2 Afforestation Experiments: Fixed Circulation Case

In this experiment, we test the response of the system to a change in vegetation at the surface, when vegetation affects only the local water and energy exchange with the atmosphere. The fluxes of air across the northern and southern domain boundaries are held fixed at their climatological values, but since the moisture and heat advection depend not only on the climatological profiles at the domain boundaries, but also on the conditions within the model domain, the advection may change even though the magnitude of the fluxes is constant.

While we chose to study afforestation in these experiments, desertification experiments may also have yielded interesting results and can be considered in future work.

6.2.1 Static Vegetation Simulations

The sensitivity of the climate to the vegetation at the land surface is tested in a simulation in which the vegetation is held fixed as deciduous forest with an LAI of 10 and a height of 50 meters. In Table 6.2, we see that the change in vegetation had very little effect on the overall water balance. While partitioning between interception loss, transpiration and soil evaporation changed, the total evaporation and the precipitation were unchanged at an annual average of 1.8 mm/day. The temperature over forest is higher than that over grassland because of a higher energy input. The lower albedo of forest allows greater absorption of solar radiation, resulting in greater heating of the land surface.

We also see a smaller net longwave radiative flux from the surface with grassland cover than from the forest, even though the air temperature in the surface layers of the atmosphere is lower. In part, this is because the upwards longwave flux is calculated from the emmission of longwave radiation not from the air but from any exposed ground surface and from the overlying vegetation canopy. A large proportion (44%)

Table 6.2: Inland Domain: Modelled Forest vs. Grassland

Variable	Climatological Fluxes		Flux Relation	
	Forest	Grass	Forest	Grass
T [K]	306.9	305.8	306.5	305.4
q [g/kg]	8.6	8.6	8.2	8.1
Precipitation [mm/day]	1.8	1.8	1.9	1.9
Total Evaporation [mm/day]	1.8	1.8	1.9	1.9
Interception Loss [mm/day]	1.2	0.4	1.3	0.7
Transpiration [mm/day]	0.5	0.6	0.6	0.9
Soil Evaporation [mm/day]	0.1	0.8	0.1	0.3
Runoff [mm/day]	0.0	0.0	0.0	0.0
Latent Heat [W/m2]	53	51	55	54
Sensible Heat [W/m2]	65	41	62	46
Net Solar [W/m2]	232	218	232	215
Net Longwave [W/m2]	-115	-127	-117	-117
Net Allwave [W/m2]	117	91	115	98
Entropy Difference [J/kg/K]	-26	-30	-31	-36

of the total evaporation takes place from the bare soil when there is grassland. Since the total evapotranspiration over grassland and forest is nearly the same, there is consequently less interception loss and transpiration to cool the canopy surfaces over grassland than over forest. The higher canopy temperatures result in larger emmission of longwave radiation and hence contributes to the smaller net longwave radiative flux. The downwards component of the longwave radiative flux is also smaller over grassland, due to smaller emmissions from the lower atmosphere which has a lower temperature. The seasonal variability of the climate under forest conditions is shown in Figure 6-14 to Figure 6-17.

6.2.2 Dynamic vegetation simulations

In the experimental run, we initialize the vegetation as deciduous forest and allow the vegetation and climate to find its own equilibrium. The sensitivity run showed that the presence of a large forest was unable to significantly alter the climate.

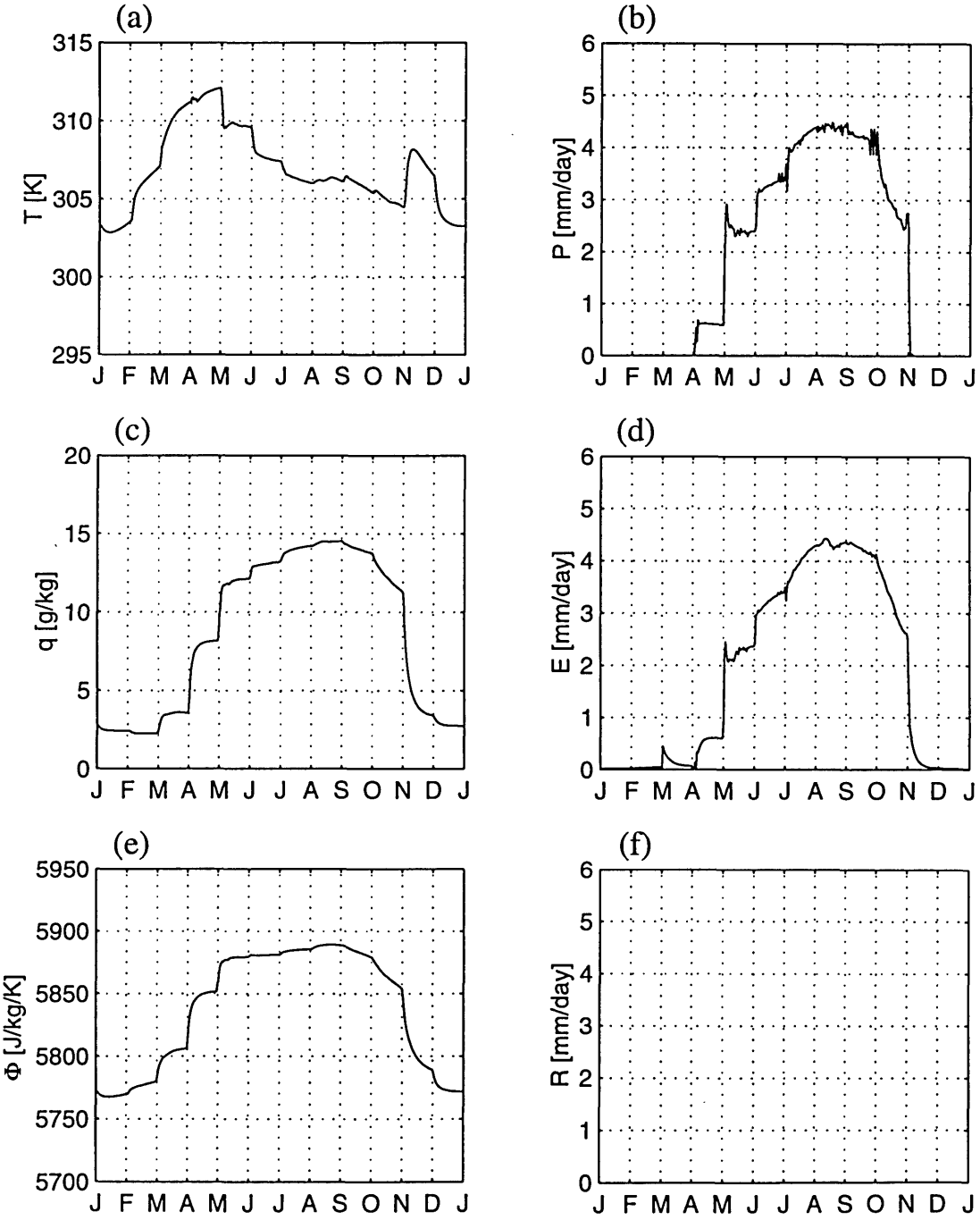

Figure 6-14: Inland domain: fixed circulation control simulation, mean annual climate, fixed deciduous forest. (a) Temperature (b) Precipitation (c) Specific humidity (d) Total evapotranspiration (e) Boundary layer entropy (f) Runoff

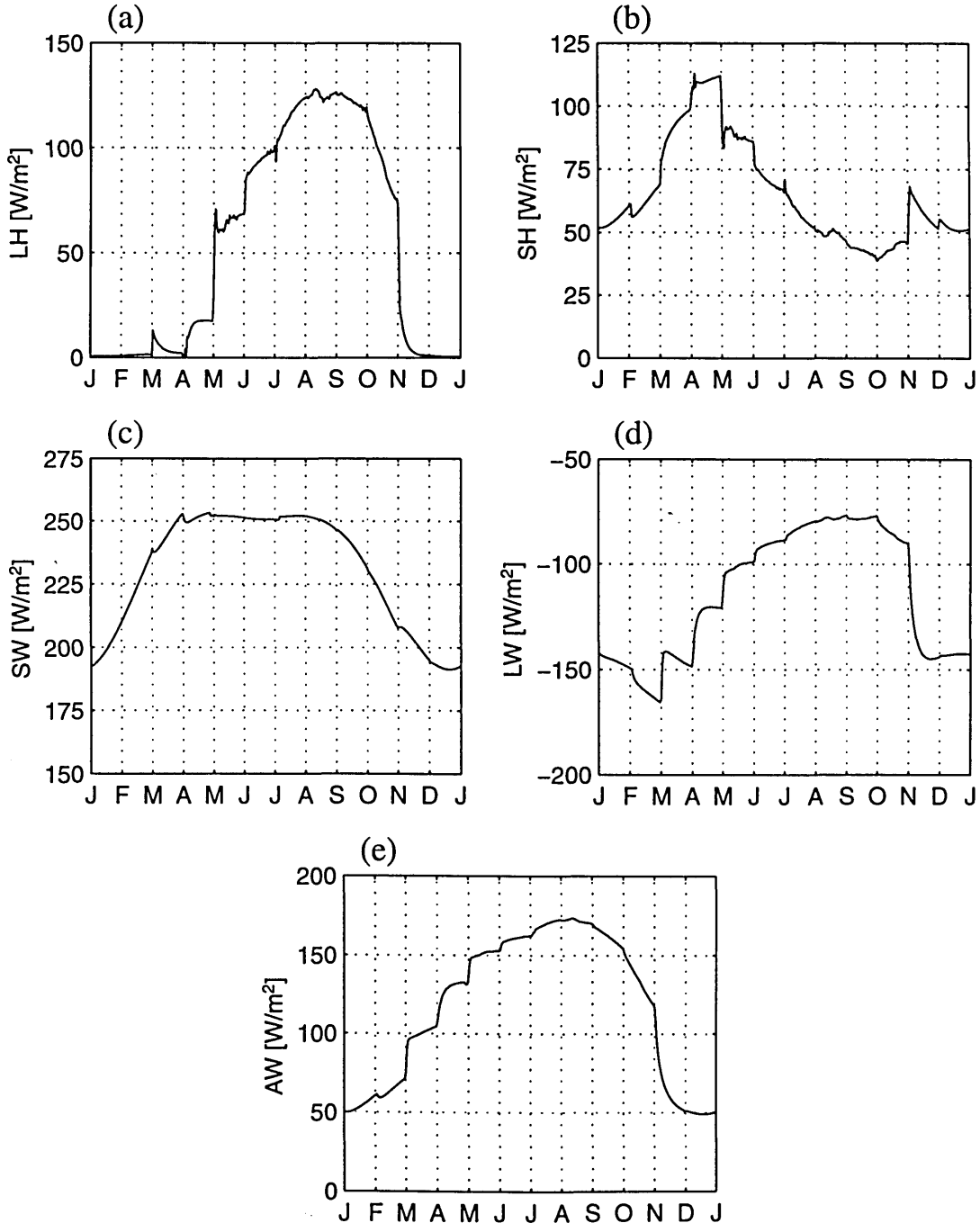

Figure 6-15: Inland domain: fixed circulation control simulation, land-atmosphere energy exchange, fixed deciduous forest. (a) Latent heat flux (b) Sensible heat flux (c) Net shortwave radiative flux (d) Net longwave radiative flux (e) Net allwave radiative flux

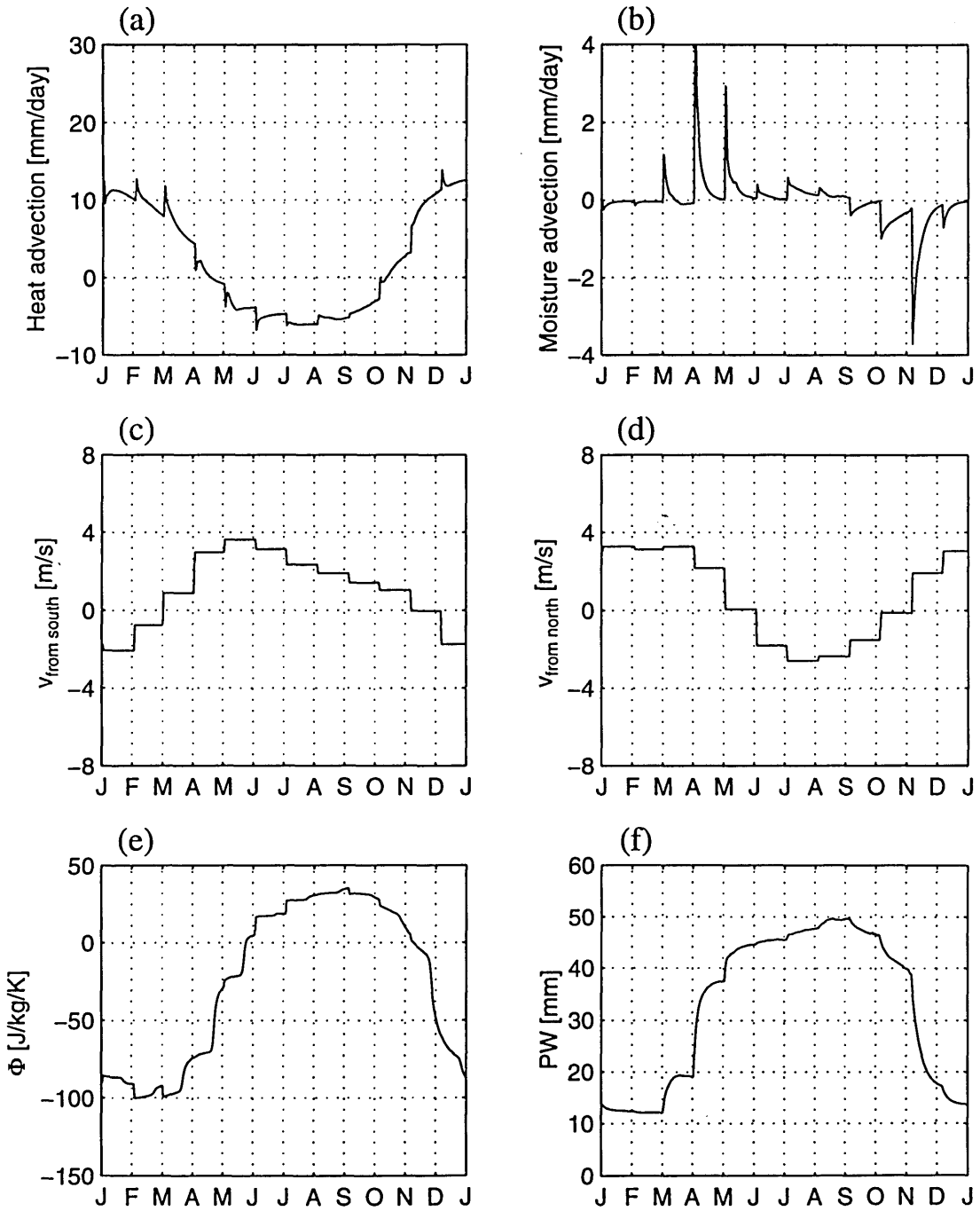

Figure 6-16: Inland domain: fixed circulation control simulation, monsoon circulation, fixed deciduous forest. (a) Heat advection (b) Moisture advection (c) Lowest level wind across southern boundary (d) Lowest level wind across northern boundary (e) Entropy difference between model domain and ocean region (f) Precipitable water

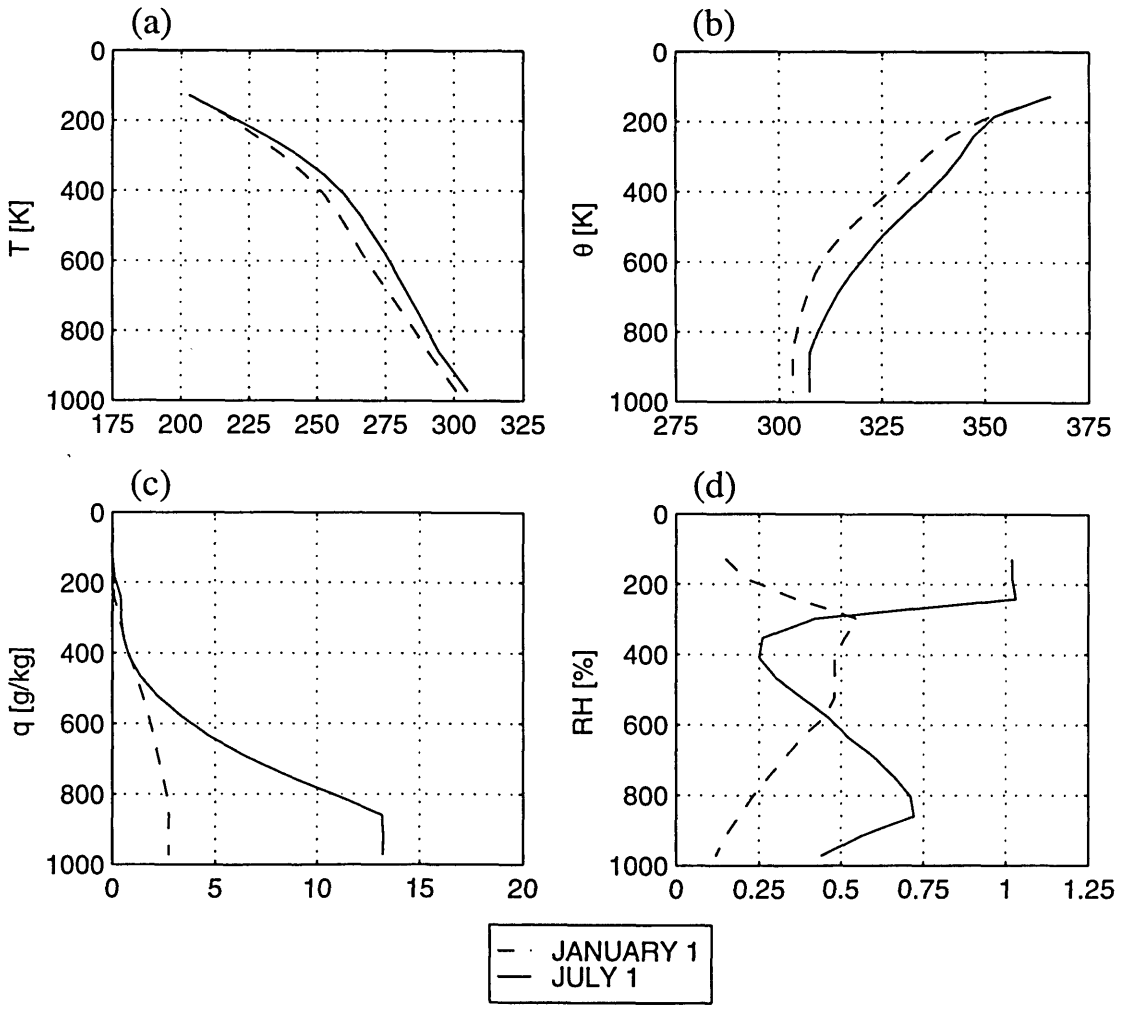

Figure 6-17: Inland domain: fixed circulation control simulation, atmospheric soundings, fixed deciduous forest. (a) Absolute temperature (b) Potential temperature (c) Specific humidity (d) Relative humidity

Not surprisingly, then, the equilibrium vegetation and climate of the experimental simulation reverted to grassland with the climate seen in the fixed circulation control simulation. In fact, the change is sudden - the LAI of the forest drops abruptly to zero, as seen in Figure 6-18. The NPP of the forest in the first year of simulation is negative, and the forest dies. Note that in Figure 6-19 the biomass never climbs above zero. This is because of an error in the biomass initialization. A higher biomass would actually have resulted in a lower (more negative) initial NPP, as the needs for maintenance respiration are increased. A higher biomass would not then have prevented the forest's demise, but the biomass would have persisted for some time while the grassland grew up around it. The biomass initialization problem is discussed further in Appendix A.

This experiment considered only afforestation of the model domain, and not desertification. Future work can include the study of desertification, which may have significant impacts on the climate.

6.3 Afforestation Experiments: Interactive Circulation Case

In this experiment we test the sensitivity of the model to initial vegetation conditions when the full effects of vegetation are felt. Changing characteristics of the land surface affect not only the local water and energy exchange but also the strength of the monsoon circulation.

6.3.1 Static Vegetation Simulations

We first test the sensitivity of the climate to vegetation type by holding vegetation fixed as deciduous forest and allowing the climate to adjust to those conditions. Table 6.2 shows the mean annual climate of this sensitivity run. The seasonal variability in the climate is shown in Figure 6-20 to Figure 6-23. As in the fixed circulation experiment, we see that the change in vegetation does not alter the climate

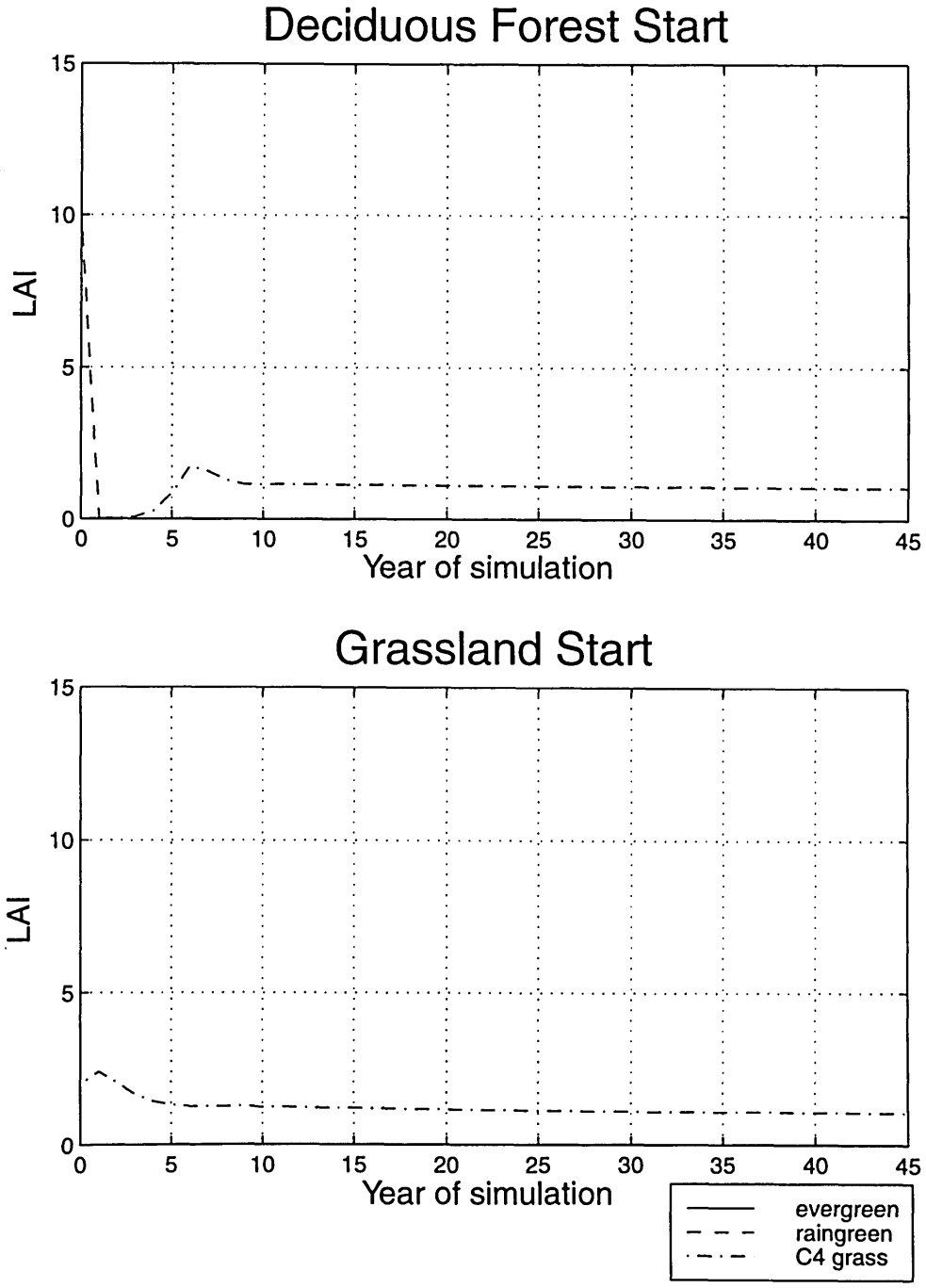

Figure 6-18: Inland domain: Fixed circulation simulations. At equilibrium, grassland is dominant with the same LAI, regardless of the initial vegetation conditions.

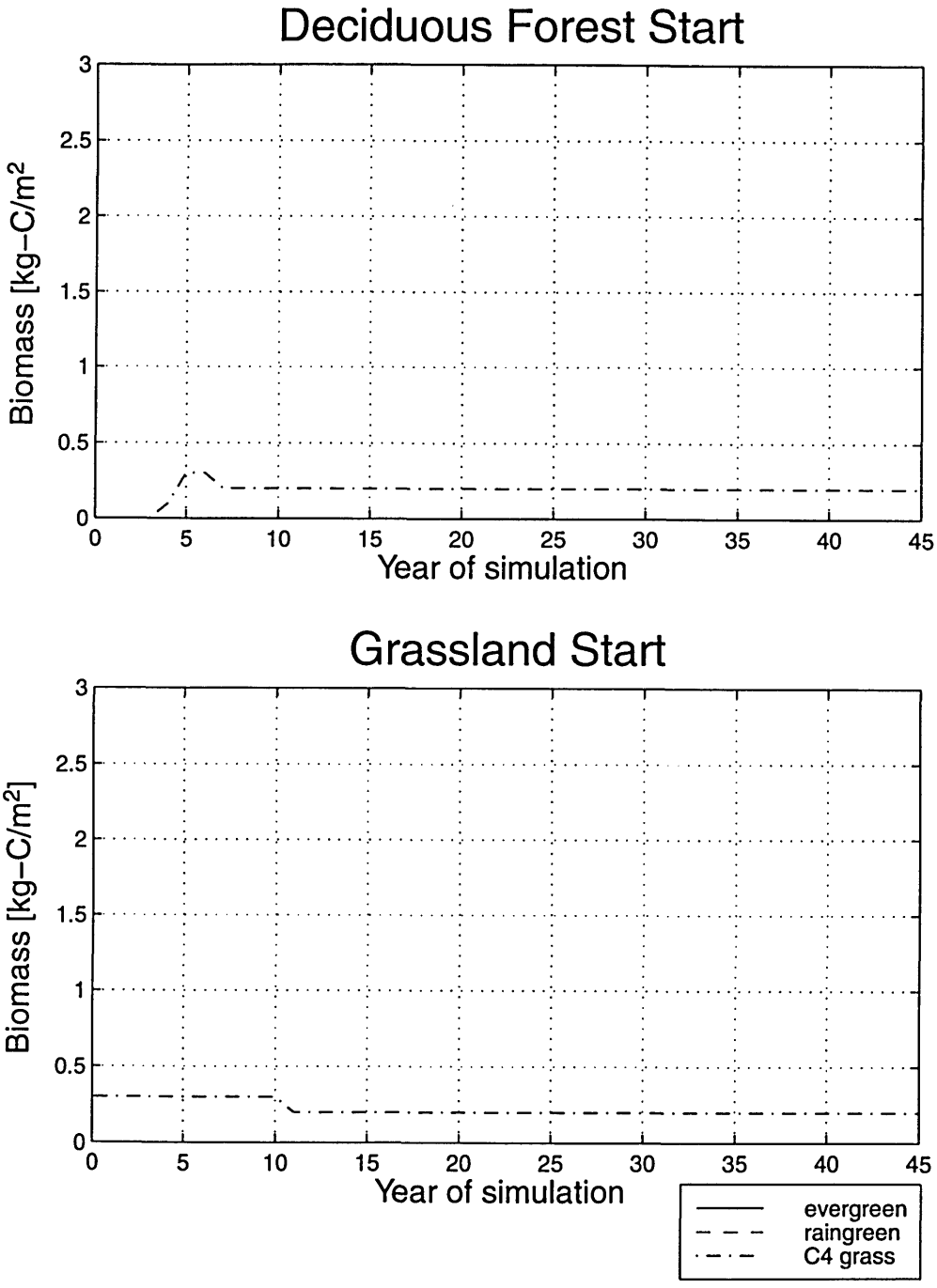

Figure 6-19: Inland domain: Fixed circulation simulations. At equilibrium, grassland is dominant with the same biomass, regardless of the initial vegetation conditions.

significantly. The presence of the forest does not significantly alter the fluxes of air into the region and moisture availability is unchanged.

6.3.2 Dynamic vegetation simulations

In the experimental simulation, we initialize the vegetation as deciduous forest and then allow the system to find its own equilibrium. The evolution of the LAI and biomass are shown in Figure 6-24 and Figure 6-25. As seen in the previous section, the climate shows little sensitivity to the vegetation type, and the equilibrium vegetaton reverts to grassland. There is insufficient water to support a forest, and as in the fixed circulation afforestation experiment, the forest NPP is negative, accounting for the abrupt transition from forest to grassland.

Again, while the equilibrium vegetation and climate do not show sensitivity to afforestation, the system may be more responsive to desertification, which may be studied in future work.

6.4 Sensitivity of Results to Slope of Empirical Flux Relationship

In this experiment, we test the sensitivity of our results to the slope of the empirical flux relationship at the southern domain boundary. The climate shows little sensitivity to these changes, as seen in Table 6.3. Neither is there significant sensitivity to vegetation type, and experimental runs show that the equilibrium vegetation in all cases is grassland (see Table 6.5). These results further support the finding of the previous sections that afforestation of this region does not enhance precipitation and that the afforestation cannot be sustained.

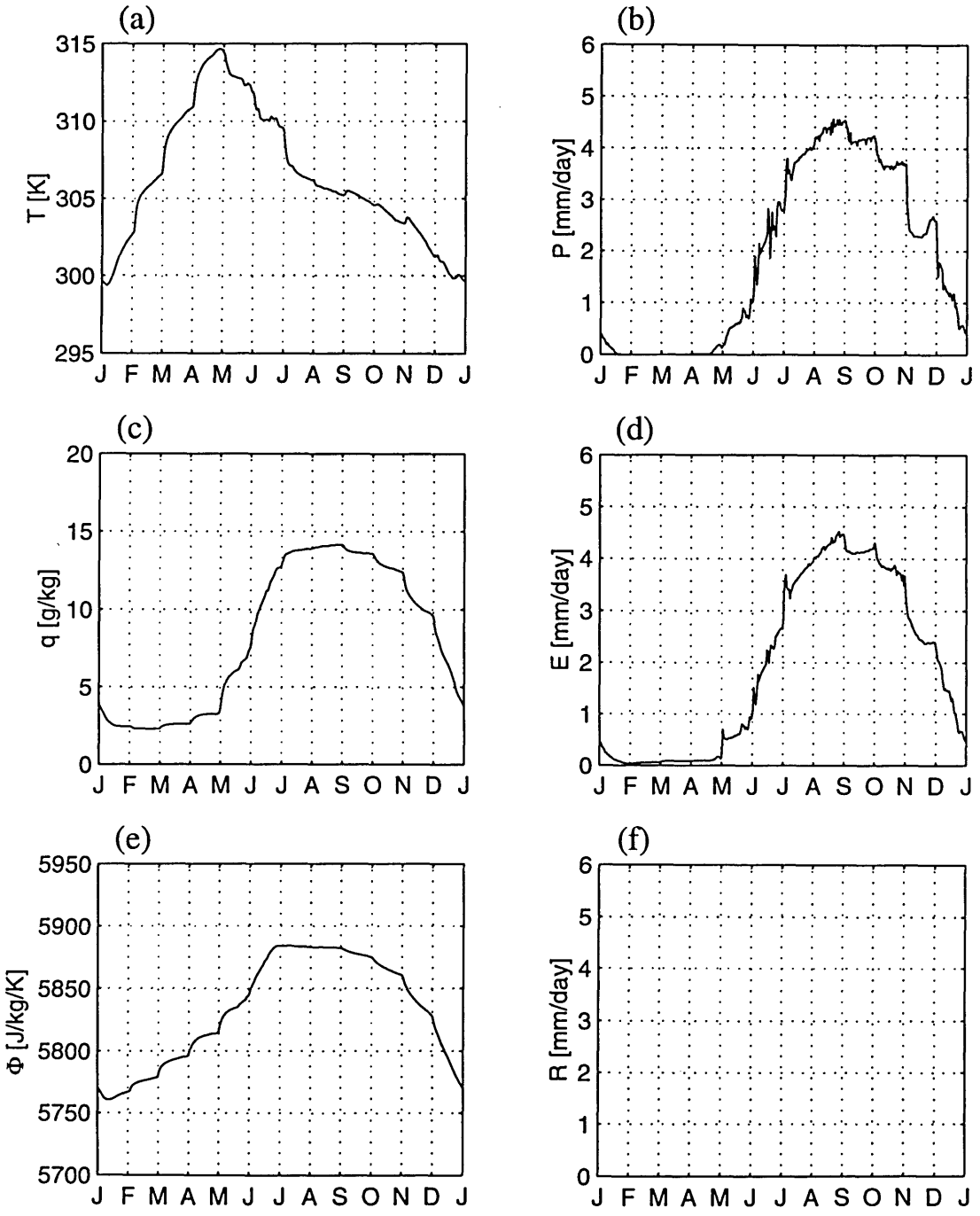

Figure 6-20: Inland domain: interactive circulation control simulation, mean annual climate, fixed deciduous forest. (a) Temperature (b) Precipitation (c) Specific humidity (d) Total evapotranspiration (e) Boundary layer entropy (f) Runoff

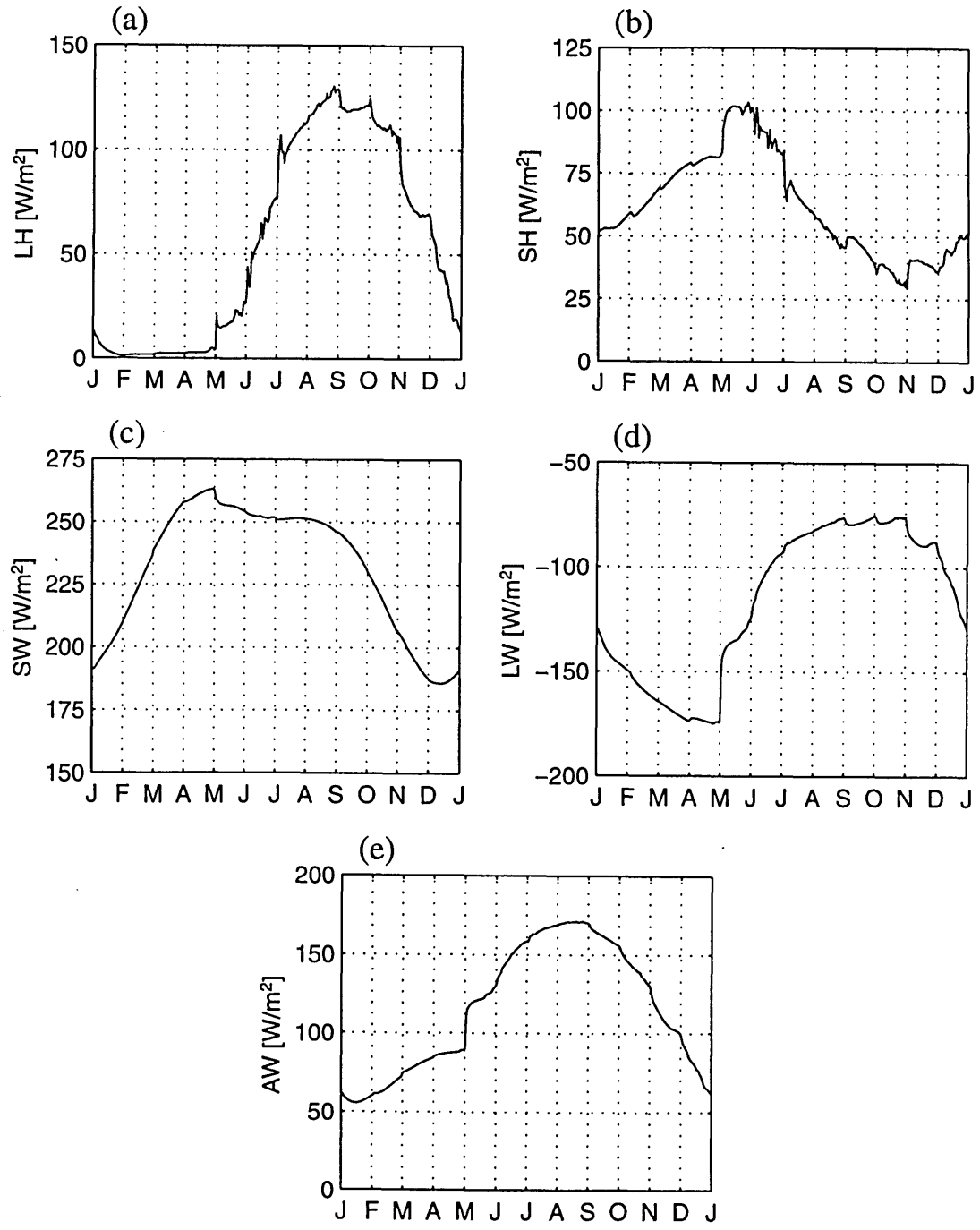

Figure 6-21: Inland domain: interactive circulation control simulation, land-atmosphere energy exchange, fixed deciduous forest. (a) Latent heat flux (b) Sensible heat flux (c) Net shortwave radiative flux (d) Net longwave radiative flux (e) Net allwave radiative flux

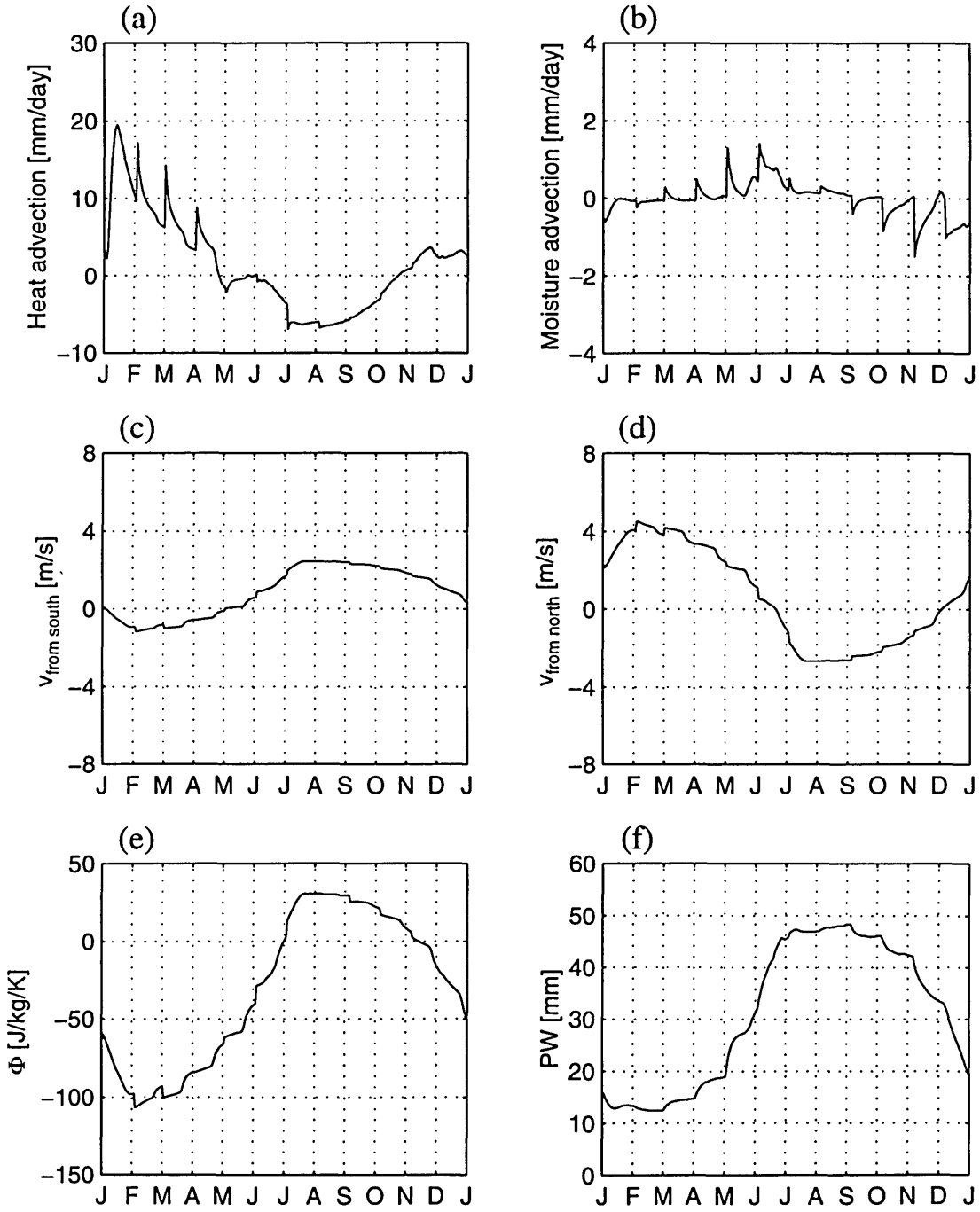

Figure 6-22: Inland domain: interactive circulation control simulation, monsoon circulation, fixed deciduous forest. (a) Heat advection (b) Moisture advection (c) Lowest level wind across southern boundary (d) Lowest level wind across northern boundary (e) Entropy difference between model domain and ocean region (f) Precipitable water

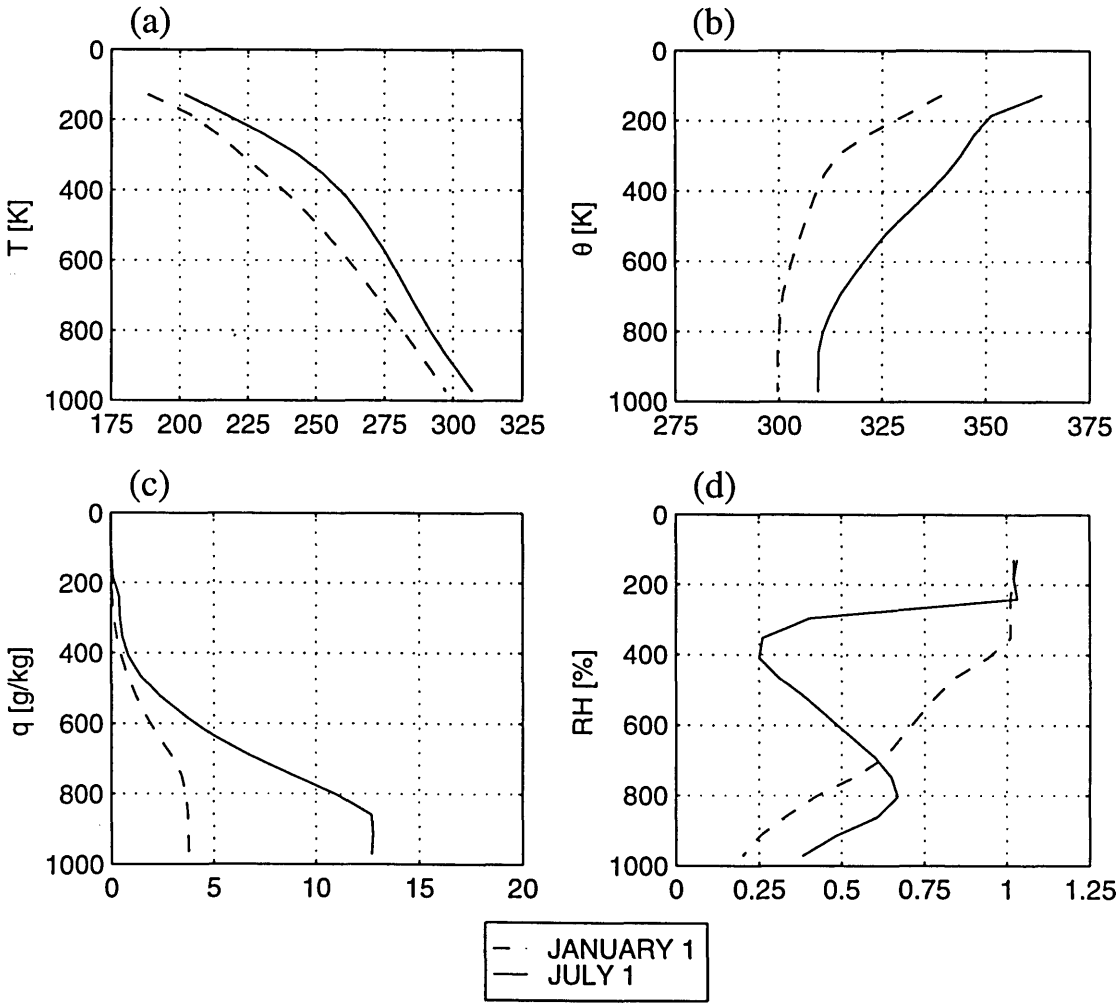

Figure 6-23: Inland domain: interactive circulation control simulation, atmospheric soundings, fixed deciduous forest. (a) Absolute temperature (b) Potential temperature (c) Specific humidity (d) Relative humidity

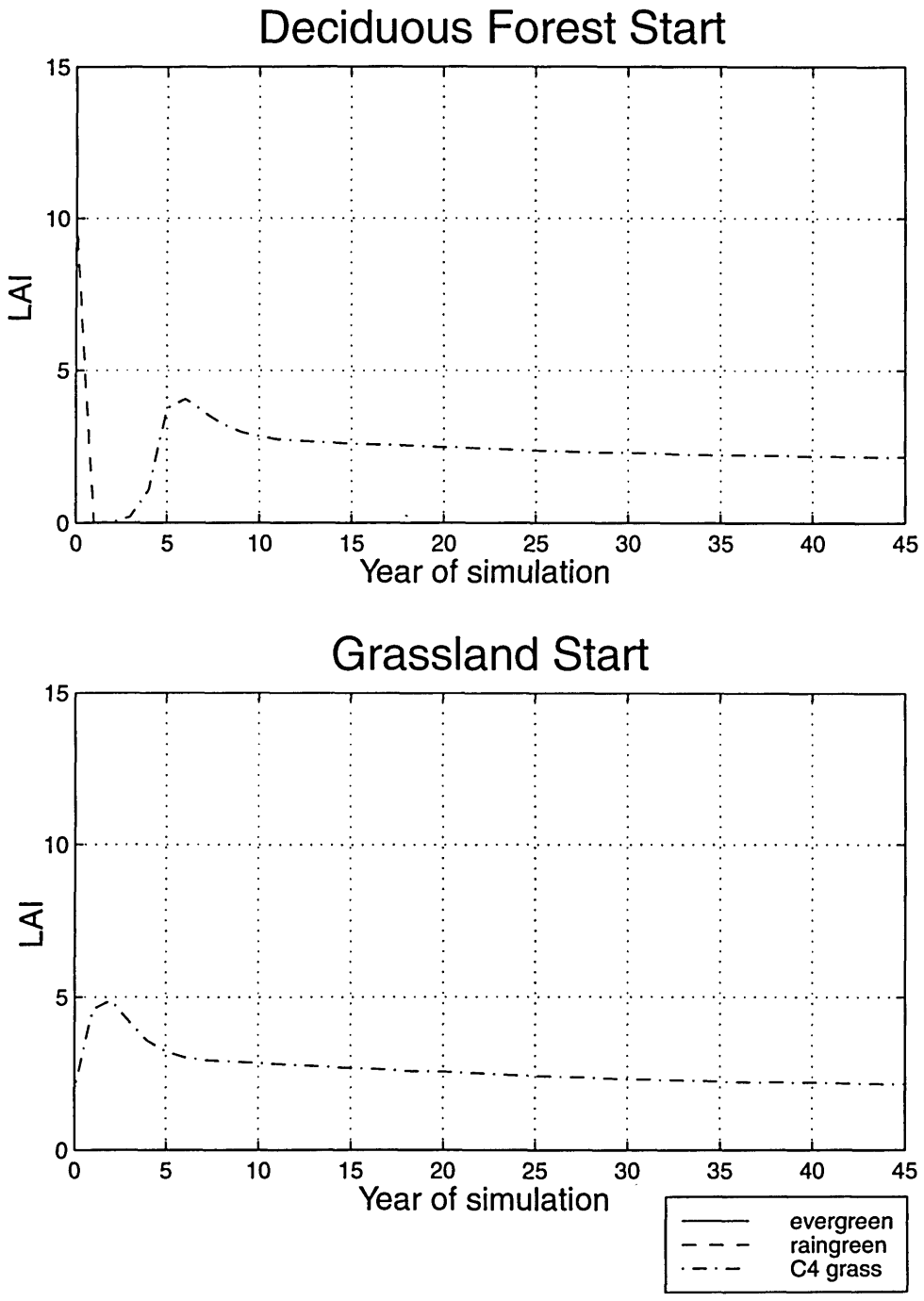

Figure 6-24: Inland domain: Interactive circulation simulations. At equilibrium, grassland is dominant with the same LAI, regardless of the initial vegetation conditions.

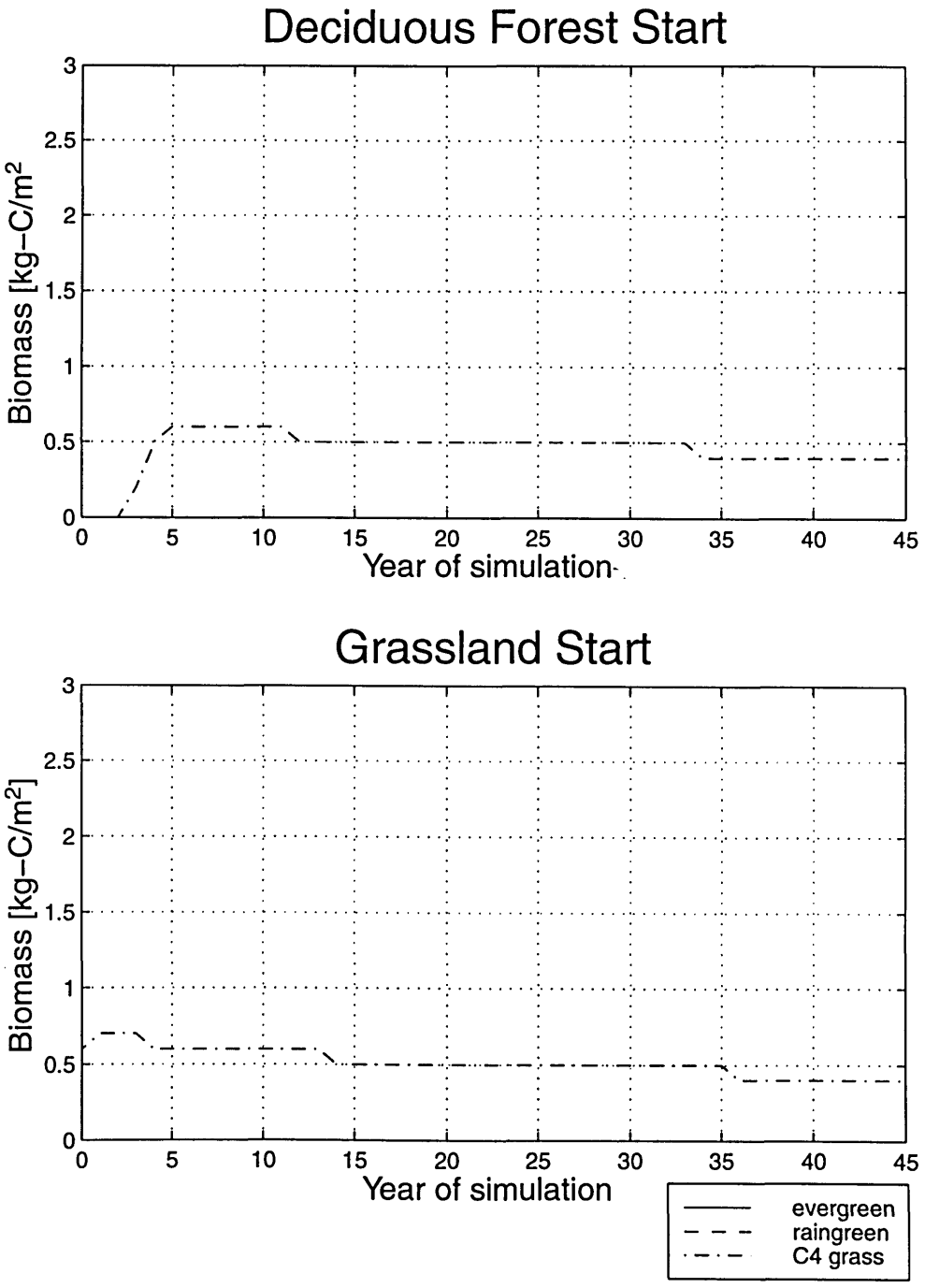

Figure 6-25: Inland domain: Interactive circulation simulations. At equilibrium, grassland is dominant with the same biomass, regardless of the initial vegetation conditions.

Table 6.3: Inland Domain: Modelled Forest vs. Grassland, with modified monsoon circulation

Variable	Ocean Flux 2.0 X Slope		Ocean Flux 0.5 X Slope	
	Forest	Grass	Forest	Grass
T [K]	307.4	306.3	305.5	304.2
q [g/kg]	8.0	7.7	8.7	8.6
Precipitation [mm/day]	1.8	1.7	2.0	2.0
Total Evaporation [mm/day]	1.8	1.7	2.0	2.0
Interception Loss [mm/day]	1.2	0.6	1.4	0.9
Transpiration [mm/day]	0.5	0.9	0.6	1.0
Soil Evaporation [mm/day]	0.1	0.3	0.1	0.1
Runoff [mm/day]	0.0	0.0	0.0	0.0
Latent Heat [W/m2]	52	48	59	59
Sensible Heat [W/m2]	63	49	62	47
Net Solar [W/m2]	234	215	232	214
Net Longwave [W/m2]	-119	-119	-112	-109
Net Allwave [W/m2]	115	96	120	105
Entropy Difference [J/kg/K]	-30	-36	-30	-35

Table 6.4: Inland Domain: Modelled Forest vs. Grassland, with modified horizontal air fluxes and advection

Variable	Ocean Advection Profile at 7.5N	
	Forest	Grass
T [K]	305.8	304.5
q [g/kg]	9.3	8.7
Precipitation [mm/day]	2.4	2.3
Total Evaporation [mm/day]	2.4	2.3
Interception Loss [mm/day]	1.5	1.0
Transpiration [mm/day]	0.9	1.7
Soil Evaporation [mm/day]	0.1	-0.5
Runoff [mm/day]	0	0
Latent Heat [W/m2]	70	66
Sensible Heat [W/m2]	56	36
Net Solar [W/m2]	231	211
Net Longwave [W/m2]	-106	-110
Net Allwave [W/m2]	125	101
Entropy Difference [J/kg/K]	-24	-33

6.5 Sensitivity of Results to Properties of the Advected Air

In this experiment, instead of using the climatological profiles of humidity and temperature of air at both domain boundaries, we used a moister and cooler profile for the the advected air at the southern boundary. This profile is taken from the NCEP climatology at 7.5N, rather than 10N. The sensitivity of the climate to this change is shown in Table 6.4. Although it is somewhat moister and cooler than the control simulation, the difference is not large. Table 6.4 also shows that the climate of this domain is not sensitive to vegetation type. As such, the equilibrium vegetation in this experiment was grassland, whether the initial vegetation was specified as grassland or deciduous forest (see Table 6.5).

Table 6.5: Inland Domain: Summary of equilibrium vegetation.

	Deciduous Start	*Grassland Start*
South Slope ÷ 2	grass	grass
South Slope x 2	grass	grass
South Profile 7.5N	grass	grass

Chapter 7

Conclusion

Our model was able to simulate the equilibrium climate and vegetation of our two domains reasonably well in the control simulations. Table 7.1 summarizes the results of our experiments for the coastal domain (5N-10N) and Table 7.2 summarizes the results of our experiments for the inland domain (10N-15N). All but one experiment gives the same equilibrium vegetation regardless of the initial vegetation. The exception is the coastal domain experiment in which the profile of air advected from the north is changed to the hotter and drier profile 5 degrees farther north. In this case, deciduous forest or grassland can become dominant, depending on the initial condition.

The stability of most of our simulations in the coastal domain suggests that even in regions where climate is significantly modified by changes in vegetation cover, there will not be multiple equilibria unless the atmospheric climate is near a threshold which separates the dominance regimes of two potential vegetation types. In tropical West Africa, forests dominate whenever the water availability is sufficient for trees to exclude competition from grasses by shading the ground with a full canopy. Thus, we can expect that forests will dominate until the availability of water begins to be insufficient to support a full canopy. At this point, grasses begin to be able to capture light and can exploit their ability to uptake water quickly and conserve water during the dry season. When water availability falls near this transition zone, we may then begin to see the effects of initial vegetation state on the equilbrium condition.

For example, a 1 mm/day (22%) decrease in precipitation resulting from altered vegetation cover in our control simulation did not affect the ultimate equilibrium state of the vegetation and climate, because the annual precipitation was well above that required to support a full-canopied forest. However, a 0.4 mm/day (16%) reduction in precipitation in our experiment with an altered profile of advected air was able to push the system into a new equilibrium. This is not because the change in climate was larger, but merely because it happened to straddle the threshold between the amount of moisture at which forest is dominant and the amount at which grassland becomess dominant.

In the coastal domain, we see that the interaction between the model domain and its surroundings has a very strong impact on the equilibrium state of both climate and vegetation. The strength of the monsoon circulation was seen to be very important for its ability to keep hot and dry air to the north from penetrating into the model domain. By changing the parameters of our empirical monsoon circulation model we were able to modify the strength of the monsoon and obtain three different equilibrium vegetation states - evergreen forest, deciduous forest and grassland. The climate which supported these different vegetation types was likewise different in each case. The greatest sensitivity was seen in the simulation in which the profile of air advected from the north was changed to one which is hotter and drier, as would likely be the case if the northern region were to undergo desertifiction. This suggests that changes in the vegetative cover of the region adjacent to our model domain may have even more significant impacts on the climate in our model domain than vegetation changes within the domain itself. This points to the need for two-dimensional and three-dimensional modeling to fully understand the coupled biosphere-atmosphere system.

Even if it is shown that forest can regrow in most deforestation scenarios, changes in climate induced by changes to vegetation cover remain important, as deforested areas are typically not left to regrow. Rather, they are used as rangeland, for agricultural crops, and for human habitation. All of these uses artificially restrict the ability of forests to regrow. Thus, despite the indications of our simulations

that forest can regrow even with the weakened monsoon circulation of the deforested regime, if forest is not in fact allowed to regrow, the weakened monsoon circulation is in essence permanent.

In the inland domain, we saw that grassland was stable in each of the experiments performed. Precipitation in the region was seen to be insensitive to changes in vegetation. It seems that this region is locked into a seasonally dry pattern due its distance from the coast. Desertification experiments, rather than our afforestation experiments may have shown more sensitivity to the vegetation.

The existence of a stable forest equilibrium at 5N-10N and a stable grassland equilibrium at 10N-15N suggests that there may be a transition region between these two domains, in which forests and grass can coexist or in which the equilibrium vegetation may depend upon the initial vegetation condition. The existence of such a region was investigated briefly in simulations for the large region 5N-15N, and intermediate regions 5N-12.5N, 7.5N-12.5N, and 7.5N-15N. Preliminary results for each of these regions also showed stable equilibrium vegetation of either grass or forest. The coarse resolution of the NCEP data, upon which our empirical monsoon circulation model is based, limits our ability to choose our domain, and the question of multiple equilibria and interactions among adjacent regions in the transition region between forest and grassland is best left for study in a two or three dimensional model with finer resolution.

7.1 Further Research

In this study, we examined the differences in climate caused by forest vs. grassland conditions. Although other studies have shown sensitivity of the equilibrium vegetation to the initial vegetation at desert margins (Claussen 1997, Levis and Foley 1997) this interaction was not examined in our study. Additional simulations looking at desertification in the inland domain (10N-15N) and a domain even further inland may yield interesting results.

Model parameters. The results of our simulations can be further explored with tests of sensitivity to different model parameters. One important parameter in our model is the LAI at which the fractional cover of vegetation reaches one, or the tree is able to completely shade a lower canopy. In the simulations described in this study, it was set at the default value, 2, given in the model code. However, this is at the low end of reasonable values. Broadleafed vegetation, or dense forest, can restrict penetration of about 95% of the available light when their LAI is in the range 2-4 (Larcher 1995). As such the model may tend to favor the growth of trees, which need only reach an LAI of 2 before competition from grasses is excluded. The sensitivity to this parameter choice should be tested in future work.

Other model parameters may be changed to study the effects of changes in atmospheric composition (for example, CO_2 doubling) and solar forcing (for example, paleoclimate investigations) on the vegetation-climate system.

Other model limitations. There are several limitations to our model, and improvement upon them may alter the behavior of the model significantly. Spatial heterogeneity in precipitation and soil moisture may play an important role in determining vegetation cover. Offline IBIS simulations forced with prescribed climatic conditions indicated that forest cannot be sustained with a precipitation rate less than 2-3 mm/day. However, the temporal distribution of the precipitation seemed to play a role in determining the exact magnitude of that threshold. In our coupled model, there are no long stretches without precipitation during the wet season. Precipitation occurs daily, with an afternoon peak, across the entire domain. If spatial heterogeneity in the precipitation were considered, then different parts of the domain might not receive precipitation every day. Longer intervals between precipitation events would allow the soils to become drier and perhaps alter the competition between trees and grasses.

Also, the vegetation model does not consider disturbance regimes, especially fires, which may play an important role in savanna ecosystems. A newer version of IBIS does include some representation of disturbance regimes. Changes in the rate of soil

Table 7.1: Coastal Domain: Summary of equilibrium vegetation.

	Evergreen Start	*Deciduous Start*	*Grassland Start*
Climatological Flux	decid	decid	decid
Flux Relation	ever	ever	ever
South Slope ÷ 2	ever	-	ever
South Slope x 2	ever	-	ever
North Slope ÷ 2	ever	-	ever
North Slope x 2	decid	decid	decid
North Profile 15N	decid	decid	grass

erosion as well as changes in nutrient cycling also occur with different vegetation types, as mentioned in Chapter 2. Consideration of these processes may also enhance the ability of the model to simulate real plant behavior.

There are also limitations to our monsoon circulation model. While our model assumes static ocean conditions, changes in the circulation might also impact the ocean, creating yet another feedback in the biosphere - atmosphere - ocean system. In addition, our monsoon circulation model looks only at meridional fluxes although tropical easterly waves may be important in the generation of precipitation in West Africa (Hayward and Oguntoyinbo 1987). Furthermore, Sud and Smith (1985), in their study on the Indian monsoon, found that surface roughness affects not only wind magnitudes but also wind direction. All these limitations point to the need for a model with better treatment of the atmospheric dynamics than is accomplished by our simple empirical model.

Table 7.2: Inland Domain: Summary of equilibrium vegetation.

	Deciduous Start	*Grassland Start*
Climatological Flux	grass	grass
Flux Relation	grass	grass
South Slope ÷ 2	grass	grass
South Slope x 2	grass	grass
South Profile 7.5N	grass	grass

Appendix A

Biomass Initialization

Due to an oversight in the model code, the biomass was not initialized at the start of the simulations which included dynamic vegetation. The effects of this error on the model behavior are discussed in this appendix. Simulations using static vegetation were unaffected by this error.

The biomass of trees plays two roles in the biosphere-atmosphere interaction described by our model, when dynamic vegetation is active. First, the height of trees are calculated as a function of the biomass, so that a larger biomass yields taller trees. The minimum tree height is 2 meters, regardless of the biomass amount. Because vegetation height affects the surface roughness, this can affect turbulent fluxes between the surface and the atmosphere. Second, the biomass affects NPP through a plant's need for maintenance respiration. The greater the biomass, the greater the plant's expenditure on maintenance respiration. However, woody tissues make up the bulk of the biomass of trees and only a fraction of this is made up of active sapwood requiring maintenance respiration. The NPP rapidly stabilizes in our simulations, indicating that the changing needs of sapwood respiration with accumulation of biomass is minimal.

Over grassland, the height of the grass is calculated as a function of the LAI, and not the biomass, and so surface roughness is unaffected by the biomass initialization error. In addition, the biomass attains a steady state much more rapidly over grassland than over forest, and thus the effects of the initialization problem are

reduced for our simulations initialized with grassland vegetation. However, we do see large spikes in NPP near the beginning of some simulations, which results in high transient values of the LAI. These spikes are shortlived. Grassland either stabilizes at smaller values of LAI and NPP as the biomass quickly builds up, or the grassland gives way to forest. The competition between forest and grassland is based on the forest's ability to block sunlight from the lower canopy when there is sufficient water, and this mechanism is unaffected by the transient bloom in grassland. As such, the biomass initialization is not considered a problem when the system is initialized with grassland conditions.

The specific conditions encountered in the coastal and inland domains initialized with forest are considered further below.

A.1 Coastal domain simulations

Using our fixed circulation control simulation as an example, we show that while the biomass initialization error can affect the competition between different tree types, it does not affect the competition between trees and grasses. By the end of our fixed circulation control simulation, the deciduous forest has reached a height of 30 meters. In two simulations in which the biomass is initialized at 15 kg-C/m^2 or 25 kg-C/m^2, conditions eventually begin to favor evergreen rather than deciduous trees (see Figure A-1 and Figure A-2). However, any shift in climate due to additional growth cannot be expected to favor grassland rather than forest. The LAI is the important determinant of competition between trees and grasses when water is abundant, as trees use shading of the ground surface as a means of eliminating competition from grasses. The initial LAI is able to shade the forest floor in all our simulations initialized with forest conditions, and the total upper canopy LAI remains high throughout the simulations. While the forest is continuing to accumulate biomass in many of our experimental simulations, this does not affect the competition between trees and grasses. As the primary intent of our experiments is to study the effects of deforestation or afforestation on climate, and not the effects of different tree types,

the biomass initialization problem does not affect the main substance of our results.

A.2 Inland domain simulations

In the inland domain, all simulations which were initialized with forest transitioned quickly into landscapes dominated by grassland. As seen in Figure A-3, this is also true when the biomass initialization problem is corrected, and biomass is initialized at 15 kg-C/m^2. As in the simulations described in Chapter 6, the upper canopy NPP is negative in this simulation because forest cannot be sustained with the limited water available in this domain. Simulations in which the vegetation is fixed as a mature forest were shown in Chapter 6. Precipitation was not increased appreciably in these simulations over the control experiments in which grassland was the dominant vegetation. The negative NPP values result in rapid death of the forest. The LAI immediately falls to zero, and the initial biomass slowly decays. Forest cannot survive in the inland domain because of insufficient moisture, and the biomass initialization does not affect this result.

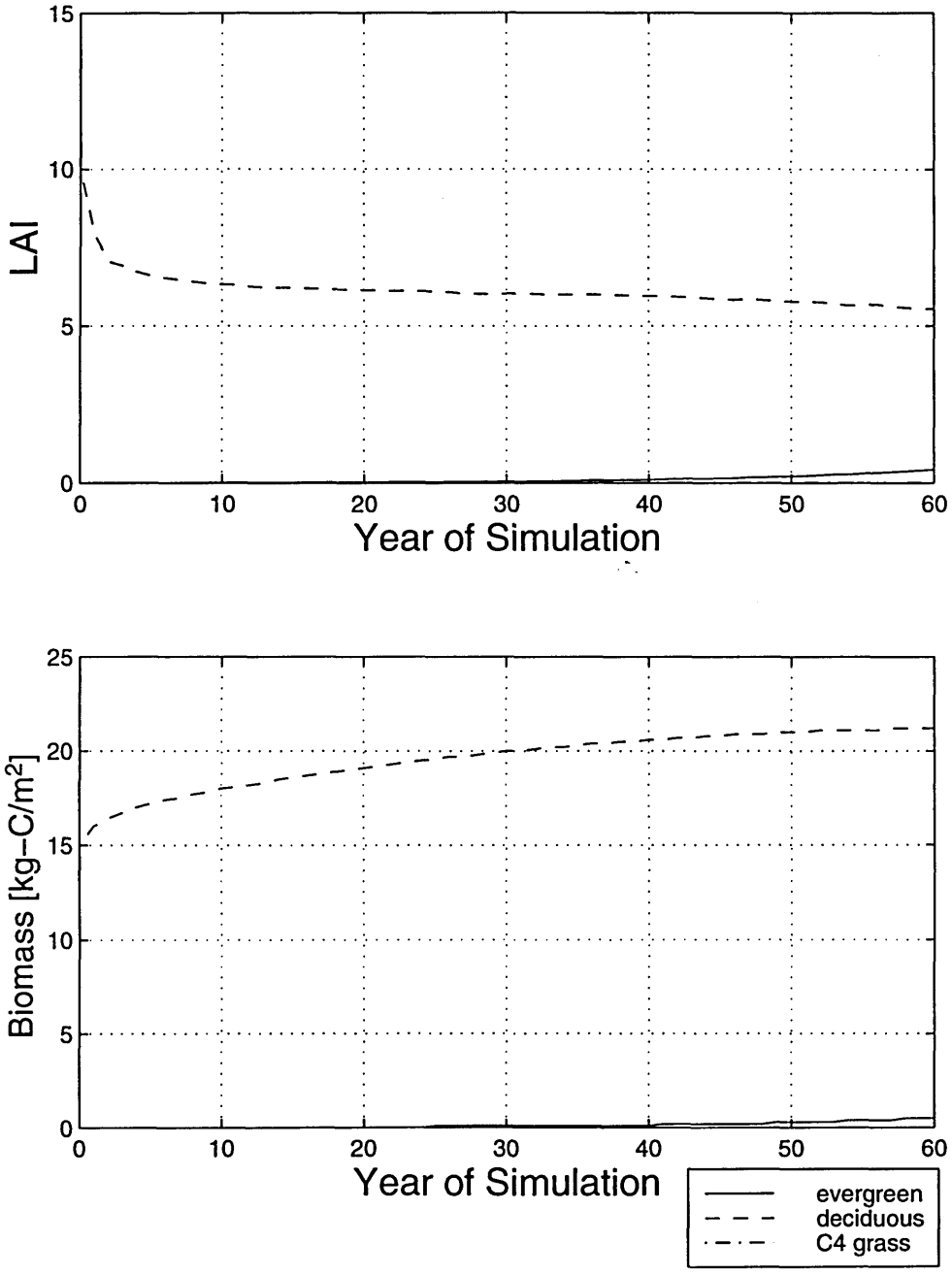

Figure A-1: Coastal domain, fixed circulation simulation, deciduous forest initialization. Both the LAI (upper panel) and the biomass (lower panel) show that evergreen forest is beginning to grow at the end of this simulation, in which the biomass is initialized at 15 kg-C/m^2.

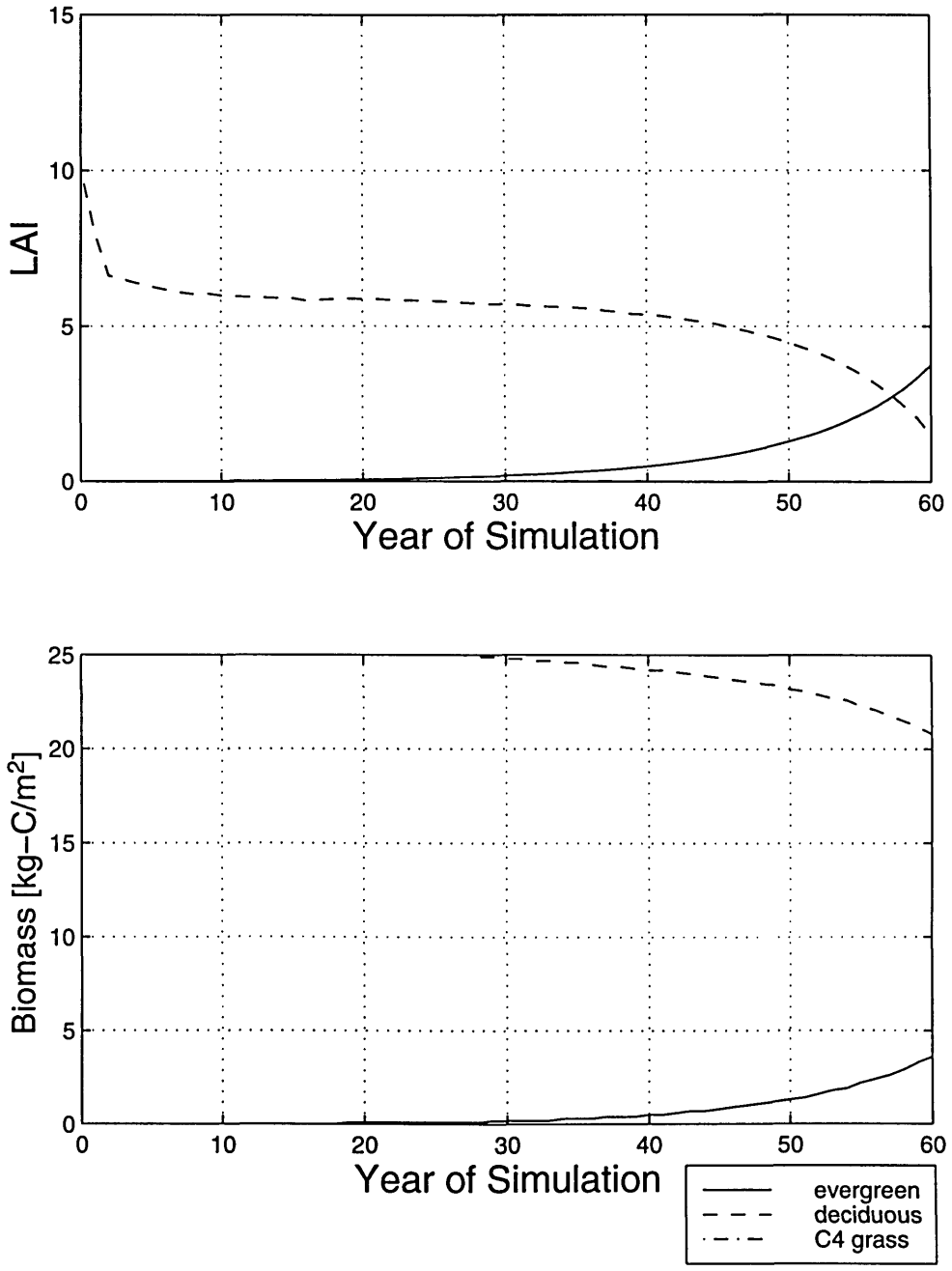

Figure A-2: Coastal domain, fixed circulation simulation, deciduous forest initialization. Both the LAI (upper panel) and the biomass (lower panel) show that the deciduous forest is giving way to evergreen forest at the end of this simulation, in which the biomass is initialized at 15 kg-C/m^2.

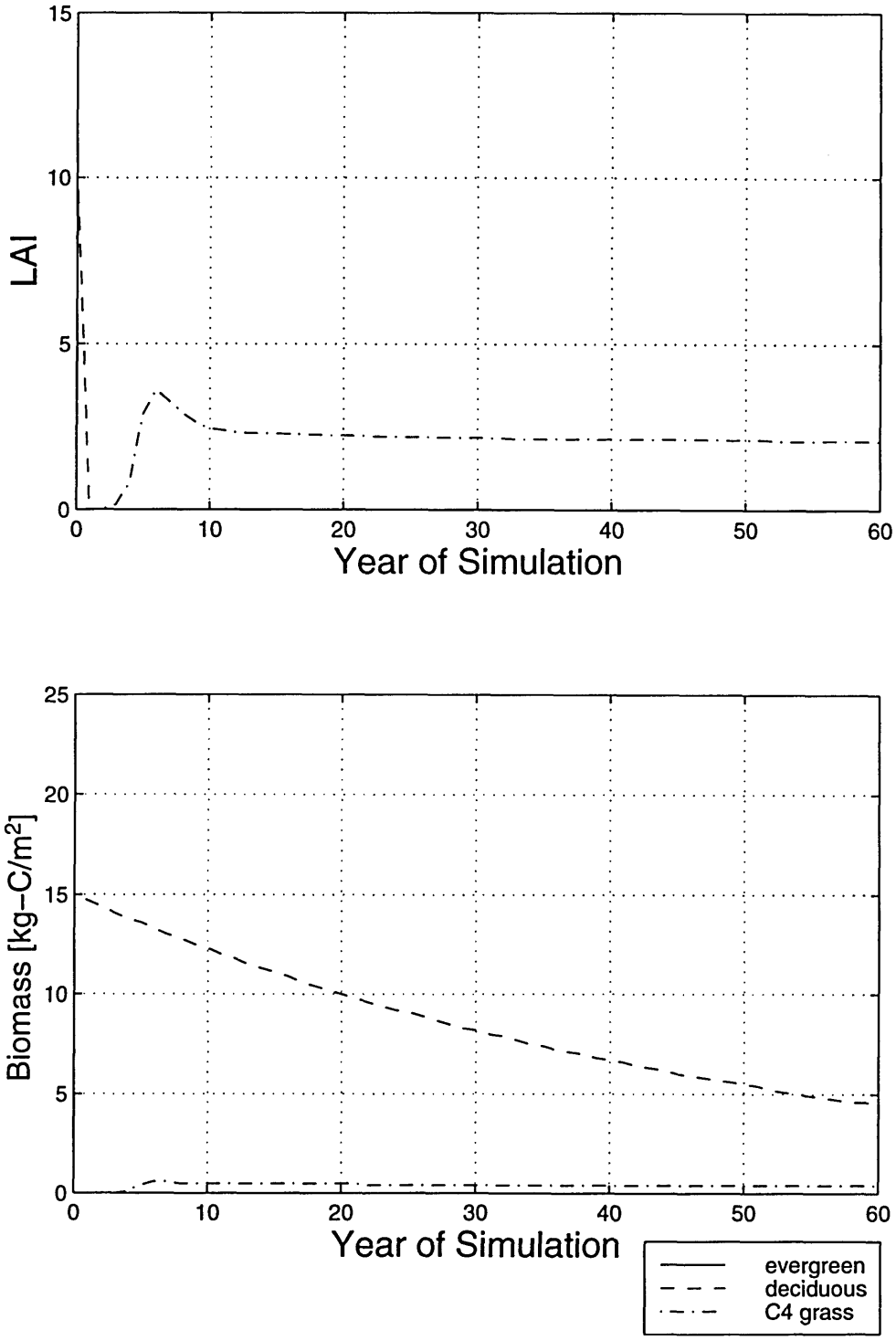

Figure A-3: Inland domain, interactive circulation simulation, deciduous forest initialization. The upper panel shows the sudden drop in LAI at the beginning of the simulation due to the negative NPP. The lower panel shows the slow decay of the initial biomass.

References

Ayoade, J. (1983). *Introduction to Climatology for the Tropics*, John Wiley and Sons.

Bastable, H. et al. (1993). Observations of climate, albedo, and surface radiation over cleared and undisturbed amazonian forest, *International Journal of Climatology* **13**: 783–796.

Bonan, G. B. (1997). Effects of land use on the climate of the united states, *Climatic Change* **37**: 449–486.

Bonan, G. B., Pollard, D. and Thompson, S. L. (1992). Effects of boreal forest vegetation on global climate, *Nature* **359**: 716–718.

Bonan, G. B., Pollard, D. and Thompson, S. L. (1995). Boreal forest and tundra ecosystems as components of the climate system, *Climatic Change* **29**: 145–167.

Brubaker, K. L., Entekhabi, D. and Eagleson, P. S. (1991). Atmospheric water vapor transport: estimation of continental precipitation recycling and parameterization of a simple climate model, *Technical report*, Ralph M. Parsons Laboratory, Massachusetts Institute of Technology.

Charney, J. (1975). Dynamics of deserts and drought in the sahel, *Quarterly Journal of the Royal Meteorological Society* **101**: 193–202.

Chou, M.-D. (1986). Atmospheric solar heating rate in the water vapor bands, *Journal of Climate and Applied Meteorology* **25**: 1532–1542.

Chou, M.-D., Kratz, D. P. and Ridgway, W. (1991). Infrared radiation parameterizations in numerical climate models, *Journal of Climate* **4**: 424–437.

Claussen, M. (1994). On couping global biome models with climate models, *Climate Research* **4**: 203–221.

Claussen, M. (1997). Modeling bio-geophysical feedbak in the african and indian monsoon region, *Climate Dynamics* **13**: 247–257.

Collinson, A. (1977). *Introduction to World Vegetation*, George Allen and Unwin.

Crawley, M. J. (1986a). *Plant Ecology*, Blackwell Scientific Publications, chapter The Structure of Plant Communities.

Crawley, M. J. (1986b). *Plant Ecology*, Blackwell Scientific Publications, chapter Life History and Environment.

Culf, A., Esteves, J., de O. Marques Filho, A. and da Rocha, H. (1996). *Amazonian deforestation and climate*, Intitute of Hydrology, chapter Radiation, temperature and humidity over forest and pasture in Amazonia.

Culf, A., Fisch, G. and Hodnett, M. (1995). The albedo of amazonian forest and ranch land, *Journal of Climate* **8**: 1544–1554.

Cutrim, E., Martin, D. W. and Rabin, R. (1995). Enhancement of cumulus clouds over deforested lands in amazonia, *Bulletin of the American Meteorological Society* **76**: 1801–1805.

da Rocha, H. R. et al. (1996). A vegetation-atmosphere intertion study for amazonia deforestation using field data and a 'single column' model, *Quarterly Journal of the Royal Meteorological Society* **122**: 567–594.

Dickinson, R. E. and Kennedy, P. (1992). Impacts on regional climate of amazon deforestation, *Geophysical Research Letters* **19**: 1947–1950.

Dickinson, R. and Kennedy, P. (1991). Land surface hydrology in a general circulation model - global and regional fields needed for validation, *Survey of Geophysics* **12**: 115–126.

Dickinson, R., Kennedy, P., Henderson-Sellers, A. and Wilson, M. (1986). Biosphere-Atmosphere Transfer Scheme (BATS) version 1E as coupled to the NCAR Community Climate Model., *Technical Report TN-275+STR*, NCAR, Boulder, Colorado. pp. 72.

Eltahir, E. A. (1996). Role of vegetation in sustaining large-scale atmospheric circulations in the tropics, *Journal of Geophysical Research* **101**: 4255–4268.

Eltahir, E. A. and Bras, R. L. (1994). Sensitivity of regional climate to deforestation in the amazon basin, *Advances in Water Resources* **17**: 101–115.

Eltahir, E. A. and Gong, C. (1996). Dynamics of wet and dry years in west africa, *Journal of Climate* **9**: 1030–1042.

Eltahir, E. and Bras, R. (1993a). A description of rainfall interception over large areas, *Journal of Climate* **6**: 1002–1008.

Eltahir, E. and Bras, R. (1993b). On the response of the tropical atmosphere to large-scale deforestation, *Quarterly Journal of the Royal Meteorological Society* **119**: 779–793.

Eltahir, E. and Bras, R. (1993c). Estimation of the fractional coverage of rainfall in climate models, *Journal of Climate* **6**: 639–644.

Emanuel, K. A. (1991). A scheme for representating cumulus convection in large-scale models, *Journal of the Atmospheric Sciences* **48**: 2313–2335.

Emanuel, K. A., Neelin, J. D. and Bretherton, C. (1994). On large scale circulations in convecting atmospheres, *Quarterly Journal of the Royal Meteorological Society* **120**: 1111–1143.

Entekhabi, D. and Eagleson, P. (1989). Land surface hydrology parameterization for atmospheric general circulation models including subgrid scale spatial variability, *Journal of Climate* **2**: 816–831.

Espenshade, E. B. J. (1990). *Goode's World Atlas*, 18th edn, Rand McNally.

Foley, J. A., Kutzbach, J. E., Coe, M. T. and Levis, S. (1994). Feedbacks between climate and boreal forests during the holocene epoch, *Nature* **371**: 52–54.

Foley, J. A. et al. (1996). An integrated biosphere model of land surface processes, terrestrial carbon balance, and vegetation dynamics, *Global Biogeochemical Cycles* **10**: 603–628.

Foley, J. A. et al. (1998). Coupling dynamic models of climate and vegetation, *Global Change Biology* **4**: 561–579.

Gutman, G. (1984). Numerical experiments on land surface alterations with a zonal model allowing for interaction between the geobotanic state and climate, *Journal of the Atmospheric Sciences* **41**: 2679–2685.

Gutman, G., Ohring, G. and Joseph, J. H. (1984). Interaction between the geobotanic state and climate: a suggested approach and a test with a zonal model, *Journal of the Atmospheric Sciences* **41**: 2663–2678.

Hayward, D. and Oguntoyinbo, J. (1987). *Climatology of West Africa*, Hutchinson.

Henderson-Sellers, A. et al. (1993). Tropical deforestation: Modelling local to regional-scale climate change, *Journal of Geophysical Research* **98**: 7289–7315.

Koster, R. and Eagleson, P. (1990). A one-dimensional interactive soil atmosphere model for testing formulations of surface hydrology, *Journal of Climate* **3**: 593 – 606.

Kutzbach, J., Bonan, G., Foley, J. and Harrison, S. (1996). Vegetation and soil feedbacks on the response of the african monsoon to orbital forcing in the early to middle holocene, *Nature* **384**: 623–626.

Larcher, W. (1995). *Physiological Plant Ecology*, 3rd edn, Springer.

Lean, J. and Rowntree, P. (1993). A gcm simulation of the impact of amazonian deforestation on climate using an improved canopy representation, *Quarterly Journal of the Royal Meteorological Society* **119**: 509–530.

Lean, J. and Rowntree, P. (1997). Understanding the sensitivity of a gcm simulation of amazonian deforestation to the specification of vegetation and soil characteristics, *Journal of Climate* **10**: 1216–1235.

Lean, J. and Warrilow, D. (1989). Simulation of the regional climatic impact of amazon deforestation, *Nature* **342**: 411–413.

Levis, S., Foley, J. A. and Pollard, D. (1997). Sensitivity of a synchronously coupled dynamic model of climate and vegetation to the choice of initial vegetation conditions, *AGU Fall Meeting* .

Meher-Homji, V. (1988). *Forests, Climate, and Hydrology Regional Impacts*, The United Nations University, chapter Effects of Forests on Precipitation in India.

Miller, G. et al. (1997). Sensitivity of the australian monsoon to vegetation type: Did aboriginal burning lead to the failure of the early holocene monsoon?, *Fall 1997 AGU Meeting* .

Pollard, D. and Thompson, S. L. (1993). Description of a land-surface-transfer model, *submitted to JGR* .

Prentice, I. C. et al. (1993). *Vegetation Dynamics and Global Change*, Chapman and Hall, chapter Modeling large-scale vegetation dynamics.

Prentice, I. et al. (1992). A global biome model based on plant physiology and dominance, soil properties and climate, *Journal of Biogeography* **19**: 117–134.

Rabin, R. M. and Martin, D. W. (1996). Satellite observations of shallow sumulus coverage over the central united states: An exploration of land use impact on cloud cover, *Journal of Geophysical Research* **101**: 7149–7155.

Rabin, R. M., Stadler, S., Wetzel, P. J., Stesnrud, D. J. and Gregory, M. (1990). Observed effects of landscape variability on convective clouds, *Bulletin of the American Meteorological Society* **71**: 272–280.

Raven, P. H. and Johnson, G. B. (1989). *Biology*, Times Mirror/Mosby College Publishing.

Rumney, G. R. (1968). *Climatology and the World's Climates*, Macmillon.

Sellers, P., Mintz, Y., Sud, Y. and Dalcher, A. (1986). A simple biosphere model (sib) for use within general circulation models, *Journal of the Atmospheric Sciences* **43**: 505–531.

Shukla, J., Nobre, C. and Sellers, P. (1990). Amazon deforestation and climate change, *Science* **247**: 1322–1325.

Shuttleworth, W. (1988). Evaporation from amazonian rainforest, *Proceedings of the Royal Society of London* **B233**: 321–346.

Smith, T. et al. (1993). *Vegetation Dynamics and Global Change*, Chapman and Hall, chapter Plant Functional Types.

Sud, Y. and Smith, W. (1985). Influence of local land-surface processes on the indian monsoon: A numerical study, *Journal of Climate and Applied Meteorology* **24**: 1015–1036.

Texier, D. et al. (1997). Quantifying the role of biosphere-atmosphere feedbacks in climate change: coupled model simulations for 6000 years bp and comparison with palaeodata for northern eurasia and northen africa, *Climate Dynamics* **13**: 865–882.

Walter, H. (1985). *Vegetation of the Earth and Ecological Systems of the Geo-biosphere*, third edn, Springer-Verlag.

Wang, G. (1998). Personal communication.

Wright, I. et al. (1992). Dry season micrometeorology of central amazonian ranchland, *Quarterly Journal of the Royal Meteorological Society* **118**: 1083–1099.

Xue, Y., Liou, K.-N. and Kasahara, A. (1990). Investigation of biogeophysical feedback on the african climate using a two-dimensional model, *Journal of Climate* **3**: 337–352.

Xue, Y. and Shukla, J. (1993). The influence of land surface properties on sahel climate. part i: Desertification, *Journal of Climate* **6**: 2232–2245.

Zheng, X. and Eltahir, E. A. (1997). The response to deforestation and desertification in a model of west african monsoons, *Geophysical Research Letters* **24**: 155–158.

Zheng, X. and Eltahir, E. A. (1998). The role of vegetation in the dynamics of west african monsoons, *Journal of Climate* **11**: 2078–2096.

Zobler, L. (1986). A world soil file for global climate modeling, *NASA* .